Compréhension des effects de l'inhibitions des protéines peroxyrédoxines humaines pour le traitement potentiel de l'inflammation post-ischemique du cerveau

Melissa L. Chow

N°d'ordre NNT : 2016LYSE1110

THESE de DOCTORAT DE L'UNIVERSITE DE LYON
opérée au sein de
l'Université Claude Bernard Lyon 1

Ecole Doctorale de chimie ED206

Spécialité de doctorat : Chimie
Discipline : Analyses biophysiques et chimiques

Soutenue publiquement le 08/07/2016, par:

Melissa L. CHOW

Understanding the effects of inhibiting human peroxiredoxin proteins for potential treatment against post-ischemic brain inflammation

---

Devant le jury composé de:

RAHUEL-CLERMONT, Sophie	MCF-HDR	Université Lorraine	Rapporteur
LEQUIN, Olivier	Professeur	Université Pierre et Marie Curie	Rapporteur
DOUMÉCHE, Bastien	MCF-HDR	Université Lyon1	Examinateur
LANCELIN, Jean-Marc	Professeur	Université Lyon1	Directeur de thèse
GUILLIERE, Florence	MCF	Université Lyon1	Invitée

UNIVERSITE CLAUDE BERNARD - LYON 1

Président de l'Université	**M. le Professeur Frédéric FLEURY**
Président du Conseil Académique	M. le Professeur Hamda BEN HADID
Vice-président du Conseil d'Administration	M. le Professeur Didier REVEL
Vice-président du Conseil Formation et Vie Universitaire	M. le Professeur Philippe CHEVALIER
Vice-président de la Commission Recherche	M. Fabrice VALLÉE
Directeur Général des Services	M. Alain HELLEU

COMPOSANTES SANTE

Faculté de Médecine Lyon Est – Claude Bernard	Directeur : M. le Professeur J. ETIENNE
Faculté de Médecine et de Maïeutique Lyon Sud – Charles Mérieux	Directeur : Mme la Professeure C. BURILLON
Faculté d'Odontologie	Directeur : M. le Professeur D. BOURGEOIS
Institut des Sciences Pharmaceutiques et Biologiques	Directeur : Mme la Professeure C. VINCIGUERRA
Institut des Sciences et Techniques de la Réadaptation	Directeur : M. le Professeur Y. MATILLON
Département de formation et Centre de Recherche en Biologie Humaine	Directeur : Mme la Professeure A-M. SCHOTT

COMPOSANTES ET DEPARTEMENTS DE SCIENCES ET TECHNOLOGIE

Faculté des Sciences et Technologies	Directeur : M. F. DE MARCHI
Département Biologie	Directeur : M. le Professeur F. THEVENARD
Département Chimie Biochimie	Directeur : Mme C. FELIX
Département GEP	Directeur : M. Hassan HAMMOURI
Département Informatique	Directeur : M. le Professeur S. AKKOUCHE
Département Mathématiques	Directeur : M. le Professeur G. TOMANOV
Département Mécanique	Directeur : M. le Professeur H. BEN HADID
Département Physique	Directeur : M. le Professeur J-C PLENET
UFR Sciences et Techniques des Activités Physiques et Sportives	Directeur : M. Y.VANPOULLE
Observatoire des Sciences de l'Univers de Lyon	Directeur : M. B. GUIDERDONI
Polytech Lyon	Directeur : M. le Professeur E.PERRIN
Ecole Supérieure de Chimie Physique Electronique	Directeur : M. G. PIGNAULT
Institut Universitaire de Technologie de Lyon 1	Directeur : M. le Professeur C. VITON
Ecole Supérieure du Professorat et de l'Education	Directeur : M. le Professeur A. MOUGNIOTTE
Institut de Science Financière et d'Assurances	Directeur : M. N. LEBOISNE

RÉSUMÉ

COMPRÉHENSION DES EFFETS DE L'INHIBITION DES PROTÉINES PEROXYRÉDOXINES HUMAINES POUR LE TRAITEMENT POTENTIEL DE L'INFLAMMATION POST-ISCHÉMIQUE CÉRÉBRALE

Les accidents vasculaires cérébraux (AVC) sont la seconde cause d'invalidité à long terme et du mortalité dans le monde entier qui résulte d'une interruption de flux sanguin cérébral. Il y a actuellement peu de médicaments pour traiter les accidents vasculaires cérébraux. Pourtant, il y a un intérêt pour trouver un traitement, ciblant spécifiquement la cascade post-inflammatoire. Il y a une attention particulière pour inhiber les protéines peroxyrédoxines humaines (hPrx) qui sont des initiateurs clés de l'inflammation. Les protéines hPrx sont des enzymes qui dégradent les peroxydes et donc protègent les cellules du stress oxydatif. Cette thèse est centrée sur l'étude de ligands potentiels des hPrx, dérivés du catéchol, susceptibles de devenir des agents thérapeutiques potentiels pour traiter les AVC, basées sur différents ligands potentiels criblés par RMN et modélisation moléculaire, nos études ont révélé que ces dérivés du catéchol pouvaient se lier à plusieurs hPrx. Deuxièmement, la capacité des dérivés du catéchol à inhiber l'activité des hPrx a été examinée au travers de tests enzymatiques *in vitro*. Il a été montré que tous les dérivés du catéchol étudiés étaient capables de les inhiber. En utilisant des simulations de dynamique moléculaire, nous avons pu expliquer le mécanisme d'action moléculaire d'inhibition. D'un point de vue général, cette recherche fournit un aperçu des ligands qui pourrait servir debase au développement de médicaments pour aider dans le processus de rétablissement de patients atteints d'attaque cérébrale.

Mots clés: peroxyrédoxines humaines, dérivés de catéchol, cinétique enzymatique, RMN

ABSTRACT

UNDERSTANDING THE EFFECTS OF INHIBITING HUMAN PEROXIREDOXIN PROTEINS FOR POTENTIAL TREATMENT AGAINST POST-ISCHEMIC BRAIN INFLAMMATION

Strokes are the second leading cause of long-term disability and death worldwide that result from a sudden loss of blood supply to the brain. Currently, there are limited drugs to treat patients when having a stroke. However, there is now interest focused on treatment after a stroke, specifically the post-inflammation cascade. In particular, there is attention to inhibit human peroxiredoxin proteins, which are key initiators of inflammation. Human peroxiredoxins are enzymes that degrade peroxides and thus, protect the cells against oxidative stress. This thesis focuses on studying ligands, catechol derivatives, to bind and inhibit human peroxiredoxin proteins to become potential therapeutic agents for strokes. First, the ligands were screened to identify if they could bind to various human peroxiredoxin isoforms with NMR and computational modeling techniques. This study revealed the catechol derivatives could indeed bind to several human peroxiredoxins. Second, the ability for the catechol derivatives to inhibit human peroxiredoxin peroxidase activity was examined through an *in vitro* enzymatic assay. All the catechol derivatives were determined to inhibit several human peroxiredoxins. In utilizing molecular dynamic simulations, it assisted in explaining the *in vitro* inhibition molecular mechanism of action. Overall, this research provides insight of molecules that could be further developed to become possibly a drug to aid in stroke patients recovery process.

Key words: human peroxiredoxins, catechol derivatives, enzymatic kinetics, inhibition mechanism, NMR.

RÉSUMÉ SUBSTANTIEL

Introduction

Les peroxyrédoxines (Prxs) sont des protéines qui permettent de réduire et détoxifier le peroxyde d'hydrogène et différents peroxydes organiques dans les cellules [1,2]. Chez l'homme, il existe six isoformes de Prxs situées dans différents compartiments cellulaires tels que le cytosol, la mitochondrie, le réticulum endoplasmique, ou encore les peroxysomes [3,4]. Les six Prxs peuvent être classées d'après leur mécanisme catalytique en trois classes basées sur le nombre de résidus cystéine impliqués dans les réactions rédox: typique à 2 cystéines (hPrx1 à 4), atypique à 2 cystéines (hPrx5) et enfin à 1 cystéine (hPrx6)[5].

Le mécanisme catalytique pour réduire les peroxydes se déroule en plusieurs étapes avec les peroxyredoxines qui subissent différents changements conformationnels. En résumé, le cycle commence avec la protéine Prx sous forme réduite qui contient une cystéine catalytique maintenue sous forme d'anion thiolate qui attaque une molécule de substrat peroxyde d'hydrogène (H_2O_2). Suite à cette réaction, la Prx devient alors oxydée et subit une modification conformationnelle passant d'un état totalement replié à un état localement déplié. Le thiolate de la cystéine catalytique de la Prx est ainsi oxydé en acide sulfénique (R-SOH) qui forme dans un état localement déplié un pont disulfure avec une autre cystéine impliquée dans la réaction et dépendant du sous-groupe de Prx. Les Prxs typiques et atypiques à 2 cystéines forment respectivement des liaisons inter- et intramoléculaires, alors que les Prx à 1 cystéine forment également des ponts disulfures mais avec d'autres protéines ou molécules. Le pont disulfure de la Prx peut ensuite être réduit par les protéines thiorédoxine, les protéines assimilées à la thiorédoxine, ou le glutathion pour compléter le cycle catalytique avec la Prx réduite et dans son état complètement replié.

Lorsque les Prxs sont oxydées, il est aussi possible qu'elles deviennent suroxydées par réaction avec une molécule additionnelle d'H_2O_2 en donnant un acide sulfinique (R-SO_2H) ou même possiblement un acide sulfonique (R-SO_3H), qui sont tous deux des formes inactives. Néanmoins, les formes suroxydées de Prxs peuvent être occasionnellement régénérées par la sulfirédoxine pour redevenir actives et retourner au cycle catalytique [1–5].

Les Prxs peuvent agir comme protéines anti-oxydantes. Les Prxs protègent la cellule contre les dommages oxydatifs qui peuvent survenir sur l'ADN, les protéines, les lipides et autres macromolécules et qui sont causés par la formation de radicaux libres tels que les espèces réactives oxygènees (ROS) ou azotées (RNS). Récemment, il a été mis en évidence que des stress oxydatifs pouvaient être liés au développement de différentes maladies dans lesquelles des fonctions cellulaires s'avéraient détériorées [2,10].

Les Prxs ont été associées à des cancers, à la maladie d'Alzheimer, à des détériorations de systèmes d'immunité. De façon intéressante, les Prxs humaines 1, 2, 5 et 6 ont aussi été reliées à la cascade inflammatoire post-ischémique [6], comme elles ont été mises en évidence dans le déclenchement de l'activation des cellules inflammatoires qui aident au remodelage du tissu cérébral endommagé [11,12]. L'étude des accidents vasculaires cérébraux (AVC) est d'une grande importance car ils sont la deuxième cause la plus fréquente de décès et d'invalidité dans le monde résultant d'une diminution soudaine d'afflux sanguin au cerveau. Les deux principaux types d'AVC sont: les AVC ischémiques et les AVC hémorragiques, dû respectivement soit au blocage ou à l'éclatement d'un vaisseau sanguin et les AVC ischémiques sont le principal type d'accident vasculaire cérébral [13-15].

Actuellement, il y a un nombre limité de médicaments pour les patients atteints d'AVC qui visent principalement à la prévention de l'apparition ou la réapparition d'un AVC. L'identification d'une inflammation cérébrale après un AVC conduit à de sérieux effets pathologiques, il y a donc un intérêt à développer des agents thérapeutiques entravant la cascade inflammatoire post-ischémique comme une méthode alternative de traitement [14,16, 17]. Sachant que les hPrxs sont des initiateurs clés de l'inflammation post-ischémique cérébrale, cette thèse se concentre sur la comprehension du mode d'action de ligands liant et inhibant l'activité peroxydase des hPrxs, comme une possible approche pour réguler l'inflammation cérébrale post-ischémique. Dans le passé, notre laboratoire a criblé une librairie de ligands par des expériences RMN (^{15}N-HQSC, Expériences de différence de Transfert de Saturation (STD), waterLOGSY) et a découvert que des dérivés du catéchol pouvaient se lier à la hPrx5 [18]. Premièrement, dans ce manuscrit, l'affinité de liaison de trois dérivés du catéchol (catéchol, 4-methylcatéchol, 4-*tert*-butylcatéchol) sera examinée au travers de méthodes RMN et de modélisation moléculaire. Ceci nous permettra de savoir s'il y a une sélectivité parmi les dérivés du catéchol pour lier les autres isoformes des hPrxs. Deuxièmement, si les dérivés du catéchol peuvent lier les hPrxs, leurs effets inhibiteurs seront ensuite évalués via un essai enzymatique *in vitro* en étudiant les mécanismes moléculaires d'action de ces inhibiteurs (MMOA).

À l'heure actuelle, il y a eu plusieurs ligands identifiés pour lier et inhiber les hPrxs. Ces ligands comprennent : l'adénanthine, H7, AMRI-59, triptolide et ses dérivés célastrol, withaferine, conoidin A et des anticorps contre les hPrxs [11,19-25]. La plupart de ces ligands sont concentrés sur les traitements possibles pour les cancers. Par conséquent, il existe encore un besoin de développer des ligands potentiels pour lutter contre une inflammation cérébrale post-ischémique. Les dérivés du catéchol pourraient être des inhibiteurs avantageux, puisque leurs composés parents (catéchine et quercétine) ont des effets anti-inflammatoires sur les cellules cérébrales résidentes macrophages. En outre, selon Zheng et al., différents dérivés du

catéchol (catéchol, 3-méthylcatéchol, 4-méthylcatéchol et 4-*tert*-butylcatéchol) se sont avérés avoir des effets anti-inflammatoires et neuroprotecteurs sur d'autres cellules du cerveau, les cellules microgliales [26].

Résultats

Comme mentionné, le catéchol, le 4-méthylcatéchol et le 4-*tert*-butylcatéchol ont été préalablement identifiés pour se lier à la hPrx5 au sein du site actif où H_2O_2 se lie. Les interactions de liaison de ces dérivés du catéchol à l'hPrx1 et l'hPrx2 ont également été examinées. En utilisant des expériences RMN (STD), les trois dérivés de catéchol ont été déterminés se lier à hPrx1 et hPrx2. Dans le classement des dérivés de catéchol, le 4-*tert*-butylcatéchol se lie toujours le mieux contrairement au catéchol qui se lie le moins pour toutes les hPrxs. Cependant, en comparant les valeurs d'affinité de liaison (K_d) pour hPrxs, il y avait des différences. Les dérivés de catéchol se lient à hPrx5 avec des valeurs de K_d inférieures (plus d'affinité) qu'aux hPrx1 et hPrx2.

En outre, pour comprendre les interactions de liaison au niveau microscopique, des expériences de modélisation moléculaire par "funnel" métadynamique (FM) ont été réalisées pour fournir plus de détails en parallèle des résultats RMN. La simulation FM permet de connaitre la dynamique des protéines en solution grâce à l'amélioration de la méthode d'échantillonnage des événements d'association et de dissociation en utilisant un potentiel de contrainte en forme d'entonnoir dirigé vers un site spécifique sur la protéine. La FM a été en mesure de déterminer que les dérivés du catéchol pourraient se lier aux sites actifs de hPrx1, hPrx2 et hPrx5. Les conformations de liaison déterminées pour les dérivés de catéchol étaient similaires aux structures cristallines aux rayons X déterminées pour hPrx5 [27]. Comme pour les résultats de RMN, des trois dérivés du catéchol, le 4-*tert*-butylcatéchol se lie le mieux aux hPrxs. En outre, les dérivés du catéchol se lient à hPrx5 avec une affinité de liaison supérieure aux autres hPrxs. Ces études ont mis en évidence les avantages de l'utilisation des simulations FM pour aider dans les premières prédictions de ligands potentiels aux protéines cibles.

Ayant déterminé que les dérivés du catéchol pouvaient se lier aux hPrxs, leur capacité à inhiber l'activité peroxydase des hPrxs a été évaluée au moyen d'un test enzymatique *in vitro*. Les effets inhibiteurs des dérivés du catéchol ont été déterminés par des essais de concentration inhibitrice médiane (IC_{50}). Tous les dérivés de catéchol se sont révélés inhiber l'hPrx5 et en classant par les valeurs d'IC_{50}, le 4-*tert*-butylcatéchol est le plus puissant inhibiteur, suivi du 4-méthylcatéchol et du catéchol. Au bilan, la force d'inhibition des dérivés du catéchol était en accord avec les études inhibitrices préliminaires accomplies dans notre laboratoire qui avaient montré que le 4-méthylcatéchol était plus puissant que le catéchol sur l'hPrx5 [18].

En outre, pour vérifier que les dérivés du catéchol se liaient aux hPrx1 et hPrx2 avec une affinité réduite, seuls les effets inhibiteurs du 4-*tert*-butylcatéchol sur ces hPrxs ont été examinés. Le 4-*tert*-butylcatéchol s'est également avéré inhiber les hPrx1 et hPrx2. Cependant, en comparant les propriétés inhibitrices du 4-*tert*-butylcatéchol à toutes les hPrxs, le 4-*tert*-butylcatéchol s'est révélé inhiber mieux l'hPrx5 que les hPrx1 et hPrx2. Par conséquent, les tendances de l'affinité de liaison déterminées par RMN et modélisation moléculaire étaient semblables aux propriétés inhibitrices examinées expérimentalement.

Après avoir confirmé que les dérivés du catéchol se liaient et inhibaient hPrx5 mieux que les autres isoformes d'hPrxs dont nous disposions, le MMOA d'inhibition a été étudié. La connaissance du MMOA fournirait un meilleur aperçu de la façon dont les dérivés du catéchol inhibent les hPrxs. Les mécanismes d'inhibition cinétiques, conformationnels, et redox ont été évalués pour chacun des dérivés du catéchol avec l'hPrx5. Le mécanisme d'inhibition cinétique a permis de comprendre si les dérivés du catéchol se liaient à l'hPrx5 de manière réversible ou irréversible. Les vitesses de réaction de l'hPrx5 ont été mesurées en l'absence et en présence de chaque dérivé du catéchol incubé avec l'hPrx5. En comparant les vitesses de réaction, les dérivés du catéchol ont été montrés ne pas perturber la vitesse de réaction de l'hPrx5. Par conséquent, cela indique que les dérivés du catéchol se lient à l'hPrx5 d'une manière réversible.

En étudiant le mécanisme conformationnel, cela nous a permis de comprendre si les dérivés du catéchol inhibent de façon compétitive, non compétitive ou incompétitive, donc si les dérivés de catéchol se lient soit à l'enzyme libre (hPrx5) ou au complexe enzyme-substrat (hPrx5-H_2O_2) provoquant l'inhibition. Le mécanisme d'inhibition conformationnelle a été mesuré en suivant la vitesse de réaction de hPrx5 à diverses concentrations d'inhibiteurs contre une gamme de concentration d'H_2O_2. Les variations de la vitesse de réaction ont été évaluées et analysées avec tous les dérivés du catéchol et déterminées inhiber l'hPrx5 d'une manière non-compétitive mixte partielle. Dans ce type de mécanisme d'inhibition, les dérivés du catéchol se lient et inhibent à la fois l'hPrx5 et le complexe hPrx5-H_2O_2, mais préfèrent l'hPrx5 seule. En outre, dans les conditions non compétitives, les dérivés du catéchol ne bloquent pas entièrement le cycle catalytique, dans lequel H_2O_2 est encore réduit en H_2O mais à des taux réduits.

Le mécanisme d'inhibition redox a aussi été examiné en identifiant s'il y avait des transformations chimiques des dérivés du catéchol pour former éventuellement des radicaux libres provoquant une inhibition. La réaction catalytique a été examinée par étapes en utilisant la RMN (1D ^{1}H et 2D ^{1}H-^{15}N-HSQC) en suivant les modifications chimiques que pourraient subir les dérivés du catéchol. Aucune transformation chimique des dérivés du catéchol n'a été observée. De plus, il n'y avait pas d'interaction non spécifique des dérivés du

catéchol aux différentes enzymes utilisées pour effectuer la réaction catalytique. Par conséquent, les dérivés du catéchol ont été montrés inhiber spécifiquement l'hPrx5.

Conclusion

Actuellement, il y a un intérêt à étudier les hPrxs et en trouvant des molécules qui pourraient être des potentiels inhibiteurs pour réguler la cascade de l'inflammation dans le cerveau après un AVC ischémique. Comme nous l'avons montré, les dérivés du catéchol se lient et inhibent l'activité peroxydase des hPrx1, hPrx2 et hPrx5. Tous les dérivés du catéchol avaient une affinité de liaison supérieure et une capacité d'inhibition plus grande contre l'hPrx5 que contre les hPrx1 et hPrx2. Le 4-*tert*-butylcatéchol a été montré être le plus affin et le plus puissant contre les hPrxs. En outre, les dérivés du catéchol ont été identifiés pour se lier spécifiquement et inhiber de manière réversible l'hPrx5 d'une manière non compétitive mixte partielle. Dans l'ensemble, les dérivés du catéchol sont des molécules qui pourraient potentiellement encore être optimisées pour devenir des candidat médicaments pour traiter l'inflammation dans le cerveau après un AVC ischémique.

SUBSTANTIAL RESUME

Introduction

Peroxiredoxins (Prxs) are proteins that reduce and detoxify a range of peroxides in the cells [6,7]. In humans there are six Prx isoforms located in various cellular compartments such as the cytosol, mitochondria, endoplasmic reticulum, peroxisomes [2,8]. The six Prxs can be classified by their catalytic function into three classes: typical 2-Cys (hPrx1-4), atypical 2-Cys (hPrx5) and 1-Cys (hPrx6) based on the number of cysteine residues involved in the redox reaction [9]. The catalytic reaction to reduce peroxides entails several steps with Prxs undergoing different conformational changes. Briefly, the cycle starts from the reduced state of Prx containing a catalytic cysteine maintained as a thiolate anion that attacks hydrogen peroxide (H_2O_2) substrate. After reaction, Prx becomes oxidized and undergoes a conformational transformation from a fully fold to locally unfolded state. As a result, the catalytic cysteine thiolate of Prx becomes oxidized in sulfenic acid (R-SOH) that form in the locally unfolded state a disulfide bond with the other cysteine involved in the reaction depending on the Prx subtypes. Typical 2-Cys Prx form intermolecular and atypical 2-Cys form intramolecular bonds whereas, 1-Cys Prx form disulfide bonds but to other proteins or molecules. Prx disulfide bond can then be reduced by thioredoxin, thioredoxin-like proteins or glutathione to complete the catalytic cycle with Prx reduced and in fully folded state again. Also, when Prx are oxidized there is the possibility to become overoxidized by reaction with an additional H_2O_2 molecule to become sulfinic acid (R-SO_2H) and can be possibly further oxidized to sulfonic acid (R-SO_3H) making Prxs catalytically inactive. However, overoxidized forms of Prxs can be occasionally regenerated by specific ATP-dependent other proteins (sulfiredoxin) to restore active forms and returned back to the catalytic cycle [1–5].

Additionally Prx can also, act as antioxidant proteins. Prx protect cells against oxidative damage to DNA, proteins and lipids, other macromolecules caused from the formation of free radicals such as reactive oxygen species (ROS) and reactive nitrogen species (RNS). Recently, oxidative stresses have been linked to the development of various diseases due to impaired cellular functions [7,10]. Prxs have been associated to cancers, Alzheimer's disease, impairing host immune systems. Interestingly, hPrxs (1,2,5 and 6) have also been linked to post-inflammation cascade after an ischemic stroke as hPrxs were discovered to trigger the activation of inflammatory cells assisting in the remodelling of damaged brain tissue [1,11,12]. Studying strokes is of importance since they are the second most common cause of death and disability globally resulting from a sudden loss of blood flow to the brain. The two main types of strokes are: ischemic and hemorrhagic strokes resulting from either a blockage or bursting of a blood vessel. Ischemic strokes are the primary type of

stroke[13–15]. At present, there are limited drugs for stroke patients that mainly focus on preventing the occurrence or reoccurrence of a stroke. Since identifying brain inflammation after a stroke leads to serious pathological effects, there is significance in developing therapeutic agents impeding the post-ischemic inflammation cascade as an alternative treatment method [14,16,17].

Recognizing hPrxs are key initiators in brain inflammation, this thesis focuses on understanding the effects of ligands binding and inhibiting hPrxs peroxidase activity, as one possible approach to regulate the brain post-inflammation cascade. In the past, our lab screened a library of ligands by NMR techniques (^{15}N-HQSC, Saturation Transfer Difference (STD), waterLOGSY) and discovered catechol derivatives could bind to hPrx5 [18]. First, in this manuscript, the binding affinity of the three-catechol derivatives (catechol, 4-methylcatechol, 4-*tert*-butylcatechol) to hPrx1 and 2 will be examined through NMR and computational modeling techniques. This will allow knowledge to know if there is selectivity amongst the catechol derivative to bind to other hPrx isoforms. Second, if the catechol derivatives can bind to the hPrxs, their inhibitory effects will be then evaluated via *in vitro* enzymatic assay in studying the inhibitors molecular mechanism of action (MMOA).

Presently, there have been several ligands identified to bind and inhibit Prxs. These ligands include adenanthin, H7, AMRI-59, triptolide and its derivatives celastrol and withaferin, conoidin A and antibodies against hPrxs [11,19–25]. Most of these ligands concentrated on possible treatments for cancers. Therefore, there is still a need to develop potential ligands for post-ischemic brain inflammation. Catechol derivatives could be advantageous inhibitors, since parent compounds (catechin and quercetin) have anti-inflammatory effects on resident brain cells macrophages. Additionally, Zheng *et al.,* found various catechol derivatives (catechol, 3-methylcatechol, 4-methylcatechol, and 4-*tert*-butylcatechol) to have anti-inflammatory and neuroprotective effects on other brain cells, microglial cells [26].

Results

As mentioned catechol, 4-methylcatechol and 4-*tert*-butylcatechol were previously identified to bind to hPrx5 within the active site where H_2O_2 binds. The binding interactions of these catechol derivatives to hPrx1 and hPrx2 were also examined. Using NMR (STD experiments) all three catechol derivatives were determined bind to hPrx1 and hPrx2. In ranking the catechol derivatives, 4-*tert*-butylcatechol always bound the best in contrast to the other catechol derivatives being the weakest. However, in comparing the binding affinity values (K_d) across hPrxs there were differences.

The catechol derivatives bound to hPrx5 with lower K_d values (greater affinity) than to hPrx1 and hPrx2.

Furthermore, to understand the binding interactions at the microscopic level computational modeling by funnel-metadynamics (FM) was completed to provide more details along with the NMR results. FM simulation allowed knowledge of the protein dynamics in solution through enhancing the sampling method of the binding and unbinding events using a funnel directed to a specific site on the protein. FM was able to determine the catechol derivatives could bind to hPrx1, hPrx2 and hPrx5 active site. The binding conformations determined for the catechol derivatives were similar to the X-ray crystal structures determined for hPrx5 [27]. Similar to the NMR results, 4-*tert*-butylcatechol bound the best out the three-catechol derivatives to the hPrxs. Also, the catechol derivatives bound to hPrx5 with a greater binding affinity than to the other hPrxs. These studies highlight the benefits of utilizing FM simulations to assist in early predictions of ligands binding to target proteins.

Determining the catechol derivatives could bind to hPrxs, their ability to inhibit hPrxs peroxidase activity was assessed through an *in vitro* enzyme assay. The inhibitory effects of the catechol derivatives were determined under a half maximal inhibition assay (IC_{50}). All the catechol derivatives were found to inhibit hPrx5 and ranking the IC_{50} values, 4-*tert*-butylcatechol was the most potent inhibitor followed by 4-methylcatechol and catechol. Altogether, the potency of the catechol derivatives was in agreement with preliminary inhibitory studies completed in our lab identifying 4-methylcatechol to be more potent than catechol to hPrx5 [18]. Also, in verifying the catechol derivatives bound to hPrx1 and hPrx2 in a reduced affinity, only the inhibitory effects of 4-*tert*- butylcatechol to these hPrxs were examined. 4-*tert*-butylcatechol was also found to inhibit hPrx1 and hPrx2 too. However, in comparing the inhibitory properties of 4-*tert*-butylcatechol to all of the hPrxs, 4-*tert*-butylcatechol was found to inhibit hPrx5 better than hPrx1 and hPrx2. Therefore, the binding affinity trends determined by NMR and computational modeling were similar to the inhibitory properties experimentally examined.

In confirming the catechol derivatives bound and inhibit hPrx5 the best for the hPrxs isoforms, the inhibition MMOA was studied. Knowledge of the MMOA would provide further insight how the catechol derivatives inhibit. The kinetic, conformational, and redox inhibition mechanisms were evaluated for each of the catechol derivative to hPrx5. The kinetic inhibition mechanism, allowed insight if the catechol derivatives bind to hPrx5 in a reversible or irreversible manner. The reaction rates of hPrx5 were measured in the absence and presence of incubating each catechol derivative to hPrx5. Comparing the reaction rates,

the catechol derivatives were found to not disrupt hPrx5 reaction rate. Therefore, this indicated the catechol derivatives bound to hPrx5 in a reversible manner.

In studying the conformational mechanism, it provided an understanding if the catechol derivatives inhibit in competitive, non-competitive or uncompetitive manner, also, if the catechol derivatives bind to the free enzyme (hPrx5) or enzyme-substrate complex (hPrx5-H_2O_2) causing inhibition. The conformational inhibition mechanism was measured by monitoring the reaction rate of hPrx5 at various set of inhibitor concentrations against a range of H_2O_2. Changes in the reaction rate were assessed and analyzed with all the catechol derivatives determined to inhibit hPrx5 in a partial mixed non-competitive manner. In this type of inhibition mechanism, the catechol derivatives were found to bind and inhibit both hPrx5 and hPrx5-H_2O_2 complex, but preferred hPrx5 alone. Also, under non-competitive conditions the catechol derivatives did not fully impair the catalytic cycle in which H_2O_2 was still reduced to H_2O but at decreased rates.

The redox inhibition mechanism was also examined identifying if there were chemical transformations of the catechol derivatives to possibly form free radicals causing inhibition. The catalytic reaction was examined step-wise using NMR (1D ^{1}H and 2D ^{1}H-^{15}N-HQSC) monitoring any chemical changes the catechol derivatives could have undergone. There were no chemical transformations of the catechol derivatives observed. Also, there were no non-specific interactions of the catechol derivative to the various enzymes used to carry out the catalytic reaction. Therefore, the catechol derivatives were found to specifically inhibit hPrx5.

Conclusion

Currently there is interest in studying hPrxs and determining potential molecules that may be inhibitors to regulate the inflammation cascade in the brain after an ischemic stroke. Shown here, the catechol derivatives were determined to bind and inhibit hPrx1, hPrx2 and hPrx5 peroxidase activity. All the catechol derivatives had a greater binding affinity and inhibitory potency against hPrx5 than hPrx1 and hPrx2. 4-*tert*-butylcatechol was found to have the greatest binding affinity and potency against the hPrxs. Also, the catechol derivatives were identified to specifically bind and inhibit hPrx5 reversibly through a partial mixed non-competitive manner. Overall, catechol derivatives are prospective molecules that could be further optimized to become drugs to treat post-inflammation in the brain after an ischemic stroke.

ACKNOWLEDGEMENTS

In completing my PhD I would first like to thank my supervisor, Jean-Marc Lancelin, for his guidance and support during my thesis. Also, his assistance when first settling in France and helping with the forever ending administrative paperwork. As well, I would like to thank my thesis reporters and committee members, Olivier Lequin, Sophie Clermont-Rahuel and Bastien Doumèche.

Additionally, I would like to thank my lab members (Florence Guillière, Laura Troussicot, Marie Martin and Corinne Sanglar) for their company and support over the past three years while in France studying. Also, the other people I've made connections with by either providing scientific support or help with experiments (Olivier Marcillat, Diane Cala).

Furthermore, I'd like to thank my family and friends for providing me constant encouragements during the ups and downs to achieve my PhD. It has sure been a journey for me learning a lot scientifically but also, personally to overcome the culture shock. In the end I survived and conquered living in France and received my PhD!

Table of Contents

Table of Figures

Table of Tables

ABBREVIATIONS

BMRB	Biological Magnetic Resonance Bank
C_p	Peroxidase cysteine
C_r	Resolving cysteine
CSP	Chemical shift perturbation
DTT	Dithiothreitol
FES	Free-energy surface
FM	Funnel-metadynamics
f_{STD}	STD amplification factors
GEM	Group epitope mapping
HMW	High molecular weight
hPrxs	Human peroxiredoxins
HSQC	Heteronuclear Single Quantum Coherence
IC_{50}	Half maximal inhibitory concentration
K_{av}	Partition coefficient
k_{cat}	Catalytic turnover number
k_{cat}/K_m	Enzyme efficiency
K_d	Dissociation constant
K_i	Inhibitory equilibrium dissociation constant between E + I and EI
K_i'	Inhibitory equilibrium dissociation constant between ES + I and ES-I
K_m	Michaelis-Menten constant
K_s	Equilibrium dissociation constant between E + S and ES
LMW	Low molecular weight
MMOA	Molecular mechanism of action
MW	Molecular weight
NADPH	Nicotinamide Adenine Dinucleotide Phosphate
Ni-NTA	Nickel-NitriloTriacetic Acid
NMR	Nuclear Magnetic Resonance
PMF	Potential mean force
SEC	Size exclusion chromatography
STD	Saturation Transfer Difference
TCEP	Tris(2-carboxyethyl)phosphine
V_{max}	Maximal velocity
yTrx1	Yeast thioredoxin 1
yTrxR	Yeast thioredoxin reductase 1
$\Delta G_b°$	Absolute binding free-energy

AMINO ACID CHART

A	Ala	Alanine
C	Cys	Cysteine
D	Asp	Aspartic acid
E	Glu	Glutamic acid
F	Phe	Phenylalanine
G	Gly	Glycine
H	His	Histidine
I	Ile	Isoleucine
K	Lys	Lysine
L	Leu	Leucine
M	Met	Methionine
N	Asn	Asparagine
P	Pro	Proline
Q	Gln	Glutamine
R	Arg	Arginine
S	Ser	Serine
T	Thr	Threonine
V	Val	Valine
W	Trp	Tryptophan
Y	Tyr	Tyrosine

1 Introduction

1.1 Peroxiredoxins and strokes

Peroxiredoxins (Prxs) are a family of proteins that reduce and detoxify hydrogen peroxide (H_2O_2), peroxynitrites ($ONOO^-$) and a range of hydroperoxides (ROOH). Also, Prxs are antioxidant enzymes that protect cells from oxidative stress against reactive oxygen species (ROS) and reactive nitrogen species (RNS) preventing the damage of DNA, lipids and other cellular proteins [6,7]. Prxs reduce more than 90% cellular peroxides at catalytic rate constant ~10^7 M^{-1} s^{-1}. Other oxidative stress defense enzymes beside Prxs include catalase (CAT), superoxide dismutase (SOD) and glutathione peroxidase (Gpx) [1,28]. Additionally, Prxs can function as chaperones, binding partners, enzyme activators and redox sensors too. These various functional states of Prxs are linked to different redox oligomeric states transitioning from reduced dimer, reduced oligomer, oxidized dimer, and hyperoxidized high molecular weight (HMW) assemblies [29].

Prxs are present in all biological kingdoms from bacteria to mammals. Humans have six Prxs (hPrxs) isoforms located in a variety of cellular compartments [8]. The six Prxs can be classified into three classes by their catalytic mechanism: typical 2-Cys (hPrx1-4), atypical 2-Cys (hPrx5) and 1-Cys (hPrx6) subfamilies. 2-Cys hPrxs contain a catalytic peroxidase cysteine (C_p) and a resolving cysteine (C_r) and the 1-Cys hPrxs only contains a C_p [9]. The catalytic cycle will be explained in more detail to follow (section 1.3.2 pg 11). hPrx1, hPrx2 and hPrx6 are mainly located in the cytosol, hPrx3 in the mitochondria, hPrx4 in the endoplasmic reticulum, and hPrx5 in the cytosol, mitochondria and peroxisomes [30]. hPrx1 and hPrx3 are the most commonly expressed proteins found in all tissues types [2].

Recently, hPrxs were discovered to be potent initiators released from the dead brain cell matter after an ischemic stroke triggering the pro-ischemic inflammation cascade [11–13]. Currently, our knowledge of the stroke process is limited due to being very complex and highly regulated. However, after a stroke research confirms that the main mechanism leading

to pathological effects are ischemic injury and inflammation [14,15,31]. There is now interest to develop alternative therapeutic agents to target and delay the inflammation cascade. Specifically, focusing on treatment against hPrx1, hPrx2, hPrx5 and hPrx6, involved to the activation of the destructive inflammation response [11,13].

The goal of my research is to identify ligands to bind and inhibit hPrxs peroxidase reaction. Since inhibiting hPrxs peroxidase activity could be an approach to regulate the inflammation cascade after an ischemic stroke. Recently, catechol derivatives have been distinguished to be ligands to bind to hPrx5 [18,27,32]. There is relevance to explore the binding affinities of these catechol derivatives to other hPrxs and determine if there are binding specificities to amongst the hPrxs family. Also, this research looks to determine if these ligands can inhibit hPrxs peroxidase activity to therefore, improve our knowledge and design drugs to be potential therapeutic agents for ischemic stroke patients.

1.2 Strokes

Strokes affect ~ 15 million people each year and is the second leading cause of death and long term disability worldwide impacting over 5 million people [33]. They are a global problem affecting all racial and/or ethnic groups [14]. There are two main types of strokes: ischemic and hemorrhagic. Ischemic strokes are the most common type of stroke resulting from the interruption of blood flow to major cerebral artery caused by blood clot (thrombosis) or blockage by foreign material in blood stream (embolism) or lack of blood delivery (hypoperfusion) leading to brain damage and permanent neurological impairments [13–15]. Whereas hemorrhagic strokes are due to the escape of blood from a ruptured blood vessel and are less common accounting for < 15% of stroke cases [13,14].

After a person experiences a stroke, it can lead to partial paralysis, difficulties with memory, thinking, speaking and physical activities [15]. Many of the ischemic stroke victims have medical and neurological complications post-stroke. Medical complications include

atherosclerotic (hardening arteries due to plaques) developing to either or both cerebrovascular and cardiovascular disease, swallowing difficulties, pneumonia, stress ulcers, thrombosis and pulmonary embolism, bladder dysfunction, bowel dysfunction, immobility issues causing body sores, and depression [34]. Various neurological complications can include brain oedema, haemorrhagic transformation, seizures and epilepsy, reoccurrences of a stroke, and delirium [35]. After a stroke, ~ 70% patients have compromised work capacity and 30% of require self-care assistance. As the population ages, the number of people affected by strokes will increase therefore, there is an urgency to improve our understanding on strokes and develop new treatments [14].

1.2.1 Treatments for strokes

There are currently limited drugs to treat ischemic stroke patients. Commonly used drugs are plasminogen activators (PAs) such as tissue-plasminogen activator (t-PA), urokinase, streptokinase, reteplase, tenecteplase and/or staphylokinase [14,16]. PAs degrade blood clots generally in the cerebrovascular artery and act by activating inactive plasminogen to become plasmin and then plasmin catalyzes the proteolysis of fibrinogen and fibrin (proteins involved in blood clots) [16,17]. The main issue with PAs is that they must be given to the patient within three hours of experiencing onset stroke symptoms and only < 10% patients are usually treated with PAs. After the three-hour mark, there is a risk in administering PAs can lead to hemorrhaging in the ischemic tissue.

Besides PAs, there are other medications for stroke patients but they are mainly for preventing a stroke occurrence or reoccurrence. These medications include anticoagulants (low-molecular weight heparin, warfarin), antihypertensive molecules (aspirin, clopidogrel, dipyridamole, ticlopidine, triflusal, GPIIa/IIIb inhibitors or lotrafiban), and lipid-lowering drugs (statin) [33]. Also, surgical approaches can be completed to open the clotted arteries or by

remove plaque formations by carotid endarterectomy, angioplasty and stenting, or bypass surgeries to prevent strokes [35].

At present, there has been little success in the development of neuroprotective agents purposed to block cellular, biochemical, and metabolic sequence of events in the inflammation cascade. Over 100 different neuroprotective agents have been tested but many have proven to be unfavourable in their efficacy [11]. As previously mentioned, the cascade of events after a stroke is very complex and is not well understood. Also, when focusing treatment on supressing the post-ischemic inflammation, there should be caution delaying or preventing inflammation. The inflammatory step can be advantageous too in aiding with brain tissue repair and regeneration and therefore, inhibiting the inflammation cascade could be a disadvantage in extending the brain injury duration. This is one factor to consider in developing new therapeutic agents against the activation of the inflammation cascade [14]. Overall, to advance knowledge and improve our current treatments against strokes, more research and drug discovery is required.

1.2.2 Inflammation cascade in strokes

After the loss of blood supply to the brain, the ischemic cascade occurs leading to a series of biochemical events resulting in the disintegration of cell membranes and neural cell death at the brain's injury site. This causes various deleterious effects such as excitoxicity, oxidative damage, blood brain barrier dysfunction and the initiation of post-ischemic inflammation. The post-ischemic inflammation process is highly coordinated and complex with the brain tissue promoting communication between the immune and nervous systems, the brains peripheral organs, and inflammatory cells to assist in remodelling the tissue injured [15].

There are several proteins released after a stroke such as nuclear protein high mobility group protein 1 (HMGB1), heat shock proteins, and β-amyloids involved in post-

inflammation cascade [13]. Most recently identified are hPrxs (hPrx1, hPrx2, hPrx5, and hPrx6) linked to promoting the post-ischemic inflammation effect (See Figure 1 pg 6)[11,13]. hPrxs are proposed to act as Danger-Associated Molecular Pattern molecules (DAMPs) signalling danger in the injured brain tissue. The DAMPs are released from dead cells and go onto bind and interact with Toll Like Receptors (TLRs) on macrophages/microglial cells (immune and resident cells in the brain) leading to activation of genes encoding for cytokines (mediators of immune systems), chemokines (class of cytokines), adhesion molecules, regulators of extracellular matrix to promote cellular recruitment, and activation leukocytes (immune cells) [7,13,15]. hPrxs were identified to interact specifically with TLR-2 and TLR-4 on macrophages and trigger the cytokines (Tumor necrosis factor-α (TNF-α), interleukins (IL; IL-1, IL-6, IL-17, IL-23)) causing inflammatory damage [11].

1.3 Peroxiredoxins

1.3.1 Structural characteristics

At the tertiary level, all the Prxs are highly conserved but with some variations with the loop lengths and conformations, and the N- and C-terminal extensions. The core structure consists of seven β-sheets and five α-helices. The structure is centered around five stranded antiparallel β-sheets (β5-β4-β3-β6-β7) surrounded in a 'sandwich' with one side covered by β1- β2- α1 and α-4, and the other side covered by α2, α3, and α5 (see Figure 2A pg 7) [36].

At the quaternary level, there are differences amongst Prxs. Prxs can form homodimers into two distinct conformational states. These homodimers are the building blocks to form other highly ordered oligomers such as octamers, decamers and dodecamers. The two dimer interfaces are defined by either: A-type or B-type (see Figure 2B & C) [36]. The A-type dimer interface is organized in a tip-to-toe manner with one monomer's α3 helix packed against the other monomer. The B-type dimer interface is organized with one subunit's β7 sheet packed against the edge of the other subunit's β-sheet forming a central 10-

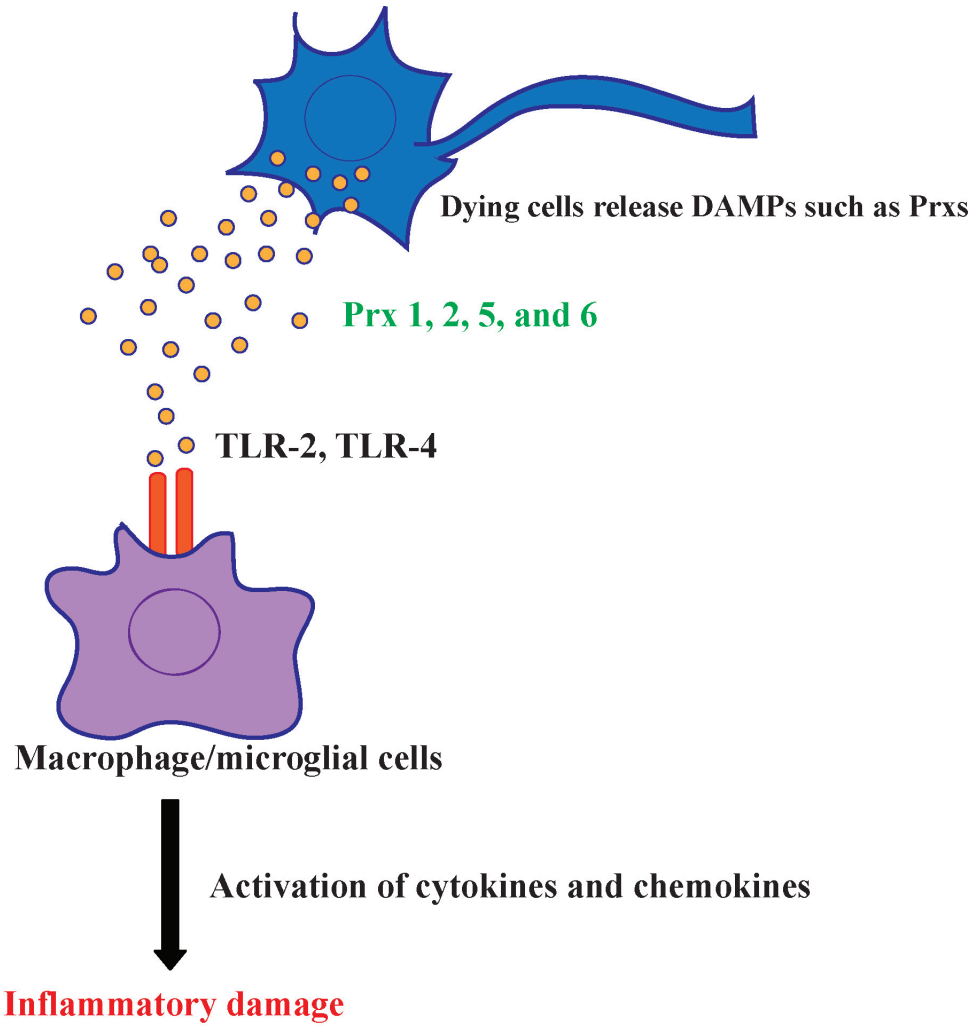

Figure 1: Post-ischemic inflammation cascade.

A scheme of the post-ischemic inflammation cascade with hPrxs released from dying brain cells. hPrxs were identified to act as Damage-Associated Molecular Pattern molecules (DAMPs) binding and interacting with Toll-Like Receptors (TLR-2, TLR-4) on macrophages and microglial cells, triggering the activation of cytokines and chemokines release overall causing inflammatory damage. This figure was reproduced under permission and adapted from Garcia-Bonilla and Iadecola, 2012 [13].

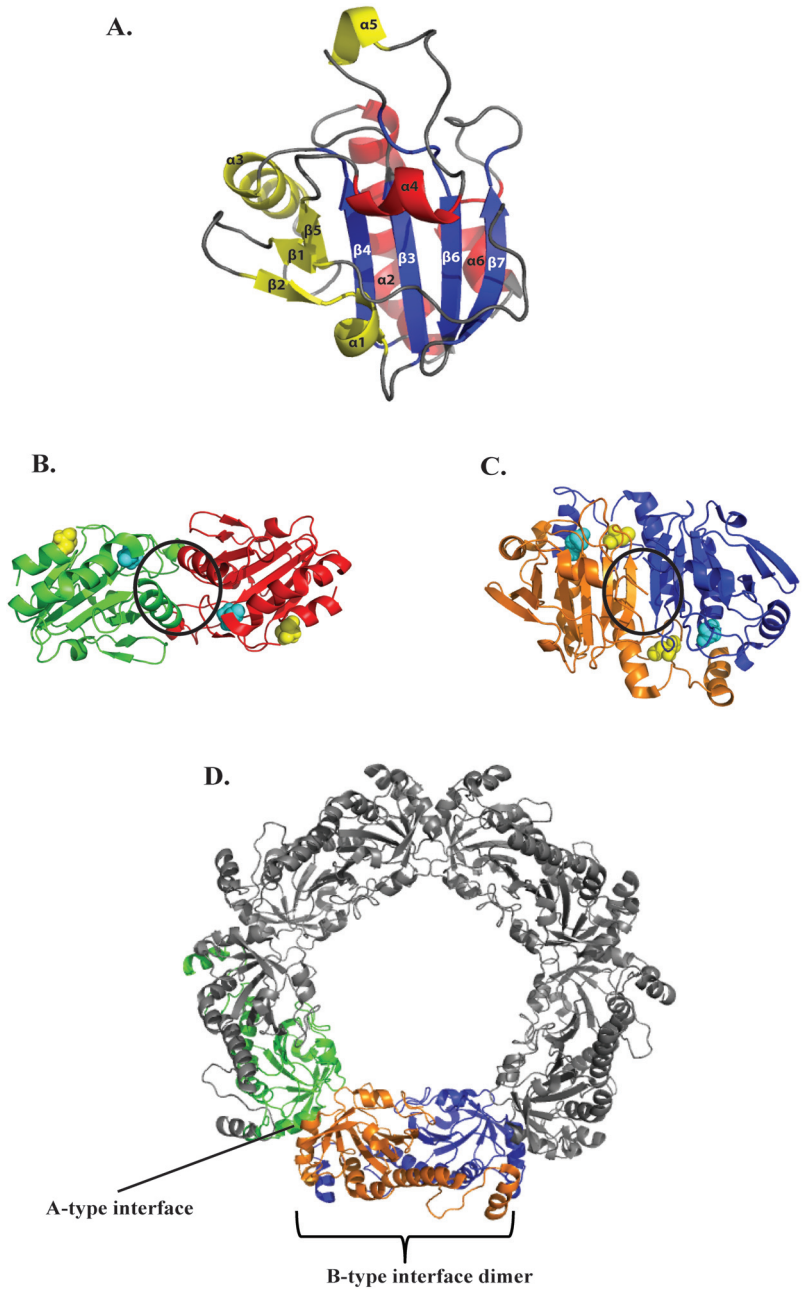

Figure 2: Prxs monomer, dimers and oligomers.

A. Monomer of hPrx5 with the α-helices and β-sheets labelled (PDB: 3MNG). **B.** The A-type dimer interface for hPrx5 (PDB: 3MNG). Circled are the interface contacts between the α-helices. Shown as spheres, are the peroxidatic cysteine (blue sphere) and resolving cysteine (yellow sphere) that form intramolecular disulfide bonds during the catalytic reaction. **C.** The B-type dimer interface for hPrx2 (PDB: 1QMV). Circled are the interface contacts between the β-sheets. Shown as spheres, are the peroxidatic cysteine (blue sphere) and resolving cysteine (yellow sphere) that form intermolecular disulfide bonds during the catalytic reaction. **D.** hPrx2 as a decamer highlighting the formation of five B-type dimers and the dimer-dimer interface are made up of the A-type interface. This figure was reproduced under permission and adapted from Knoops *et al.* 2011 and Flohe and Harris, 2007 [36,37].

stranded β-sheet between the two subunits. In a dimer B-type interface, the C-terminus end of one subunit (α-helix) that reaches over the dimer interface and interacts with the other subunit in which this feature is not present in the A-type dimer state [9]. hPrx1-4 and hPrx6 all form B-type interface dimers, whereas hPrx5 form A-type interface dimers [29,36].

Additionally, Prx1-4 can form highly ordered-oligomers building from the common B-type interface dimers with the addition of five or six dimers through A-type interfaces (see Figure 2D). The formation of highly ordered Prxs oligomers is dependent on several factors such as the redox state, ionic strength, protein concentration, pH and phosphorylation [9,29]. In contrast to Prx1-4, Prx5 and Prx6 are less commonly reported as highly ordered oligomers, since Prx5 slowly polymerizes but has been reported to be dimers, tetramers and hexamers. Prx6 has been observed as a dimer but their physiological function as a dimer is not well understood [29]. Comparing the two types of dimer interfaces, the B-type interface appears to be the more stable interface linked to Prxs catalytic activity transitioning from oxidized to reduced state. As the Prx decamers (seen for Prx1-4) were found to weaken and disassemble to basic B-type dimers interface, with the C-terminus one subunit (that contains C_p) acting like a molecular switch between the oligomeric state [29,38].

In addition to structural differences amongst Prxs, there are some similarities at the amino acid sequences and structural arrangement within the active site region. All Prxs contain an active site motif **P**XXX**T**XX**C$_p$** and the C_p is located in the loop-helix (α2) structure. During the peroxidase reaction, the loop-helix structure region moves and partially unwinds [2]. The C_p in the active site pocket is surrounded by a conserved H-bond network with three conserved amino acid residues: Pro43, Thr47 and Arg126 (amino acid numbering for Prx2; see Figure 3 & Figure 4). Pro43 limits solvent and hydrogen peroxide accessibility to the C_p. Also, Pro43 shields the reactive cysteine sulfenic acid (C_p-SOH) intermediated from further oxidation by hydrogen peroxide [9]. Thr47 is within H-bond distance from the Sγ of the C_p and is purposed to enhance the nucleophilicity of the C_p and maintain its side chain orientation properly assisting in hydrogen peroxide reactivity. Arg126 is assumed to assist in

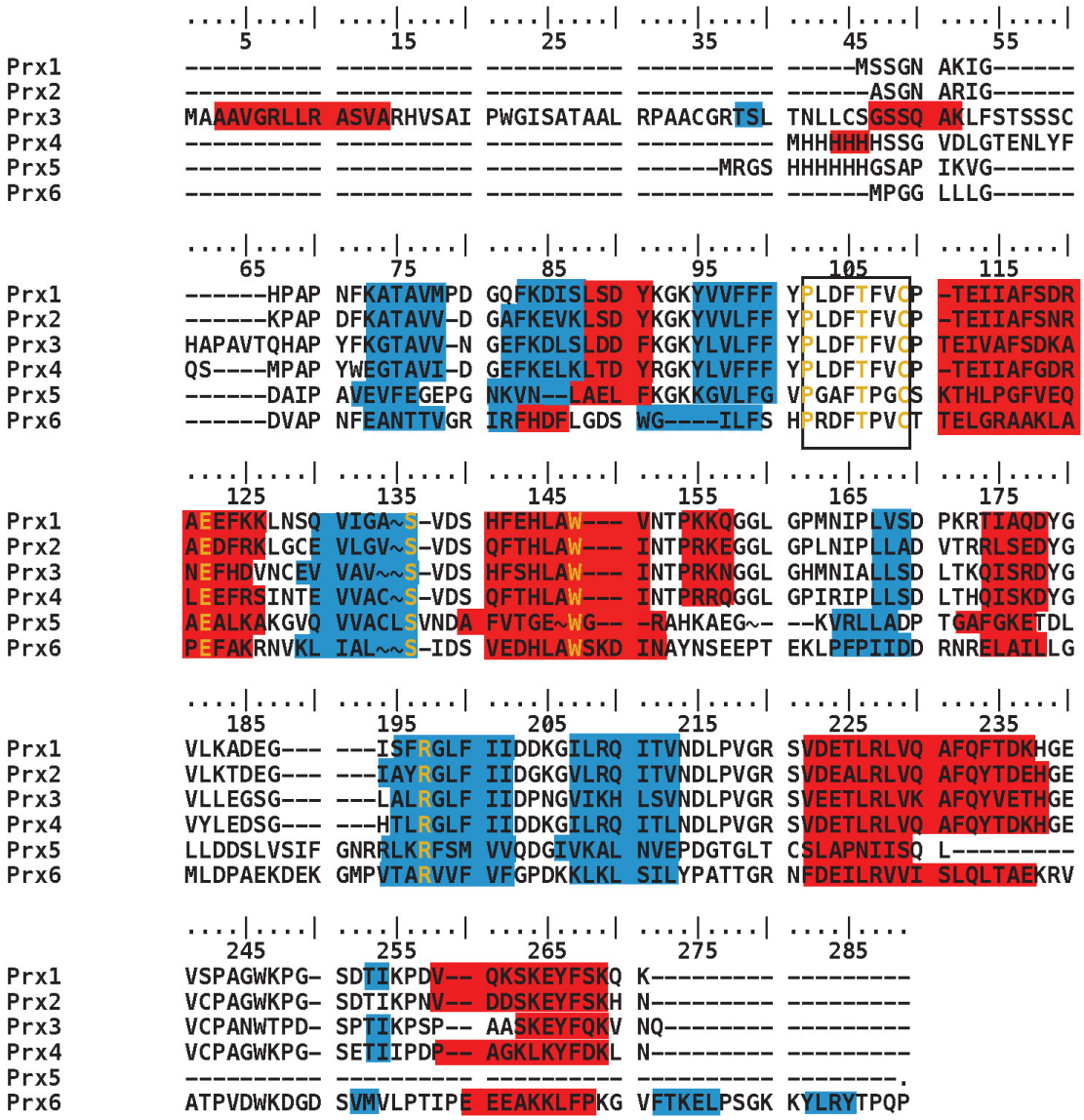

Figure 3: Conserved amino acid residues in hPrx1-6.

Shown here is the amino acid sequence alignment for hPrx1-6. Highlighted in blue are the β-sheets and in red are the α-helices. Also, emphasized are the conserved amino acid residues for hPrxs in yellow. Within the active site regions the amino acids include Pro43, Thr47, Cys50 and Arg126 (numbering in reference to hPrx2). Additionally, Glu62, Ser75 and Trp85 are also the other conserved amino acids involved in the H-bond network in the arrangement for the active site of hPrxs. The amino acid sequence alignment was completed by the PRALINE website and modified by BioEdit software.

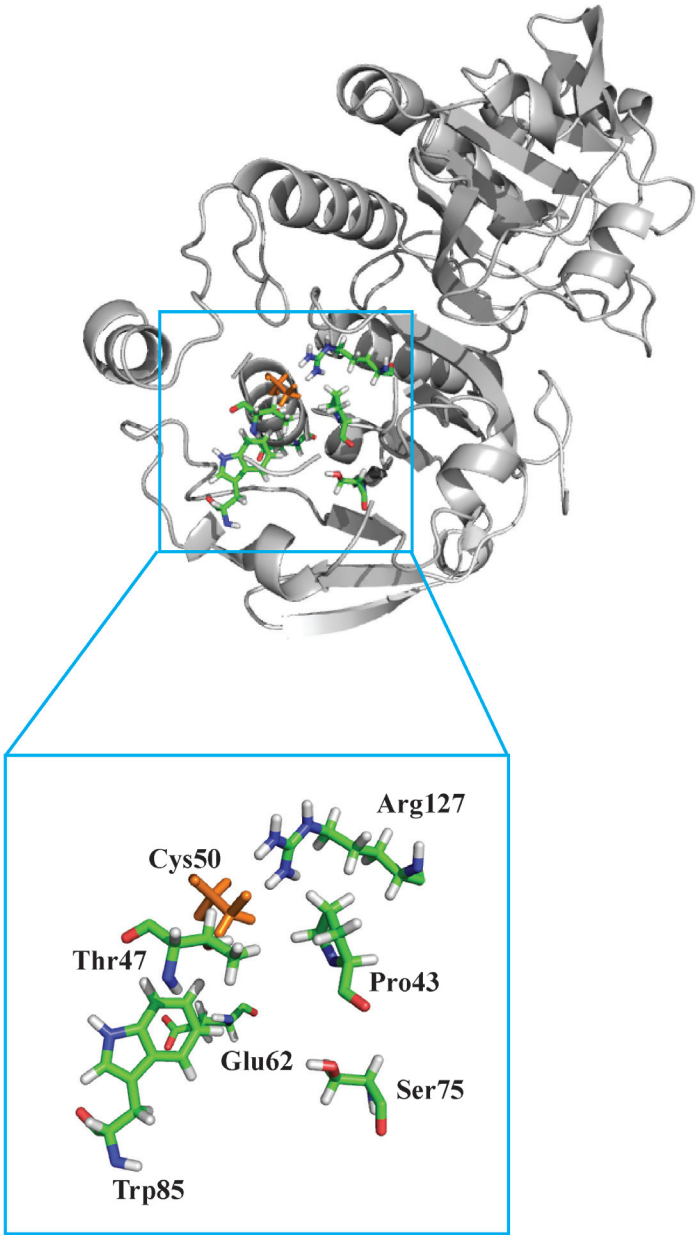

Figure 4: Conserved amino acid residues shown on hPrx2 protein structure.

Highlighted here are the conserved amino acids located around the peroxidatic cysteine (C_p; orange) for hPrx2 active site. The amino acids include Pro43, Thr47, Glu62, Ser75, Trp85 and Arg127.

lowering the pKa due to the electrostatic influenced by the positively charged guanidino group [9,36]. Also, sequence alignment of Prxs by subfamilies (six subfamilies AhpC/Prx1, Prx6, Prx5, BCP/PrxQ and AhpE) have also indicated three additional conserved amino acids: Glu62, Ser75 and Trp85 (amino acid numbering to hPrx2). Trp85 and Ser75 are located between the active site and the A-type interface that is involved in the H-bond network with the other conserved amino acids (Pro43, Thr47, Arg126). Also, Glu62 is able to interact and form H-bond to Arg126 in the active site too. These three additionally conserved amino acids are proposed to interact with Arg126 which is important and have an indirect role influencing the pK_a of the C_p too [39] (see Figure 3 & Figure 4).

1.3.2 Catalytic mechanism of Prxs

The main catalytic mechanism of Prxs consists of three chemical steps along with two conformational states but can include two additional steps. Figure 5 shows the differences observed for the three classes of Prxs. The three main chemical steps consist of peroxidation, resolution, and recycling. Whereas, Prxs can undergo additional steps that include hyperoxidation (or overoxidation) and resurrection depending on the cellular environment Prxs are exposed to. The two conformational states are either fully folded (FF) or locally unfolded (LU) (see Figure 6 & Figure 7).

The first step is peroxidation, with Prx in the FF states and its active site pocket being well defined with the C_p-thiolate (C_p-S^-) residue ready to bind and react with hydrogen peroxide. Peroxidation occurs when the C_p-thiolate attacks and reacts with hydrogen peroxide. As a result, the C_p-thiolate residue becomes oxidized to C_p-SOH (sulfenic acid) and a water molecule is produced. The active site of Prx now transitions to its LU state. In this state, the active site pocket becomes a loosely defined conformation and there is a rearrangement of the amino acids in the active site with the C_p-loop moving and the α2 helix becoming partially unwound (see Figure 7) [1,2,40]. The second step is resolution, as C_p-SOH

then becomes attacked by another thiol forming a disulfide bond and another water molecule is released. The disulfide bond is formed by the C_p-C_r making either intermolecular (typical 2-Cys) or intramolecular (atypical 2-Cys) disulfide bonds. Whereas for the 1-Cys class, it forms a disulfide bond through another protein or small molecule [2]. The third step is recycling, with the disulfide bond being reduced to C_p-SH by thioredoxin, thioredoxin like protein, or glutathione and the FF conformational state is restored [1,2,10] (see Figure 6 & Figure 7).

Also, Prx can undergo a hyperoxidation step (step 4), in which the C_p-SOH is attacked and reacts with a second and/or third hydrogen peroxide forming C_p-SO_2^- (sulfinic acid) and/or C_p-SO_3^- (sulfonate). At this point the catalytic cycle is inactivated, but can be reactivated through a resurrection step (step 5) with sulfiredoxin (Srx). Srx along with ATP, Mg^{2+}, and a thiol as an electron donor are required to carry out the catalysis the conversions of inactive Prx to C_p-SOH (sulfenic acid) state [1–3]. Hyperoxidation has previously been determined to occur in hPrx1-4 and hPrx6 but not hPrx5 [4,41]. It is purposed Prxs are more prone to hyperoxidation, which linked to structural characteristics containing the YF and GGLG motifs (no present in hPrx5). These motifs are thought to hinder or slow down the ability of the C_r to react with the C_p. This short kinetic pause leaves the C_p-SOH intermediate prone to being attacked by another hydrogen peroxide molecule [41].

1.4 Other roles of Prxs

In addition to peroxidase and antioxidant properties, Prxs have also been identified to have a role in regulating cellular level of hydrogen peroxide assisting in cell signalling pathways through non-stress and stress related manners. The exact details on how Prxs influence or trigger these effects linked to cell signalling is still not clear [1,42,43]. An example of a non-stress related cell signalling role of Prxs, was observed by Woo *et al*. when Prx1 became phosphorylated at Tyr194 by Src kinase through the simulation of a growth factors or

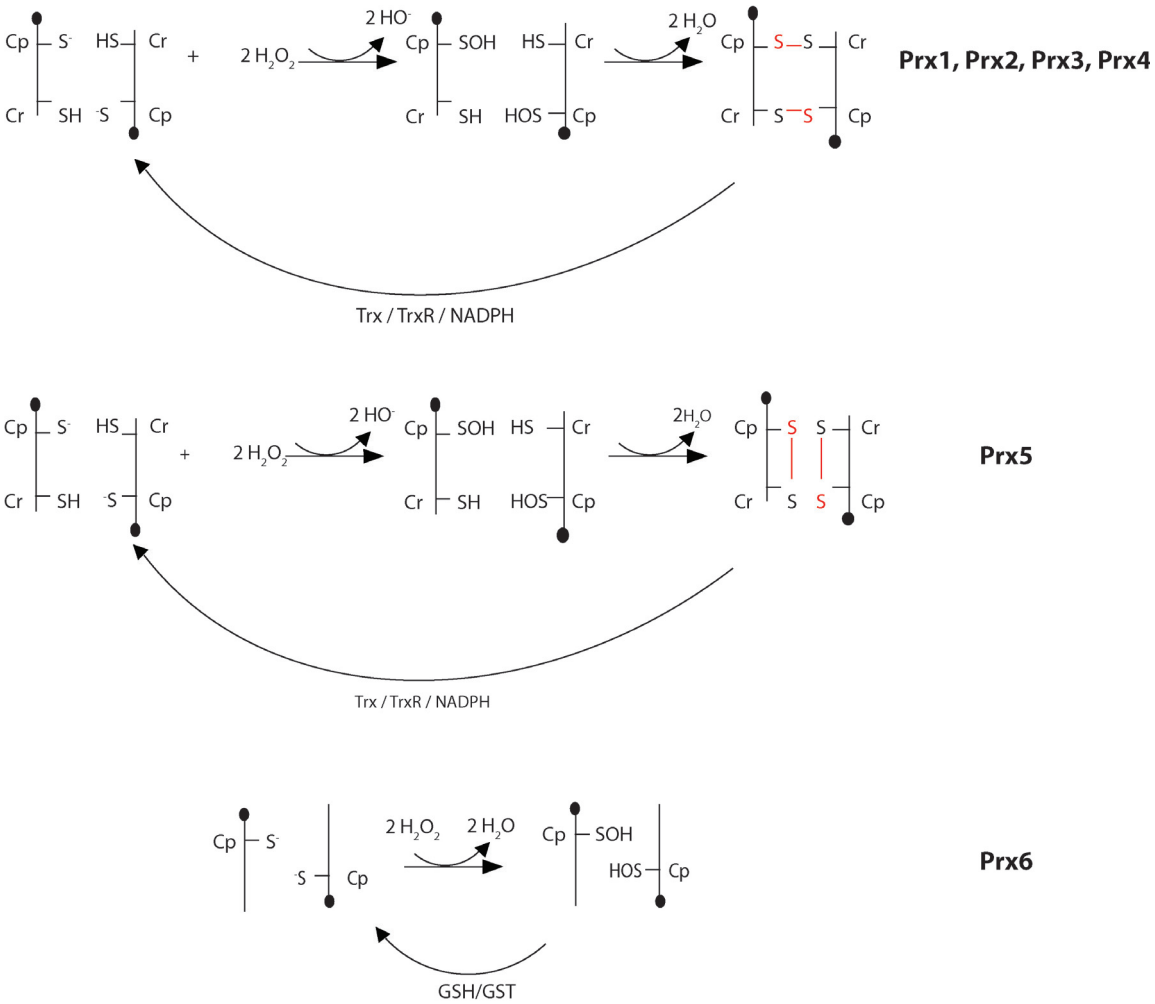

Figure 5: Catalytic mechanism for three Prxs classes.

Shown here are the differences in the catalytic mechanisms between the typical 2-Cys (Prx1-4), atypical 2-Cys (Prx5) and 1-Cys Prxs. First, Prxs are in the reduced state (C_p-SH and C_r-SH) and then attack hydrogen peroxide (H_2O_2) with the release of a water molecule (H_2O). Second, in an intermediate state the Prxs peroxidatic cysteine (C_p) are oxidized to C_p-SOH, leading to a rearrangement of Prx active site and the C_p-C_r disulfide bonds are formed. Typical 2-Cys Prxs form intermolecular disulfide bonds and the atypical 2-Cys Prxs form intramolecular disulfide bonds. For 1-Cys, the C_p forms a disulfide bond to another protein or small molecule. Third, Prxs are in the oxidized state and are regenerated being reduced by thioredoxin system (thioredoxin (Trx), thioredoxin reductase (TrxR), NADPH) or glutathione system (glutathione (GSH), glutathione transferase (GST)). This figure was reproduced under permission and adapted Rhee *et al.* 2012 and Flohe and Harris 2007 [30,36].

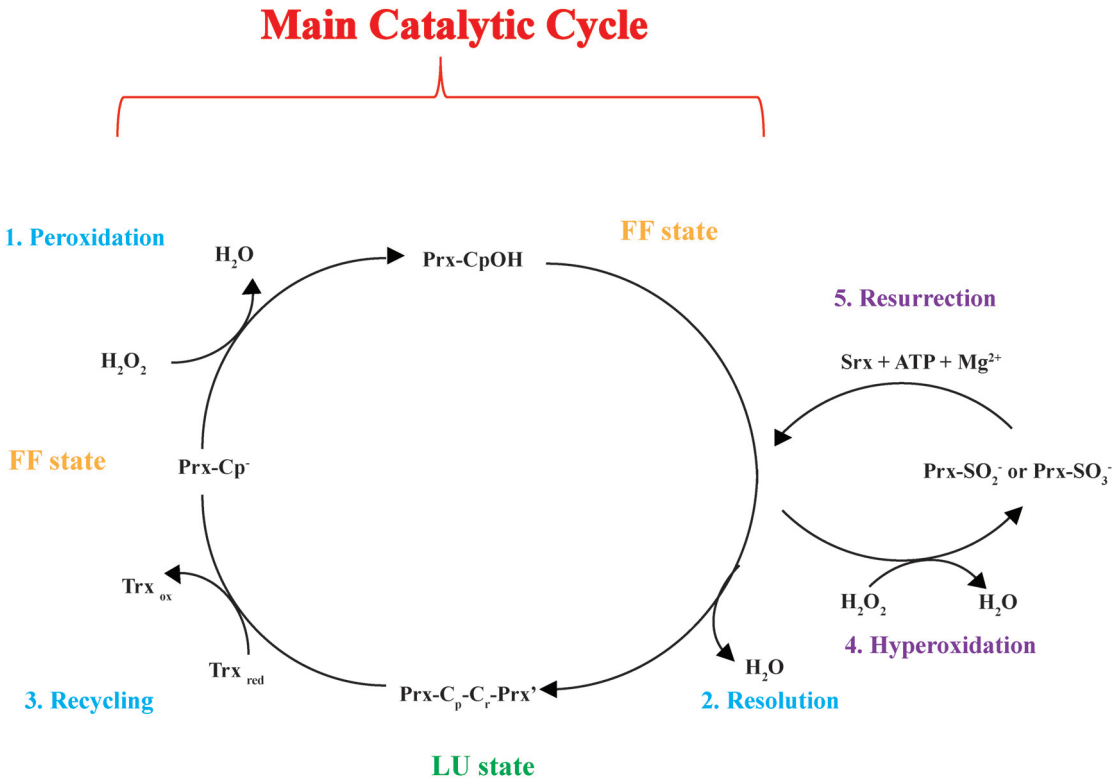

Figure 6: Five catalytic steps and two conformational states of Prxs catalysis.

Shown here are the catalytic steps and conformational states Prx undergo reducing peroxides. The steps in blue are the three main steps Prx go through (peroxidation, resolution, and recycling). In this cycle, Prx starts in the reduced state (Prx-C_p^-) in the fully folded state (FF state) and transition to locally unfolded state (LU) when becoming oxidized. After peroxidation step, Prx can be further oxidized to Prx-SO_2^- or Prx-SO_3^- becoming hyperoxidized and inactive. However, Prx can become reactivated by the enzyme sulfiredoxin (Srx) and become resurrected to continue on in the peroxidase catalytic cycle. This figure was reproduced under permission and adapted from Perkins *et al*. 2014[6].

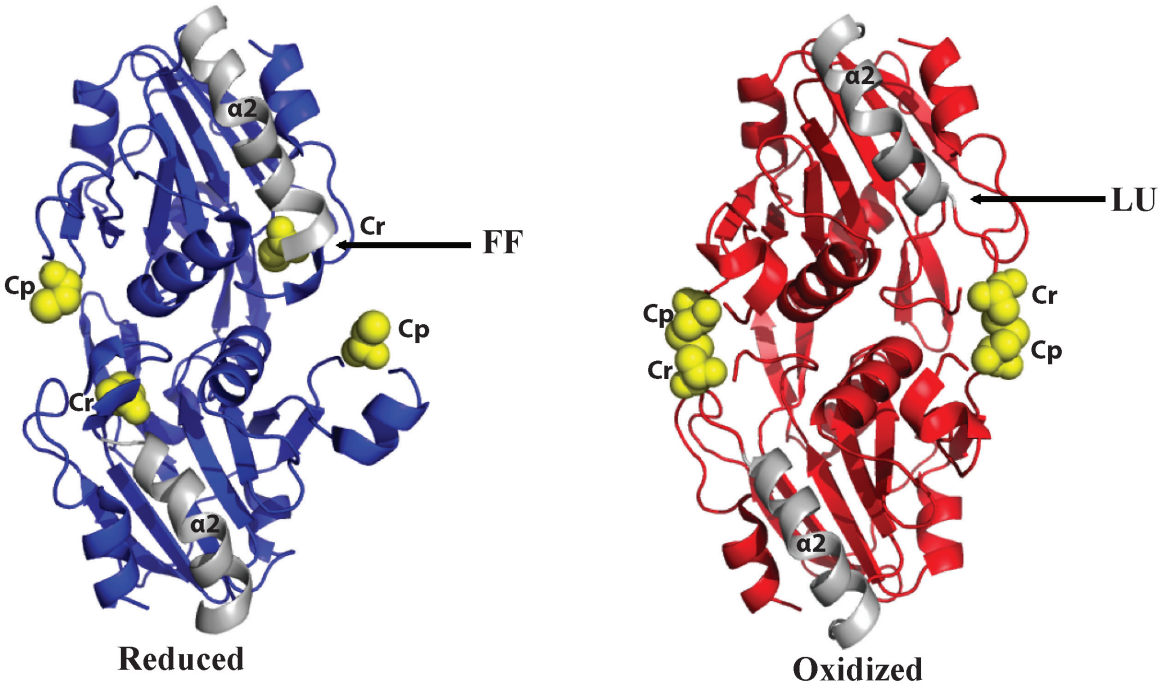

Figure 7: Yeast peroxiredoxin Ahp1 oxidized and reduced states highlighting the conformational changes.

Shown here is yeast peroxiredoxin Ahp1 highlighting the changes from the reduced (red) and oxidized (blue) states. During the peroxidase reaction, reduced Prx attacks a hydrogen peroxide molecule and reduces it to water. The catalytic reaction results in the loop-helix (α2) to partially unwind transitioning from the fully folded (FF) to locally unfolded (LU) state and the catalytic active site undergoes rearrangement. The catalytic cysteine (Cp) and resolving (Cr) cysteine shown in yellow forms a disulfide bond and Prx becomes oxidized. Afterwards, oxidized Prx can be reduced by the thioredoxin system completing the catalytic cycle (See section 1.3.2 and Figure 6). This figure was reproduced under permission and adapted from Lian *et al.* 2012 [40]. (**PDB**: 4DSQ and 3DSR).

immune receptors. As a result, phosphorylated Prx1 became inactive and therefore lead to the accumulation of hydrogen peroxide near receptor complexes. This triggered the inactivation of protein tyrosine phosphatase (PTP), a regulatory component in cell signalling transduction pathway [42].

An example of stress related role of Prxs was observed by studying yeast Prx (cPrxI) in identifying Prxs becoming chaperone proteins through heat shock and oxidative stress (hyperoxidation). As a chaperone, Prx was found to prevent oxygen radical-mediated denaturation and aggregation of α-synuclein (abundant brain protein) and therefore, protect the yeast cells against oxidative stress. Aggregates of α-synuclein are found in Lewy bodies in brains of patients with Parkinson's and Alzheimer's diseases [44].

1.5 Drug discovery

1.5.1 Approaches to drug discovery

Identifying drugs have mainly focused on targeting proteins linked to diseases causing pathogenesis [45,46]. The process of identifying and developing a drug is very lengthy which involve many steps that are well regulated to achieve a drug available to the market. The various steps include: target identification (step 1), target validation (step 2), lead identification (step 3), lead optimization (step 4), preclinical (step 5), and clinical trails (step 6) (See Figure 8) [47].

Recognizing the target protein(s) the compound/ligand interact with can be evaluated through two main approaches; either target based and phenotypic based screening. The traditional method for drug discovery has been phenotypic-screening that involves screening potential drugs in the physiological environments in either cells or whole organism to provide a direct view of the side effects and desired response that are under unbiased conditions [48]. This approach allows identification of multiple proteins or pathways not previously known. Although there are some drawbacks such as in identifying the molecular targets of the active drug hits requires 'target deconvolution'. Therefore, this entails characterizing the molecular

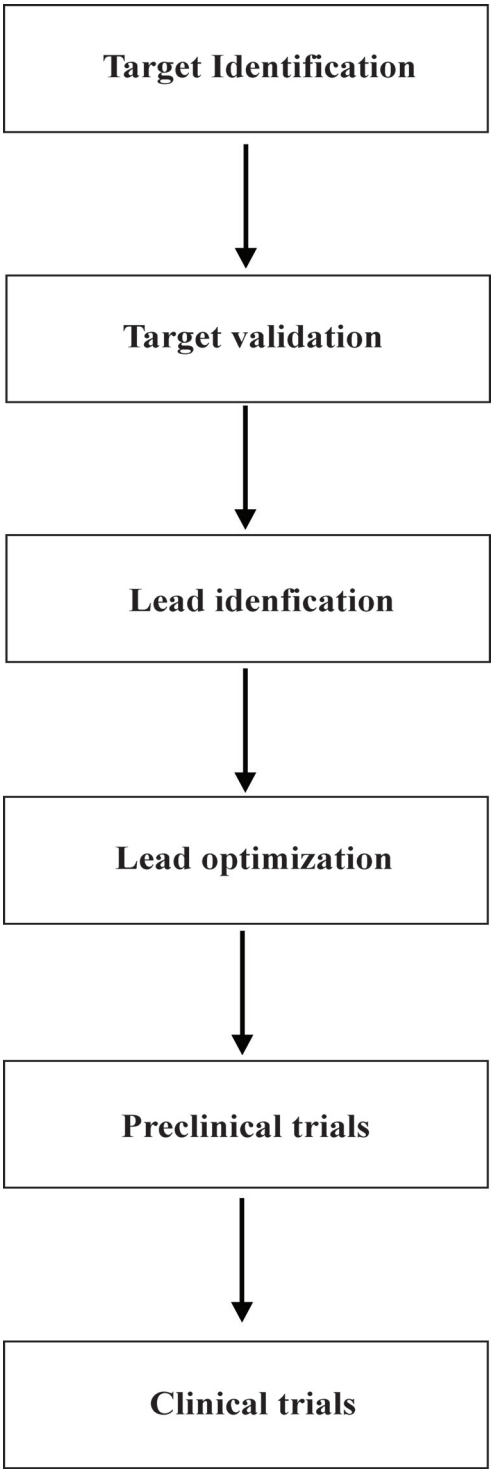

Figure 8: Flow chart of the drug discovery process.

In determining a ligand as a potential inhibitor to become a therapeutic drug entails a long process, from identifying the target up until the clinical trials. Each step of the process requires rigour testing and observing understanding effects of the ligands identified as inhibitors.

mechanism of action (MMOA) of lead drugs identified from the phenotypic screening to result in optimization of the drugs. This is a main issue with the phenotypic approach leading to a lower throughput of lead drugs found [46]. However, there have been advancements with phenotypic screening approaches pinpointing the molecular targets with proteomics and genomic-based approaches. For example there have been improvements with high-throughput imaging platforms and computational analysis to aid to finding the relevant pathways and proteins due to phenotypic changes observed [48].

Whereas with target based drug-screening approach, it involves a large number of compounds being screened against a single target protein and the active hits are further optimized through medicinal chemistry efforts [48]. This approach applies molecular and chemical knowledge to investigate specific molecular hypothesis. The three hypotheses are: the methods used in preclinical screenings to select a drug candidate will translate to effective clinical meaning at the patient level, the target selected is important to human disease, and the MMOA of the drug candidates at the target are capable to achieve the desired response [46]. There are some limitations to this approach since sometimes the specific molecular hypotheses may not be always relevant to the disease pathogenesis and provide sufficient therapeutic evidence. Currently there is interest in the target-based approach because it uses molecular tools of genetics, chemistry and biological information to drive drug discovery and this approach allows the ability to monitor the drug discovery progress [46]. This thesis focuses in particular exploring target-based approach to assess the development of catechol derivatives as potential lead drugs to be a therapeutic agent in post-inflammation brain effects after an ischemic stroke.

1.5.2 Target-based drug discovery approach

The drug discovery process involves many different areas of science including chemical and structural biology, computational chemistry, synthetic organic chemistry and

pharmacology [47]. To identify hit ligands as potential drugs, different methods such as high-throughput screening (HTS), and/or fragment based lead discovery (FBLD) can be used[49,50]. HTS involves screening millions of relatively complex drug sized compounds with the goal of identifying the most potent hits. The compounds tested through HTS range in molecular weight (MW) between 250-600 Da and have potency from low μM to high nM. The rate of identifying a hit is often low. Many of the hits fail to become potential drugs since the MW of the hit compound must be further adapted and the potency must be retained or increased which is an issue to achieve.

Whereas FBDL, small fragments with a low MW (LMW) between 120-250 Da with <1000 fragments are screened with a high sensitivity in detecting hits. The hits identified have low potency from low mM to μM. More hits are more frequently recognized than HTS, since fragments have more options in molecular designs, which can be increased exponentially as the MW decreases. Also, the identified hit fragments that become leads fragment, the potency has to be increased and this can be acquired by increasing the MW [50]. Distinguishing hit fragments is achieved through various techniques such as X-ray crystallography, nuclear magnetic resonance (NMR), isothermal titration calorimetry (ITC), surface plasmon resonance (SPR), nano-electrospray mass spectroscopy (MS), thermal shift (TS), optical waveguide grating (OWG), biophysical methods and bioassay techniques [51]. Specifically focused in this thesis are the NMR techniques to assist in early drug screening stages.

1.6 Drug screening by NMR techniques

NMR is a highly sensitive technique to screen and identify hit fragments or ligands. This method is able to detect and quantify binding interactions of the ligand without any prior understanding of the protein function. Also, NMR can provide information about both the ligand and/or protein to assist in optimizing the weak binding hits into high affinity leads [52].

Here, the basic NMR techniques will be focused on drug discovery screening but there are more complex and combinational NMR techniques that can furthermore be used to provide other details to assist in detecting hit ligands accurately.

1.6.1 NMR protein-based drug screening studies

The most common method for protein-based NMR technique is 2D ^{1}H-^{15}N or ^{1}H-^{13}C heteronuclear single quantum correlation (HSQC) with ^{15}N and/or ^{13}C isotope labelled proteins. Using 2D HSQC, the spectra are recorded with the labelled protein in the absence and presence of a ligand. When the ligand is present and binds to a protein, there will be alterations in the mean chemical environment around the binding site of the protein. These changes are then detected by a change in the isotropic NMR chemical shift so called chemical shift perturbation (CSP) of the observed nuclei [52,53]. From the 2D spectra, the CSPs are monitored by following the shifts in amino acid residues or by a decrease in amino acid signal intensities. Additionally, if the amino acid residues are assigned to the different observed NMR signals and if a 3D structure is known, the binding site and/or an induced conformational change on the protein can be potentially mapped. 2D NMR is advantageous to X-ray crystallography because the protein-ligand is in solution at equilibrium for its binding interaction. Also, obtaining stable and well-established crystals of a protein and protein-ligand is very resource intensive and time consuming. The electron density map only provides knowledge of one binding conformation in contrast, NMR allows an understanding of weighted average of the various binding conformations [51]. As well, 2D HSQC experiments can be conducted as a titration by following the chemical shifts as a function of the ligand concentration and dissociation constant values (K_d's) can be extracted for the protein-ligand complex [53]. Furthermore, there are limitations with 2D HSQC experiments since they require relatively high amounts of protein (~ 0.1 mM) isotope labelled, and is restricted to small to medium size proteins (~ 40 kDa) since the MW influences the nuclear-spin relaxation [51]. As

small proteins have a slower transverse relaxation rates (T_2) than large proteins that slowly reorienting themselves and have rapid transverse relaxation rates. As a result, large proteins have NMR signal line broadening with poor sensitivity and resolution detection [49,52]. Therefore, from set backs due to protein size, labelling, and concentration, this can be overcome by examining the binding conformation of the protein-ligand through ligand-based NMR techniques as an alternative approach.

1.6.2 NMR Ligand-based drug screening studies

Ligand-based NMR techniques commonly used in drug screening are saturation transfer difference (STD) and/or water ligand observation by gradient spectroscopy (waterLOGSY). For these NMR experiments, the protein does not need to be isotope labelled, and low concentration (i.e. 5 μM) can be used to detect weak binding interactions of ligand(s) [52,53]. Both techniques use 1D ^{1}H spectra for the detection of the ligand binding to the protein but there are differences in how the detection is observed. WaterLOGSY experiments detects the transfer of magnetization from the bulk water to the protein's binding site and onto the bound ligand [52]. Whereas, STD experiments detects the transfer of magnetization from the protein to the bound ligand. Both waterLOGSY and STD NMR spectroscopy have been used in the past in our lab and in this thesis to assist ligand screening to hPrx5, which will be explained shortly (see section 1.10 Current drug discovery screening against Prxs). Specifically, in this thesis STD NMR spectroscopy will be used for drug screening.

In STD NMR spectroscopy, the interaction of the ligand to the protein is monitored in the presence of low protein concentrations (10^{-7} to 10^{-8} M) and in a large molar excess (1:10 to 1:1000) of the test ligand(s). Also, in contrast to HQSC NMR experiments the protein size is not a constrain since the MW of the protein can be > 15 kDa [54]. In STD, two 1D ^{1}H spectra

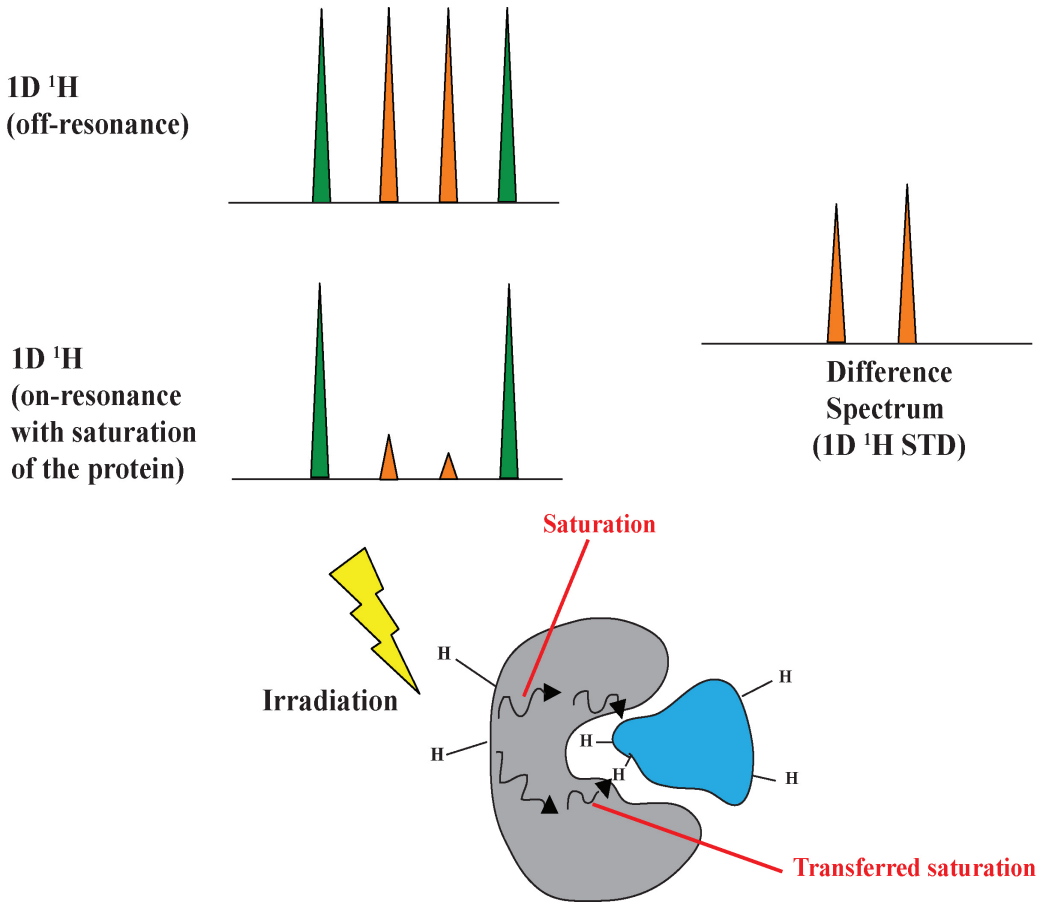

Figure 9: Schematic of the 1D ^{1}H-^{1}H STD NMR experiment.

First a 1D ^{1}H spectrum is recorded detecting the protons of a ligand (top left; off-resonance). Then after a 1D ^{1}H spectrum is recorded, with the target protein being irradiated for a saturation time (bottom left; on-resonance). If a ligand is bound to the target protein, the irradiation magnetization is transferred to the ligand (difference spectrum;1D ^{1}H STD spectrum). Shown here, four protons were originally detected for the ligand but after the irradiation of the protein, only two of the protons were detected to be in contact. The difference between the two spectra indicates the protons involved in the binding interaction (right). This figure is reproduced under permission and adapted from Angulo and Nieto, 2011[54].

are recorded without (^{1}H) and with irradiation of the proteins resonance (^{1}H STD) (See Figure 9). In the ^{1}H STD spectrum, the protein is irradiated in a region generally ~ -1 to 2 ppm that represents the methyl groups of the proteins and not the ligand [49]. If the ligand is bound to the protein, when the protein is irradiated, the magnetization will be transferred to the ligand, which will be detected in the ^{1}H STD spectrum [52]. The difference of the two spectra can identify the specific protons of the ligand involved in the binding interaction. Also, the protons of the ligand interacting with the protein can be interpreted through group epitope mapping (GEM). STD experiments can be conducted as a titration by monitoring the proton signal intensities between the two spectra referred as the STD amplification factor (f_{STD}), as a function of ligand concentration and a dissociation constant (K_d) can be obtained for the protein-ligand complex [55].

1.7 Computational modeling aiding in drug design and discovery

Drug discovery and development takes on average between 10 to 15 years and is a costly process ranging from $800 million to $ 1.8 billion (USD) spent [47]. Many of the drugs developed are not successful with only ~ 3% of the new drugs making it to the market [56]. To assist in the early stages of drug screening, computational tools have become integrated in the process in hopes to improve the drug development pathway and reduce costs [47]. Various computation tools are available from high throughput virtual screening, docking and hit development based on structure-activity relationships. Many of these methods rely on very simplified assumptions and limitations when screening ligands and identifying hits against target proteins [57]. There have been developments in more advances computational tools such as molecular dynamic (MD) simulations to assess ligand binding to target proteins.

MD simulations can combine Newtonian physics and the entire flexible atoms representative on a protein, in the presence of water and other molecules present showcasing the dynamic interactions between all of them. In which, both qualitative information such as

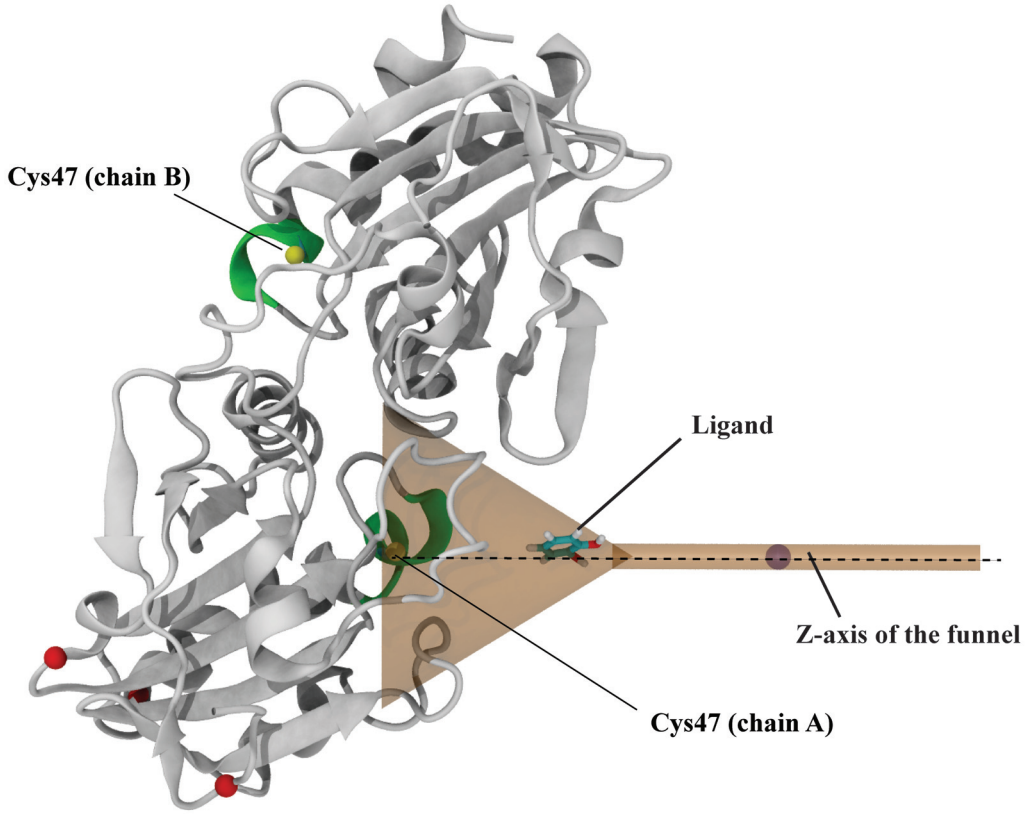

Figure 10: External funnel restraint potential applied to hPrx5 active site with a ligand present.

Shown here is the funnel applied to hPrx5 active site (signified by Cys47 residue) used to enhance the binding and unbinding sampling of a ligand. The free-energy surface (FES) of the ligand binding to hPrx5 is obtained by computing a reweighted algorithm as a function of the projection on the z-axis (the funnel) and from the ligands center of mass distance to the z-axis (see Figure 15 and this will be further explained in section 1.10.1 pg 35). The FES provides information of the binding conformation of the protein-ligand interaction. This figure is from Troussicot *et al.* 2015 [32].

where and how the ligands bind to a protein and quantitative information about the binding affinities and kinetics of the interaction can be obtained [57,58]. Advancements in computer hardware technology such as the graphic processing unit (GPU) and parallel computing, has allowed MD simulations to process a large amount of data more quickly and observe microsecond simulations within a few days [57].

At present, there have been improvements on MD simulations with a new method funnel-metadynamics (FM). FM simulations allow enhanced sampling of the protein-ligand binding events in solution. As a funnel shaped restraint potential is applied to the system which enables monitoring a specific region on the target protein to be explored amplifying the sampling of the binding and unbinding states (see Figure 10 which is an example used for hPrx5[32]). FM simulations are possible when there is known structural information (i.e. NMR) of the ligands local binding site to the target protein. This technique allows accurate estimation of binding free-energy surface (FES) interaction between the target protein and ligand of interest, whereas MD simulations only provide qualitative estimations of the FES. FM has been applied to studying ligand binding to a target protein with some success in examining benzamidine binding to trypsin, and potential inhibitor SC-558 binding to cyclo-oxygenase 2 (COX-2). These FM simulations produced comparable results to other computer screening techniques [59]. Therefore, FM is another computer tool is assist in drug discovery screening process. FM simulations have been utilized in the past in our lab (see section 1.10 pg 35) and will be covered briefly in this thesis to assist in drug discovery screening to hPrxs.

1.8 Optimization of lead ligands to become potential inhibitors

Upon identifying lead ligands (step 3) that bind to a validated target protein, the next step in drug discovery process is lead optimization phase (step 4) that focuses on target potency and selectivity (Figure 8 pg 17). This thesis specifically centers around this step in the drug discovery process. Lead optimization involves of designing and synthesizing

structural analogues of lead ligands. The goal of this step is to understand structural properties of the protein-ligand binding affinity through the development of structure-activity relationships (SAR) and also, entails carrying out *in vitro* enzyme assay screening to assist in optimization [45]. The enzymatic screenings are designed to identify ligands that are inhibitors and subsequently the molecular mechanism of action (MMOA) can be further investigated. Additionally, at this step cell-based assays can be completed to assess the biochemical activities of the ligands identified as potential inhibitors too. The *in vivo* screening provides information on the inhibitors solubility, membrane permeability, protein binding, selectivity, metabolism and toxicity properties important for hit ligands to become drugs [60].

1.8.1 Screening lead ligands through *in* vitro enzymatic assay

This thesis specifically concentrates on screening fragments (ligands) in an *in* vitro enzyme assay. Inspecting the ligands effects at the enzymatic level, involves carefully setting up the assay properly to measure potential inhibitory affects. Enzymatic assays comprise of monitoring and detecting the enzyme-catalysis reaction with a chemical transformation occurring [61]. Detecting the enzyme catalysis reaction can be done through various methods with absorbance and/or fluorescence spectroscopy being the most common methods but also radioisotope measurements can be used. Either of these methods can involve labelling or non-labelling the substrate or protein [61,62].

Monitoring the enzymatic activity is based on measuring the initial velocity of the reaction in the absence and presence of the potential inhibitors. Measuring the enzymatic activity can be completed by three approaches: continuous, discontinuous, and endpoint assays. Continuous enzymatic assay is the most often utilized in either measuring the product formation or substrate depletion over the reaction time course detecting the reaction signal via absorbance or fluorescence spectroscopy [45]. Whereas, discontinuous enzymatic assays involve stopping or quenching the reaction prior to obtaining a detection signal. This is usually

completed over several time points. Endpoint enzymatic assays is a type of discontinuous assay with only one time point used to monitor the initial velocity of the enzymatic reaction [45].

1.8.2 Identifying ligands as inhibitors via IC_{50} assay

Upon setting up the ideal enzymatic reaction conditions to monitor and detect the target protein, the ligands are screened through a half maximal inhibition concentration (IC_{50}) assay. The IC_{50} assay is conducted with the target enzyme (protein) at the substrate concentration required to reach the reactions half maximal velocity (V_{max}) known as the K_m or Michaelis-Menten constant [45,60,63]. The target proteins enzymatic activity is assessed through a titration with increasing ligand concentrations. In testing ligands and their analogs or library of ligands, IC_{50} values can be determined and the ligands are ranked to compare their inhibitory potency (assuming the same experimental conditions are maintained) [45]. In completing the IC_{50} assay, it provides insight if the ligands are inhibitors and the structural characteristics required to target the protein of interest. From this knowledge, ligands identified as inhibitors can be built upon if the ligand(s) are fragments to increase the MW as previously mentioned and the ligand(s) potency can be increased to become more drug like. Also, to contribute to a greater understanding of the lead ligands identified as inhibitors the molecular mechanism of action (MMOA) can be examined to aid in drug development [46,60].

1.9 Inhibitors molecular mechanism of action (MMOA)

The inhibitors MMOA allows characterization of how the inhibitor interacts and binds to inhibit the target enzyme causing a desired response [46,60]. The MMOA consists of different aspects including kinetic, conformational and redox mechanisms as shown in Figure 11. Each of these mechanisms requires further analysis to provide insight into the binding preferences and how the catalytic reaction is implicated.

To evaluate an inhibitor's MMOA, it is generally performed under classical steady-state conditions. Steady-state refers to when the concentration of the *ES* complex is balanced with the rate of formation of the *ES* complex equalling the rate of decomposition of the *ES* complex and is shown by the following equations 1-3 [45,63]:

$$E + S \underset{k_{-1}}{\overset{k_1}{\rightleftharpoons}} ES \xrightarrow{k_2} E + P \qquad \text{(Equation 1)}$$

$$K_m = \frac{k_{-1} + k_2}{k_1} \qquad \text{(Equation 2)}$$

$$v = \frac{V_{max}\,[S]}{K_m + [S]} \qquad \text{(Equation 3)}$$

Steady-state is influenced by all three rate constants: k_{-1}, k_2 (also known as the catalytic rate, k_{cat}) and k_1 (equation 1). The rate constant variables can be simplified and represented by the K_m or the Michaelis-Menten constant, which is a measure of the relative apparent affinity in establishing the *ES* complex when half of the maximal velocity (V_{max}) is obtained under saturating conditions (equation 2). When the concentration of the *ES* complex is maintained at a constant therefore, the reaction rate (or velocity, *v*) is constant and can be expressed as shown in equation 3 [45,63]. As a result, the reaction should be generally measured within the initial phase of the reaction (less than 10% completion). Plotting the product or substrate concentration (when $S \cong S_o$) as a function of time, a linear plot is obtained and the initial slope value can be extrapolated and converted into a rate value. After the initial phase of the reaction, the concentration of the substrate diminishes and the rate slowly decreases with the reaction reaching an equilibrium phase.

In enzyme kinetic, K_s or equilibrium dissociation constant is defined when the first step ($E+S \rightleftharpoons ES$) reaches equilibrium before the product is formed (in agreement to the rapid equilibrium hypothesis). Therefore, the equilibrium phase occurs shortly after the initial phase at the beginning of the reaction. As a result, K_s includes the enzyme and could be defined as $K_s = [E][S]/[ES]$ or same as K_m when $k_{cat} = 0$. The equilibrium phase is represented by the k_1 and k_{-1} shown in the following equation:

$$K_s = \frac{k_{-1}}{k_1} \qquad \text{(Equation 4)}$$

When an inhibitor inhibits an enzyme, this leads to changes in the steady-state kinetic conditions, affecting the catalysis in maintaining the formation and decomposition of the *ES* complex [45,63]. The MMOA is examined through measuring changes of the enzyme catalysis in the V_{max} and K_m of the substrate over a range of inhibitor concentrations (specifically used in the conformational mechanism discrimination) [45,60,63]. Traditionally MMOA studies are tedious, time consuming, requiring laborious efforts and only a few molecules can be studied at once. However, there have been advances with automation such as plate readers and enhanced data processing improving this area of research [60].

1.9.1 Kinetic mechanism of inhibition

The kinetic mechanism mainly focuses on the binding kinetics and residence time of the inhibitor interacting with the target protein. This mechanism is influenced depending on if the inhibitor binds causing an affect under equilibrium or non-equilibrium conditions. In equilibrium conditions, the inhibitor binds to the protein with a fast binding rate on (k_{on} or k_1) and a slow off rate (k_{off} or k_{-1}) in a reversible manner, in which the kinetic mechanism is under competition between the substrate and ligand for the target protein.

In contrast in non-equilibrium conditions, this can lead to a slow reversible binding or irreversible mechanism. The inhibitor binds to the protein with slow binding rates (k_{on} and k_{off}) without the reacting reaching the equilibrium state. Under these conditions, there is less competition between substrate and ligand for the target protein [46]. Inhibitors that act in an irreversible manner are due to the formation of covalent bonds between the inhibitor and protein. To understand the kinetic mechanism of an inhibitor, the binding reversibility can be examined and determine if the inhibit binds reversible, slow reversible or irreversible [45].

1.9.2 Conformational mechanism of inhibition

Additionally, knowledge of the conformational mechanism of an inhibitor is vital in gaining insight on the MMOA. The conformation mechanism focuses on the binding of the inhibitor to the protein, which can involve the inhibitor binding the free enzyme (*E*), enzyme-substrate complex (*ES*) or possibly the enzyme-substrate-inhibitor complex (*ESI*) [46,60,63]. The binding conformations are based on three classic and basic mechanisms: competitive, non-competitive and/or uncompetitive manner. Following Figure 12 and Table 1 show the following mechanisms and the effects on the K_m and V_{max} values.

In the competitive inhibition mechanism, the inhibitor binds to the free enzyme preventing the substrate from binding and therefore the substrate and inhibitor are mutually exclusive (Figure 12 A). In the classic non-competitive inhibition mechanism, the inhibitor has no effect on the substrate binding and vice versa (Figure 12B). The inhibitor and substrate bind reversibly, randomly, and independently to different sites on the target enzyme. The inhibitor can bind to either the *E* or *ES* complex. In classic non-competitive mechanism, the inhibitory dissociation constants K_i (represent the *EI* complex) and the K_i' (represents the *ESI* complex) are equal. However, with non-competitive inhibition mechanism there can be partial types depending on the binding preference of the inhibitor to the *E* or *ES* complex. When $K_i' > K_i$, the inhibitor would rather bind to the *E* instead of the *ES* complex and vice versa when $K_i' < K_i$ (See Table 1). In the uncompetitive inhibition mechanism, the inhibitor binds reversibly to the *ES* forming *ESI* complex but not the free *E* alone (Figure 12C) [45,60,62,63].

Besides the three main types of inhibition, there can be other inhibitory events such as partial (as briefly mentioned), allosteric, tight-binding and time-dependent inhibition [46,60]. As stated, an inhibitor can partially inhibit depending on the binding affinity to the *ES* or *E* for non-competitive mechanism. There can also be partial competitive inhibition, with the inhibitor partially binding to the enzyme at different site forming *ES*, *EI*, and *ESI* complexes too. Or even the inhibitor binding partially to two sites on the enzyme. These are very

complex partial inhibition mechanisms that can occur [63]. Whereas for allosteric inhibition, it involves the inhibitor decreasing the activity of the enzyme by binding to an allosteric site other than or in addition to the active site. As a result, the binding of the inhibitor leads to a conformational change to the enzyme structure that effects the formation of the *ES* complex. Tight-binding inhibition is when the population of the free inhibitor is reduced through the formation of the *EI* or *ESI* complex and generally the inhibitor binds with the apparent affinity (K_i) is near the concentration of the enzyme present in the enzyme. Time-dependent inhibition occurs when the inhibitor binds slowly to the enzyme on the time scale of the enzymatic turnover in the catalytic reaction. Therefore, to observe this type of inhibition it is not initially apparent until incubating the inhibitor with the enzyme or monitoring the resident time of the inhibitor (k_{off}) [46,60].

1.9.3 Redox mechanism of inhibition

The reduction-oxidation (redox) mechanism focuses on the electron transfer between the inhibitor and enzyme. Some inhibitors, when interacting with the target enzyme under specific experimental conditions can lead to the inhibitor to become oxidized and become a free radical. As a result, the free radical form of the inhibitor can act on the protein causing inhibition. An example of a redox MMOA is with the drug verteporfin administered to reduce vision loss as verteporfin is thought to form hydroxyl radicals that contribute to its inhibitory effect to damaging cells [46].

Overall, to understand the MMOA of an inhibitor against a target protein requires various levels of knowledge in deciphering the binding interaction and inhibition preferences to cause a desired response. Each aspect from the kinetic, conformational and redox mechanisms is a complex focus entailing laborious efforts. Many of the lead ligands identified to be inhibitors are optimized thoroughly prior to understanding the MMOA and

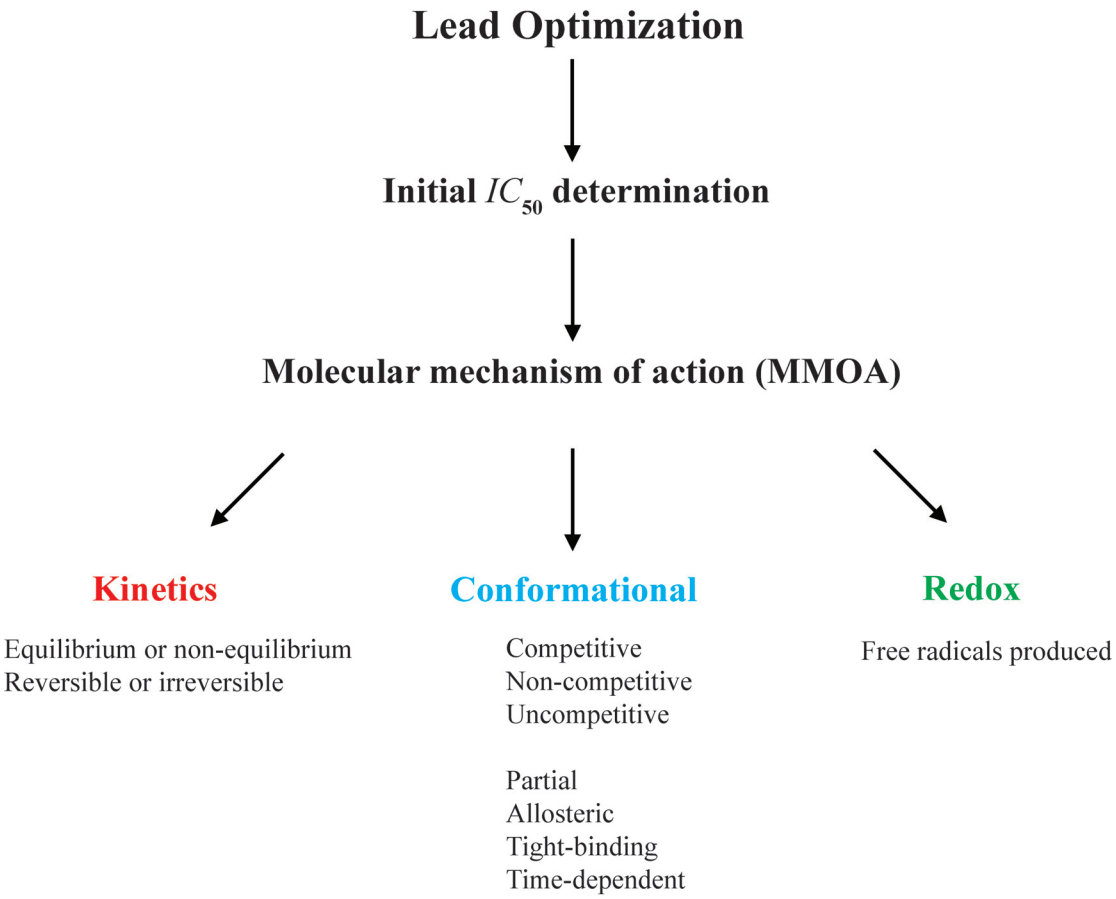

Figure 11: Flow chart for lead optimization steps.

Upon determining lead ligands, they are further optimized in examining their inhibitory properties in carrying out an IC_{50} assay and identifying the ligands as inhibitors. Additionally, the molecular mechanism of action can be explored examining kinetic, conformational and redox mechanism to aid in optimizing lead inhibitors. This figure was reproduced under permission and adapted from Copeland, 2005 [45].

Table 1:The effects on K_m and V_{max} values for the various conformational mechanisms and the equations to solve the mechanisms.

Measuring the MMOA under classic steady-state conditions, changes in the K_m and V_{max} values are evaluated to determine the inhibition mechanism. The three basic inhibition mechanisms include: competitive, non-competitive and uncompetitive. The table was reproduced under permission and was adapted from Copeland, 2005 [45].

	Competitive	Non-competitive			Uncompetitive
		$K_i' > K_i$	$K_i' = K_i$	$K_i' < K_i$	
K_m	• Increases with increasing [I]	• Increases with increasing [I]	• No effect	• Decreases with increasing [I]	• Decreases with increasing [I]
V_{max}	✓ Not effected	✓ Decreases with increasing [I]	✓ Decreases with increasing [I]	✓ Decreases with increasing [I]	✓ Decreases with increasing [I]
	$v = \frac{V_{max}[S]}{[S] + K_m\left(1 + \frac{[I]}{K_i}\right)}$	$v = \frac{\frac{V_{max}}{\left(1 + \frac{[I]}{K_i'}\right)}[S]}{[S] + K_m\left(\frac{\left(1 + \frac{[I]}{K_i}\right)}{\left(1 + \frac{[I]}{K_i'}\right)}\right)}$			$v = \frac{\frac{V_{max}}{\left(1 + \frac{[I]}{K_i'}\right)}[S]}{[S] + \frac{K_m}{\left(1 + \frac{[I]}{K_i'}\right)}}$

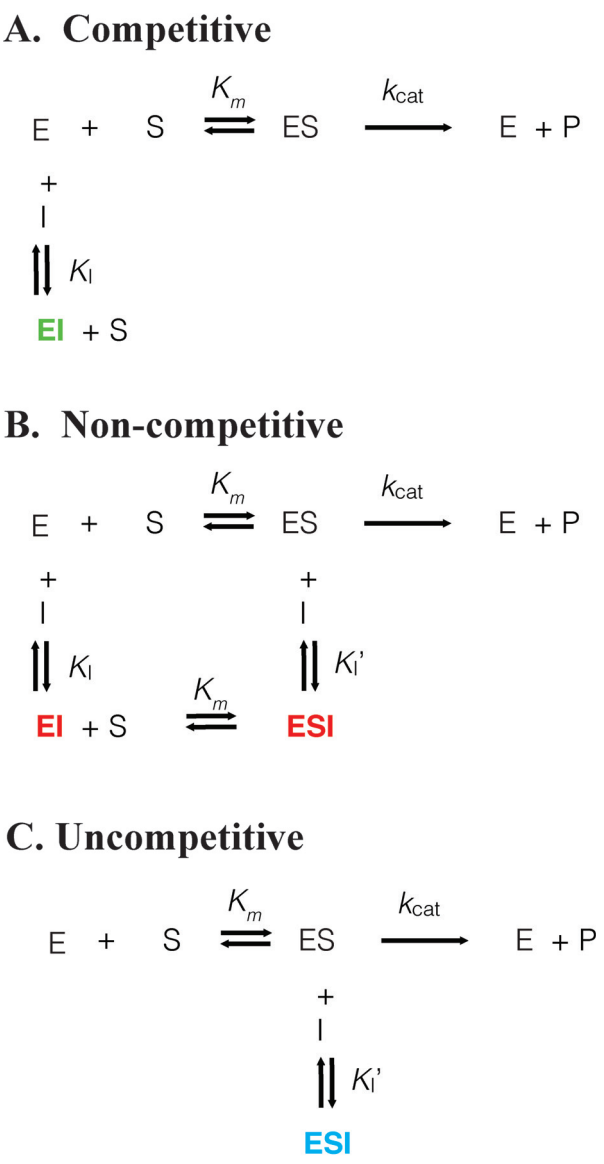

Figure 12: Schemes for the three basic inhibition mechanisms.

Competitive. The inhibitor (*I*) binds to the free enzyme (*E*) forming the *EI* complex and prevents the substrate (*S*) from binding and any product (P) from being produced. A competitive inhibitor only acts on the apparent K_m and the V_{max} is not affected. When the K_i value is reduced, the degree of inhibition is greater at any given [I] and [*S*]. **B. Non-competitive.** The inhibitor binds to both the free enzyme and the *ES* complex. The product production is not completely impaired. This depends on the specific type of non-competitive inhibition mechanism, with respect to the preference in the inhibitor binding to the *E* or *ES* complex. In the classic non-competitive mechanism, the K_m is not affected but the V_{max} decreases (*I* binds equally to both *E* and *ES* complex). The degree of inhibition depends on the [*I*], K_i, K_i' values. **C. Uncompetitive.** The inhibitor only binds to the *ES* complex. The substrate must bind to the enzyme first for the inhibitor to cause an effect therefore; it does affect the production of a product. Both the K_m and V_{max} decrease. The degree of inhibition depends on the [*S*], in which the inhibition increases with the [*S*] increasing [45,63].

biochemical properties at *in vitro* and *in vivo* levels in hopes to be developed as drugs and continue on in the drug discovery process [46,60,64].

1.10 Current drug discovery screening against Prxs

As previously mentioned, the interest of this thesis is to identify lead ligands against hPrxs to aid in regulating the post-ischemic brain inflammation cascade and specifically, understanding in-depth how the ligands bind and inhibit hPrxs. At present, there have been developments of various types of inhibitors to inhibit Prxs and will be next discussed.

1.10.1 Catechol derivatives

Recent studies have taken an interest in using catechol and its derivatives as potential inhibitors against hPrxs. Catechol and its derivatives are found in a variety of products and Figure 13 shows the chemical structure of some catechol derivatives. Humans are commonly exposed to catechols in a range of forms such as metabolites from the degradation of benzene or oestrogen hormones. Also, the simple catechol skeleton is found in endogenous compounds such as neurotransmitters and their precursors (adrenaline, noradrenaline, dopamine, L-DOPA)[65] (see Figure 14A). Catechol derivatives are metabolites from the digestion of polyphenols found in fruits and vegetables and polyphenol compounds (caffeic acid, tea catechin, quercetin) (see Figure 14B) [26,65]. These properties presented for the catechol derivatives are enticing that further development of these ligands could become prospective drugs to treat the post-inflammation cascade after an ischemic stroke.

Previously in our lab, Barelier *et al.* have utilized both STD and waterLOGSY to screen over 200 fragments from a library against hPrx5 [18]. Both NMR techniques were sensitive in identify six fragments to bind to hPrx5. STD NMR was further applied to determined the binding affinities (K_d) of these six fragments ranging from 1-3 mM and one of the simple fragments determined to bind to hPrx5 was catechol [18]. In identifying a simple fragment like catechol could bind, other derivatives were explored to identify improved

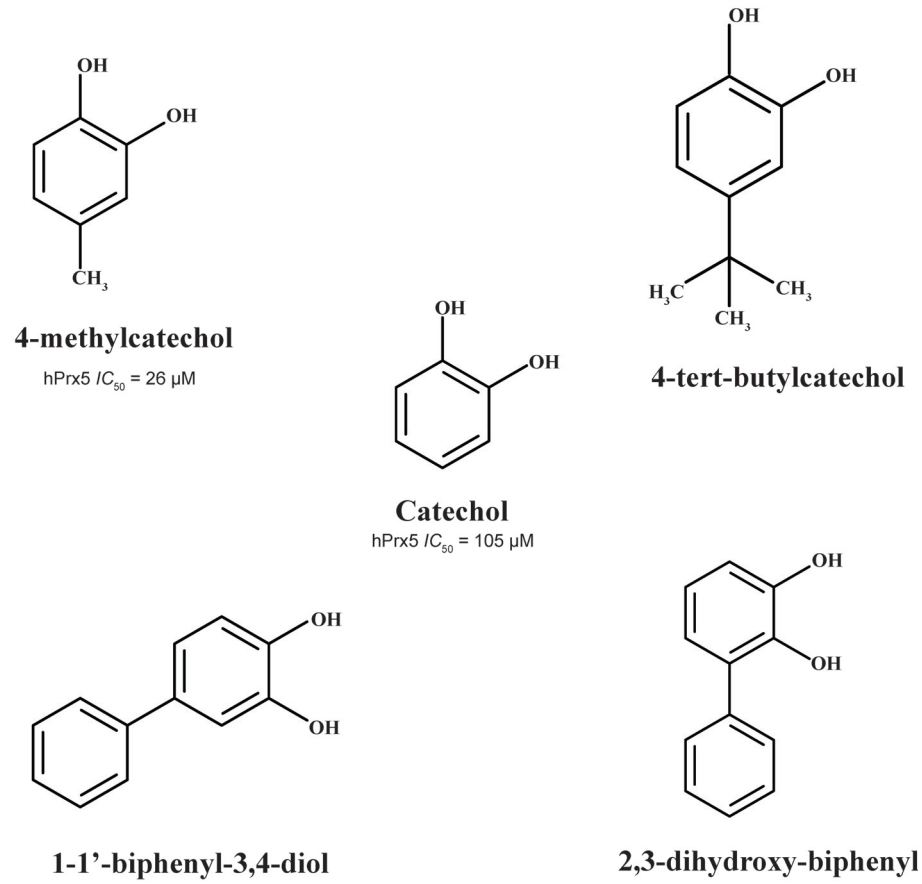

Figure 13: The chemical structure of catechol and some of its derivatives.

Shown here are some of the catechol derivatives screened against hPrx5. Catechol (center) consists of the basic phenol structure with an additional alcohol group. Whereas, for its derivatives different function groups are added such as methyl (top left), *tert*-butyl (top right) or a benzene ring at different carbons (bottom left and right). The IC_{50} values shown here are for inhibiting hPrx5 peroxidase activity [18,27,32].

A. Neurotransmitters

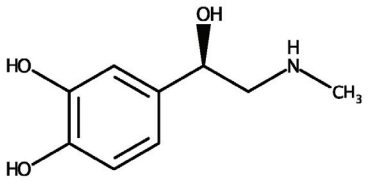

Adrenaline

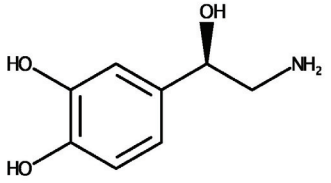

Noradrenaline

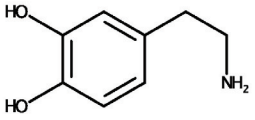

Dopamine

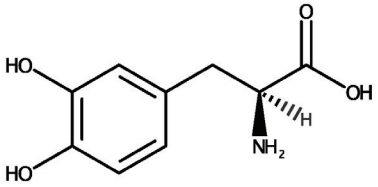

L-DOPA

B. Polyphenols

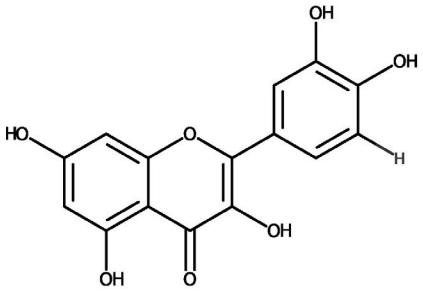

Quercetin

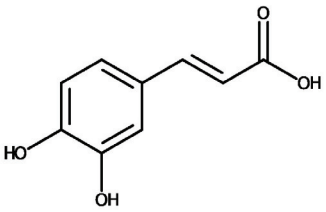

Caffeic acid

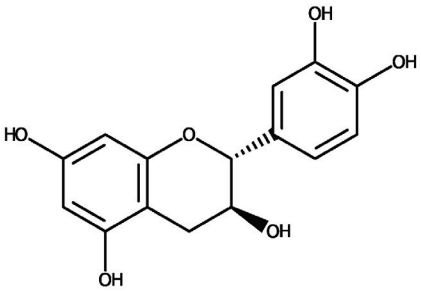

Catechin

Figure 14: The chemical structure of neurotransmitters and polyphenols.

Shown here are some of the chemicals structures of **A. neurotransmitters** and **B. polyphenols** that have the catechol skeleton backbone structure [66,67].

binding specificity. Catechol derivatives examined included 4-methylcatechol, 4-*tert*-butylcatechol, 1-1'-biphenyl-3,4-diol and 2,3-dioxyl-biphenyl (see Figure 13) [27]. The binding affinity of these catechol derivatives were screened with STD NMR spectroscopy and 4-*tert*-butylcatechol was discovered to have the best binding affinity to hPrx5. Therefore, adapting the simple catechol structure improved the binding affinity was achieved. Using STD NMR spectroscopy, GEM exploited the catechol derivatives protons most implicated in the binding interaction between hPrx5-catechol derivative and it was the protons within the benzene ring of the catechol derivatives that were found to be most involved as opposed to the functional groups[27].

Additionally, chemical shift mapping NMR technique (2D HQSC) has been utilized to understand the protein binding interactions to the catechol derivatives against hPrx5. Similar to the results of STD NMR, 4-*tert*-butylcatechol was determined to bind best with a binding affinity (K_d) of 0.19 mM [27,32] (Chow *et al.* 2016; to be further explained in section 3.3.1). The binding of 4-*tert*-butylcatechol involved interacting with the amino acid residues of hPrx5 within its active site and a loop plus a small α-helix perpendicular to the active site. 4-*tert*-butylcatechol interacted with the catalytic cysteine (C_p; Cys47) along with Ala42, Thr44, and Ser48 having the most significant chemical shift perturbation (CSP) detected (Chow *et al.* 2016) [27]. Overall, applying these NMR techniques to screen the catechol derivatives against hPrx5 provided insight of the binding interaction details.

Catechol derivatives have also previously been studied in their binding ability to hPrx5 through computer tools such as docking and FM. Docking determined the catechol derivatives (catechol, 4-methylcatechol, 4-*tert*-butylcatechol, 1-1'-biphenyl-3,4-diol and 2,3-dioxy-biphenyl) could bind within the active site of hPrx5. However, in further examining the possible binding conformation, co-crystallizing all of these catechol derivatives was not successful. Only catechol, 4-methylcatechol and 4-*tert*-butylcatechol were able to co-crystallize [27]. Therefore, highlighting the limitations with docking as it is generally used for

screening high number of ligands but there are set backs on the accuracy in identifying lead hits resulting to false positives [47,59].

FM computer simulations have provided more insight of dynamics catechol derivatives binding to hPrx5 in solution. This computational simulations provided information on the binding conformations revealing details about the chemical bonds, bond angles and free-energy values [58,59]. FM was used to understand the binding interactions of catechol and 4-methylcatechol to hPrx5 active site. In simulating the binding events of the catechol derivatives to hPrx5, a FES map was obtained providing insight into the binding conformations. Figure 15 shows the FES map acquired for catechol binding to hPrx5, in which two reversible binding conformations were observed (two energy basins). Whereas, the FM simulation of 4-methylcatechol to hPrx5, revealed there were also, two reversible binding conformations seen. Additionally, when 4-methylcatechol bound to hPrx5 the active site underwent a conformational change with the binding pocket shrinking to accommodate the binding providing dynamic information. Also, the absolute binding free-energy values ($\Delta G°$) obtained were converted to binding affinity (K_d) values assisting in comparing the binding interactions between the two-catechol derivatives. 4-methylcatechol was found to bind to hPrx5 with a better affinity than catechol with a K_d of ~ 2 mM [32]. The binding conformations observed by FM for catechol and 4-methylcatechol to hPrx5, complemented the co-crystal structures previously seen for X-ray crystallography [27]. Nevertheless, FM simulations were shown to be another computational tool advantageous in drug discovery screening.

In identifying catechol derivatives bound to hPrx5, there has been a preliminary study in assessing their inhibitory properties. hPrx5 peroxidase activity was monitored through an *in vitro* enzymatic assay, and both catechol and 4-methylcatechol were determined to inhibit hPrx5. 4-methylcatechol was the most potent inhibitor with an IC_{50} value of 0.026 mM [18]. Although, in identifying 4-*tert*-butylcatechol binds the best to hPrx5 the inhibitory effect has yet to be examined. Also, the inhibition mechanisms of the catechol derivatives to hPrx5 have not been assessed to provide more knowledge to further develop catechol derivatives

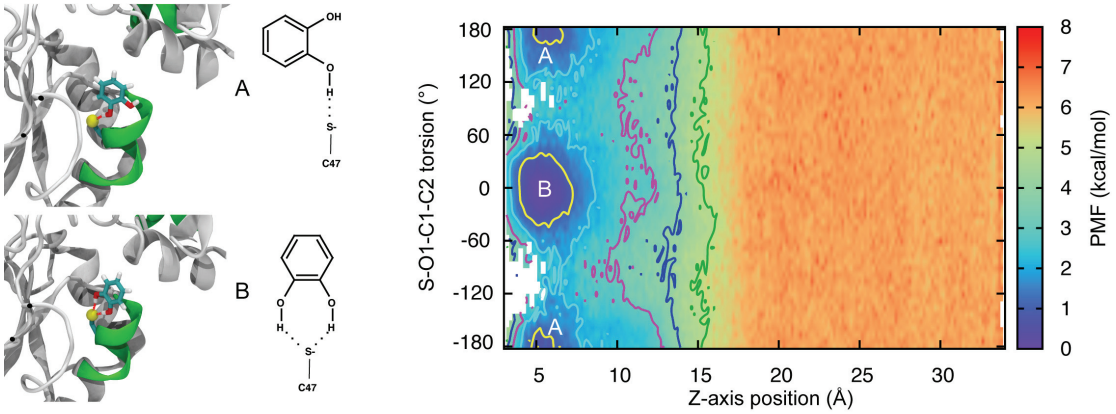

Figure 15: Free energy surface map for catechol binding to hPrx5 using FM.

Shown here are the free-energy surface (FES) basins observed for catechol interacting to hPrx5 active site. The free-energy (shown as Potential Mean Force (PMF)) is represented by iso-energetic colour contours ranging from 0 (blue indicating the lowest free energy) to 8 kcal/mol (red indicating the highest free energy). The free energies obtained are function of catechol's center of mass position during the projection along the z-axis of the funnel. The binding conformation angle (torsion) of catechol to hPrx5 is defined by hPrx5 catalytic Cys47-SH residue and catechol's O1, C1 and C2 atom. This FES map shows the two reversible binding conformations (**A** & **B**) observed for catechol when binding to hPrx5 through H-bonds. The figure is from Troussicot *et al.* 2015 [32].

into ideal drugs. Therefore, there is interest to further explore the inhibitory properties of the catechol derivatives as future drugs as a vital therapeutic agent for post-ischemic brain inflammation.

Independently, there have also been several studies examining the antioxidant effects of polyphenols and their metabolites, catechol derivatives, having anti-inflammatory effects on cellular activity in the brain. Zheng *et al.* found catechol, 3-methylcatechol, 4-methylcatechol and 4-*tert*-butylcatechol to influence the inflammatory activation and neurotoxicity on resident brain cells, microglial. The catechol derivatives lead to inhibiting the expression of inflammatory cytokines (mediators immune response) and suppress specific cell signalling factors. Therefore, highlighted the neuroprotective effect of the catechol derivatives in preventing neurotoxicity to microglial cells [26].

1.10.2 Other inhibitors or methods to target Prx activity

There have also been other drug discoveries of other prospective drugs against various Prxs. Other studies have not focused on NMR techniques to screen compounds but have utilized computer tools such as virtual screening using docking, X-ray crystallography and high-throughput *in vitro* screening method on cells or target proteins [19–21,25].

Potential drugs adenanthin, H7 and AMRI (Albany Molecular Research Inc.)-59 (specific molecule from their library) have been identified to bind and inhibit hPrx1 and hPrx2 (see Figure 16). These drugs have mainly focused on therapeutic treatments towards cancers, since elevated levels of certain Prxs have been linked to enhance cancer cells survival resulting in resistance to chemotherapy and radiotherapy treatments [19–21]. Adenanthin and H7 were found to induce the differentiation of acute promyelocytic leukemia (APL) cells through targeting and inhibiting hPrxs peroxidase activity. Adenanthin inhibited hPrx1 and hPrx2 with IC_{50} values of 1.5 μM and 15 μM and were found to bind to the C_r (Cys173/2) of the Prxs [19]. H7 inhibited specifically hPrx1 and not hPrx2-4 with an IC_{50} value of 7.85 μM,

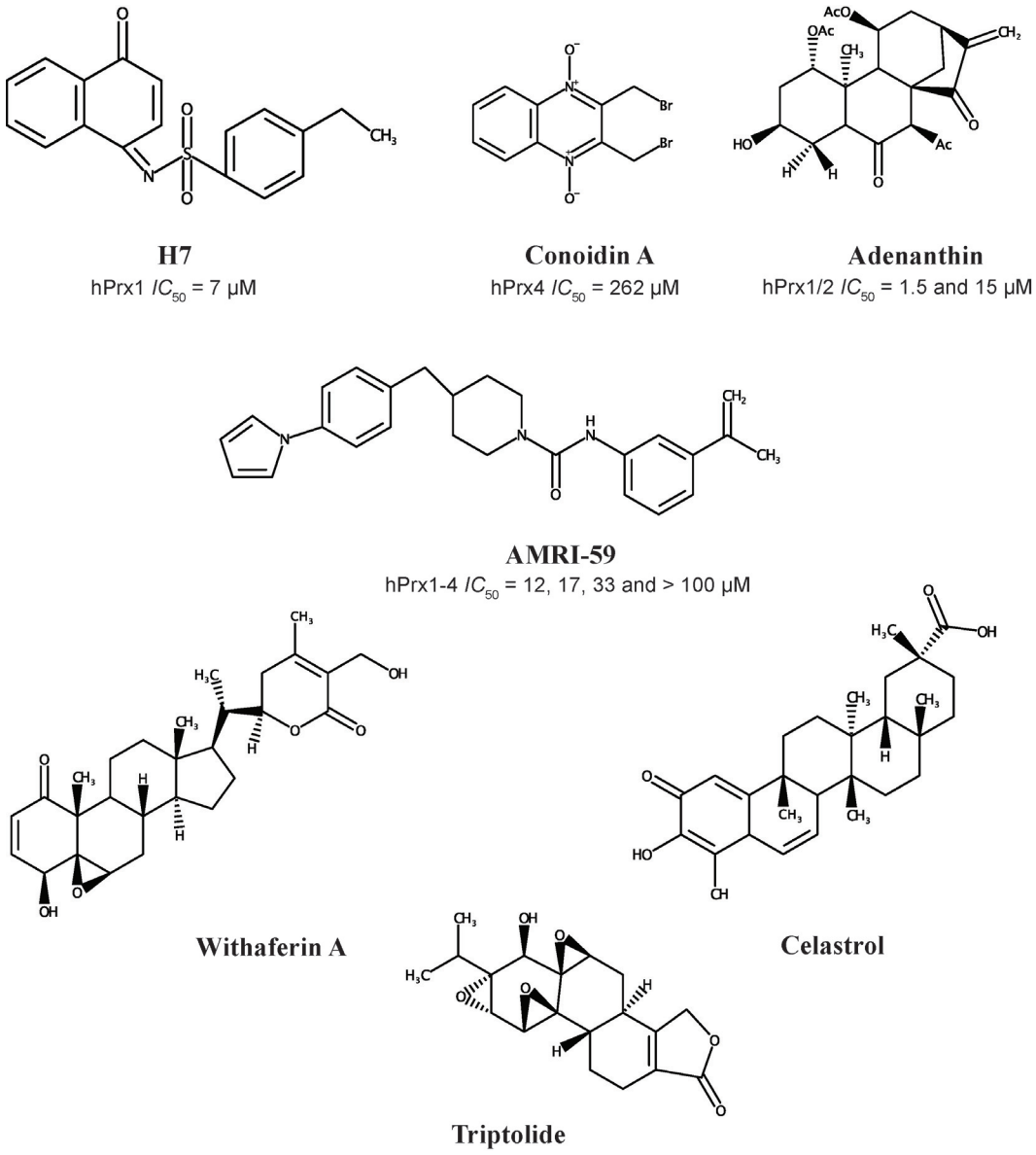

Figure 16: Other inhibitors chemical structure against hPrxs.

Shown here are the chemical structures of the various inhibitors identified to bind and inhibit hPrxs. Adenanthin, H7 and AMRI-59 have been identified to inhibit hPrx1 and hPrx2. Conoidin A to known in inhibit hPrx1, hPrx2, and hPrx4. Withaferin A, triptolide, and celastrol are known to inhibit hPrx1. The respective IC_{50} values shown here are for inhibiting the various hPrxs peroxidase activity [19–21].

binding and interacting in the active site region including the C_p (Cys52) [20]. AMRI-59 was found to target human lung cancer cells inhibiting hPrxs peroxidase activity by impairing the reduction of hPrxs leading the cell death. Specifically, AMRI-59 inhibited hPrx1-4 but was most potent against hPrx1 with an IC_{50} value of 12 μM [21]. These inhibitors were identified to inhibit hPrxs through impairing the peroxidase activity.

Moreover, modifications of Prxs through other post-translation modifications have also been linked to regulating their redox activity. Manipulating acetylated hPrx1 and hPrx2 through histone deacetylase (HDAC) 6 activity have been purposed as a therapeutic strategy for treatment to cancers, neurodegenerative diseases, and other disorders. Since acetylation of hPrx1 and hPrx2 was found to increase peroxidase activity and protect the Prxs from hyperoxidation. Elevated levels of hPrxs have been linked to various disease such as cancer as previously mentioned [68]. Triptolide and its derivatives celastrol and withaferin, were found to inhibit the oligomerization of hPrx1 but not inhibit the peroxidase activity when tested. These inhibitors were found to bind to Cys83 and Cys173, which are key amino acids in the decameric structure and chaperone activity of hPrx1. Through cysteine alkylation of these key amino acids lead to the hPrx1 to have a loss in its ability form highly ordered oligomers and chaperone activity [22]. Conoidin A and its analog conoidin B, have been determined to inhibit hPrxs (1,2, and 4), hookworm *Ancylostoma ceylanicum* (Ace-Prx1), and *Toxoplasma gondii* (TgPrx2) [23–25]. Conoidin A was identified as the more potent inhibitor against the Prxs and inhibited Ace-Prx1, hPrx2 and hPrx4 with IC_{50} values of 374, 358 and 262 μM. Specifically for conoidin A inhibitory properties on Ace-Prx, were found to bind and inhibit through cysteine alkylation of Cys49 or Cys79 or both and also hyperoxidation to Cys170 in an irreversible oxidized state [25] (see Figure 16).

Targeting and inhibiting Prxs the main attraction has been on the cysteine residues of the proteins as they are involved in regulating the redox activity. Also, there has been developments of antibodies to hPrx5 and hPrx6 designed to bind on more conserved regions, β4-sheet and α3-helix region (amino acids 66-93). Anti-hPrx5 and anti-hPrx6 were found to

be beneficial in treatment on mouse models after an ischemic stroke reducing the severity of neurological pathophysiology [11].

1.11 Research objectives

As introduced in the previous sections, peroxiredoxins are peroxidase proteins involved in reducing various peroxides and but are also, antioxidant enzymes assisting in the defense of cellular free radicals. Recently, peroxiredoxins were identified as a key protein released after an ischemic stroke apart of a cascade leading to post-ischemic inflammation in the brain. As a result, regulating the inflammation cascade is an attractive therapeutic treatment to aid and assist stroke patients in the recovery process.

There is great appeal in studying human peroxiredoxins and determining potential molecules that may act as inhibitors to help control the post-inflammation cascade. Hence, my thesis focuses on investigating the interactions of lead ligands identified to bind to hPrxs (1,2 and 5) and understanding their possible inhibitory properties to inhibit hPrxs activity. First the ligands, catechol, 4-methylcatechol and 4-*tert*-butylcatechol, will be further studied by NMR spectroscopy techniques to assess the binding interactions and affinities to hPrx1, hPrx2, and hPrx5. Previous work has already examined the binding interactions of the catechol derivatives to hPrx5. Specifically, I will concentrate on examining the binding interaction and affinities of the catechol derivatives to hPrx1 and hPrx2. I will incorporate past findings of the binding affinities of the catechol derivatives to hPrx5 and understand if there is specificity amongst lead ligands to hPrx1, hPrx2 and hPrx5. Additionally, to assist in understanding the protein-ligand interactions, computational modeling will accompany the research, which will be completed by Jean-Marc Lancelin and Laura Troussicot. Secondly, I will also determine if these lead ligands can inhibit hPrxs peroxidase activity through an *in vitro* enzymatic assay. Identifying the ligands that can inhibit hPrxs, their molecular

mechanism of action (MMOA) will be examined. Knowledge of the MMOA can contribute to further optimizing the lead ligands to potentially become drugs as a therapeutic treatment for ischemic stroke patients.

2 Materials and methods

2.1 Reagents

All buffer reagents were obtained from Thermo Fisher Scientific (Fair Lawn, USA), Carl Roth GMBH + Co. KG (Karlsruhe, Germany), and/or Sigma-Aldrich (St. Louis, USA) unless otherwise indicated. The chromatography columns were obtained from Qiagen (Hilden, Germany) and GE Healthcare Life Sciences (Buckinghamshire, United Kingdom).

2.2 Standard protocols

2.2.1 Protein purification

Recombinant human peroxiredoxin 1, 2 and 5 (EC 1.11.1.15), yeast Trx1 (EC 1.8.1.9), and yeast TrxR1 (EC 1.8.1.9) were in the pQE-30 expression vector (Qiagen) with a N-terminal fusion with hexahistidine (6xHis) tag. The plasmids were provided through the collaboration with Dr. Bernard Knoop's lab at the Université Catholique de Louvain, Belgium. The expression and purification of the proteins were adapted from Declercq *et al.* 2000[69]. Briefly, the plasmids were transformed in to *E.coli* strain M15 (pRep4) and grown in LB medium at 37°C with 50 µg/mL ampicillin and kanamycin. The bacterial cultures were induced at an O.D. 600 at of 0.6 with 1 mM isopropyl-thio-galactopyranoside (IPTG) for 4 to 5 hours. The bacterial cells were then harvested by centrifugation at 2000 g-forces for 20 minutes (Thermo Fisher Scientific, rotor F15-8 x 50 cy). The bacterial cell pellets were then lysed with 50 mM sodium phosphate, 300 mM NaCl, 10 mM imidazole, pH 8 by sonication (Sartorius Stedim Biotech, Aubagne, France). The cell lysate was then centrifuged for 45 minutes at 16500 g (Thermo Fisher Scientific, rotor TX-750). The cell supernatant was then loaded onto a Ni^{2+}-NTA column after an equilibration with the lysis buffer. The column was then washed with the lysis buffer and the protein was eluted with a gradient of imidazole using the following buffer (50 mM sodium phosphate, 300 mM NaCl, 250 mM imidazole,

pH8). The eluted protein was pooled and dialyzed overnight against PBS pH 7.4 at 4°C. The homogeneity of the protein was analyzed by SDS-PAGE and stored at -80°C until used.

2.2.2 ^{15}N-isotope protein expression and purification

The expression and purification for hPrx1, hPrx2, hPrx5, yTrx1, yTrxR1 labeled with ^{15}N-isotope was the same to the unlabeled protein except for the bacterial cell growth medium. The bacterial cells were grown in M9 minimal medium (6g/L Na_2HPO_4, 3g/L KH_2PO_4, 0.5g/L NaCl) supplemented with 50 μg/mL ampicillin and kanamycin, 6 μg/L thiamine, 1 mM $MgSO_4$, 1 mM $CaCl_2$, 10 mL/L of trace metal solution (5g EDTA, 0.5g $FeCl_3$, 0.005g ZnO, 0.001g $CuCl_2$, 0.001g $Co(NO_3)_2 \cdot 6H_2O$ and 0.001g $(NH_4)6Mo_7O_{24} \cdot 4H_2O$ per liter), 4g/L D-glucose, and 1g/L $^{15}NH_4Cl$.

2.2.3 Quantification of protein concentration

The concentration of a protein was determined by absorbance (measuring between the wavelengths of 240-440 nm using a UV-Vis spectrum Jasco France SAS, France). The absorbance value at the wavelength 280 nm was then converted to a concentration by the proteins extinction coefficient at A_{280} (ε, calculated from expasy.org/protparam from the amino acid sequence). yTrx1, ε = 10095 M^{-1} cm^{-1}; yTrxR1, ε = 24660 M^{-1} cm^{-1}, hPrx1 ε = 18450; hPrx2 ε = 21555 M^{-1} $cm^{-1}M^{-1}$ $cm^{-}1$; hPrx5 ε = 5625 M^{-1} cm^{-1}.

2.2.4 Polyacrylamide gel electrophoresis

The gels were made in the laboratory using 30% acrylamide/bis-acrylamide solution. All SDS-PAGE gels consisted of a 5% polyacrylamide stacking and 15% polyacrylamide separating gel. The protein samples run on the gels were prepared in a 2x Laemmli buffer solution (50 mM Tris, pH 6.8, 2% SDS, 0.1% bromophenol blue, 10% glycerol with the

addition of 10 mM DTT to the samples prior to running the gel). The gels were run on a Bio-Rad Mini PROTEAN Tetra cell system (Bio-Rad Laboratories Ltd., France) using running buffer (25 mM Tris pH 8.3, 192 mM glycine, and 0.1% SDS) at 90 V through the stacking layer and 120 V through the separating layer until reaching the end. For visualization, the gels were stained using Coomassie brilliant blue dye (R-250) and destained using destain buffer (10% acetic acid / 40% of ethanol / 50% of distilled water).

2.2.5 Hydrogen peroxide quantification

Hydrogen peroxide (H_2O_2) was quantified by a titration in monitoring the chemical reaction in neutralizing H_2O_2 with potassium permanganate. Shown here is the following chemical reaction:

$$2MnO_4^- + 5H_2O_2 + 6H^+ \rightleftarrows 2Mn^{2+} + 5O_2 + 8H_2O$$

The protocol was adapted from Mendham *et al.*, 2000[70]. A titrated solution consisted of an unknown concentration of H_2O_2 with 2 M H_2SO_4 in a final volume of 5 ml with H_2O. Then potassium permanganate was titrated into the solution until a faint pink colour was reached signifying the neutralization of H_2O_2. The volume of potassium permanganate used to titrate was then used to calculate the concentration of H_2O_2 that was neutralized using the balanced equation. The concentration of H_2O_2 stocks was re-quantified every several months to ensure the H_2O_2 did not decompose.

2.2.6 Size exclusion chromatography (SEC)

Size exclusion chromatography was used to estimate the MW of yTrx1, yTrxR1, hPrx1 and hPrx2. The redox proteins were pre-treated with either 10 mM of DTT or oxidized with 500 μM H_2O_2. Then 3mg/ml of protein was loaded onto a column pre-equilibrated in 50

mM $NaHPO_4$, 150 mM NaCl, 3mM KCl, pH 7.2. Either the Superdex200 10/300 GL (for high molecular weight (HMW) proteins 10 to 600 kDa) or Superdex75pg (for low molecular proteins (LMW) from 3 to 70 kDa) was used depending on the size of the protein. The protein's elution volume was obtained from the UV-Vis chromatogram monitoring the absorbance at 280 nm with the ÄKTAprimeplus system (GE Healthcare Science). The elution volume was then converted to a partition co-efficient value (K_{av}) from the following equation:

$$K_{av} = \frac{V_e - V_o}{V_c - V_o}$$

V_e represents the elution (or retention) volume, V_o is the void (or interstitial) volume and V_c is the geometric column (or intra-particle) volume. The molecular weight for a protein was determined from the column's calibration curve. Both columns were calibrated with high and low molecular weight protein mixture obtained from GE Healthcare Life Sciences (Buckinghamshire, United Kingdom). A mixture of calibration proteins (LMW and HMW protein kits from GE Healthcare Science) was loaded onto the column and the K_{av} values were determined. The K_{av} values were plotted against their known molecular weights to generate a calibration curve.

2.3 Peroxidase activity assay

2.3.1 Half maximal concentration assay (IC_{50})

The inhibitory concentration assay of hPrx1, hPrx2 and hPrx5 was adapted from Kim et *al.* 2005 and Barelier et *al.* 2010[18,71]. Inhibition activity of hPrx1, hPrx2 and hPrx5 was measured indirectly by the coupling reaction of TrxR oxidizing NADPH, monitored by the absorbance at 340 nm. The reaction conditions consisted with catechol derivatives at various concentrations (0-75 mM catechol, 0-15 mM 4-methylcatechol, and 0–5 mM 4-*tert*-butylcatechol) in PBS, 15 µM yTrx1, 2 µM yTrxR1, 0.15 µM hPrx5, 200 µM NADPH

(Sigma-Aldrich) and 25 μM H_2O_2 (at ~ K_m value) in 1000 μl total reaction volume. The reaction was carried out by a mixture of all three proteins diluted in PBS (10 mM $NaHPO_4$, 137 mM NaCl, 3 mM KCl) with 1mM EDTA at a pH 7.0 with the addition of the catechol derivatives and NADPH. Lastly, H_2O_2 was added to the mixture and mixed to initiate the reaction and the inhibition activity of hPrx1, hPrx2 or hPrx5 was monitored at room temperature (23°C). The reaction was measured at A_{340} for 200 seconds and the initial rate of the reaction was determined from linear portion of the curve and is expressed in μmol mg^{-1} min^{-1} in reference to the amount of hPrx used. The IC_{50} values were determined from plotting the reaction rates against the catechol derivative concentrations and fitting the data to a hyperbolic decay equation using SigmaPlot (San Jose, USA). The catechol derivatives were ranked on the inhibition potency by their IC_{50} values. In monitoring the inhibition activity for hPrx1 and hPrx2, they were conducted under similar conditions as hPrx5 with the exceptions: hPrx1 and hPrx2 at 0.38 μM and 4-*tert*-butylcatechol was reconstituted with 100% (v/v) DMSO initially and then further diluted in PBS pH 7.4 with 1mM EDTA (~ 10 000 folds). The IC_{50} values are representative of three individual experiments (n=3).

2.3.2 Conformational inhibition mechanism

The conformational inhibition mechanism assay was conducted with three to four concentrations of the catechol derivatives above and below the IC_{50} value, 15 μM yTrx1, 2 μM yTrxR1, 0.15 μM hPrx5, 200 μM NADPH and a range of H_2O_2 from 0-500 μM. The reaction was initiated by mixing all three proteins together with a catechol derivative and NADPH and the addition of H_2O_2. The reaction was monitored A_{340} for 100 seconds and the initial rate of the reaction was determined from linear portion of the curve and is expressed in μmol mg^{-1} min^{-1}. The Data was plotted in a Michaelis-Menten and/or Hanes-Woolf representations. The V_{max} and K_m values were calculated for each inhibitor concentration using SigmaPlot (San Jose, USA). Since data was not fitting well under linear regression fit, DynaFit (BioKin, Ltd., Watertown, USA) software was then used with the steady-state

approximation, for model discriminations and parameter determination[63,72]. See the "Appendix" for an example of the script used to assess the conformational inhibition mechanism. DynaFit used the Levenberg-Marquardt algorithm[73] to fit the data and the Savitzky-Golay algorithm[74] to smooth out the data (see the Appendix for more details). The data values are representative of three individual experiments (n=3).

2.3.3 Kinetic inhibition mechanism

The kinetic inhibition mechanism assay (reversibility) was carried out by incubating hPrx5 with 100-fold the concentration required (15 μM) and with each catechol derivative (catechol, 4-methylcatechol, 4-*tert*-butylcatechol) at 10-fold and 5-fold the concentration of the IC_{50} value. The protein and ligand mixture was then incubated for 30 minutes at room temperature. After the hPrx5 and the specific catechol derivative mixture were diluted 100-fold transitioning from high to low inhibition concentration conditions into the enzymatic mixture containing 15 μM Trx, 2 μM TrxR, 200 μM NADPH and 25 μM H_2O_2. The reaction was monitored A_{340} for 100 seconds and the initial rate of the reaction was determined from linear portion of the curve. The rates are expressed in μmol mg^{-1} min^{-1} for hPrx5. The reversibility reaction rates were measured for three independent experiments (n=3).

2.4 NMR

2.4.1 2D HSQC NMR spectroscopy

The NMR samples consisted of 200 μM for the specific protein, in the absence or presence of 2.5 mM of the specific ligand (catechol, 4-methylcatechol, 4-*tert*-butylcatechol) in PBS pH 7.4, and 2 mM of tris (2-carboxyethyl)phosphine (TCEP) in PBS at pH 7.4 and 10% D_2O. The NMR spectra were acquired at 301K (28°C) with a Varian Inova 600 MHz spectrometer equipped with a 5 mm standard triple resonance ($^1H/^{13}C/^{15}N$) inverse probe with a z-axis field gradient. To obtain the protein NMR fingerprint, a 2D ($^{15}N,^1H$)- heteronuclear single quantum coherence (HSQC) experiment was performed [75]. Two ^{15}N-HQSC spectra

were obtained: in the absence of the ligand and then in the presence of the ligand. Prior to recording the protein in the presence of the ligand, the mixture was incubated at room temperature for five minutes.

2.4.2 STD NMR spectroscopy

The STD NMR samples were prepared with 20 μM hPrxs (Prx1 and/orPrx2), a concentration range of a ligand in 100% DMSO (maximum total concentration of 5% DMSO (v/v); catechol 0-54 mM; 4-methylcatechol 0-54 mM; 4-*tert*-butylcatechol 0-4 mM), 10% D_2O (v/v) in PBS buffer pH 7.4 with 2 mM TCEP. ^{1}H and STD NMR spectra were monitored at 301K (28°C) with Varian Inova 600 MHz Spectrometer equipped with a room temperature 5 mm triple-resonance inverse probe with z-axis field gradient. Both ^{1}H and STD NMR experiments were conducted with identical experimental conditions (interscan delays) and the parameters for STD experiment (saturation frequency and saturation time) were identical for each sample. The selective saturation of the protein NMR spectrum was achieved with the decoupler offset 3000 Hz up field from the carrier frequency and the non-saturation control was performed at 15000 Hz downfield. The number of scans for ^{1}H consisted of 512 and for STD consisted of 1024. The STD signals were measured for protons in the aromatic region (6-8 ppm). The binding dissociation constant (K_d) was acquired for the ligand by monitoring the STD amplification factors (f_{STD}) as a function of ligand concentration. The f_{STD} was derived from the following equation:

$$f_{STD} = \frac{I_{STD}}{I_0} \text{x} \frac{[L]_{tot}}{[Prx]_{tot}}$$

Where I_{STD} and I_0 are the integral peaks in the STD and ^{1}H experiments and the $[L]_{tot}$ and $[Prx]_{tot}$ are the total concentration of the ligand and peroxiredoxin. The K_d value was obtained by fitting the plot f_{STD} vs. $[L]_{tot}$ to hyperbolic curve [76]. The K_d values are

representative of three independent experiments (n=3) for 4-*tert*-butylcatechol interactions to hPrx1 and hPrx2. For the catechol and 4-methylcatechol interactions to hPrx1 and hPrx2, the K_d values are representative of one independent experiment (n=1).

2.4.3 1D NMR spectroscopy to monitor the peroxidase activity

Peroxidase chemical reaction (i.e. redox inhibition mechanism) samples were prepared under the same conditions as the enzymatic reaction (0.15 μM hPrx5, 15 μM Trx, 2 μM TrxR, 200 μM NADPH, and 25 μM H_2O_2 in PBS pH 7.0 with 1 mM EDTA) in the presence of 1mM of each catechol derivative (catechol, 4-methylcatechol, 4-*tert*-butylcatechol) in 10% (v/v) D_2O.^{1}H NMR spectra were recorded at 301K (28°C) on a Varian Inova 600 MHz Spectrometer equipped with a room temperature 5 mm triple-resonance inverse probe with z-axis field gradient. The peroxidase reaction was broken down sequentially in the presence of the specific catechol derivative and each component was incubated for five minutes at room temperature prior to a ^{1}H NMR spectrum recorded. The reaction order consisted of the catechol derivative alone initially with the addition of each following components: NADPH, H_2O_2, Trx, TrxR, and hPrx5.

2.5 Protein structure and sequence alignment

All protein sequences and structures were obtained from the Protein Data Base with the following numbers: hPrx1 (2RII), hPrx2 (1QMV), hPrx3 (PDB not known; fasta sequence PRDX3_HUMAN), hPrx4 (2PN8), hPrx5 (3MNG), and hPrx6 (1PRX). The sequence alignments were completed using Praline sequence assignment site (http://www.ibi.vu.nl/programs/pralinewww/) and BioEdit software (Ibis Biosciences, Carlsbad, USA) [77]. The figures highlighting key regions on the proteins were created using PyMOL (The PyMOL Molecular Graphics System, Version 1.8 Schrödinger, LLC.).

3 Results

3.1 Characterization of hPrx1, hPrx2, hPrx5, yTrx1, yTrxR1

3.1.1 Expression and purifying redox recombinant proteins

My first objective in starting the hPrxs project was to purify and characterize all the recombinant redox proteins required for the peroxidase reaction (hPrxs, yTrx1, and yTrxR1). Previously in our lab, hPrx5 was extensively studied and characterized, so I mainly focused on studying hPrx1, hPrx2, yTrx1 and yTrxR1. I first wanted to ensure we had all of the proper recombinant redox proteins.

All the recombinant proteins were successfully expressed and purified. The general protein yield varying from 60 to 80 mg per liter of bacterial culture. Upon purifying the recombinant redox proteins molecular weight and purity were confirmed by SDS-PAGE. Under reducing conditions all the recombinant proteins apparent molecular weights (MWs) were: 25 kDa for hPrx1, 25 kDa for hPrx2, 19 kDa for hPrx5, 12 for kDa yTrx1 and 36 kDa for yTrxR1 representing the proteins in their monomeric forms (see Table 2 pg 65). Figure 17 is an example for a purification of hPrx5.

3.1.2 Fingerprints of the recombinant redox proteins by ^{15}N-HQSC NMR spectroscopy

Under physiological conditions, redox proteins can exist as monomers, homodimers and other higher ordered oligomers [36,78,79]. I was interested to know what state the recombinant redox proteins were in upon purifying and also, if they were well folded to be functional in measuring their enzymatic activity. All the recombinant proteins were ^{15}N-isotope labelled to possibly achieve a 2D ^{1}H-^{15}N NMR spectrum, a fingerprint of each protein under a set of experimental conditions (concentration, pH and temperature). For yTrx1, a high resolution ^{15}N-HQSC NMR spectrum was acquired under reduced conditions representing a homogenous reduced state and the peaks were well separated and sharp (see Figure 18). The number of peaks observed on the spectrum was in accordance to the predicted

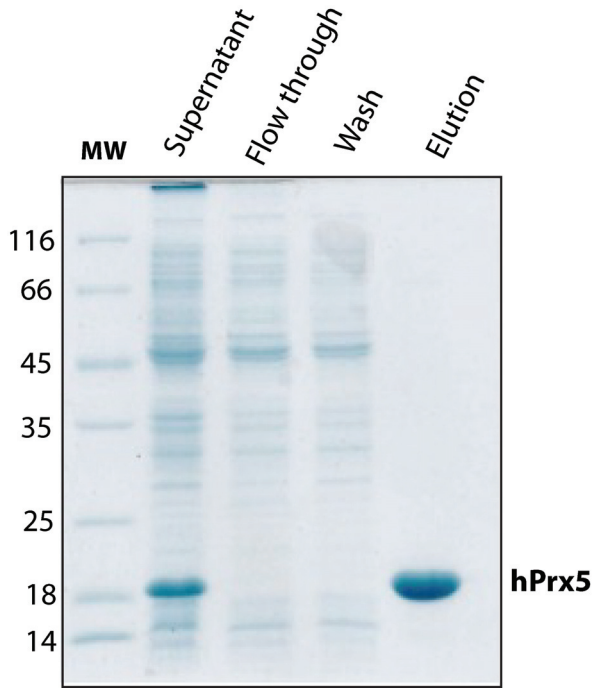

Figure 17: SDS-PAGE gel for a purification of human Prx5.

hPrx5 was expressed in *E. coli* cells with a N-terminal fusion hexahistidine (6xHis) tag and purified through Ni-NTA affinity chromatography. Shown here is a SDS-PAGE gel of the various steps followed in the purification of hPrx5. First, the bacterial cells were lysed and then the cell supernatant was loaded onto Ni-NTA affinity column (shown as supernatant). In loading the supernatant, only the His-tagged hPrx5 protein was bound to the Ni-NTA column and any unspecific proteins was removed (flow through). After, the column was further washed to remove any impurities bound to the column (wash). Lastly, His-tagged hPrx5 was eluted (elution). The purity of hPrx5 was evaluated by 15% SDS-PAGE under reducing conditions (10mM DTT) and had a MW ~ 19 kDa (monomer).

number of peaks from the amino acid sequence. Additional, yTrx1 NMR spectrum was compared to previously published spectra of yTrx2 (BMRB 6912)[80]. Both spectra had similar peak characteristics but there were some moderate differences between yTrx1 spectrum and yTrx2 spectrum. yTrx1 had a His-tag, and the amino acid sequence between yTrx1 and yTrx2 are ~70% identical. Also, yTrx1 amino acid sequence had additional amino acids, and the experimental conditions were not exactly the same. Nevertheless, the spectra overall were comparable and therefore confirmed the native form of yTrx1.

However, in acquiring ^{1}H-^{15}N-HSQC NMR spectra for ^{15}N-hPrx1, hPrx2 and yTrxR1, the spectra had poor quality even under reducing conditions. The signals were not detected well separated and there were only a few peak signals detected (see Figure 19 for hPrx2). This suggested that hPrx1, hPrx2 and yTrxR1 are either a high MW (HMW) oligomer possibly under conformational exchanges [81]. Examining hPrx2 ^{15}N-HSQC spectra, even under reduced or oxidized conditions there was no change observed in the signal peak pattern. Overall, the ^{15}N-HSQC spectra show the amide protons between 6 to 8 ppm (center of the spectrum), this suggested these signal peaks could correspond to mobile parts of hPrx2 and possibly the C- or N-terminal region of the protein in which the His-tag is present at the N-terminus. hPrx2 structure has been previously characterized and determined to form a decamer [82]. Therefore, size exclusion chromatography was further used to examine the recombinant redox proteins apparent MWs and determine if they existed in higher oligomeric states in solution state.

3.1.3 Determining recombinant redox proteins MW by size exclusion chromatography

The MWs for the redox recombinant proteins were determined by size exclusion chromatography (SEC) in separating the proteins based on their size. Prior to determining the MWs for the recombinant redox proteins, the size exclusion columns were first calibrated.

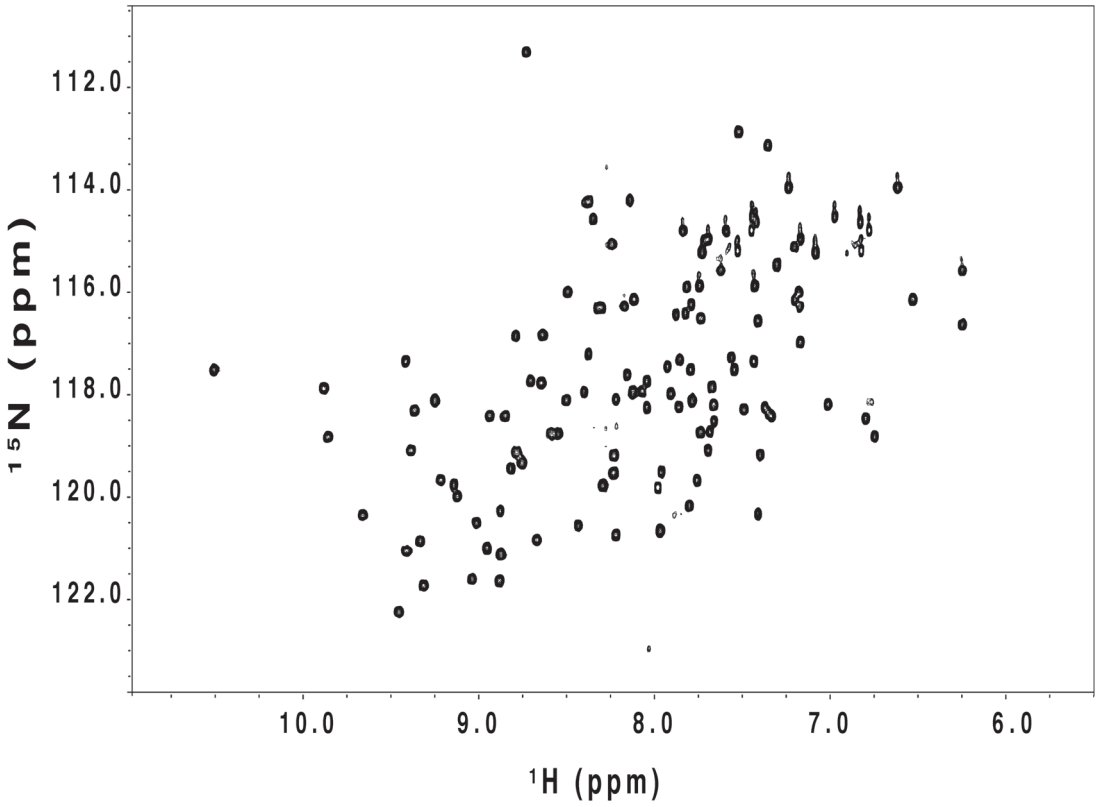

Figure 18: ^{15}N-HSQC spectrum for reduced ^{15}N-thioredoxin.

Thioredoxin (yTrx1) was labeled with ^{15}N isotope to generate a 2D ^{1}H-^{15}N HSQC NMR spectrum. The N-H peaks observed in the spectrum were sharp and well separated. Additionally, the NMR spectrum was comparable to previously published spectrum confirming yTrx1 structure properties (BMRB 6912). The experimental conditions were: 200 µM ^{15}N-yTrx1, 10% D_2O, 2 mM TCEP in PBS pH 7.4 at 28°C on a 600 MHz NMR spectrometer.

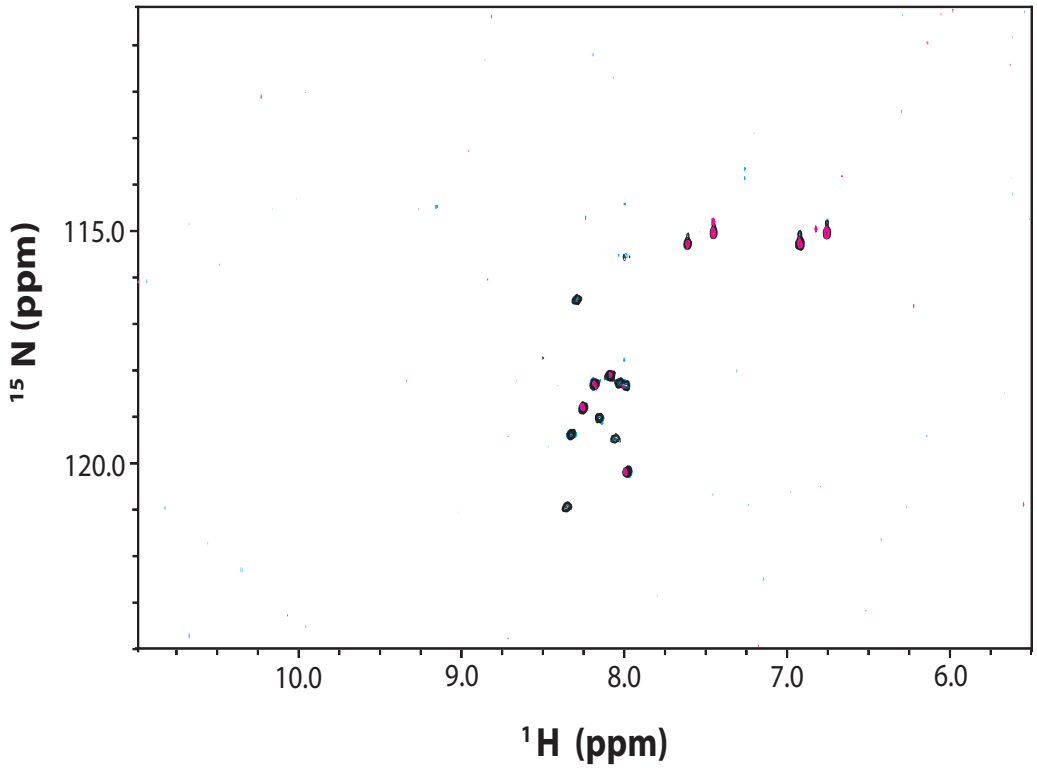

Figure 19: ^{15}N-HSQC spectra for ^{15}N-peroxiredoxin 2.

Human peroxiredoxin 2 (hPrx2) was labeled with ^{15}N isotope to generate a 2D ^{1}H-^{15}N HSQC NMR spectrum. hPrx2 spectra were examined under reduced (pink) and oxidized (blue) conditions (black represents untreated protein). Observing the spectra, there were very few peaks in the 6 to 8 ppm regions suggested only the protein's mobile parts such as the C- or N-terminus (His-tag) are observed and the rest of the protein is not detectable due to being a HMW oligomer under exchange. The experimental conditions were: 200 µM ^{15}N-hPrx2, 10% D_2O, 1 mM TCEP and/or 1 mM H_2O_2, in PBS pH 7.4 at 28°C on a 600 MHz NMR spectrometer.

Two columns were used to accommodate the possibility recombinant redox proteins were highly ordered oligomers. The Superdex 200 column was used to separate high molecular weight (HMW) proteins ranging from 10 to 660 kDa and the Superdex 75pg column was used to separate low molecular weight (LMW) proteins ranging from 3 to 70 kDa. Figure 20A and Figure 21A are an example for the calibration chromatogram obtained for the two columns. Calibrating the columns a mixture of proteins in a range of sizes was separated with the largest MW proteins eluting first and the smallest MW proteins eluting last. From the UV-Vis chromatogram (A_{280}) the elution volumes (retention volume) were noted for each protein in the calibration protein mixture, the partition coefficient (K_{av}) values were determined. Plotting the protein's K_{av} values against their known MW (log scale) a calibration curve was acquired and fitted to a linear regression (see Figure 20B and Figure 21B). From the calibration curve the equation of the line (y = -0.45 x + 2.32 LMW; y = -0.39 x + 2.38 HMW) was obtained and used to estimate MW for the various recombinant redox proteins.

For all the recombinant redox proteins, their MW was determined under both redox states. However, there were no differences in the MWs observed for the proteins. Figure 22A & B are examples for the separation of yTrx1 and yTrxR1 under both redox states. yTrx1 had a MW of ~ 11.0 kDa indicating it to be a monomer. yTrxR1 had a MW ~ 55.9 kDa suggesting it be more of a dimer (monomer ~ 35kDa) and would support the poor signal detection of large proteins observed for the ^{15}N-HQSC spectrum as yTrxR1 is a large protein > 40 kDa [49,53]. Also, similar to yTrxR1, hPrx1 had an apparent MW ~ 300 kDa (14 x monomer 21 kDa) and hPrx2 had a MW ~ 290 kDa (13 x monomer 22 kDa) and were large proteins in size (Figure 23). Overall, all the recombinant redox proteins with the exception of yTrx1 behaved as large oligomers upon purification. Table 2 is a summary of all the characterization results for the recombinant redox proteins.

A.

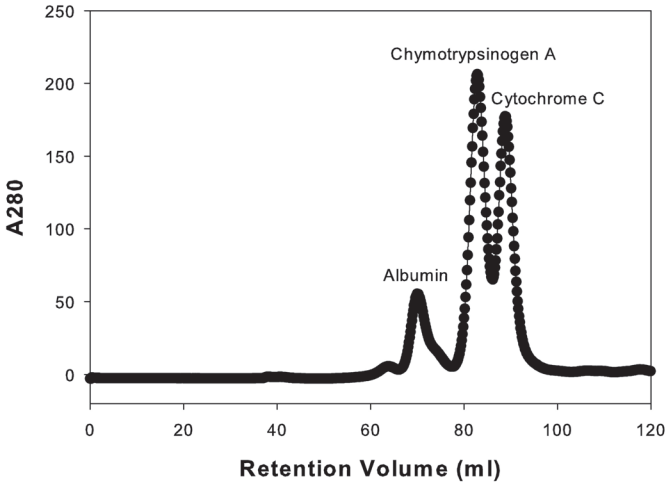

B.

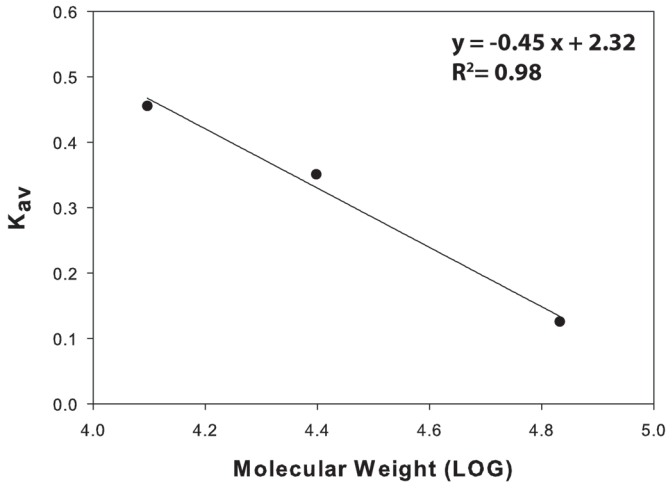

Figure 20: Calibration chromatogram and plot for Superdex 75pg column.

A. Calibration chromatogram (A_{280}). 3 mg/ml of low molecular weight (LMW) proteins: albumin (45 kDa), chymotrypsinogen A (25 kDa) and cytochrome C (12.5 kDa) were loaded and separated on the Superdex 75 column at 0.5 ml/min flow rate. UV-Vis chromatogram at 280 nm was obtained from monitoring the protein's retention volume. **B**. **Calibration curve.** For each protein the partition coefficient (K_{av}) was calculated and was plotted against their molecular weight. The calibration curve was used to estimate the MW of proteins between 3 to 70 kDa. The follow values were obtained to generate the calibration curve: V_c = 120 ml, V_o = 62 ml, V_e (albumin, chymotrypsinogen A, cytochrome C) = 69, 82, 88 ml.

A.

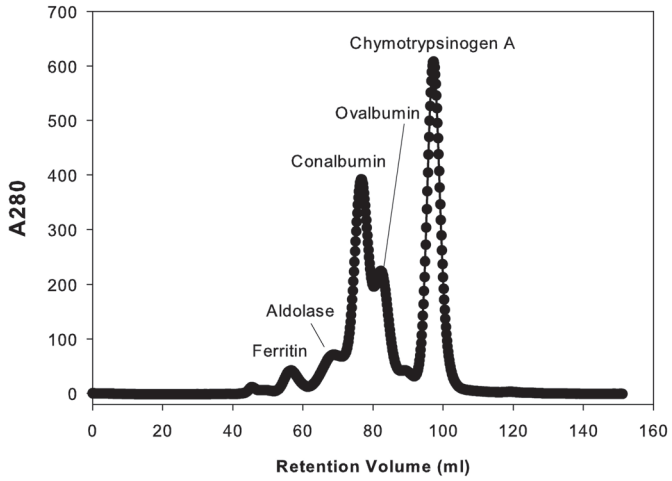

B.

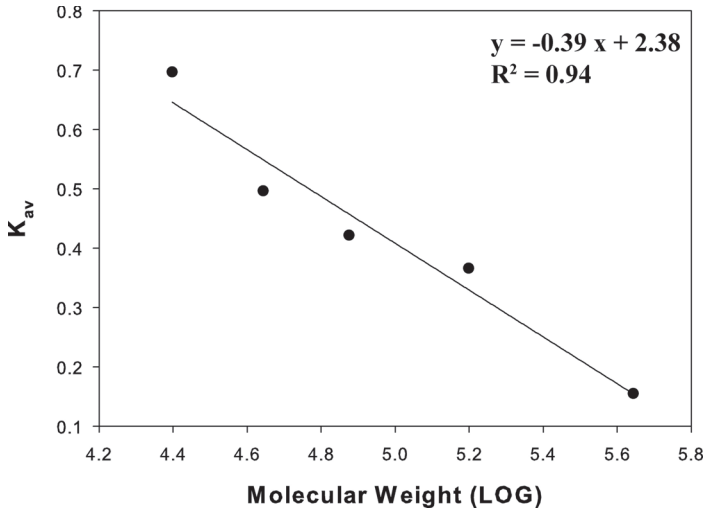

Figure 21: Calibration chromatogram and plot for Superdex 200 column.

A. Calibration chromatogram (A_{280}). 3 mg/ml of high molecular weight (HMW) proteins: ferritin (440 kDa), aldolase (158 kDa), conalbumin (75 kDa), ovalbumin (44 kDa), and chymotrypsinogen A (25 kDa) were loaded and separated on the Superdex 200 column at 0.5 ml/min flow rate. UV-Vis chromatogram at 280 nm was obtained from monitoring the protein's retention volume. **B**. **Calibration curve.** For each protein the partition coefficient (K_{av}) was calculated and plotted against their molecular weight. The calibration curve was used to estimate the MW of proteins between 44 to 440 kDa. The following values were generated to obtain the calibration curve: V_c = 120 ml, V_0 = 45 ml, V_e (ferritin, aldolase, conalbumin, ovalbumin, chymotrypsinogen A) = 56, 68, 76, 82 and 97 ml.

A.

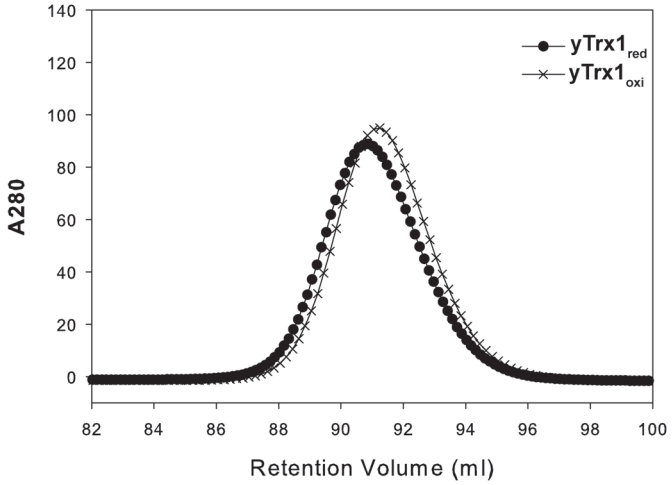

B.

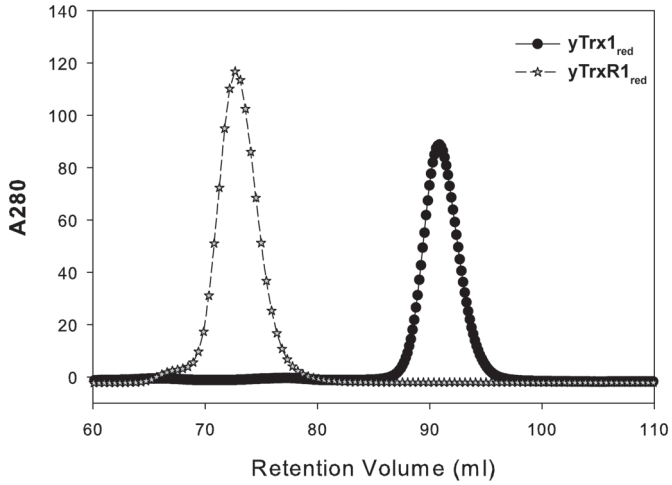

Figure 22: UV-Vis (A_{280}) chromatogram for reduced and oxidized thioredoxin and thioredoxin reductase.

A. Reduced and oxidized chromatograms of thioredoxin. 3 mg/ml of yTrx1 pre-treated to be reduced (10 mM of DTT) or oxidized (500 μM of H_2O_2) was loaded and separated on the Superdex 75 pg column at 0.5 ml/min flow rate. From the calibration curve (Figure 20 B) for the LMW proteins, reduced yTrx1 estimated MW was ~ 11 kDa (V_e = 91 ml) and oxidized yTrx1 estimated MW was ~ 11 kDa (V_e = 90 ml). **B. Reduced thioredoxin and reduced thioredoxin reductase chromatograms.** Similar to figure A, reduced yTrxR1 was loaded and separated on the Superdex 75 column at 0.5 ml/min flow rate. Reduced yTrxR1 estimated MW was ~ 56 kDa (V_e = 72 ml).

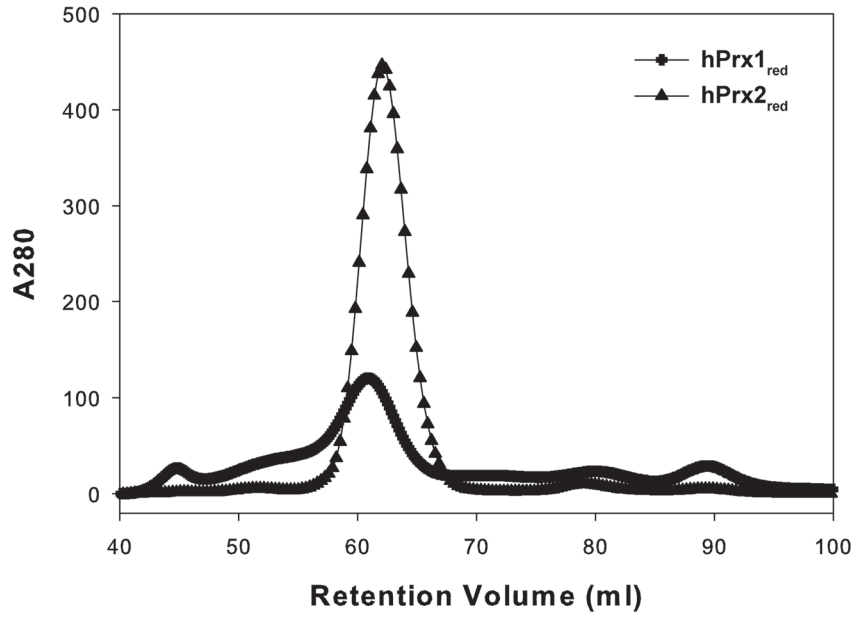

Figure 23: UV-Vis (A_{280}) chromatogram for reduced peroxiredoxin 1 and 2.

Both hPrx1 and hPrx2 were reduced with 10 mM of DTT and then 3 mg/ml of each protein was loaded onto the Superdex 200 column separately. Each protein was eluted at flow rate of 0.5 ml/min. From the calibration plot of the high molecular weight (HMW) proteins the MW was estimated for each protein. Reduced hPrx1 estimated MW was ~ 310 kDa (main peak ~ 60 ml; V_e = 60 ml) and reduced hPrx2 estimated MW was ~ 290 kDa (V_e = 62 ml).

Table 2: Summary of characterizing recombinant redox proteins.

The following values were obtained from SDS-PAGE, and SEC for reduced proteins.

Protein	SDS-PAGE (kDa)	SEC (kDa)	Calculated MW from the monomeric sequence (kDa)
yTrx1	11.0	11	11.2
yTrxR1	36.0	56	35.0
hPrx1	25.0	313	22.1
hPrx2	25.0	288	21.7

3.2 Setting up the peroxidase activity assay

After characterizing all the redox recombinant proteins, my next objective was to set up the peroxidase activity assay. The overall goal was to set up the assay to determine if the catechol derivatives could inhibit hPrx1, hPrx2, and hPrx5. I first started with setting up with the assay for hPrx5 and followed by hPrx1 and hPrx2.

To monitor the peroxidase activity of hPrx, it is through a coupling reaction via the oxidation of NADPH with yTrx1 and yTrxR1 as electron transporters (Figure 24). For hPrx activity to be measured properly, hPrx must be maintained at rate limiting conditions[45]. To achieve hPrx under rate limiting conditions, yTrx1 and yTrxR1 must be sustained in excess and therefore, the ideal conditions for yTrx1 and yTrxR1 were first assessed. The concentrations of yTrxR1 was fixed and a range of yTrx1 concentrations were evaluated since yTrx1 concentration was suggested to be 10 fold higher to hPrx and yTrxR1 concentrations from past assay protocols [83]. The assay conditions used to determine the best concentration ratio between yTrx1 and yTrxR1 was 0.5 μM hPrx5, 2 μM yTrxR1, 200 μM NADPH, 100 μM H_2O_2. Figure 25 shows the Michaelis-Menten plot for the peroxidase reaction rates monitored against increasing concentrations of yTrx1 used. The K_m and V_{max} values were extrapolated and examined to assist in choosing the concentrations of yTrx1. The V_{max} was ~ 8 μmol $min^{-1}mg^{-1}$ and a K_m was ~ 10 μM of yTrx1. The concentration of 15 μM for yTrx1 was chosen, since the concentration was within the range when the peroxidase react was at it's V_{max} and would ensure the reaction between yTrx1 and yTrxR1 was balanced and maintained at a continuous reaction rate. Also, under these experimental conditions ~10% of NADPH was only oxidized and therefore 200 μM of NADPH was selected as there was an excess of NADPH present to monitor the reaction [83]. A similar approach was taken for hPrx1 and hPrx2 to determine the ideal concentrations of yTrx1 and yTrxR1 and the same conditions were achieved with yTrxR1 at 2 μM and yTrx1 at 15 μM.

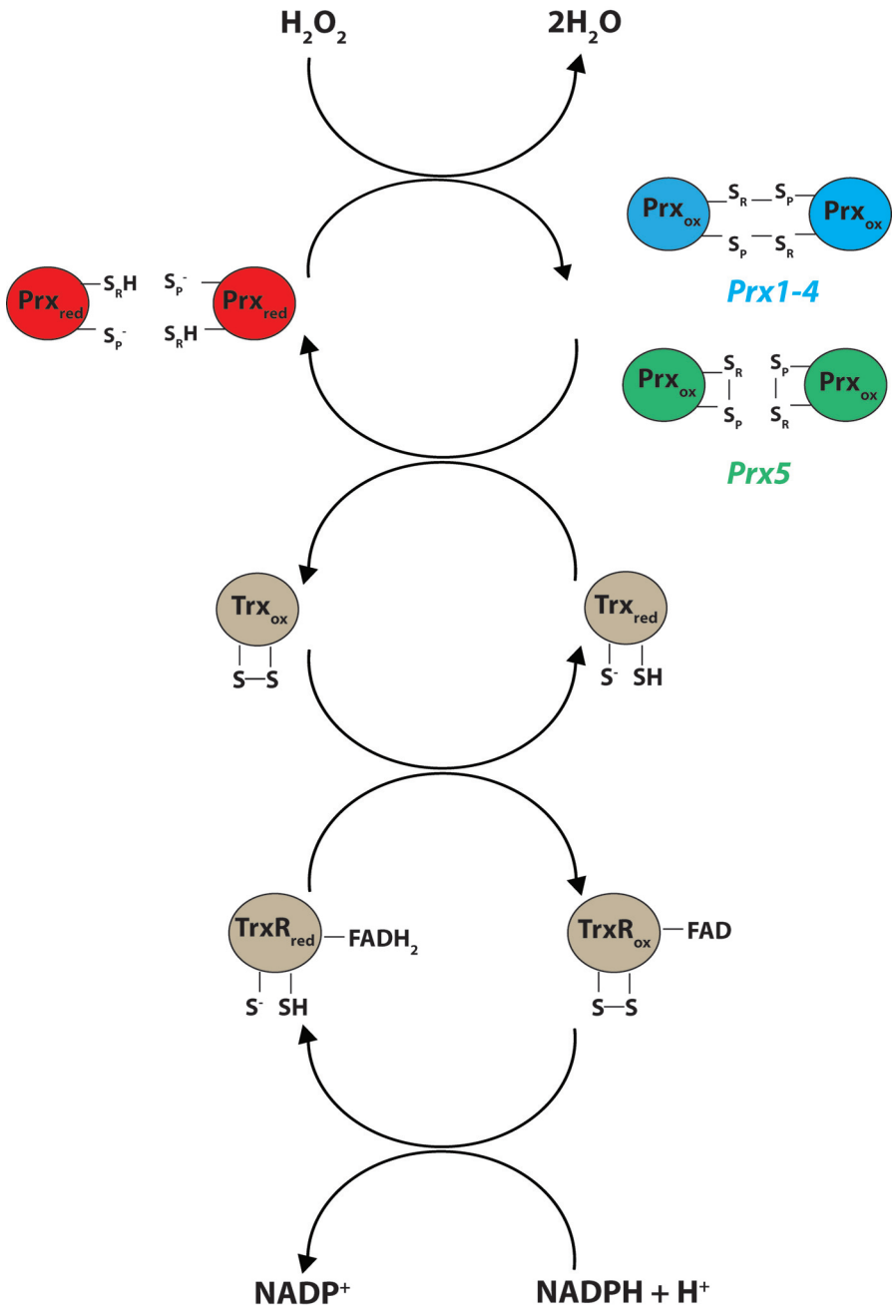

Figure 24: Schematic of the peroxidase activity reaction

Here Prx reduces hydrogen peroxide (H_2O_2) cycling through its reduced and oxidized states signified by chemical transformation of the peroxidatic cysteine sulfur (S_P) and resolving cysteine sulfur (S_R). When Prxs are reduced S_P-S_R they can either form intermolecular (Prx1-4 blue) or intramolecular (Prx5 green) disulfide bonds. The peroxidase reaction is measured through a coupling reaction with other redox proteins thioredoxin (Trx) and thioredoxin reductase (TrxR) also undergoing redox changes via the oxidation of NADPH at 340 nm. The figure is reproduced under permission and adapted from Lu and Holmgren, 2013 [84].

Next, the concentration of hPrx5 was optimized to properly and accurately measure the initial phase of the peroxidase reaction. A concentration rate of hPrx5 was examined under the following assay conditions 2 μM yTrxR1, 15 μM yTrx1, 200 μM NADPH and 100 μM H_2O_2. To determine the ideal concentration of hPrx5 to use, the peroxidase reaction rate was plotted against the concentration of hPrx5 shown in Figure 26. The plot shows the peroxidase reaction rate was proportional to the concentration of hPrx5 represented by a linear plot trend. Also, the plot trend indicated the yTrx1 to yTrxR1 conditions were well maintained and only hPrx5 reaction was being influenced. Therefore, in evaluating the plot 0.15 μM of hPrx5 was chosen as the ideal concentration to measure the peroxidase reaction. Whereas, for hPrx1 and hPrx2 the concentration selected was 0.38 μM in which the reaction rate was equivalent to hPrx5 activity. Overall, the following conditions used to monitor the peroxidase reaction was 0.15 μM hPrx5, 0.38 μM hPrx2, 0.38 μM Prx1, 2 μM yTrxR1, 15 μM yTrx1, and 200 μM NADPH.

Depending on the interest for monitoring the peroxidase assay, the H_2O_2 concentration range can be varied. Specifically, in measuring the hPrxs inhibition properties against the catechol derivatives, it was best to work around the K_m of H_2O_2 (substrate) for the hPrxs [45]. As a result, the K_m for H_2O_2 was determined for all the hPrxs. Under the following conditions 0.15 μM hPrx5, 2 μM yTrxR1, 15 μM yTrx1 and 200 μM NADPH, the ideal concentration of H_2O_2 was examined to measure the peroxidase reaction. Figure 27 shows the assays data plotted, with the reaction rate against the concentration of H_2O_2 to achieve a Michaelis-Menten plot and the K_m and V_{max} values were determined from the plot. hPrx5 had a V_{max} of ~ 12 μmol $min^{-1}mg^{-1}$ and a K_m of ~ 25 μM. For hPrx1 and hPrx2, their activity was similar with a V_{max} of ~ 1 μmol $min^{-1}mg^{-1}$ and a K_m ~ < 5 μM (See Table 3). In measuring hPrx1 and hPrx2 K_m for H_2O_2, was challenging as the typical 2-Cys Prx are more sensitive to lower H_2O_2 concentrations and there were limitations on the sensitivity on the spectrophotometer to monitor the differences. Therefore the K_m of H_2O_2 for hPrx1 and hPrx2 was not accurately

measured compared to hPrx5. Figure 28 A and B shows the difference in reaction activity between hPrx5 and hPrx1with increasing H_2O_2 concentrations.

Additionally the k_{cat} values representing the catalytic turnover rate and k_{cat}/K_m values representing the catalytic efficiency were determined. hPrx5 had a k_{cat} of ~ 3 s^{-1} and k_{cat}/K_m of ~ 9 x 10^4 M^{-1} s^{-1}. hPrx1 and hPrx2 had similar values with k_{cat} of ~ 2 s^{-1} and k_{cat}/K_m was not applicable due to inaccuracies in the K_m determination (See Table 3). Overall, to monitor half maximal (IC_{50}) inhibition assay the following conditions were used: 0.15 µM hPrx5, 0.38 µM hPrx1/2, 2 µM yTrxR1, 15 µM yTrx1, 200 µM NADPH and 25 µM H_2O_2. The IC_{50} assay was initially conducted for hPrx5 distinguishing the catechol derivatives could inhibit. Therefore, to compare the inhibitory actions of the catechol derivatives the same assay conditions were required to be maintained for hPrx1 and hPrx2, and the H_2O_2 was sustained at 25 µM.

3.3 Article 1: "Predicting and understanding the enzymatic inhibition of human peroxiredoxin 5 by 4-substituted pyrocatechols combining funnel-metadynamics, solution NMR and steady-state kinetics"

The full version of article 1 is in section 4 pg 107.

3.3.1 Catechol derivatives bind to hPrx5 by ^{15}N-HSQC and FM simulations

To provide further insight on the binding interaction of the catechol derivatives to hPrx5, ^{15}N-HSQC NMR and funnel-metadynamics (FM) computational simulations were used. Laura Troussicot and Jean-Marc Lancelin carried out these experiments assessing the hPrx5-catechol derivative binding interaction and affinities.

Briefly as mentioned in the article, the ^{15}N-HSQC NMR experiments determined the key amino acids on hPrx5 involved when interacting and binding to the catechol derivatives. In which, hPrx5 was exposed to increasing concentrations of the specific catechol derivative and the N-H cross peaks chemical shift perturbation (CSP) were monitored examining the 2D^{1}H-^{15}N NMR spectra. hPrx5 was found to interact with all the catechol derivatives with the

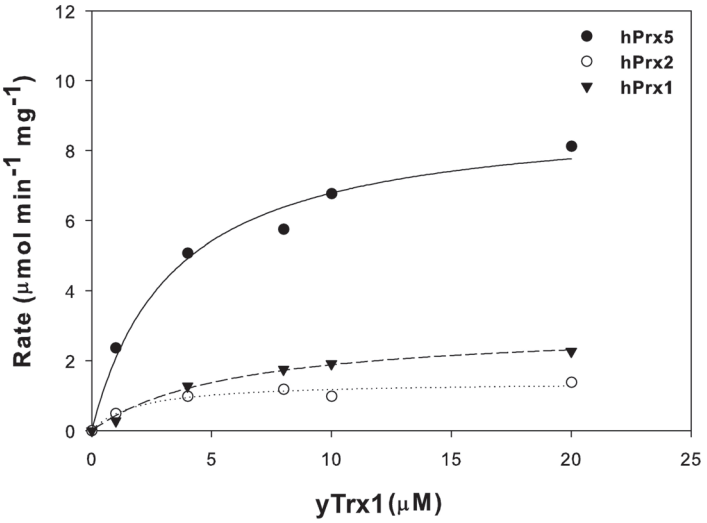

Figure 25: Determining the ideal ratio concentration between yTrx1 and yTrxR1.

Plotted is the rate as a function of the concentration of yTrx. The plots show with increasing concentrations of yTrx1 that the reaction rate reaches a maximum at ~ 8 μM of yTrx1. To maintain hPrxs at rate limiting conditions, yTrx1 at 15 μM and yTrxR1 at 2 μM were chosen to sustain saturated reaction rate. Since after ~ 10 μM of yTrx1 shown here, the reaction rate is well regulated. The following conditions shown here are: 0.15 μM hPrx5, 0.38 μM hPrx 2, 0.38 μM Prx1, 2 μM yTrxR1, varying μM yTrx1, 200 μM NADPH, 25 μM H_2O_2.

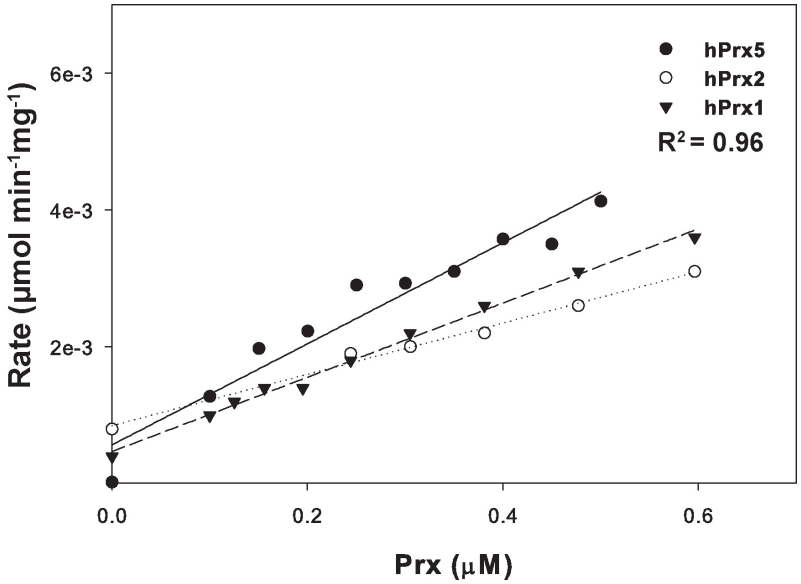

Figure 26: Determining the ideal concentration of hPrxs

Plotted is the reaction rate versus varying concentrations of hPrxs. Increasing the concentration of hPrx the reaction rate increased following a linear trend. To measure the initial phase of the peroxidase reaction 0.15μM hPrx5, 0.38 μM hPrx2 and 0.38 μM hPrx1 were chosen. The assay conditions shown are: 15 μM Trx, 2 μM TrxR, 200 μM NADPH, 25 μM H_2O_2 and varying concentrations of hPrx5, hPrx2, and hPrx1.

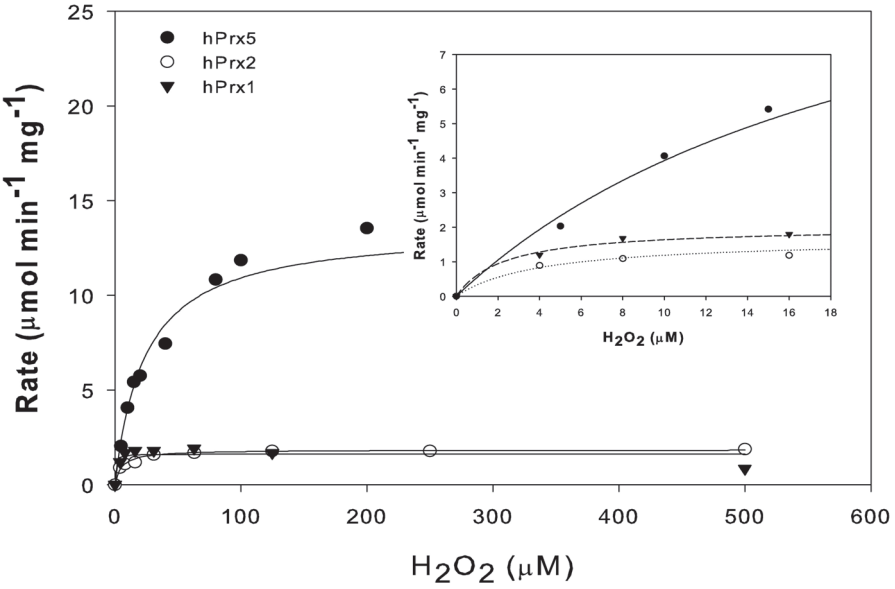

Figure 27: Determining hPrxs K_m for H_2O_2.

Plotted are the reaction rates for hPrx1, hPrx2, and hPrx5 against increasing concentrations of H_2O_2 fitting to a Michaelis-Menten curve to determine K_m of H_2O_2. Increasing concentration of H_2O_2 the peroxidase reaction rate increased and eventually reaches a maximum rate. Figure 28 shows the plots obtained in monitoring the peroxidase showcasing the data in a different representation. Overall, hPrx5 was determined to have a K_m of ~ 25 μM and V_{max} of 8 μmol min^{-1} mg^{-1}, and hPrx2 and hPrx1 had a K_m < ~ 5 μM and a V_{max} of ~ 1 μmol min^{-1} mg^{-1}. The assay conditions shown are: 0.15 μM hPrx5, 0.38 μM hPrx2 and hPrx1, 15 μM yTrx1, 2 μM yTrxR1, 200 μM NADPH, and varying concentrations of H_2O_2.

A.

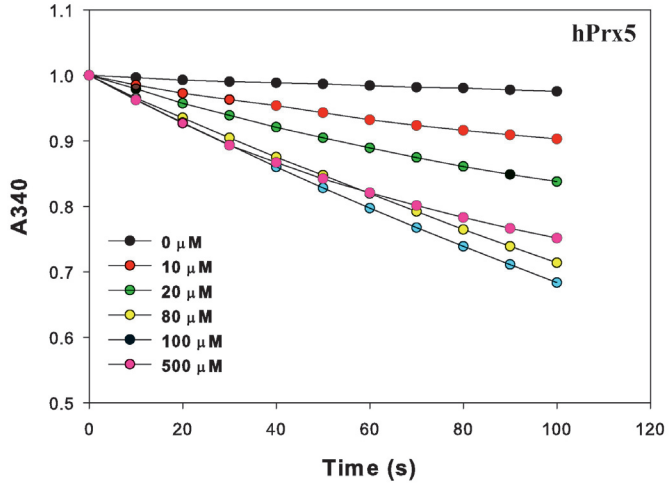

B.

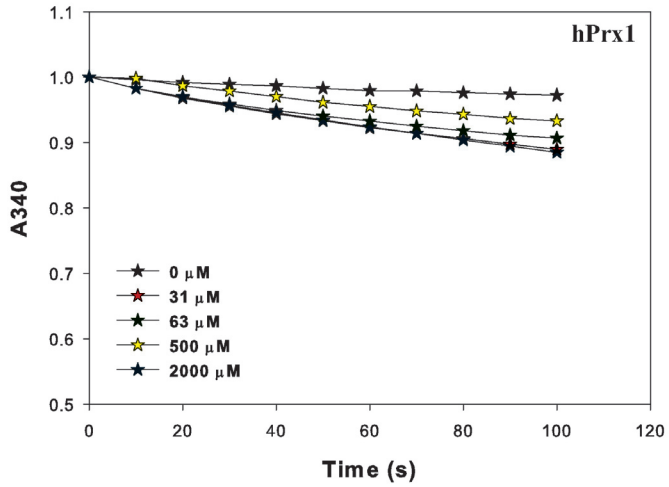

Figure 28: Monitoring hPrx5 and hPrx1 peroxidase activity with increasing H_2O_2 concentrations.

Plotted is the A_{340} of NADPH against time monitoring the peroxidase activity of the hPrxs. The reaction activity is shown for hPrx5 **(A)** and hPrx1 **(B)** against time with a varying concentration of H_2O_2. The plots show with increasing concentration of H_2O_2, the reaction rates of the hPrxs are increased illustrated by more NADPH oxidized. The assay conditions shown here are: 0.15 µM hPrx5, 0.38 µM hPrx1, 15 µM yTrx1, 2 µM yTrxR1, 200 µM NADPH and varying concentrations of H_2O_2 (0-500 µM).

Table 3: Comparison of the peroxidase activity for hPrx1, hPrx2, and hPrx5.

Here is a summary of the catalytic activity parameters measured for the peroxidase activity for hPrx5, hPrx2, and hPrx1. Comparing the activities, hPrx1 and hPrx2 had similar catalytic activities in contrast to hPrx5 (values are extrapolated from Figure 27). Note: the rate values from the graph are in μmol min^{-1} mg^{-1} but in the table the values are represented as μmol L^{-1} min^{-1}. The protein concentrations used are 0.38 μM for hPrx1/2 and 0.15 μM for hPrx5.

	hPrx1	**hPrx2**	**hPrx5**
K_m **(μM)**	<5.00 ± 2.50	<5.00 ± 2.50	24.24 ± 3.23
V_{max} **(μmol L^{-1} min^{-1})**	15.37 ± 2.86	13.28 ± 2.64	38.62 ± 1.45
k_{cat} **(s^{-1})**	0.67 ± 0.12	0.58 ± 0.12	4.29 ± 0.16
k_{cat}/K_m	N/A	N/A	(9.63 ± 0.55) x 10^4

amino acids mainly in the active site. The CSPs were plotted against the ratio concentrations of the catechol derivatives to hPrx5 and were fitted to a square root fit. A K_d value was obtained for hPrx5 binding affinity to each of the catechol derivative. 4-*tert*-butylcatechol had the greatest binding affinity to hPrx5 and the amino acids Ala42, Thr44 and Ser48 were determined to contribute the most in binding interaction with a K_d value of 0.19 ± 0.03 mM (see article Figure 6 pg 128).

FM simulations were used to monitor the dynamic binding events of hPrx5 and the catechol derivatives in solution. A funnel was used to assist in enhancing the binding events measurements specifically within the active site region of hPrx5 as a homodimer. The binding conformations of the catechol derivatives to hPrx5 were determined. Also, a quantitative estimation of the hPrx5-catechol derivative complex absolute binding free-energy value ($\Delta G_b°$) was obtained and was converted into a binding affinity value (K_d). FM was used to simulate both hPrx5 alone and a mimicked hPrx5-H_2O_2 complex to assess the possible binding conformations the catechol derivatives could undergo to inhibit hPrx5 peroxidase activity within the active site region. Modeling the binding interactions, all the catechol derivatives had a binding affinity to both hPrx5 and hPrx5-H_2O_2 complex but preferred to bind to hPrx5 alone within the active site. 4-*tert*-butylcatechol was found to bind the best to hPrx5 than catechol and 4-methylcatechol with a K_d of 0.11 mM. The improved binding affinity for 4-*tert*-butylcatechol was contributed from forming H-bonds and along with more pronounced Van der Waal interactions than seen in catechol and 4-methylcatechol (see Table 4). 4-*tert*-butylcatechol bound to hPrx5 active site involved Thr44, Pro45, Leu119, Ile119, Phe118, Arg127, and Phe79 (B), Pro20 (B), Gly19 (B) from the neighbouring monomer (see Figure 4 & 5 in the article pg 123 & 127). Overall, FM simulations were valuable to assist in interpreting the binding interaction at the microscopic level along with the NMR techniques used. The results from both methods complied with each other too. Identifying the catechol derivatives bound to hPrx5, the inhibitory properties were then examined.

Table 4: Summary of the catechol derivatives binding affinities to hPrx5 determined by ^{15}N-HSQC and FM simulations.

Here is a summary of the data collected from both experimental and simulated approaches to monitor the binding interactions and affinities of the catechol derivatives to hPrx5.

	FM Simulations		^{15}N-HSQC
	K_d for hPrx5 (mM)	**K_d for hPrx5-H_2O_2 (mM)**	**K_d (mM)**
Catechol	6.90 ± 2.10*	40.00 ± 30.00	4.50 ± 0.60*
4-methylcatechol	0.90 ± 0.40*	69.00 ± 26.00	1.00 ± 0.20*
4-*tert*-butylcatechol	0.11 ± 0.09	0.80 ± 0.70	0.19 ± 0.03

* Data from Troussicot *et al.* 2015 [32].

3.3.2 Catechol derivatives inhibit hPrx5 peroxidase activity

Briefly as shown in the article, the catechol derivatives inhibitory properties against hPrx5 were evaluated by an IC_{50} assay. This assay was conducted with increasing concentrations of the catechol derivatives and the peroxidase activity of hPrx5 was monitored. The half-maximal inhibitor concentration (IC_{50}) value was obtained and the catechol derivatives inhibitory potency could be determined by ranking the IC_{50} values. As mentioned in section 1.10.1 pg 33, preliminary have already determined catechol and 4-methylcatechol inhibited hPrx5, however, the conformational MMOA was not further explored[18]. Also, 4-*tert*-butylcatechol was recently identified to bind to hPrx5 but there was no evidence it could inhibit[27,32]. This study examined the inhibition properties of catechol, 4-methylcatechol and 4-tert-butylcatechol against hPrx5. Figure 29 is an example measuring the peroxidase activity of hPrx5 in the presence of increasing concentrations of 4-*tert*-butylcatechol with the peroxidase reaction rate decreasing. In all, the IC_{50} assay determined the three-catechol derivatives could inhibit hPrx5 peroxidase activity. Ranking the catechol derivatives by their IC_{50} values, 4-*tert*-butylcatechol was found to be the most potent inhibitor (See Table 5). Shown in the article are the IC_{50} curves all three catechol derivatives (article Figure 7 pg 131). The IC_{50} curves display that all the catechol derivatives inhibit ~ 80% of hPrx5 with some residual activity of hPrx5 still present. Overall this study showed the catechol derivatives could inhibit hPrx5 peroxidase activity. Also, other hPrxs have been implicated in the post-ischemic inflammation cascade (also hPrx1, hPrx2 and hPrx6). The inhibition properties of the catechol derivatives to hPrx1 and hPrx2 were studied and the results will follow in section 3.4.3 pg 104.

3.3.3 Catechol derivatives specifically bind and inhibit hPrx5

In determining the catechol derivatives inhibit hPrx5, there was a possibility the catechol derivatives could also inhibit through forming free radicals or bind to Trx system components (yTrx1, yTrxR1, NADPH) as the reaction is measured through a coupling

reaction. Therefore, the redox MMOA was measured utilizing ^{1}H and ^{15}N-HQSC NMR spectroscopy methods (data shown in supplementary section).

^{1}H NMR spectroscopy was used to analyze the chemical reaction by breaking down the reaction and individually adding in each reaction component monitoring any changes in the chemical shift pattern. Figure 30 pg 82 shows the ^{1}H NMR spectra recorded over the course of the reaction for catechol present. First, 1 mM catechol was added to the NMR tube and a ^{1}H spectrum was recorded. Sequentially, each of the reactions components (NADPH, H_2O_2, yTrx1, yTrxR1, and hPrx5) was added and a ^{1}H spectrum was recorder to monitor the chemical reaction. The ^{1}H spectra shows the aromatic protons of catechol were observed at ~ 6 ppm chemical shift region and upon the addition of NADPH, its protons were observed in the ~ 7.5 to 8 ppm and ~ 5.5 ppm regions. However, none of the recombinant redox proteins were observed due to their low concentration and had broad signals as the reaction was carried under the enzymatic conditions. Overall in examining the ^{1}H spectrum, there were only changes to the chemical shift pattern upon the addition of yTrxR1 and hPrx5. The changes observed represented NADPH proton signals becoming slightly reduced, which signified hPrx5 reduced H_2O_2 and NADPH becoming oxidized with the catalytic reaction happened. As a result, there were no changes to the proton signals for catechol observed since no chemical reaction detected the transformation of catechol into other organic compounds or free radicals, suggesting there were no interactions of catechol to hPrx5 catalytic components. This was completed for 4-methylcatechol and 4-*tert*-butylcatechol as well and neither of them were detected to be chemically transformed too.

Additionally, ^{15}N-HSQC NMR spectroscopy was used to further assess if the catechol derivatives had any binding interaction to yTrx1 and yTrxR1. Both yTrx1 and yTrxR1 were isotope labelled with ^{15}N and ^{15}N-HSQC spectra were recorded for each of the proteins in the absence and in the presence of each of the catechol derivatives. Figure 31 is an example of the ^{15}N-HSQC spectra recorded for ^{15}N-yTrx1 in the absence and presence of catechol. Both spectra in the absence and presence of catechol for ^{15}N-yTrx1 were superimposed, and there

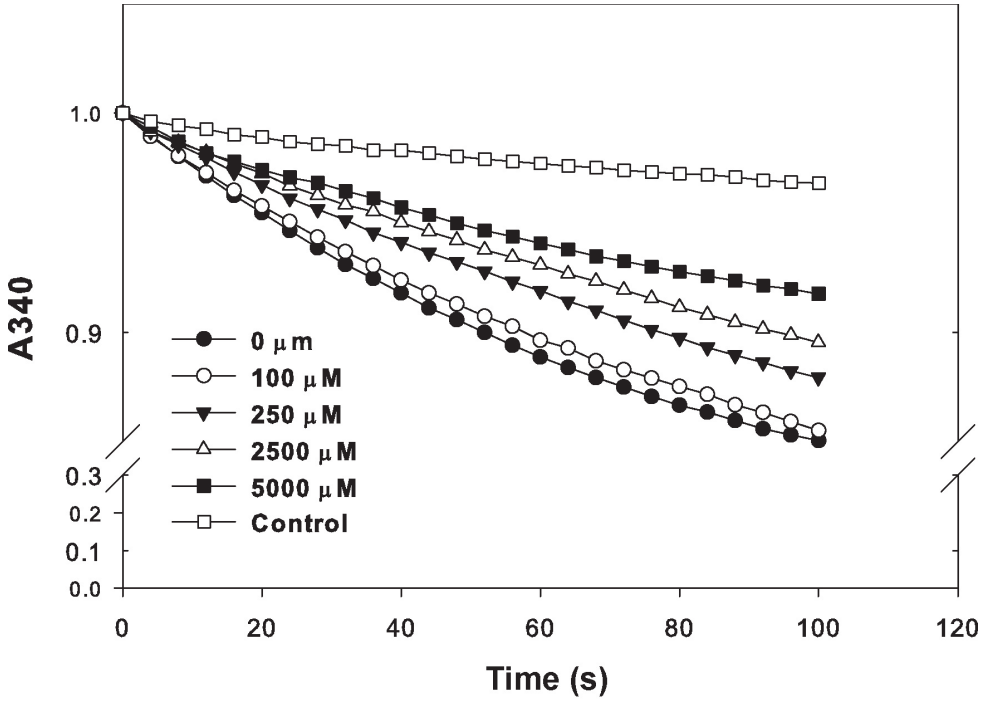

Figure 29: 4-*tert*-butylcatechol inhibits hPrx5 peroxidase activity.

hPrx5 peroxidase activity was monitored by the Trx system (yTrx1, yTrxR1 and NADPH) as electron donor via the absorbance at 340 nm. Shown here is hPrx5 peroxidase activity being inhibited when exposed to increasing concentrations of 4-*tert*-butylcatechol (0-5000 μM; control no Prx5 present). Overall, 4-*tert*-butylcatechol was determined to be an inhibitor to hPrx5. The experimental conditions were: 0.15 μM hPrx5, 15 μM yTrx1, 2 μM yTrxR1, 200 μM NADPH, 25 μM H_2O_2 in PBS pH 7.0 with 1 mM EDTA at 23 °C monitoring absorbance at 340 nm.

Table 5: IC_{50} values for the catechol derivatives against hPrx5.

Here shown are the IC_{50} values obtained when monitoring the inhibitory effects of the catechol derivatives against hPrx5. The data is represented as the mean ± standard error for three independent experiments.

	IC_{50} (mM)
Catechol	3.73 ± 0.85
4-methylcatechol	0.82 ± 0.14
4-*tert*-butylcatechol	0.25 ± 0.06

were no chemical shift perturbations observed for yTrx1. Therefore confirming yTrx1 does not have binding interactions to catechol. This was completed for 4-methylcatechol and 4-*tert*-butylcatechol, confirming yTrx1 to not interact with these ligands too. Whereas, for yTrxR1 as mentioned previously, a ^{15}N-HSQC spectrum could not be obtained and therefore, STD NMR spectroscopy was used to characterize any potential binding affinity of the catechol derivatives to yTrxR1. Figure 32 is an example for the interaction of catechol to yTrxR1 examined. Comparing the ^{1}H and ^{1}H STD spectra, there was no STD signals observed for catechol and this indicated there are no interactions between catechol and yTrxR1. This was completed for the other catechol derivatives with similar results and indicated there were no binding interactions to yTrxR1. Overall, all the catechol derivatives were determined to not bind hPrx5 peroxidase components or become chemically transformed when monitoring the hPrx5 peroxidase activity. Consequently, the catechol derivatives indeed inhibit hPrx5 specifically.

3.3.4 Catechol derivatives inhibit hPrx5 in a partial mixed type non-competitive manner

Upon determining the catechol derivatives inhibit hPrx5, their conformational inhibition MMOA was investigated. Inhibitors can inhibit enzymes through the basic competitive, non-competitive and/or uncompetitive manners. As briefly explained in the article, the conformational inhibition mechanism was examined using five concentrations of the catechol derivative (above and below the IC_{50} value) against range of H_2O_2 concentrations (0-500 μM). The conformational inhibition MMOA was first assessed by analyzing changes in the V_{max} and K_m values through graphical methods. Two different graphical methods were applied: the Hanes-Woolf (linear) and the Michaelis-Menten (non-linear), to ensure the trends analyzed were consistent. Figure 33 shows the Michaelis-Menten plots (rate versus [H_2O_2]) and Figure 34A-C shows the Hanes-Woolf plots ([H_2O_2]/rate versus [H_2O_2]). Table 6 shows the K_m and V_{max} extrapolated from the Michaelis- Menten and Hanes-Woolf plots. For both

graphical methods, the trends were consistent with the K_m values increasing and the V_{max} values decreasing with increasing catechol derivative concentrations. Therefore, the catechol derivatives inhibit hPrx5 was in a non-competitive mechanism. This conformational MMOA indicates the inhibitor can inhibit both the free enzyme (*E*) and the enzyme-substrate complex (*ES*). However, to further assess the conformational MMOA, the inhibitory dissociation constant values (K_i and K_i') were determined as there are various subtypes of non-competitive inhibition mechanism and this would provide details how the inhibitors operate.

Initially, linear regression fitting methods were used to determine the inhibitory dissociation constant values. The K_i value established by plotting the K_m/V_{max} versus the inhibitor concentration and represents when the inhibitor binds just to *E*. Whereas the K_i' was extrapolated from plotting the $1/V_{max}$ versus the inhibitor concentration and represents when the inhibitor binds to the *ES* complex. Figure 34A-C (middle and lower plots) show the graphical plots generated. In examining all the plots and the K_i values, the $K_i' > K_i$ indicating the catechol derivatives preferred to bind and inhibit *E* instead of the *ES* complex. However, in examining the K_i and K_i' plots for catechol, the linear regression fitting did not fit well (curvature to the plot points) suggesting the inhibition model could be more complex than just a non-competitive model. Therefore, a non-linear regression fitting method was used to further examine the inhibition model.

The software program DynaFit was used to determine the best inhibition model for the catechol derivatives against hPrx5 through non-linear fitting methods [72]. Several types on inhibition models were tested (competitive, mixed type non-competitive, partial mixed type, dual site partial mixed type) fitting the data to determine the ideal conformational MMOA. Shown in the article, Figure 8 pg 132, are the inhibition models determined by DynaFit. Both 4-methylcatechol and 4-*tert*-butylcatechol were determined to fit partial mixed type non-competitive model. Figure 35 is a schematic of the conformational MMOA. The both

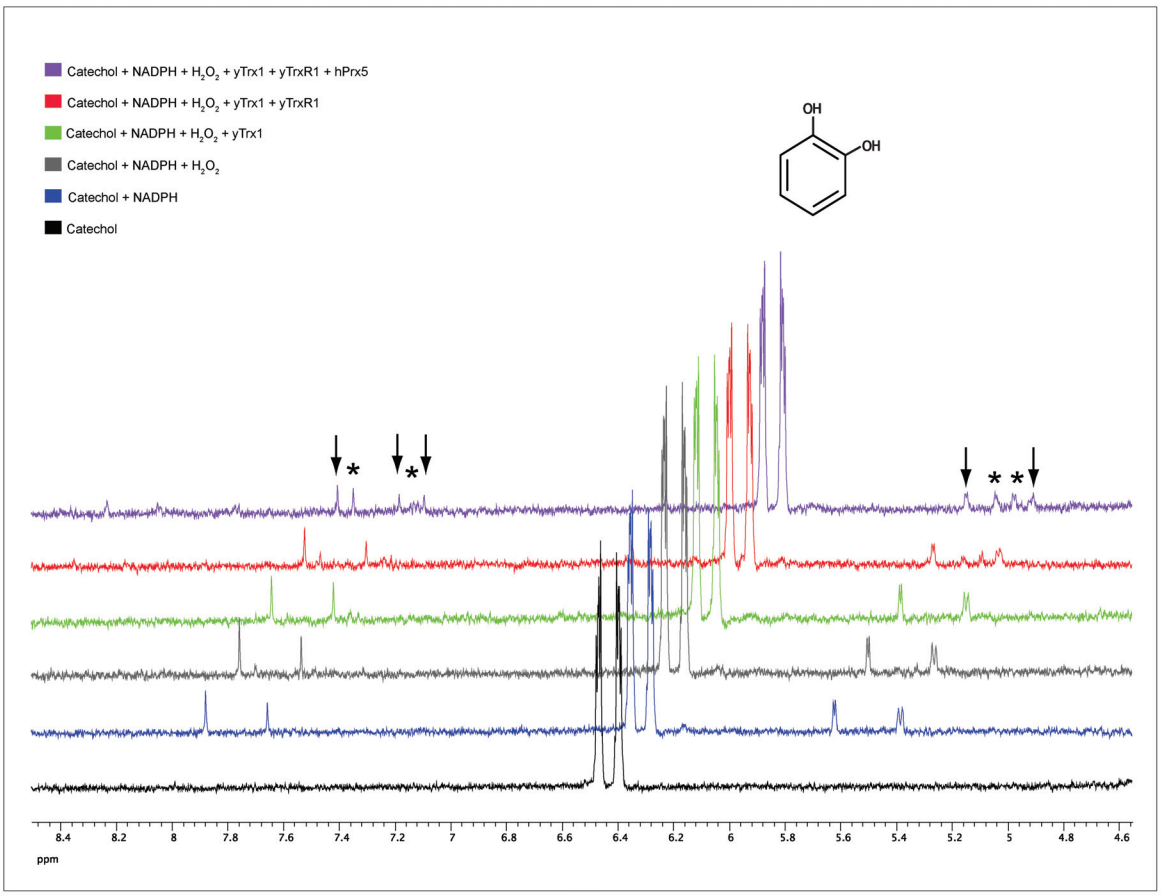

Figure 30: ^{1}H NMR spectra for the peroxidase reaction in the presence of catechol

hPrx5 reaction was broken down sequentially with the addition of each reaction component (NADPH, H_2O_2, yTrx1, yTrxR1, and hPrx5) with catechol present (shown in the aromatic region ~6.5 ppm) to monitor any chemical transformations. The reaction components were added and incubated for 5 minutes at room temperature followed by a 1D ^{1}H NMR spectrum recorded on a 600 MHz NMR spectrometer at 28°C. The only chemical reaction monitored was the oxidation of NADPH. The signals of NADPH are indicated with vertical arrows and those of $NADP^+$ by an asterisk. NMR assignments for NADPH and $NADP^+$ were taken from BMRB entries 55 and 263. Overall, catechol was neither transformed in the presence of the different reagents or during the enzymatic reaction. The experimental conditions shown here are: 1 mM catechol, 200 µM NADPH, 25 µM H_2O_2, 15 µM yTrx1, 2 µM yTrxR1, 0.15 µM hPrx5 in PBS with 1 mM EDTA pH 7.0 and 10% D_2O.

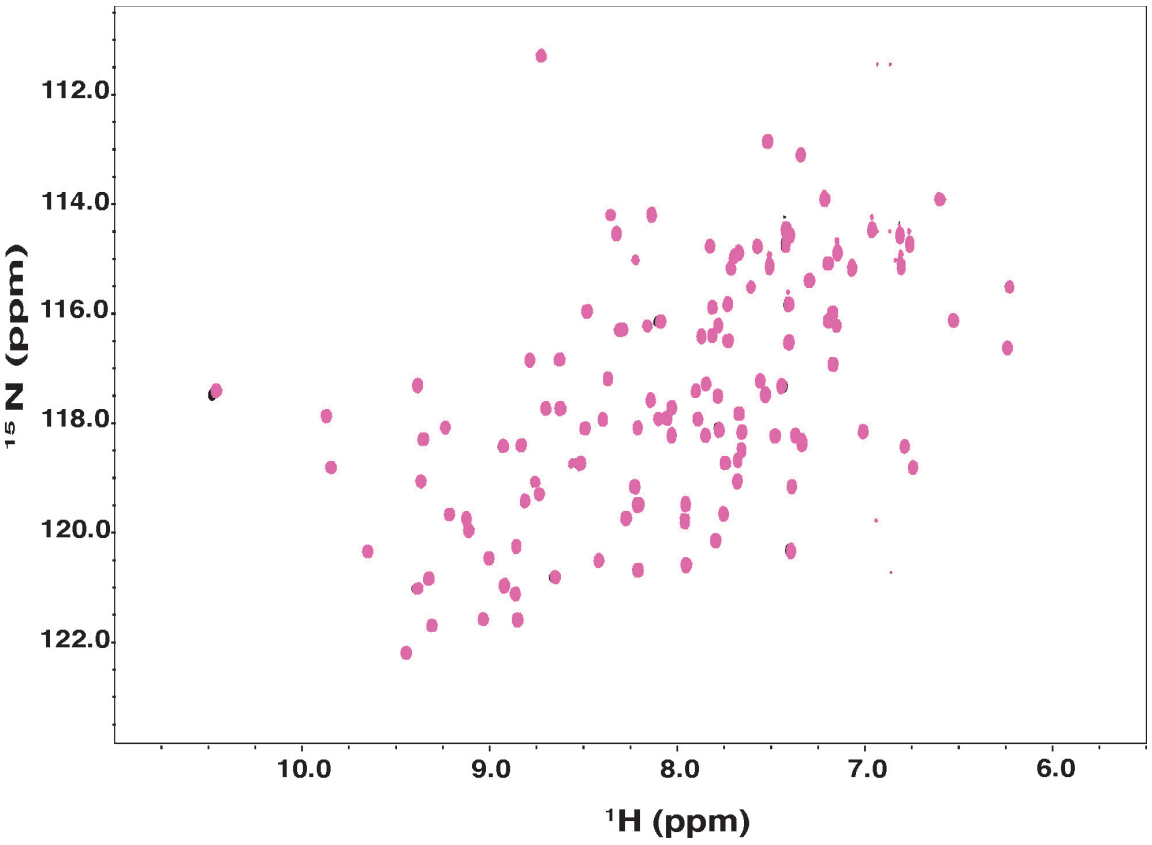

Figure 31: ^{15}N-HQSC spectra of ^{15}N-thioredoxin1 in the absence and presence of catechol.

The ^{15}N-HSQC spectra were used to examine any chemical interactions between catechol and yTrx1. yTrx1 ^{15}N-HSQC was recorded initially without catechol (black) and then after in the presence of 8 mM of catechol (pink). After, both spectra were overlaid and there were no chemical shift perturbations detected. Therefore, indicating yTrx1 does not interact with catechol. The experimental conditions shown here were: 200 µM ^{15}N-yTrx1, 10% D_2O, 1 mM TCEP in PBS pH 7.4 at 28°C on a 600 MHz NMR spectrometer.

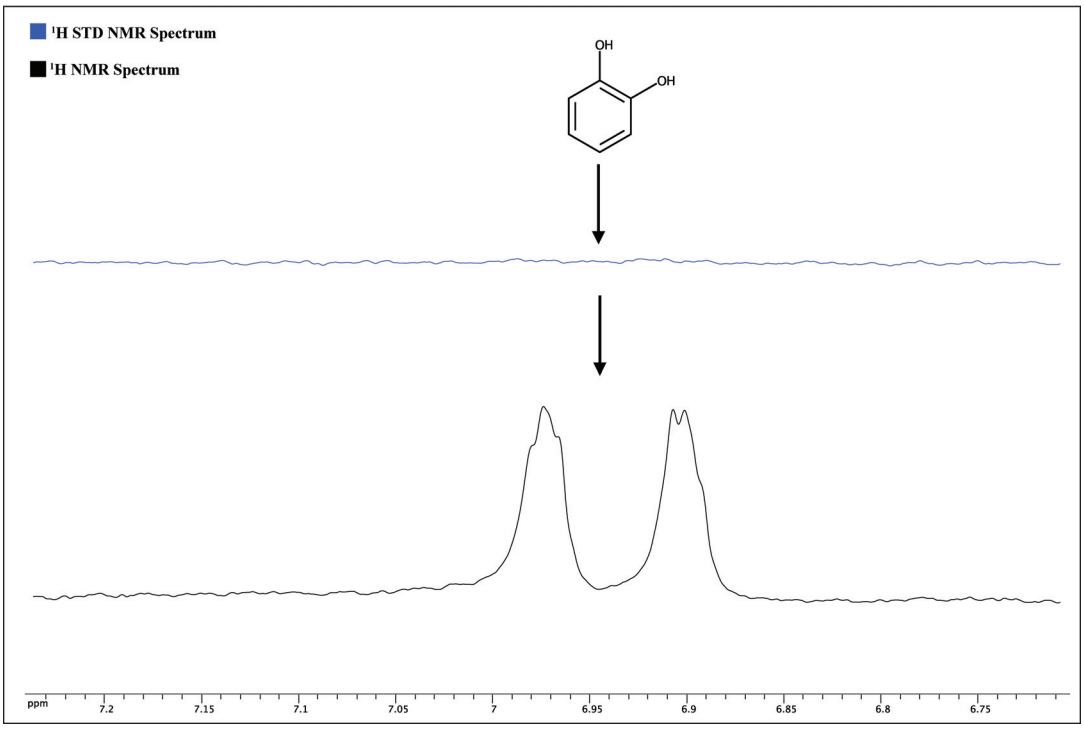

Figure 32: ^{1}H and ^{1}H STD NMR spectra evaluation the interaction of catechol to yTrxR1.

The ^{1}H (black) and ^{1}H STD (blue) spectra obtained when monitoring any possible binding interaction of 1 mM of catechol to 20 µM of yTrxR1. Comparing the spectra, 1D ^{1}H spectrum shows the aromatic protons of catechol at ~ 7-6.9 ppm. However, in the ^{1}H STD spectrum, yTrxR1 was irradiated (below 0 ppm region) and catechol was not bound to yTrxR1 since the saturation was not transferred and no signal was detected in the ~7 ppm region. Therefore, this indicated catechol has no binding affinity to yTrxR1. The experimental conditions shown here were: 20 µM yTrx1R, 10% D_2O in PBS pH 7.4 with 1 mM of catechol at 28°C on a 600 MHz NMR spectrometer.

inhibitors preferred to bind to *E* since K_i'>K_i value. Additionally, with hPrx5 was partially inhibited and H_2O_2 is still reduced through the *ES* and *ESI* complexes represented by k_{cat} and k_{cat}' values. Table 7 shows all the inhibition mechanism values determined to under the model discriminated by DynaFit.

For catechol's conformational MMOA model to hPrx5 it was not as simple to interpret the results from DynaFit. Two inhibitor mechanisms were determined: mixed type and partial mixed type non-competitive for catechol. In evaluating the inhibitory dissociation constants and k_{cat} values (Table 7) for partial mixed type non-competitive model, the K_i and K_i' values determined were within reason with error to 4-methylcatechol and 4-*tert*-butycatechol values. However, for catechol's k_{cat} values, the k_{cat}' value was ~ 0 with a large error indicating there was only one pathway for hPrx5 to reduce H_2O_2 via *ES* complex. Therefore, the pathway for H_2O_2 to be reduced via the *ESI* complex would not exist and would suggest catechol is more likely fit the mixed type non-competitive model. In examining the mixed type non-competitive model, the data did not fit well using DynaFit for catechol (see Figure 35). Additionally, the inhibitory dissociation constant values and the k_{cat} values determined had a larger error. Therefore, this suggested this model does not fit best for catechol (See Table 7 and Figure 36).

Overall, in evaluating catechol's conformational inhibition MMOA determined by DynaFit, catechol was found to inhibit hPrx5 in between both models. However, partial mixed type non-competitive mechanism was the more probable mechanism because when comparing the inhibitory trends observed they were more similar to the other catechol derivatives. Therefore, all the catechol derivatives discovered to inhibit hPrx5 in a partial mixed type non-competitive manner. In which the K_i'>K_i indicating the catechol derivatives prefer to bind and inhibit *E* over the *ES* complex. hPrx5 peroxidase activity is partially impaired and can still reduce H_2O_2 via *ES* or *ESI* complexes.

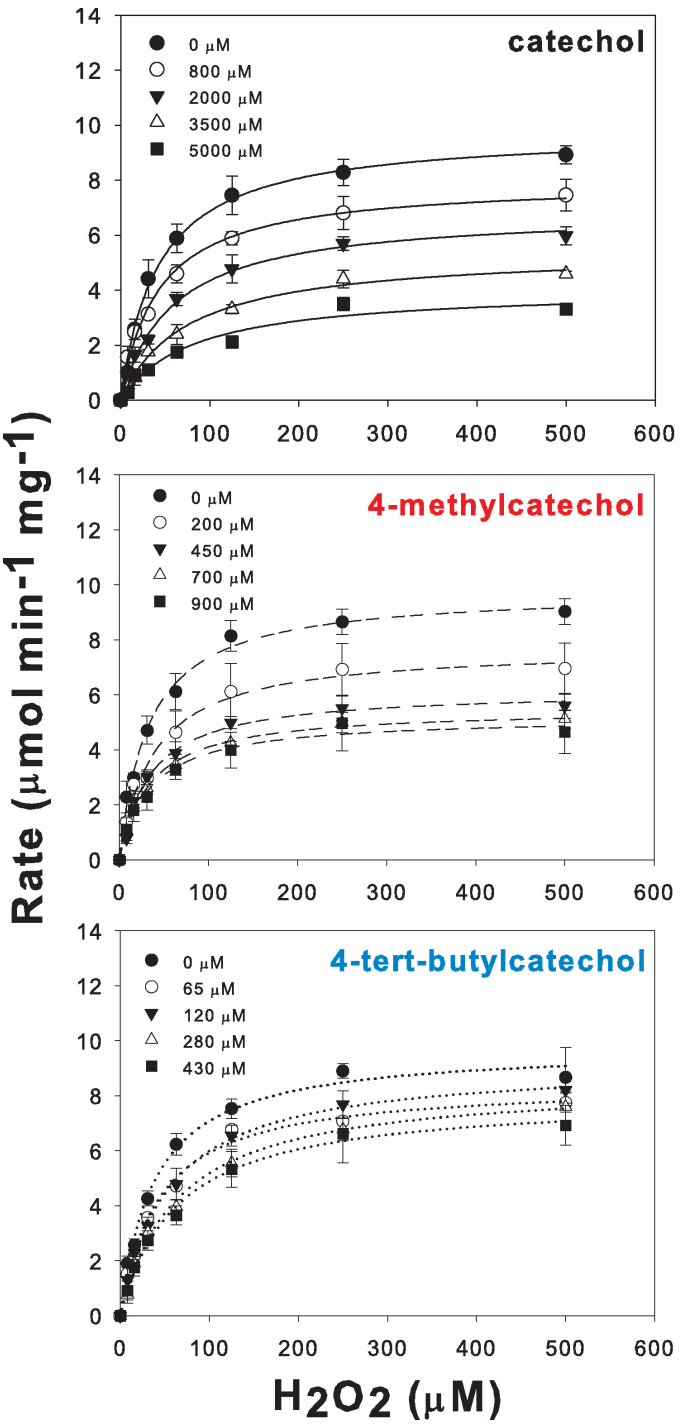

$$v = \frac{V_{max}'\,[S]}{K_m' + [S]}$$

Figure 33: Michaelis-Menten curves for the inhibition of hPrx5 against each catechol derivative.

Plotted are the initial reaction rates (µmol min^{-1} mg^{-1} of hPrx5) for each catechol derivative versus a hydrogen peroxide concentration range (µM). The data was fitted to the Michaelis-Menten equation and V_{max}' and K_m' apparent values were obtained (see **Table 6** pg 90). All three catechol derivatives were determined to inhibit hPrx5 in a non-competitive manner with the V_{max} decreasing and the K_m increasing with increasing inhibitor concentrations. The trends for the V_{max} and K_m complemented the findings with the Hanes-Woolf plot in Figure 34.

A.

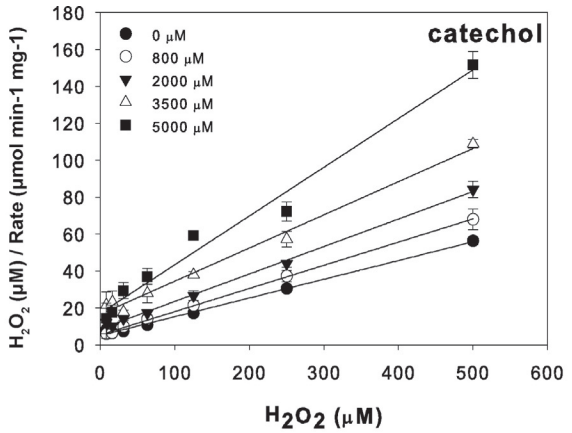

Hanes-Woolf Plot

$$\frac{[S]}{Rate} = \frac{1}{V_{max}}[S] + \frac{K_m}{V_{max}}$$

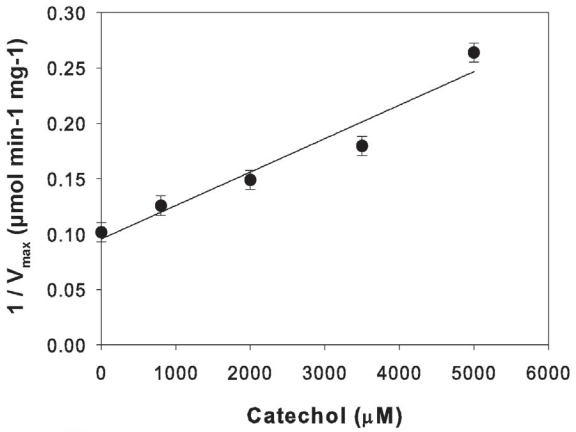

Determine K_i'

$$\frac{1}{V_{max}'} = \frac{1}{K_i' V_{max}}[I] + \frac{1}{V_{max}}$$

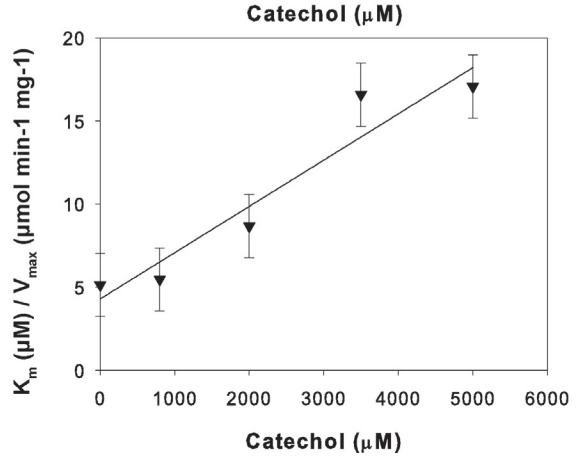

Determine K_i

$$\frac{K_m'}{V_{max}'} = \frac{K_m}{K_i V_{max}}[I] + \frac{K_m}{V_{max}}$$

Figure 34: Inhibition mechanism determined by linear regression fitting methods.

(A) catechol, (B) 4-methylcatechol, and (C) 4-*tert*-butylcatechol. Upper plot: the Hanes-Woolf plot with the [H_2O_2] (µM) /initial rate (µmol min^{-1} mg^{-1}) plotted against [H_2O_2]. The initial rates are expressed in µmol min^{-1} mg^{-1} in reference to the mg of hPrx5. The K_m (µM) and V_{max} (µmol min^{-1} mg^{-1}) values were generated from this plot. Middle plot: The K_i' value was determined from plotting the $1/V_{max}$ versus the inhibitor concentration. Lower plot: The K_i value was determined from plotting K_m/V_{max} versus the inhibitor concentration. Plotting the data it was not always linear, therefore the fitting was not accurate enough to determine the inhibition model. To further improve the inhibition model discrimination, non-linear model fitting methods were conducted using DynaFit. Note: K_m and V_{max} notation in the equations represent 0 µM of the inhibitor and K_m' and V_{max}' notation in the equations represents the various concentrations of the inhibitor used.

B.

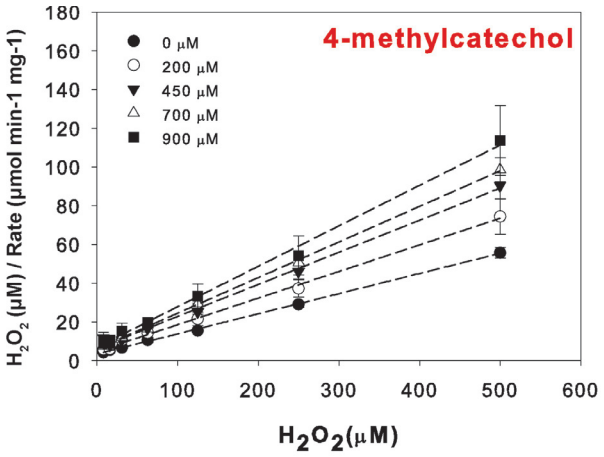

Hanes-Woolf Plot

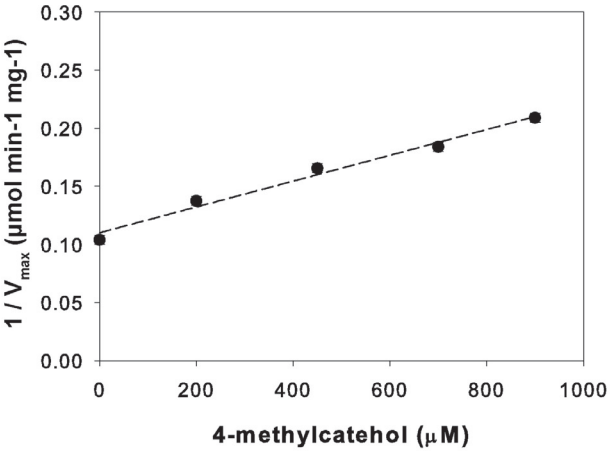

Determine K_i'

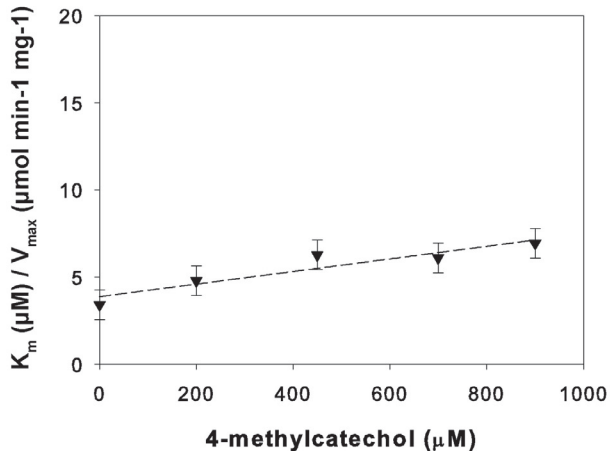

Determine K_i

C.

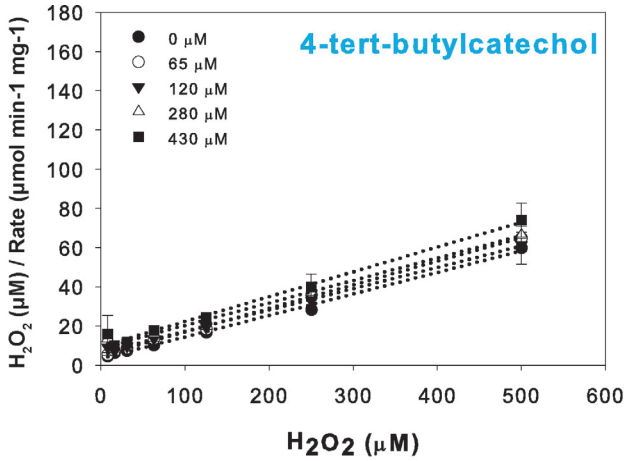

Hanes-Woolf Plot

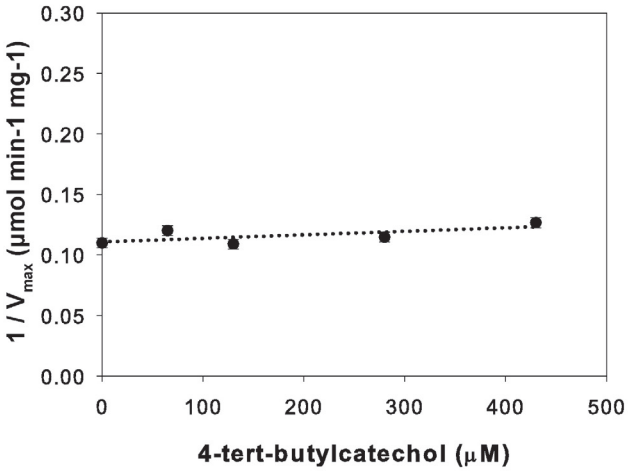

Determine K_i'

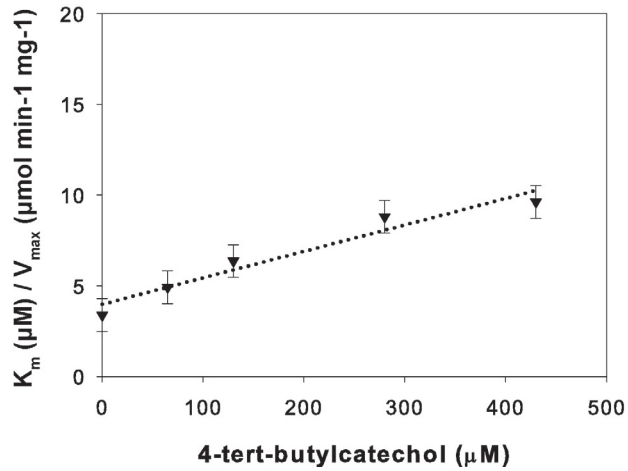

Determine K_i

Table 6: K_m and V_{max} values from the Michaelis-Menten and Hanes-Woolf plots.

A. Michaelis-Menten. B. Hanes-Woolf. The K_m (Michaelis-Menten constant) and V_{max} (maximum velocity) values were determined by Michaelis-Menten plots (non-linear) plotting initial rate values vs. $[H_2O_2]$ and by Hanes Woolf plots (linear) plotting $[H_2O_2]$ / rate vs. $[H_2O_2]$. The K_m values increased and the V_{max} decreased with increasing inhibitor concentrations and were shown for both methods. These trends were seen for all three catechol derivatives. Therefore, indicating the catechol derivatives inhibit hPrx5 in a non-competitive manner. The trends of the K_m and V_{max} values complement the Hanes-Woolf plots. See Figure 33& Figure 34 pg 86.

A.

Catechol			4-methylcatechol			4-*tert*-butylcatechol		
Ligand (µM)	**K_m (µM)**	**V_{max} (µmol min^{-1} mg^{-1})**	**Ligand (µM)**	**K_m (µM)**	**V_{max} (µmol min^{-1} mg^{-1})**	**Ligand (µM)**	**K_m (µM)**	**V_{max} (µmol min^{-1} mg^{-1})**
0	42.36 ± 3.33	9.77 ± 0.22	**0**	32.96 ± 2.65	9.77 ± 0.21	**0**	38.14 ± 2.90	9.77 ± 0.21
800	42.22 ± 4.07	7.95 ± 0.22	**200**	38.35 ± 3.99	7.72 ± 0.23	**65**	42.83 ± 3.84	8.46 ± 0.22
200	58.10 ± 6.95	6.85 ± 0.26	**450**	34.29 ± 4.40	6.16 ± 0.22	**130**	53.30 ± 4.61	9.18 ± 0.24
3500	74.58 ± 12.08	5.43 ± 0.29	**700**	33.91 ± 4.87	5.50 ± 0.22	**280**	63.91 ± 6.25	8.49 ± 0.27
5000	81.45 ± 18.16	4.05 ± 0.31	**900**	34.33 ± 5.22	5.20 ± 0.22	**430**	62.97 ± 6.54	7.96 ± 0.26

B.

Catechol			4-methylcatechol			4-*tert*-butylcatechol		
Ligand (µM)	**K_m (µM)**	**V_{max} (µmol min^{-1} mg^{-1})**	**Ligand (µM)**	**K_m (µM)**	**V_{max} (µmol min^{-1} mg^{-1})**	**Ligand (µM)**	**K_m (µM)**	**V_{max} (µmol min^{-1} mg^{-1})**
0	50.60 ± 23.07	9.86 ± 0.85	**0**	32.83 ± 9.41	9.62 ± 0.36	**0**	30.81 ± 9.35	9.11 ± 0.34
800	43.51 ± 18.14	7.96 ± 0.55	**200**	34.91 ± 7.17	7.28 ± 0.21	**65**	41.02 ± 8.89	8.33 ± 0.28
200	58.29 ± 16.17	6.72 ± 0.39	**450**	37.93 ± 6.03	6.04 ± 0.14	**130**	58.50 ± 10.47	9.19 ± 0.35
3500	92.35 ± 15.04	5.57 ± 0.27	**700**	33.18 ± 5.32	5.44 ± 0.12	**280**	76.87 ± 10.60	8.73 ± 0.31
5000	64.73 ± 9.33	3.79 ± 0.13	**900**	33.21 ± 4.69	4.79 ± 0.09	**430**	76.01 ± 9.57	7.90 ± 0.26

Table 7: Inhibition mechanism values for the catechol derivatives against hPrx5.

The inhibitory constant values determined by DynaFit modeling discrimination. The data is represented as the mean ± standard error for three independent experimental days.

	Catechol		4-methylcatechol	4-*tert*-butylcatechol
Model Type	Mixed	Partial	Partial	Partial
K_s (µM)	23.62 ± 4.27	40.70 ± 4.00	33.70 ± 4.60	36.9 ± 4.40
K_i (mM)	0.42 ± 2.21 x 10^{6}	1.81 ± 0.46	0.33 ± 0.13	0.09 ± 0.04
K_i' (mM)	1.00 x 10^{6} ± 1.42 x 10^{-2}	4.04 ± 1.13	0.36 ± 0.12	0.18 ± 0.10
k_{cat} (s^{-1})	2.69 ± 1.18 x 10^{-1}	3.08 ± 0.08	3.11 ± 0.01	3.05 ± 0.10
k_{cat}' (s^{-1})	--	~ 0	1.07 ± 0.25	2.35 ± 0.18
k_{cat} / K_s (M^{-1} s^{-1})	(1.40 ± 0.13) x 10^{5}	(1.14 ± 0.14) x 10^{5}	(9.24 ± 1.10) x 10^{4}	(8.25 ± 0.82) x 10^{4}

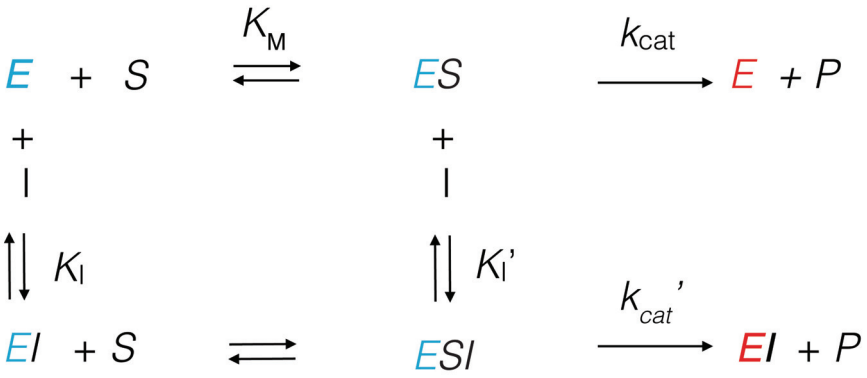

Figure 35: Partial mixed type non-competitive inhibition mechanism scheme for hPrx5 inhibited by the catechol derivatives.

When inhibiting reduced hPrx5 in blue (*E*) by an inhibitor (*I*) there are two pathways. The *I* can bind either to the free enzyme or the Michaelis-Menten complex (*ES*). Under these conditions, hPrx5 is not fully inhibited and can produce product (*P*): either by *ES* or *ESI* represented by k_{cat} and k_{cat}' rate constants. Oxidized hPrx5 state in red (Cys47-SOH or sulfenic acid) and can be regenerated to its reduced state by the thioredoxin system.

3.3.5 Catechol derivatives bind to hPrx5 in a rapid reversible manner

In addition to identifying the catechol derivatives are inhibitors against hPrx5, the kinetic MMOA was examined assessing the binding interaction between the catechol derivatives and hPrx5 were evaluated. Depending on the kinetic MMOA, an inhibitor can bind to enzyme through rapid reversibility, slow reversibility or irreversibility[45]. The reversibility of the catechol derivatives to hPrx5 were tested by incubating hPrx5 at 10-fold IC_{50} with a catechol derivative and then after mixture was diluted (by 100-fold factor) with the reaction rate monitored. Figure 38 shows the activity of hPrx5 after being incubated with 4-*tert*-butylcatechol. hPrx5 activity seemed to be marginally unaffected but similar to the control. Evaluating the reaction rates for all of the catechol derivatives, the rates are relatively unchanged. There was no big difference in the reaction rate values when incubating hPrx5 with 10- or 5-fold [IC_{50}] of each inhibitor (See Table 8). Overall, hPrx5 peroxidase activity rate was unaffected and therefore indicated the catechol derivatives bind in a rapidly reversible manner.

3.4 Article 2 " Comparing the binding and inhibition properties of the catechol derivatives to other hPrx isoforms"

Article 2 is currently in preparation.

3.4.1 Catechol derivatives bind to hPrx1 and hPrx2

In determining the catechol derivatives bind and inhibit hPrx5, there was interest to assess if the catechol derivatives could also, bind and inhibit other hPrx isoforms. I examined the binding and inhibiting properties of the catechol derivatives to hPrx1 and hPrx2. Both hPrx1 and hPrx2 are in a different class of hPrxs, typical 2-Cys class, and are structurally different from hPrx5. Both hPrx1 and hPrx2 were identified to be involved in the inflammation cascade after an ischemic stroke too [11].

A. **B.**

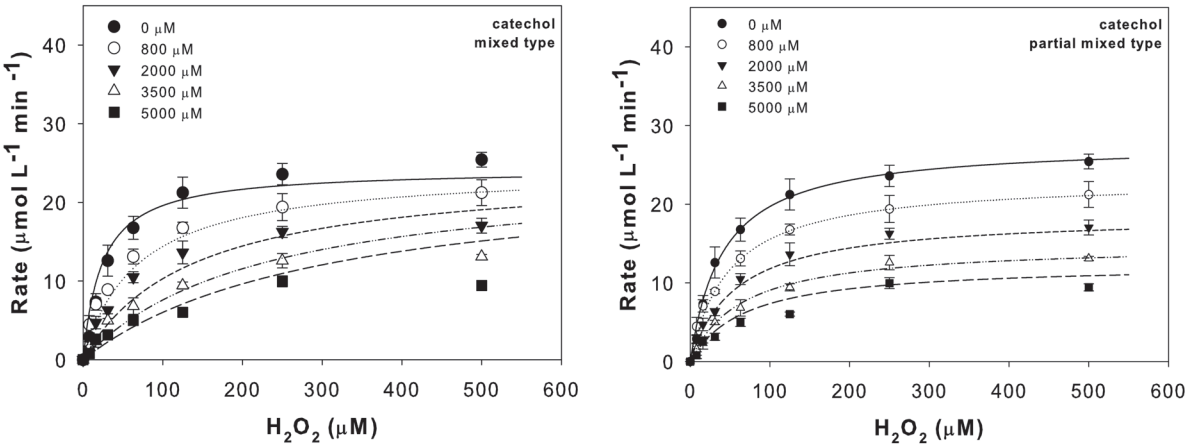

Figure 36: Inhibition models fitted by DynaFit for the inhibition of hPrx5 by catechol.

A. Mixed non-competitive type model. B. Partial mixed non-competitive type model. In determining the inhibition model for catechol against hPrx5 there were two (Figures A and B) models purposed. In comparing the model fittings, catechol's data fits more precisely to partial mixed type. In addition, the inhibitory constant values determined also, complied with the inhibition trends seen for 4-methylcatechol and 4-*tert*-butylcatechol (Table 7).

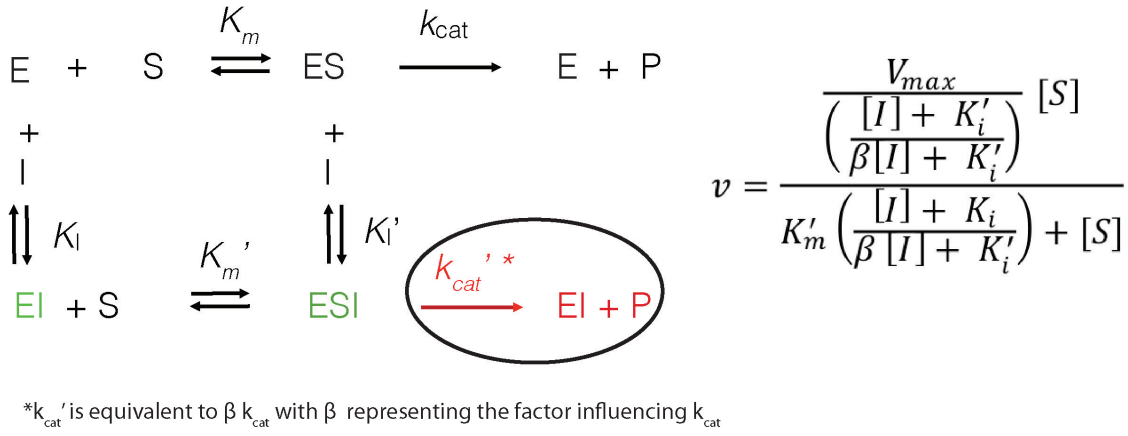

$$v = \frac{\frac{V_{max}}{\left(\frac{[I] + K_i'}{\beta[I] + K_i'}\right)}[S]}{K_m'\left(\frac{[I] + K_i}{\beta[I] + K_i'}\right) + [S]}$$

Figure 37: Inhibition mechanism scheme for mixed versus partial mixed type non-competitive.

Here is a scheme highlighting the differences between the two-inhibition mechanism: mixed and partial mixed type non-competitive. In both mechanisms the inhibitor inhibits the *E* and *ES* complex (green). However, for mixed non-competitive type, the *ESI* complex cannot produce any product (circled and in red) but only through the *ES* complex and no k_{cat}' value exists. Whereas, for partial mixed type non-competitive, the *ESI* and *ES* complexes can both produce product and have both k_{cat} and k_{cat}' values.

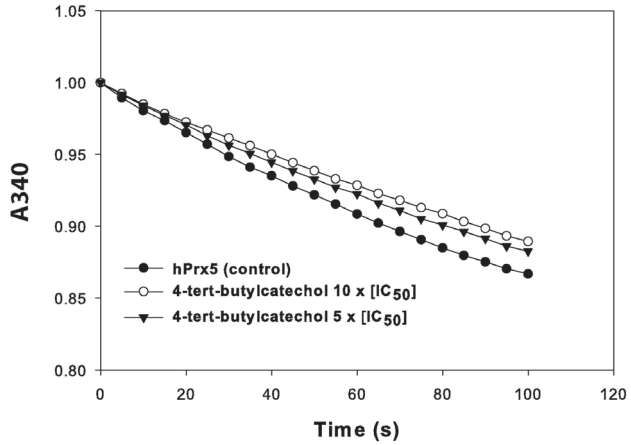

Figure 38: Binding reversibility plots for 4-*tert*-butylcatechol to hPrx5.

4-*tert*-butylcatechol was incubated at 10- and 5-fold the concentration of the IC_{50} value and after the reaction rate was measured. Comparing the reaction rates from before and after, 4-*tert*-butylcatechol incubated with hPrx5 the reaction rates were not significantly affected. Therefore, this indicated 4-*tert*-butylcatechol bound to hPrx5 in a reversible manner. The experimental conditions shown here were: 0.15 µM hPrx5, 15 µM yTrx1, 2 µM yTrxR1, 200 µM NADPH and 25 µM H_2O_2 in PBS pH 7.0 with 1 mM EDTA with varying concentrations of the catechol derivative monitoring the absorbance at 340 nm.

Table 8: Binding reversibility rates for the catechol derivatives to hPrx5.

The catechol derivatives were determined if they bind to hPrx5 in a reversible or irreversible manner. The catechol derivatives were incubated at high concentrations with hPrx5 and after the reaction rates were measured. Comparing the reaction rates before and after the incubation, the catechol derivatives bind reversibly to hPrx5, as the rates are marginally unaffected. The data is representative as the mean ± standard error for three independent experiments (n=3).

Inhibitor	IC_{50} (mM)	Rate (µmol min^{-1} mg^{-1})	
		10 X [IC_{50}]	5 x [IC_{50}]
hPrx5		0.32 ± 0.02	
4-*tert*-butylcatechol	0.25 ± 0.06	0.25 ± 0.01	0.28 ± 0.01
4-methylcatechol	0.82 ± 0.14	0.26 ± 0.01	0.26 ± 0.01
Catechol	3.73 ± 0.85	0.25 ± 0.02	0.26 ± 0.01

First, the binding interaction for the three catechol derivatives to hPrx1 and hPrx2 were examined by Saturation Transfer Difference (STD) NMR spectroscopy. STD NMR spectroscopy characterized the ligand binding affinity events: the free ligand and bound ligand to the protein [85]. The bindings of the catechol derivatives to the hPrxs were monitored over a titration with increasing concentrations of the catechol derivatives (catechol 0-54 mM, 4-methylcatechol 0-54 mM, 4-*tert*-butylcatechol 0-4 mM).

All the catechol derivatives were determined to bind and interact with both hPrx1 and hPrx2, as there were changes in the STD signals observed in examining the ^{1}H and ^{1}H STD NMR spectra. Figure 39 shows the overlay of the ^{1}H (black) and ^{1}H STD (red) NMR spectrum highlighting the implicated proton signals for 4-*tert*-butylcatechol to hPrx2. ^{1}H spectrum represents the reference spectrum and ^{1}H STD spectrum represents after hPrx2 was irradiated for a period of time 2 sec and in which, 4-*tert*-butylcatechol was bound to hPrx2. As a result, the saturation from hPrx2 was transferred to 4-*tert*-butylcatechol and STD signal for the protons of 4-*tert*-butylcatechol were detected [54]. There was a little difference in the STD signals detected between 4-*tert*-butylcatechol's protons H3, H5, and H6, which were the most saturated in comparison to *tert*-butyl group. The binding interaction of the ligands protons can also be interpreted from the group epitope mapping. Figure 40 and Figure 41 are the STD saturation curves for hPrx1 and hPrx2. The f_{STD} was plotted against the catechol derivative concentration and the curves were fitted determining an apparent dissociation constant (K_d). Also, shown in the figures (right) is the epitope mapping distinguishing the catechol derivatives proton's averaged apparent binding interaction that occurred represented as a percentage to the specific hPrx. In comparing the apparent binding interaction of the catechol derivatives to hPrx1 and hPrx2, the catechol derivatives have a slightly better affinity hPrx2. Both hPrxs had similar binding affinities when ranking the K_d values of the catechol derivatives. 4-*tert*-butylcatechol had the best affinity and catechol had the least affinity to both hPrx1 and hPrx2. 4-*tert*-butylcatechol binding affinity to hPrx1 and hPrx2, had K_d values of 26.0 ± 7.0 mM (hPrx1) and 5.9 ± 1.0 mM (hPrx2) (see Table 9). Overall, STD NMR spectroscopy was able to detect an apparent binding of the catechol derivatives to both hPrx1 and hPrx2**.**

3.4.2 Catechol derivatives bind to hPrx2 determined by FM simulations

To assist in determining if the catechol derivatives could bind to hPrx2 active site, hPrx2 binding interaction to the catechol derivatives was examined by FM computational modeling similar to hPrx5. Jean-Marc Lancelin assisted in modeling and monitoring the binding events of

hPrx2 and the catechol derivatives. Only hPrx2 was modelled since hPrx2 structure organization is homologous to hPrx1. Examining the binding events of the catechol derivatives to the active site of hPrx2 homodimer, the binding conformations were assessed through the FES plots and $\Delta G_b°$ values were obtained and to K_d values too. All the catechol derivatives were determined to bind to hPrx2 and 4-*tert*-butylcatechol was found to bind the best with a K_d value of 5.60 ± 1.80 mM (See Table 10). 4-*tert*-butylcatechol bound to hPrx2 active site through H-bonds and Van der Waals interactions interacting with the following amino acids Pro44, Leu45, Thr48, Pro52, Phe49, Glu122, Ile124, Leu146, Pro147, and Val171, Leu183 and Pro185 from the second monomer.

Table 9: STD amplification factor values and catechol derivatives epitope mapping.

The binding dissociation constant (K_d) values were determined from fitting the STD curves from Figure 40 and

Figure 41 representing the binding interaction of the catechol derivatives to the hPrxs. The K_d values are shown as the mean ± standard error for three independent experiments (except for catechol and 4-methylcatechol with the K_d representing one experimental day). Also, shown are the f_{STD} % values corresponding to the epitope mapping for the protons involved in the binding interaction. Similar to the K_d values, error is only reported for 4-*tert*-butylcatechol and it is assumed for the other the ligands a maximum of ± 10% error occurred for the f_{STD} % values.

Protein	Ligand	Proton Assignment	Average K_d (mM)	Normalized f_{STD} (%)
Prx1	Catechol	H3/H6 H4/H5	95.6 ± 14.6	100 100
	4-methylcatechol	H6 H3 H5 Methyl group	26.8 ± 20.3	90 100 97 66
	4-*tert*-butylcatechol	H3 H6 H5 *Tert*-butyl group	26.0 ± 7.0	63 ± 3 48 ± 4 100 ± 10 78 ± 3
Prx2	Catechol	H3/H6 H4/H5	55.5 ± 9.4	100 97
	4-methylcatechol	H6 H3 H5 Methyl group	54.1 ± 13.1	86 100 94 59
	4-*tert*-butylcatechol	H3 H6 H5 *Tert*-butyl group	5.9 ± 1.0	70 ± 6 100 ± 2 93 ± 5 50 ± 7

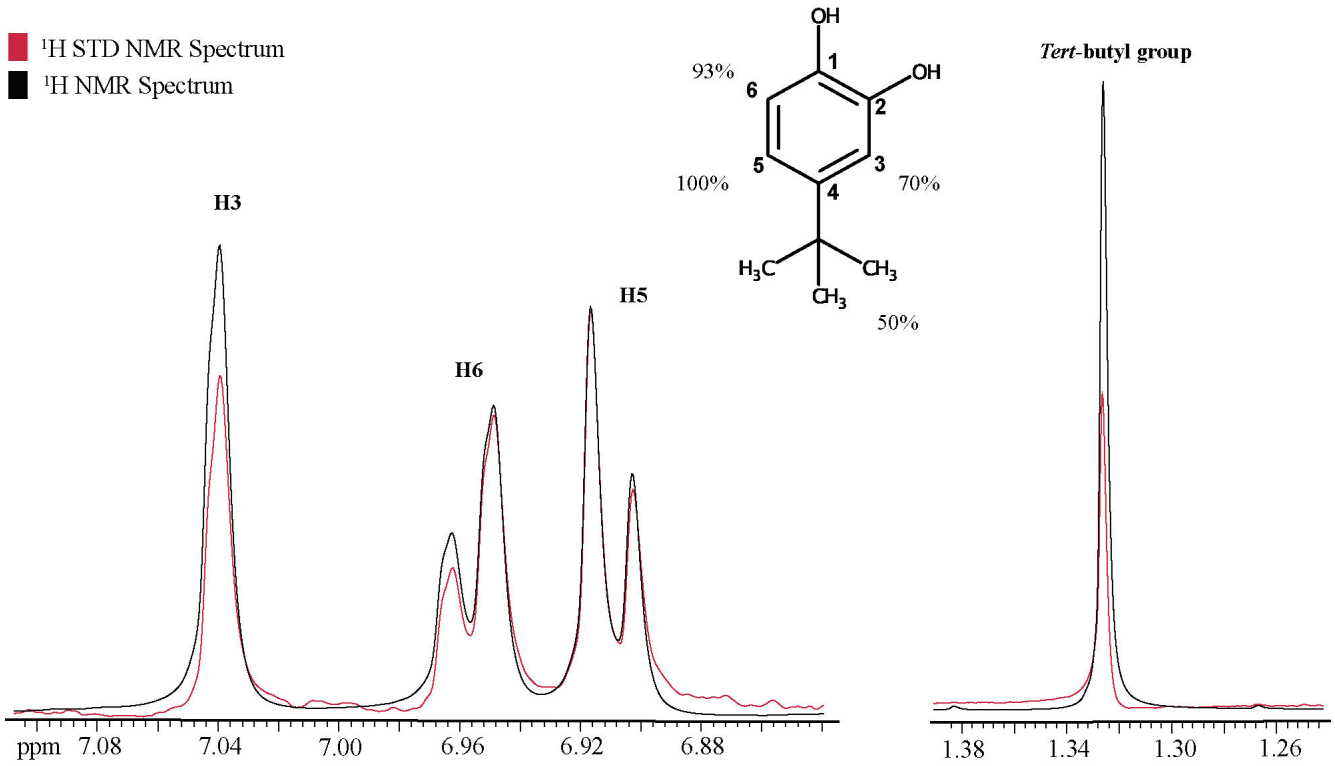

Figure 39: Overlay of ^{1}H and ^{1}H STD NMR spectra for 4-*tert*-butylcatechol binding interaction to hPrx2.

The ^{1}H (black) and ^{1}H STD (red) spectra obtained monitoring the binding interaction of 4.36 mM of 4-*tert*-butylcatechol to 20 µM of hPrx2. Overlaying the spectra, the aromatic protons (H3, H6, H5) of 4-*tert*-butylcatechol are more implicated in the binding interaction than the *tert*-butyl group protons. Also, shown is the group epitope mapping determined for all the protons involved in the binding even

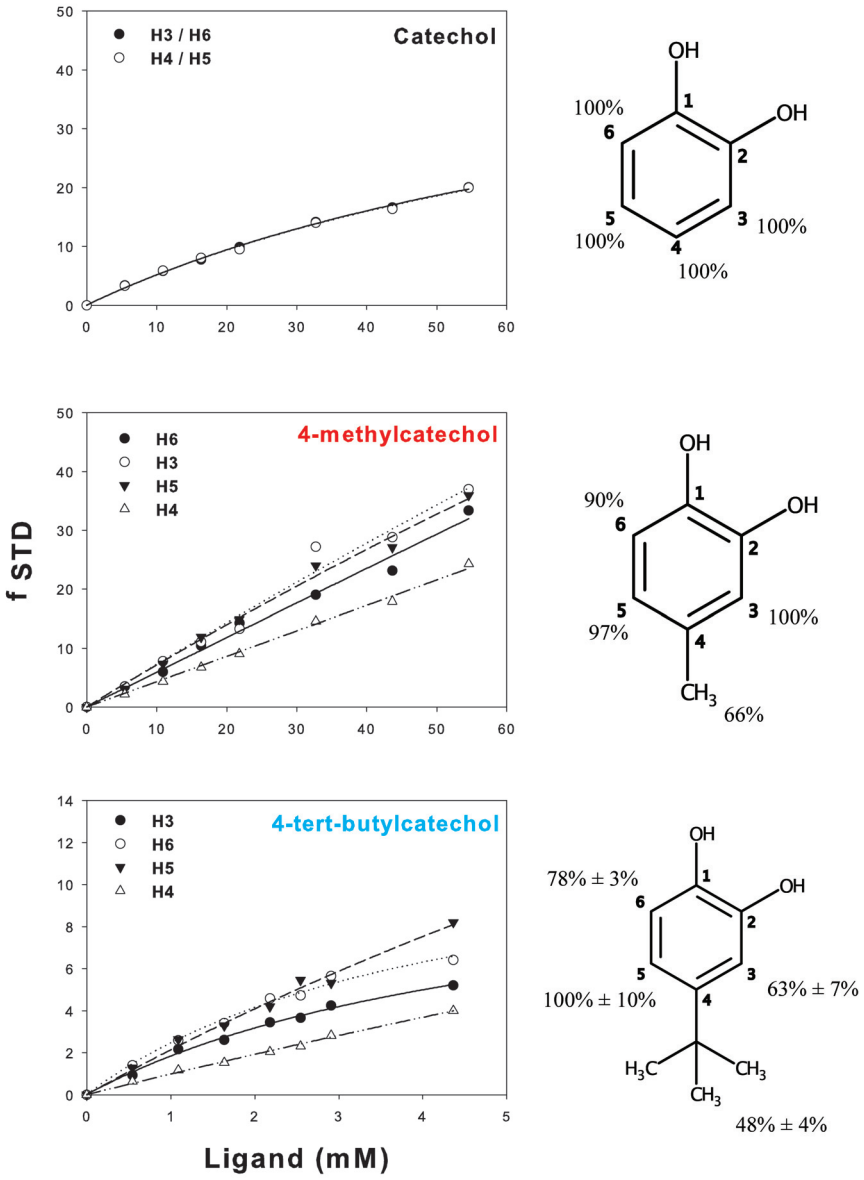

Figure 40: STD curves for the catechol derivatives binding interaction to hPrx1.

The following curves represent STD factors (f_{STD}) of the three-catechol derivatives plotted against the catechol derivatives concentration range. The data was fitted and K_d values were determined for each of the catechol derivatives interaction to hPrx1 (see Table 9 pg 96). All the catechol derivatives were determined to have a binding affinity to hPrx1. 4-*tert*-butylcatechol had the greatest binding affinity to hPrx1. Also, shown is the group epitope mapping determined for the protons of the catechol derivatives involved in the binding event. The protons in the aromatic ring are the most implicated in the binding. Note: 4-*tert*-butylcatechol was the only ligand examined in three independent experiments and therefore there is error shown for the epitope mapping. It can be assumed for catechol and 4-methylcatechol the error on the group epitope mapping is at maximum ± 10%.

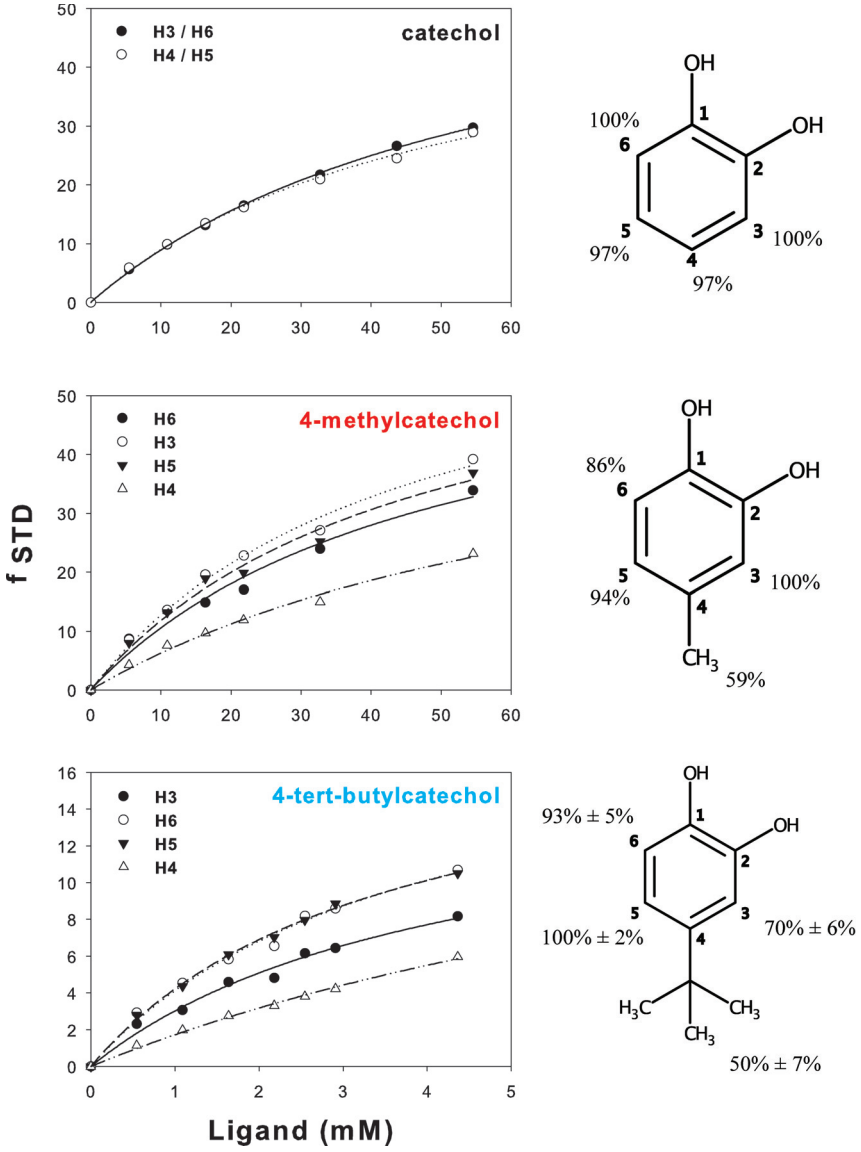

Figure 41: STD curves for the catechol derivatives binding interaction to hPrx2.

The following curves represent STD factors (f_{STD}) of the three-catechol derivatives plotted against the catechol derivatives concentration range. The data was fitted and K_d values were determined for each of the catechol derivatives interaction to hPrx2 (see Table 9 and pg 96). All the catechol derivatives were determined to have a binding affinity to hPrx2. 4-*tert*-butylcatechol had the greatest binding affinity to hPrx2. Also, shown is the group epitope mapping determined for the protons of the catechol derivatives involved in the binding event. The protons in the aromatic ring are the most implicated in the binding. Note: 4-*tert*-butylcatechol was the only ligand examined in three independent experiments and therefore there is error shown for the epitope mapping. It can be assumed for catechol and 4-methylcatechol the error on the group epitope mapping is at maximum ± 10%.

Table 10:The catechol derivatives binding affinities to hPrx2 by FM simulations.

Here are the binding affinity (K_d) values determined for the catechol derivatives to hPrx2 from monitoring the binding event by FM modeling simulations.

	K_d for hPrx2 (mM)
Catechol	14.5 ± 7.2
4-methylcatechol	84.0 ± 110.0
4-*tert*-butylcatechol	5.60 ± 1.80

3.4.3 Catechol derivatives do inhibit hPrx1 and hPrx2 peroxidase activity

Upon determining the catechol derivatives could bind to hPrx1 and hPrx2, their ability to inhibit the peroxidase activity was assessed. However, as determined by STD NMR spectroscopy the binding affinities were poor for catechol and 4-methylcatechol with K_d values ~100 to 50 mM range which are likely above the limit of non-selective interactions of the ligands. Therefore, only the inhibition properties of 4-*tert*-butylcatechol was examined [86]. To monitor the IC_{50} assay for 4-*tert*-butylcatechol to hPrx1 and hPrx2 there were slight modifications to maintain the same experimental conditions as hPrx5 and be able to come IC_{50} assay results. The concentration of hPrx1 and hPrx2 was 0.38 μM instead of 0.15 μM (hPrx5). The H_2O_2 concentration was kept at 25 μM even though the K_m measured for hPrx1 and hPrx2 was < 5 μM.

In conducting the IC_{50} assay, 4-*tert*-butylcatechol was determined to also inhibit hPrx1 and hPrx2. Figure 42 shows the overlay IC_{50} curves obtained for the three hPrx isoforms. Ranking the IC_{50} values 4-*tert*-butylcatechol inhibits hPrx1 the best followed by hPrx2 and hPrx5 (see Table 11). However, in examining the curves there were differences in the residual relative activity achieved. 4-*tert*-butycatechol was found to inhibit hPrx5 better by reaching a relative activity at ~ 0.40 compared to hPrx1 and hPrx2 with ~ 0.80 and ~ 0.65 (see Figure 42). Overall, 4-*tert*-butylcatechol could inhibit hPrx1, hPrx2 and hPrx5 but on varying degrees of inhibition.

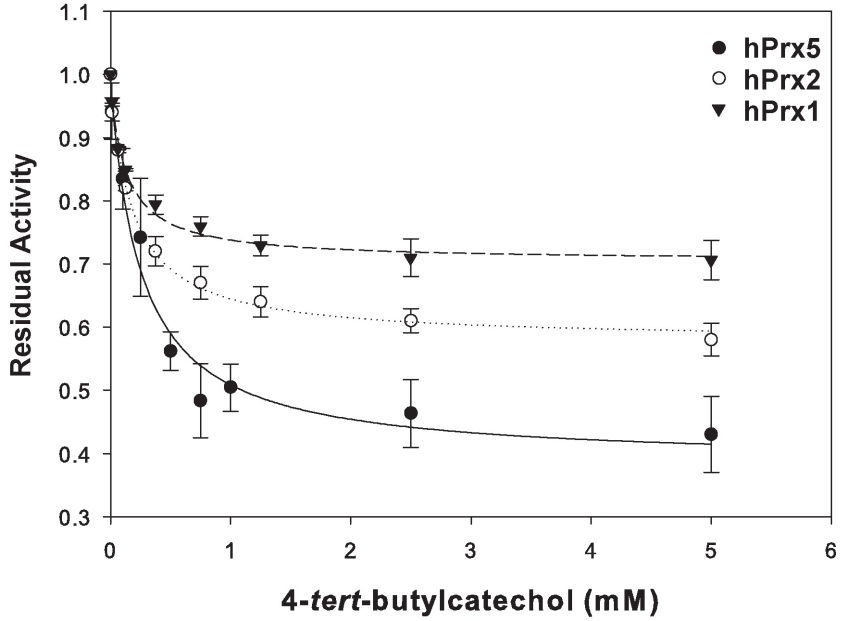

Figure 42: Comparison of the IC_{50} curves of 4-*tert*-butylcatechol inhibition properties to hPrxs.

Plotted are the IC_{50} curves obtained measuring the peroxidase activity of the various peroxiredoxins against increasing concentrations of 4-*tert*-butylcatechol. 4-*tert*-butylcatechol can inhibit hPrx1, hPrx2 and hPrx5 but at vary degrees of inhibition.

Table 11: Comparison of the IC_{50} values for hPrxs isoforms inhibited by 4-*tert*-butylcatechol.

The ability of 4-*tert*-butylcatechol to inhibit hPrxs was measured through an IC_{50} assay (see Figure 42). Comparing the hPrxs, hPrx5 is inhibited the best in comparison to hPrx1 and hPrx2. The data is represented as the mean ± standard error for three independent experiments (n=3).

hPrx isoform	IC_{50} (mM)
hPrx5	0.25 ± 0.04
hPrx2	0.19 ± 0.05
hPrx1	0.13 ± 0.04

4 Article 1

"Predicting and Understanding the Enzymatic Inhibition of Human Peroxiredoxin 5 by 4-Substituted Pyrocatechols Combining Funnel-Metadynamics, Solution NMR and Steady-State Kinetics."

Melissa L. Chow[§], Laura Troussicot[§], Marie Martin[§], Bastien Doumèche[¶], Florence Guillière[§], Jean-Marc Lancelin[§*]

[§] Université de Lyon, Institut des Sciences Analytiques, UMR 5280, CNRS, Université Lyon 1, ENS Lyon - 5, rue de la Doua, F-69100 Villeurbanne, France.[¶] Université de Lyon, Institut de Chimie et Biochimie Moléculaires et Supramoléculaires, UMR 5246, Université Claude Bernard Lyon1, CNRS, INSA, CPE-Lyon, 43 Bd du 11 novembre 1918, F-69622, Villeurbanne, France

KEYWORDS: Funnel-metadynamics, enzyme kinetics, enzyme inhibition, solution NMR, absolute binding free-energy, human peroxiredoxin5.

Accepted by Biochemistry (American Chemical Society Publications).

4.1 Abstract

Funnel metadynamics is a kind of computational simulation used to enhance the sampling of protein−ligand binding events in solution. By characterization of the binding interaction events, an estimated absolute binding free energy can be calculated. Nuclear magnetic resonance and funnel metadynamics were used to evaluate the binding of pyrocatechol derivatives (catechol, 4-methylcatechol, and 4-tert-butylcatechol) to human peroxiredoxin 5. Human peroxiredoxins are peroxidases involved in cellular peroxide homeostasis. Recently, overexpressed or suppressed peroxiredoxin levels have been linked to various diseases. Here, the catechol derivatives were found to be inhibitors against human peroxiredoxin 5 through a partial mixed type noncompetitive mechanism. Funnel metadynamics provided a microscopic model for interpreting the inhibition mechanism. Correlations were observed between the inhibition constants and the absolute binding free energy. Overall, this study showcases the fact that funnel metadynamics simulations can be employed as a preliminary approach to gain an in-depth understanding of potential enzyme inhibitors.

4.2 Introduction

Enzyme catalysis is one of the more fascinating properties of biological macromolecules. Since the seminal reports of Henri, Michaelis, and Menten, it has been known that the rate of enzyme catalysis of a chemical reaction is directly proportional to the concentration of the enzyme−substrate complex. This concept was predicted by the original Henri− Michaelis−Menten equations.[1−4] A century of enzymology and enzyme kinetics established the different classical models of the enzyme catalytic mechanisms and models for their inhibitions.[5] In basic enzyme catalysis, an enzyme binds reversibly to its substrate and forms an enzyme−substrate complex that is slightly stabilized. From this state, the reaction evolves to a chemical transition state with a decrease in free energy and the production of a

product. This reaction is represented here (eq 1):

$$E + S \underset{k_{-1}}{\overset{k_1}{\rightleftharpoons}} ES \overset{k_2}{\rightarrow} ES^{\ddagger} \rightarrow E + P \qquad (1)$$

where E is the enzyme, S its substrate, ES the enzyme− substrate complex or Michaelis−Menten complex, $ES^{\ddagger}$ the enzyme transition-state complex, and P the product of the reaction. The complete catalytic cycle can be complicated by modifications to the enzyme after the reaction and its regeneration involving another enzyme or cofactor (coen- zyme). Many types of enzymatic inhibition models are known, including sophisticated allosteric inhibitions.[6] The simplest inhibition model is based on the affinity of an inhibitor (I), analogous to the substrate, for the enzyme's active site leading to a nonproductive enzyme−inhibitor complex (EI) (eq 2).[4]

$$E + I \rightleftharpoons EI \qquad (2)$$

Competition between a substrate and an inhibitor for the active site is either reversible or irreversible when the inhibitor reacts by forming covalent bonds to the enzyme. In the case of reversible competitive inhibition, the greater the affinity (and the higher the stability of the enzyme−inhibitor complex), the more potent the inhibition.

Protein−ligand binding interaction is the fundamental basis for understanding any type of inhibition mechanism. Also, it is the core and the key point for designing inhibitors for developing selective drugs or effectors. Recently, the process of binding and unbinding of a ligand to a protein could be rationalized more easily using accelerated molecular dynamics protocols along with high-performance computing (HPC) at the laboratory scale.[7] This has led to advancements in obtaining statistical descriptions of protein−ligand interactions at the microscopic level for macroscopic measurements.

Previously, Troussicot et al. demonstrated that nuclear magnetic resonance (NMR)

assays of protein−ligand affinity measurement of the chemical shift perturbations were in agreement with binding affinities calculated by funnel metadynamics (FM) simulations.[8,9] Human peroxiredoxin 5 (hPrx5), a 2 × 19 kDa homodimer, was determined to weakly but selectively bind to catechol and 4-methylcatechol within the active site.[8] hPrx5 is part of the peroxiredoxin (Prx) family that reduces and detoxifies hydrogen peroxide, peroxynitrites, and a range of hydroperoxides (ROOH). Prxs are antioxidant defense enzymes along with superoxide dismutase (SOD), catalase, and glutathione peroxidase (GPX).[10,11] Antioxidant enzymes provide protection from reactive oxygen species (ROS) such as superoxide radical anions, hydrogen peroxide (H_2O_2), and hydroxyl radicals.[10] Additionally, Prxs are involved in regulating the levels of peroxides in cells linked to both stress- and non- stress-related signaling.[11,12]

There are six mammalian Prx members that can be organized into three classes: typical 2-Cys (Prx1−4), atypical 2-Cys (Prx5), and 1-Cys (Prx6) reflecting the number of cysteine residues involved in the redox reaction.[13,14] Prx catalytic activity reduces H_2O_2 to water. The first step is common for all classes: the active site is fully folded (FF) with a peroxidatic cysteine (Cp) that attacks and reacts with hydrogen peroxide. Cp (Cys- S^-) is then oxidized to sulfenic acid (Cys-SOH) and produces water or alcohols.[13,15] The active site of Prx then becomes locally unfolded (LU), and Prx either can be overoxidized to sulfinic acid (Cys-SO_2H) after reacting with another H_2O_2 becoming inactivated or can be regenerated back to Cys-SH. The recycling of reduced Prx depends on the Prx class.[12,15] The most common classes are 2-Cys (typical and atypical), in which the oxidized Cys-SOH reacts with the resolving cysteine (Cr) from the same subunit or another subunit forming a disulfide bond. Cp−Cr bond formation leads to the rearrangement of the active site. Lastly, the disulfide bond is reduced by thioredoxin (Trx), by a thioredoxin-like protein, or by glutathione (GSH),

returning Prx to the Cys-SH state with an FF active site.[10,11,16]

Oxidative stresses from the ROS have been linked to the development of many diseases and aging, which result in the impairment of several cellular functions.[16] Prxs have been linked to cancers by influencing signaling cascades, growth control, tumor suppression, and chemotherapy resistance.[17] Also, Prxs were identified in playing a role during the inflammation cascade in the brain after an ischemic stroke.[18] Deficiencies of Prxs in prokaryotic and eukaryotic pathogens have been linked to compromising host immune systems leading to infections. Prxs have been associated with various diseases, and therefore, there is an interest in identifying drugs that target Prxs for therapeutic treatments.[11,15] There have been some advancements in identifying drugs for inhibiting or modulating Prxs activity such as conoidin A,[19] adenanthin,[20] H7,[21] triptolide, celastrol, withaferin A,[22] and disulfide BNP7787.[23]

Here, NMR and FM simulation experiments were used to characterize the binding and inhibition of hPrx5 by the three pyrocatechol (or catechol) derivatives: catechol, 4-methylcatechol, and 4-tert-butylcatechol. FM was used to provide details at the microscopic level, specifically for the binding interaction between hPrx5 with hydrogen peroxide and the three ligands within the active site. Additionally, the binding interaction between a mimicked ES complex and the ligands was also assessed. Evaluating these binding states contributed to there being more information about the binding preference among the catechol derivatives binding for hPrx5. Also, solution NMR experiments were able to determine that hPrx5 has binding affinity for 4-tert-butylcatechol, and the ligand bound to the hPrx5 active site in a manner similar to that of catechol and 4- methylcatechol as previously determined. Furthermore, the potential for the catechol derivatives to bind and inhibit hPrx5 catalytic activity was evaluated. The *in vitro* enzyme assays proved that all the catechol derivatives can inhibit hPrx5 catalytic activity and inhibit via a partial mixed type non- competitive

mechanism. Overall, this study highlights the prospects of FM being utilized as a method for predicting ligands as inhibitors assisting in drug design.

4.3 Materials & methods

4.3.1 System preparation and equilibration for MD

Systems subjected to MD protocols were prepared as previously described[8] starting from the conformation of the high- resolution crystal structure of homodimeric hPrx5 corresponding to Protein Data Bank (PDB) entry 3MNG.[24,25] Only the crystallographic water molecules were retained from the PDB coordinate file in addition to the protein, and the rest were eliminated. Hydrogen peroxide and/or ligands were positioned manually near one of the two active sites of the homodimer. Simulations were conducted using the AMBER99SB-ILDN force field[26–28] for the protein and the TIP3P water model for the explicit solvent.[29] Active site Cys47 was modeled as a thiolate (residue CYM of Amber). Na^+ and Cl^- were added to match 150 mM sodium chloride aqueous solutions, close to the experimental conditions used. The Amber charges were applied to the protein, substrate, ligands, ions, water atoms, and the restrained electrostatic potential charges were used for the ligands using the Antechamber program suite[30] and the General Amber Force Field GAFF.[31] Using ACEMD code,[32] the system was minimized and equilibrated under constant-pressure and -temperature (NPT) conditions at 1 atm and 300 K using a time step of 4 fs because of the use of the hydrogen mass repartitioning scheme[33] implemented in ACEMD, with a nonbonded cutoff of 9 Å, rigid bonds, and particle mesh Ewald long-range electrostatics with a grid with spacing of 1 Å. The systems were equilibrated first using 500 steps of steepest- descent minimization, followed by running the isothermal NVT ensemble for 0.1 ns, using a Langevin thermostat set at 300 K, followed by 5 ns of the isothermal–isobaric NPT ensemble using a Langevin thermostat at the same temperature and the Berendsen barostat of ACEMD. During

minimization and equilibration, the heavy protein and ligands atoms were restrained spatially using a spring constant of 10 kcal mol^{-1} $Å^{-2}$. The magnitude of the restraining force constant was then reduced to 1 kcal mol^{-1} $Å^{-2}$ during 100 ps of NVT. The barostat was switched on at 1 atm for 1 ns of NPT simulation. During that period, the force constant of the position constraint of all heavy atoms was gradually reduced every 100 ps steps by a factor of 0.65 to a final value of ~0.1 kcal mol^{-1} $Å^{-2}$, allowing the systems to relax smoothly. Finally, the volume was allowed to relax for a further 4 ns under NPT conditions, reaching a final box size. During this run, Cα atoms of the protein and ligands were restrained with a 1 kcal mol^{-1} $Å^{-2}$ harmonic potential to prevent the system from reorienting. Then, the equilibrated systems were used for MD.

4.3.2 Funnel-metadynamics

The PLUMED plugin[34] was used to conduct funnel metadynamics calculations. Because the funnel external potential is fixed in space,[9] the hPrx5 dimer is diffusion-restrained by three atoms chosen far from the dimer interface and the active site as previously described.[8] Cα atoms of G6, G31, and K65 of chain A were used as positional restrains to inhibit the whole protein diffusion with a force constant of 20 kcal mol^{-1} $Å^{-2}$ in ACEMD. The bias was added on a distance CV (see Results). A Gaussian width of 0.35 Å was used, and a Gaussian deposition rate of 0.25 kcal mol^{-1} ps^{-1} (1 kcal = 4.18 kJ) was initially used and gradually decreased on the basis of the adaptive bias with a ΔT of 3600 K. Trajectories and geometrical clustering were analyzed using the VMD software.[35] In the FM calculation with hydrogen peroxide bound to hPrx5, a wall potential was used with PLUMED from the sulfur to the hydrogen of hydrogen peroxide of 20 kcal mol^{-1} $Å^{-2}$ applying beyond a maximal interatomic distance of 2.0 Å. This term is not taken into account in the free energy

calculations from PLUMED outputs.

4.3.3 Protein expression and purification

Recombinant human peroxiredoxin 5 (hPrx5, EC 1.11.1.15), yeast thioredoxin 1 (yTrx1, EC 1.8.1.9), and yeast thioredoxin reductase 1 (yTrxR1, EC 1.8.1.9) were in the pQE-30 expression vector (Qiagen) with an N-terminal fusion with a hexahistidine (6xHis) tag. The plasmids were provided through collaboration with B. Knoop's lab at the Université Catholique de Louvain (Louvain-la-Neuve, Belgium). The expression and purification of the proteins were adapted from ref 36. Briefly, the plasmids were transformed into Escherichia coli strain M15 (pRep4) and grown in LB medium at 37 °C with 50 μg/mL ampicillin and kanamycin. For the production of [^{15}N]hPrx5, M9 minimal medium was used (6 g/L Na_2HPO_4, 3 g/L KH_2PO_4, and 0.5 g/ L NaCl) supplemented with 50 μg/mL ampicillin and kanamycin, 6 μg/L thiamine, 1 mM $MgSO_4$, 1 mM $CaCl_2$, a 10 mL/L trace metal solution [5 g of EDTA, 0.5 g of $FeCl_3$, 0.005 g of ZnO, 0.001 g of $CuCl_2$, 0.001 g of $Co(NO_3)_2{\cdot}6H_2O$, and 0.001 g of $(NH_4)_6Mo_7O_{24}{\cdot}4H_2O$ per liter], 4 g/L D- glucose, and 1 g/L $^{15}NH_4Cl$.[37] The bacterial cultures were induced at an O.D.600 of 0.6 with 1 mM isopropyl thiogalactopyranoside (IPTG) for 4−5 h. The bacterial cells were harvested by centrifugation for 20 min at 2000g [Thermo Fisher Scientific, F15-8 × 50 cy rotor]. The bacterial cell pellets were lysed with 10 mM imidazole, 50 mM phosphate, and 300 mM NaCl (pH 8) by sonication (Sartorius Stedim Biotech, Aubagne, France). The cell lysate was then centrifuged for 45 min at 16500g (Thermo Fisher Scientific, TX-750 rotor). The cell supernatant was then loaded onto a Ni^{2+}-NTA column (Qiagen). The column was washed with the lysis buffer. The protein was eluted and dialyzed overnight against PBS (pH 7.4) at 4 °C. The homogeneity of the protein was analyzed by sodium dodecyl sulfate−polyacrylamide gel electrophoresis and the purified hPrx5 stored at −80 °C until it was used. The protein concentration was quantified by UV spectrometry (UV−vis spectrometer, Jasco France) using

the following protein extinction coefficients at A_{280} (ε calculated via expasy.org/protparam): for yTrx1, ε = 10095 M^{-1} cm^{-1}; for yTrxR1, ε = 24660 M^{-1} cm^{-1}; and for hPrx5, ε = 5625 M^{-1} cm^{-1}.

4.3.4 NMR assays

The binding of hPrx5 to the catechol derivatives was examined through two-dimensional ($^{1}H–^{15}N$) NMR experiments, also termed heteronuclear single-quantum coherence (HSQC). The experimental procedure was adapted from Troussicot et al.[8] with hPrx5 amino acid residues previously assigned. Briefly, 200 µM ^{15}N-labeled hPrx5 reduced (2 mM TCEP) in PBS (pH 7.4) was exposed to increasing concentrations of catechol derivatives (in 110 mM DMSO or H_2O) until binding saturation was exhibited. The binding interactions were monitored at 28 °C on a Varian Inova 600 MHz NMR spectrometer equipped with a 5 mm standard triple-resonance ($^{1}H/^{13}C/^{15}N$) inverse probe with a z-axis field gradient. The $^{1}H–^{15}N$ spectra were processed using the NMRPipe/NMDraw package.[38] The chemical shift perturba- tions (CSPs) were assigned using NMRViewJ.[39] The combined amide CSP Δδ was defined according to the following expression[40] (eq 3):

$$\Delta\delta = \sqrt{\frac{\Delta\delta_H^2 + \frac{1}{25}\Delta\delta_N^2}{2}} \quad (3)$$

Upon characterization of the amide CSP Δδ for the specific amino acid residues involved in the binding interactions, a binding dissociation constant (K_D) was extrapolated from the plot of CSPs versus [catechol derivative]/[hPrx5] as previously described[8] using MatLab (Mathworks, Meudon, France). Data were acquired in duplicate.

4.3.5 Half maximal inhibitory concentration Assay (IC_{50})

The inhibitory concentration assay of hPrx5 was adapted from Kim et al.[41] and Barelier et al.[37] The inhibition activity of hPrx5 was measured indirectly by the coupling reaction of yTrxR1 oxidizing NADPH, monitored by the absorbance at 340 nm as shown in Figure 7. The reaction conditions consisted of catechol derivatives at various concentrations (catechol at 0−75 mM, 4-methylcatechol at 0−15 mM, and 4-tert-butylcatechol at 0−5 mM) in PBS, 15 μM yTrx, 2 μM yTrxR, 0.15 μM hPrx5, 200 μM NADPH (Sigma-Aldrich), and 25 μM H_2O_2 (at approximately the K_M value) in a total reaction volume of 1000 μL. The reaction was conducted with a mixture of all three proteins diluted in PBS [10 mM $NaHPO_4$, 137 mM NaCl, and 3 mM KCl] with 1 mM EDTA at pH 7.0 upon addition of the catechol derivatives and NADPH. Lastly, H_2O_2 was added to the mixture and the solution mixed to initiate and monitor the inhibition of hPrx5 at room temperature (23 °C). The reaction was monitored at A_{340} for 200 s, and the initial rate of the reaction was determined from the linear portion of the curve and was expressed in micromoles per liter per minute in reference to the amount of hPrx5 used. The IC_{50} values were determined by plotting the reaction rates versus the catechol derivative concentration and fitting the data to a hyperbolic decay equation using SigmaPlot. The catechol derivatives inhibitory potency against hPrx5 was ranked based on their IC_{50} values. The data are representative of three individual experimental days (n = 3).

4.3.6 Inhibition Mechanism Assay

The inhibition mechanism assay was conducted with three or four concentrations of the catechol derivatives above and below the IC_{50} value, 15 μM yTrx, 2 μM yTrxR, 0.15 μM hPrx5, 200 μM NADPH, and a range of H_2O_2 concentrations from 0 to 500 μM. The reaction was initiated by mixing all three proteins together with a catechol derivative and NADPH and

adding H_2O_2. The reaction was monitored by measuring the A_{340} for 200 s, and the initial rate of the reaction was determined from the linear portion of the curve and is expressed in micromoles per milligram per minute. Data were plotted in a Michaelis− Menten and/or Hanes−Woolf representation.[4] The V_{max} and K_M values were calculated for each inhibitor concentration using SigmaPlot. Since the data sets were not ideally linear, DynaFit software was used with the steady-state approximation for model discriminations and parameter determination.[42,43] The data are triplicate results from three individual experiments (n = 3).

4.4 Results

4.4.1 Unbiased NVT molecular dynamics simulating H_2O_2 binding to reduced hPrx5

To study how hydrogen peroxide (H_2O_2) binds to reduced human peroxiredoxin 5 (hPrx5) and to deduce the pertinent collective variables for metadynamics simulations, the reduced hPrx5 system was first equilibrated in the presence of 6 mM H_2O_2 (i.e., six molecules of H_2O_2 were introduced around the protein in the solvation cell that includes ~55000 water molecules) before a run of 350 ns of NVT molecular dynamics (MD). H_2O_2 molecules were initially dispersed at arbitrary positions around the protein surface from 20 to 25 Å. The NVT MD trajectory was analyzed for possible binding events between H_2O_2 and hPrx5, by searching for hydrogen bonds (H-bonds) formed between the active site amino acids, in particular involving Cys47 thiolate and H_2O_2. Three short binding events were detected for H_2O_2 bound within the two active sites of hPrx5 as a homodimer. The longest binding event observed was ~1.5 ns. During a binding event, H_2O_2 made a H-bond with the sulfur atom of Cys47 with a H−S distance of 1.8−2.0 Å. The S···H−O bond angle is ~180° (Figure 1).

4.4.2 Hydrogen peroxide funnel-metadynamics

To enhance the sampling of infrequent events (i.e., occurring on a long time scale) in a reasonable computation time, well-tempered metadynamics was proposed. Metadynamics provides a free energy landscape of the investigated processes.[44,45] Free energy maps can be computed at the end of the calculation using the history-dependent bias potential added during the simulation with a few degrees of freedom of the system, called collective variables (CVs). FM provided a quantitative estimate of the binding event yielding an absolute binding free energy difference ($\Delta G_b°$) value between the free solvated state and the bound forms of any ligands. Using FM, the binding constant, K_b, can be computed as eq 4:

$$K_b = \pi R_{cyl}^2 \int_{site} dz.e^{-\beta[W(z)-W_{ref}]} \quad (4)$$

where πR_{cyl}^2 is the surface of the cylinder used as the external restraint fixed potential. Potential W(z) and its value in the unbound state, W_{ref}, are derived from the potential mean force (PMF) obtained through metadynamics calculations. β is a constant, where $\beta = (k_B T)^{-1}$ (k_B is Boltzmann's constant and T the temperature of the system). Equilibrium binding constant K_b is directly proportional to the absolute protein−ligand binding free energy, $\Delta G_b°$, following eq 5:

$$\Delta G_b^0 = \frac{1}{\beta} ln(C^0 K_b) \quad (5)$$

where $C° = 1/1660$ Å^{-3} represents the standard concentration of 1 M. The equilibrium binding constant, K_b, is the inverse of the dissociation equilibrium constant, K_D, of the ligand−protein complex measured here during NMR experiments (see below).

The funnel was aligned to the Z-axis, which was oriented to the solvent with respect to the direct access to the active site of hPrx5 (see Figure 2). The FM simulation started with H_2O_2 bound to hPrx5, and afterward, 11 successive rebinding events occurred for H_2O_2

during 200 ns of FM simulation (Figure S1). The binding of the hPrx5 substrate, hydrogen peroxide, converged to a nearly zero free energy difference and indicated that H_2O_2 diffuses freely from the solvent to the active site with a negligible affinity (Figure S2). Figure 3 (top right) shows only a tiny basin of low energy attributed to the interaction within the active site standing for ES in the simulation. The energy basin cannot be easily distinguished from other nonspecific surface interactions.

When the binding events were geometrically clustered, a single H-bond was detected between the H_2O_2 as a donor and the Cys47 thiolate. The apparent ES complex in the FM simulation is equivalent to the bound form observed in the unbiased NVT trajectories and is characterized by a geometric arrangement between hPrx5 and H_2O_2 shown in Figure 3 (bottom right). The free energy surfaces (FES) plot shows the free energy basin between H_2O_2 and hPrx5, and the bond angle conformation of the two oxygen atoms of H_2O_2 with the Cys47 sulfur exhibited an ~45° bond angle (and ~110° due to H_2O_2 symmetry).

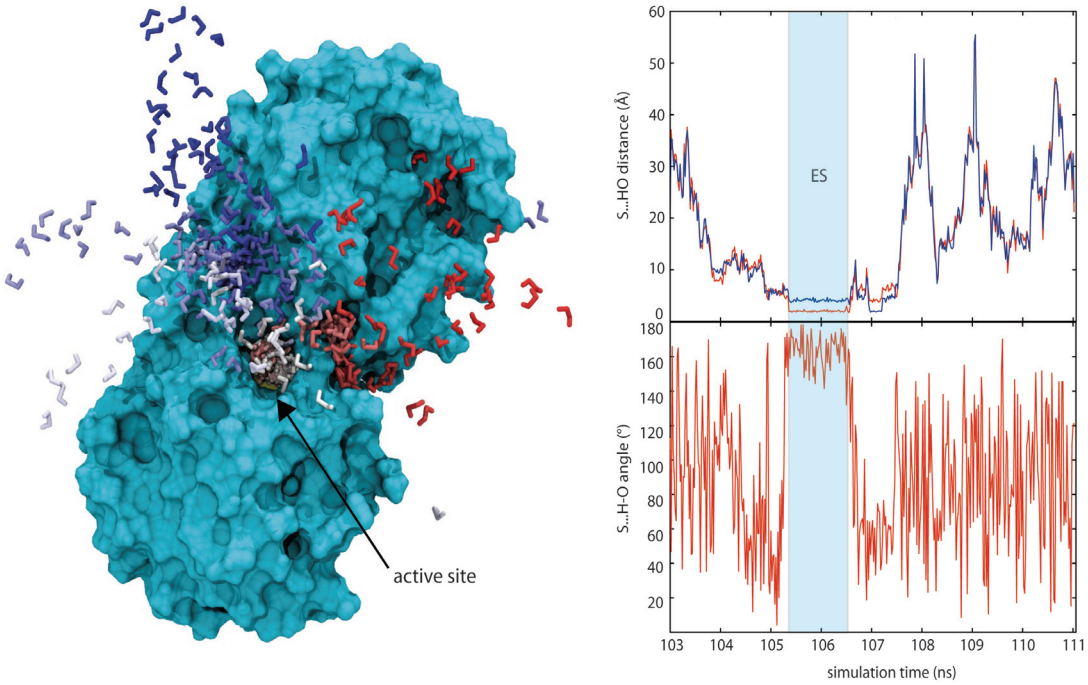

Figure 1 - Illustration of a binding event between hydrogen peroxide to hPrx5 simulated by unrestrained NVT molecular dynamics during 1.2ns between 105 and 107 ns of a 350 ns unrestrained NVT trajectory. In the left panel, hPrx5 is represented with the water-accessible surface colored light blue and hydrogen peroxide with bonds colored using a deep blue–white–red continuous spectrum depending of the simulation time. The time step between two frame shots is 20 ps. The hydrogen peroxide bound to hPrx5 corresponds to the Michaelis–Menten complex colored white in one of the two active sites of the homodimer (indicated with an arrow). The right panels show interatomic distances (top) from the Cys47-S– thiolate to a hydrogen of H2O2 (blue and red traces) as a function of simulation time. The bond angle is defined by the sulfur atom of the Cys47 thiolate, the one hydrogen atom of the hydrogen peroxide, and the oxygen atom attached (plotted in the bottom panel). The binding event is depicted in the blue highlighted region.

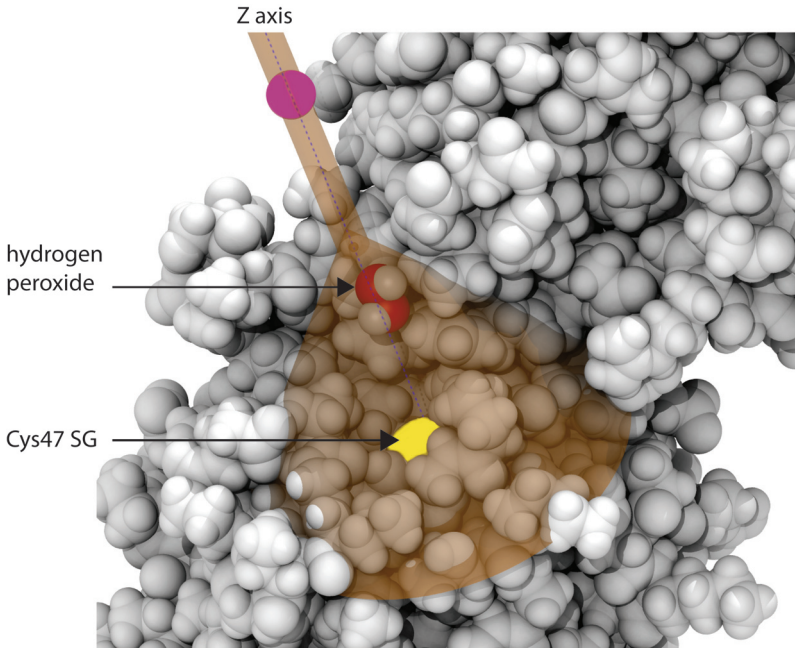

Figure 2 – External funnel restraint potential (transparent orange surface) applied to hPrx5 active site with its substrate, hydrogen peroxide. The catalytic thiolate of Cys47 (SG) is represented with a yellow sphere. The cylinder part of the funnel is aligned and centered on the Z-axis with a radius Rcyl of 1 Å. The funnel potential is limited to 35 Å from the Z-axis origin (SG atom of Cys47) by a wall potential represented by a pink sphere on the top. The cone region is defined by a vertex height Zcc of 18 Å from the origin and an angle α of 1.1 rad.

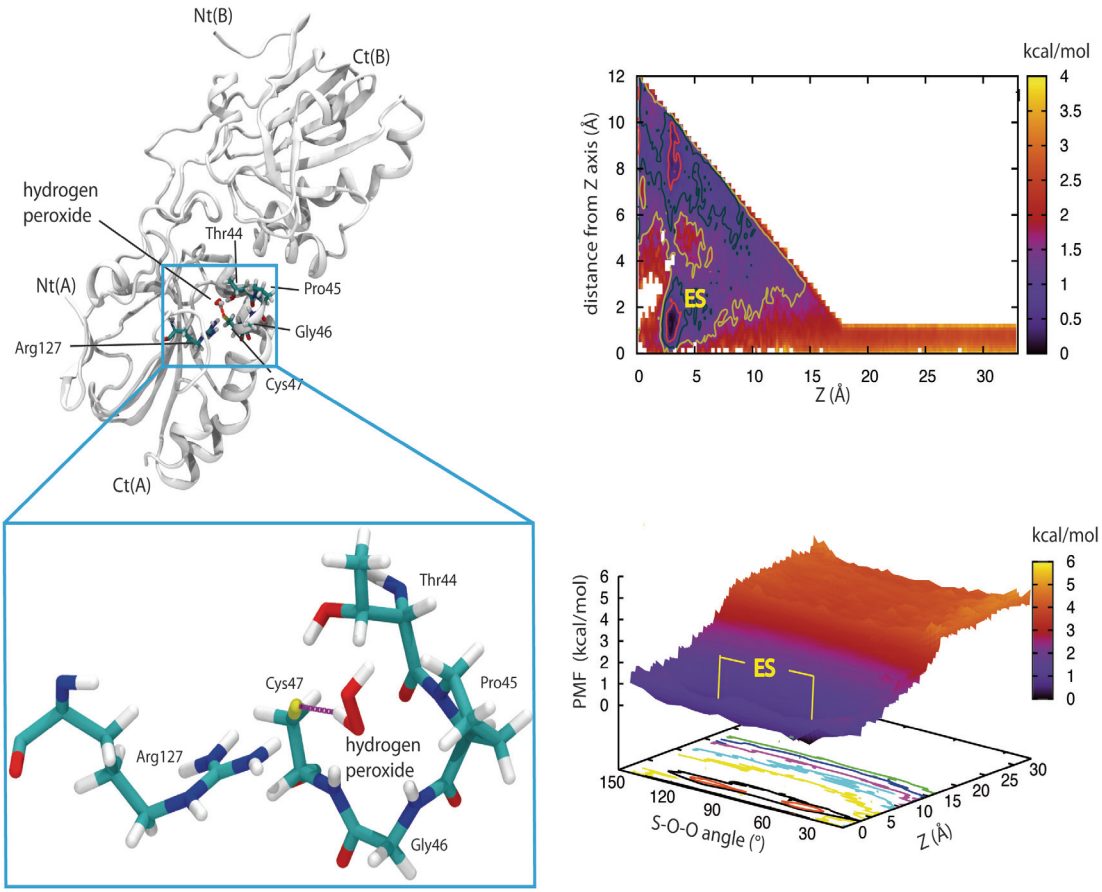

Figure 3 – Michaelis-Menten complex (*ES*) of hPrx5 and hydrogen peroxide determined using Funnel-metadynamics (FM). The top left panel is a structure of hPrx5 complexed with hydrogen peroxide during FM. The active site is located at the interface between chains A and B of the homodimer. The main amino acids participating in hydrogen peroxide reduction (Thr44, Pro45, Gly46, Cys47 thiolate, and Arg127) are represented as cyan sticks. N- and C-termini of each chain are denoted as Nt (A or B) and Ct (A or B), respectively. The bottom left panel is an enlarged view of ES corresponding to hydrogen peroxide H-bonded to the thiolate of Cys47. The H-bond is indicated with a purple dotted line. H-Bond formations fluctuated along the MD trajectory, alternating between Arg127 or Thr44 as the donor and Cys47 thiolate as the acceptor. The right panels show free energy surfaces (FES) represented as a function of the three collective variables used in FM calculations. The potential mean force (PMF) is mapped with iso-energy contours using 0.5 kcal mol^{-1} intervals.

4.4.3 Binding affinity of 4-*tert*-butylcatechol for the free-reduced form of hPrx5 using FM

The converged FM trajectory (Figures S3 and S4) showed that 4- tert-butycatechol bound to hPrx5 with an enhanced $\Delta G_b°$ of at least −1 kcal mol^{-1} compared to the reported affinity of 4- methylcatechol.[8] This was in agreement with the experimentally determined K_D measured by NMR (see below). FM simulations lead to a $\Delta G_b°$ value of −5.5 ± 0.9 kcal mol^{-1} and a K_D value of 0.11 ± 0.09 mM.

The improved binding of 4-tert-butycatechol may be related to the enhanced van der Waals contacts occurring between the 4-tert-butyl group and the neighboring patch of Leu116, Ile119, and Phe120 located in a small helix capping the active site as shown in Figure 4, although this improved interaction does not modify the dispersion of the bound states shared in different conformations. This conformational dispersion was detected after geometrical clustering of the bound conformations (Figure S5), and a similar dispersion was also noticed for 4- methylcatechol.[8] One cluster included the conformation found in a crystal of hPrx5 in complex with 4-tert-butylcatechol (PDB entry 4K7O).[46]

Compared to catechol and 4-methylcatechol, 4-tert-butylca- techol bound more on the protein surface next to the active site (green cluster in Figure 4 and Figure S5) with a less stable conformation observed. This surface interaction is stabilized by a H-bond between the hydroxyl groups of 4-tert-butylcatechol and the side-chain carboxylate of Glu19 (chain B) located in a neighboring loop of the active site. Additionally, there were van der Waals contacts that occur with the hydrophobic patch of amino acids (Leu116, Ile119, and Phe120) mentioned above and contacts with Pro20 (chain B) and Phe80 provided by the other side chain of the homodimer (see

Figures 4 and 5). The surface conformation is located on the edge of the free energy basin (Figure 4, bottom right), near 8 Å on the Z-axis and approximately 1.5–2 kcal mol^{-1} above the conformations of the direct interaction with the catalytic Cys47 thiolate. This sort of surface binding was also detected in unbiased NVT trajectories conducted prior to FM. The FES plot features the free energy basin with the angles formed between the catalytic Cys47 sulfur and the oxygen atoms of the hydroxyl groups of 4-tert- butylcatechol. The angles are ~180° for conformation A and ~60° for conformation B (Figure 4, top right).

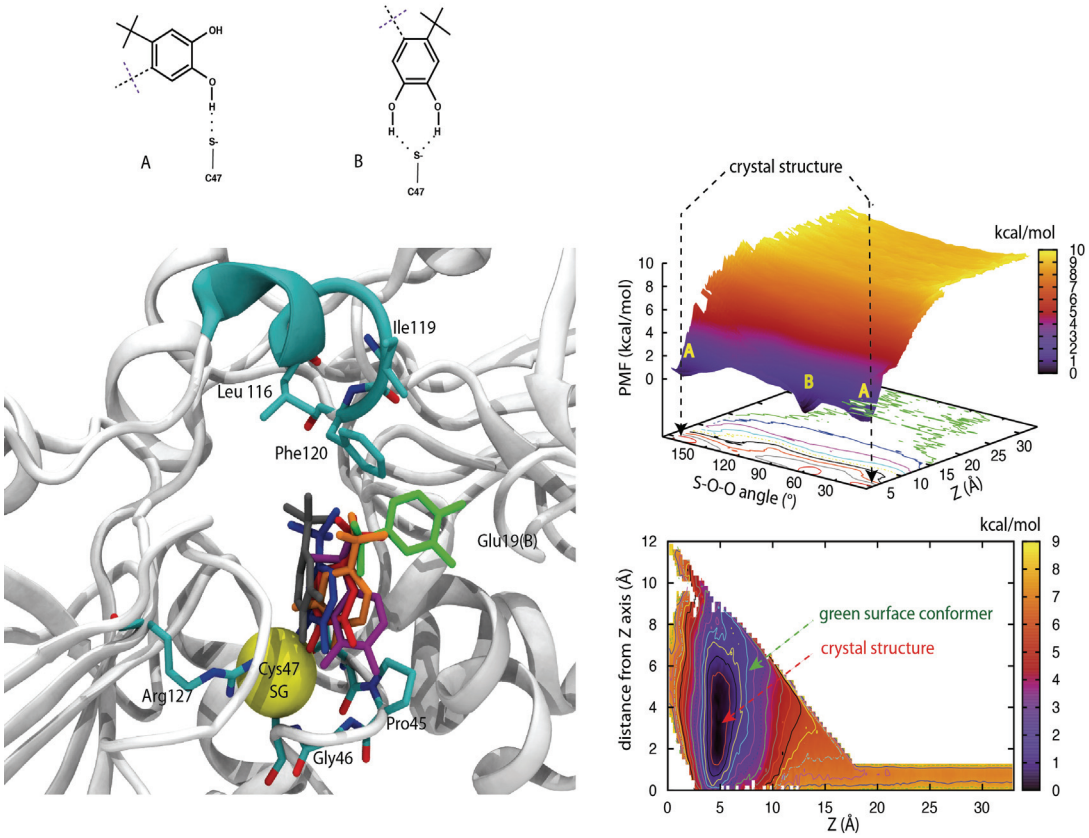

Figure 4 – Binding a 4-*tert*-butylcatechol to hPrx5 active site determined using FM. The top left panel is a schematic of the bound conformations for the ligand to Cys47 thiolate involving H-bonds. Alternative conformations are indicated with dashed bonds for the tert-butyl group. The bottom left panel shows six representative bound conformations (dark gray, navy blue, red, orange, purple, and green) after geometrical clustering of the whole FM trajectory. The Cys47 SG atom is represented as a yellow van der Waals sphere. Invariant amino acids Pro45, Gly46, and Arg127 are represented as cyan sticks as well as Leu116, Ile119, and Phe120 located in a two-turn helix (cyan) capping the active site. The right panels show the FES represented as a function of the three collective variables used in FM calculations. Conformations of type A and B and the crystal structure are located on the top FES. Contours of iso-energy are drawn on the map using a 1 kcal mol^{-1} interval (top FES) or a 0.5 kcal mol^{-1} interval (bottom FES) with the positions of the conformer indicated in green and the crystal structure indicated in red.

4.4.4 FM of catechol derivatives with a simulated ES complex

Determining the relative affinities for the reduced free state of hPrx5 and for the ES complex would improve our understanding and characterization of the type of inhibition mechanism.[4] The ES complex was modeled by instilling a wall potential limiting the interatomic distance between the sulfur atom of the catalytic Cys47 thiolate and one of the two protons of H_2O_2. The distance of 2.0 Å was retained from the analysis of the bound states of the substrate in the unbiased NVT MD (see above). No other restraints were used, allowing hydrogen peroxide to adapt continuously to the active site of hPrx5 and the solvent dynamics. The catechol derivatives were then subjected to FM runs and analyzed (Figures S6−S12).

The catechol derivatives were found to have alternative binding modes in the presence of H_2O_2. However, all the catechol derivatives acquired a free energy penalty to form H-bonds with the catalytic thiolate. Figure 5 exemplifies the case of 4-tert-butylcatechol with a shift observed in the minimum of the free energy basin. A similar phenomenon was noticed for the two other catechol derivatives given in the Supporting Information (Figures S6−S10). For 4-tert-butylcatechol, the major bound conformation fell into the basin corresponding the surface interaction mentioned above for the free enzyme (see the preceding paragraph and Figure 4).

Table 1 gives the estimated $\Delta G_b°$ for each catechol derivative for both the free enzyme and the simulated ES complex. In comparing of the absolute free energy values, the catechol derivatives have a greater affinity for the reduced free state hPrx5 than for the ES complex. Although the catechol derivatives still had an affinity for the ES complex and can still be measured using FM. Therefore, the ability of the catechol derivatives to bind to hPrx5 in a mixed state could suggest the inhibition models against hPrx5.

4.4.5 High-precision NMR affinity assay of 4-*tert*-butylcatechol for reduced hPrx5

The binding affinity of 4-tert- butylcatechol for hPrx5 was examined by ^{15}N HSQC titration over increasing ligand concentrations. Via assessment of the spectra, the amino acids of hPrx5 having the most significant chemical shift perturbations (CSPs) were distinguished. As in the cases of catechol and 4-methylcatechol,[8] Ala42, Thr44, and Ser48 contribute to the greatest CSP perturbations for 4-tert- butylcatechol (Figure S13). The CSPs were plotted against the ratio concentrations of 4-tert-butylcatechol to hPrx5 and were fitted to a hyperbolic isotherm, and a binding dissociation constant (K_D) was obtained (Figure 6). 4-tert-Butylcatechol bound to hPrx5 with a K_D of 0.19 ± 0.03 mM, which correlated to the K_D of 0.11 ± 0.09 mM estimated by FM (Table 1). In comparison to all of the catechol derivatives, 4-tert- butylcatechol bound to hPrx5 with a binding affinity greater than that of 4-methylcatechol (K_D = 1.00 ± 0.20 mM) or that of catechol (K_D = 4.50 ± 0.60 mM).

4.4.6 IC_{50} determination

The ability of the catechol derivatives to bind and inhibit hPrx5 enzymatic activity was first analyzed. hPrx5 enzymatic activity was evaluated through hPrx5 reducing H_2O_2 by NADPH with thioredoxin (yTrx1) and thioredoxin reductase (yTrxR1) as electron transporters (Figure 7). yTrx1, NADPH, and yTrxR1 were used at high concentrations, allowing hPrx5 to be the rate-limiting enzyme.[47] hPrx5 activity was measured using a substrate concentration around the Michaelis−Menten constant (K_M) value (e.g., ~25 μM). The IC_{50} value was determined for each catechol derivative, and the potencies of the inhibitors were established by ranking the IC_{50} values. Under these experimental conditions, 4-tert-butylcatechol was determined to be the most potent inhibitor with an IC_{50} value of 0.25

± 0.06 mM and catechol was the least potent inhibitor with an IC_{50} value of 3.73 ± 0.85 mM (Table 2). Nevertheless, even at high concentrations of the catechol derivatives, the catalytic activity was not fully abolished, suggesting hPrx5 is inhibited through a partial inhibition mechanism (see below).

The possibility of any side reactions or nonspecific interactions of the catechol derivatives with yTrx1, yTrxR1, or NADPH was considered. Using two-dimensional (^{1}H vs ^{15}N) NMR, ^{15}N isotope-labeled yTrx1 and yTrxR1 chemical shift peaks were monitored before and after their incubation with high concentrations (2−10 mM) of the catechol derivatives. Both yTrx1 and yTrxR1 were determined not to bind to any of the catechol derivatives (Figure S14). Also, one- dimensional (1D) ^{1}H NMR was used to demonstrate that catechol derivatives were not transformed into other by- products that could possibly interfere with any of the reaction components during the enzymatic reaction. For each of the catechol derivatives, the only transformation detected after completion of the enzymes reactions was the full oxidation of NADPH into $NADP^{+}$ identified in the 1D spectra (Figure S15).

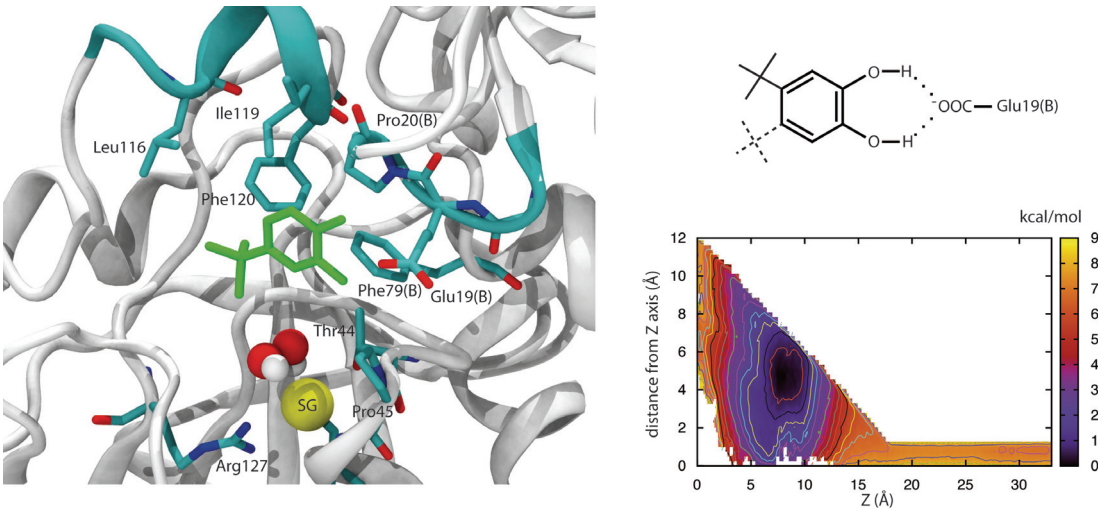

Figure 5 – Binding a 4-*tert*-butylcatechol to hPrx5 active site in the presence of hydrogen peroxide simulated as Michaelis-Menten complex of hPrx5. The left panel is a representative conformation of the lowest region of the free energy basin. 4-tert-Butylcatechol is represented as green sticks and the sulfur of the catalytic Cys47 thiolate as a yellow van der Waals sphere as well as hydrogen peroxide above. Essential amino acids of the active as well as the hydrophobic patch for capping the hPrx5 active site are colored cyan. The top right panel is a schematic of the bound conformation for the ligand's interaction in the lower region of the basin with H-bonds to the Glu19 (chain B) side chain. Alternative conformations are indicated with dashed bonds for the tert-butyl group. The bottom right panels is an FES plot represented as a function of the two collective variables used in FM calculations. Contours of iso-energy are drawn on the map using 0.5 kcal mol−1 intervals.

Table 1. Estimation of the Absolute Free Energy Binding Differences (ΔGb°) and Dissociation Constants (KD) Using FM for the Free Reduced State (E) of hPrx5 and a Simulated Michaelis−Menten Complex (ES) with Hydrogen Peroxide.

	ΔG_b^0 *E* (kcal.mol^{-1})	ΔG_b^0 *ES* (kcal.mol^{-1})	K_D *E* (mM)	K_D *ES* (mM)
Catechol	-3.0 ± 0.2[a]	-2.0 ± 0.3	6.9 ± 2.1[a]	40 ± 30
4-Methylcatechol	-4.2 ± 0.3[a]	1.6 ± 0.2	0.9 ± 0.4[a]	69 ± 26
4-*tert*-Butylcatechol	-5.5 ± 0.9	-4.4 ± 0.5	0.11 ± 0.09	0.8 ± 0.7

[a] value from Reference 8.

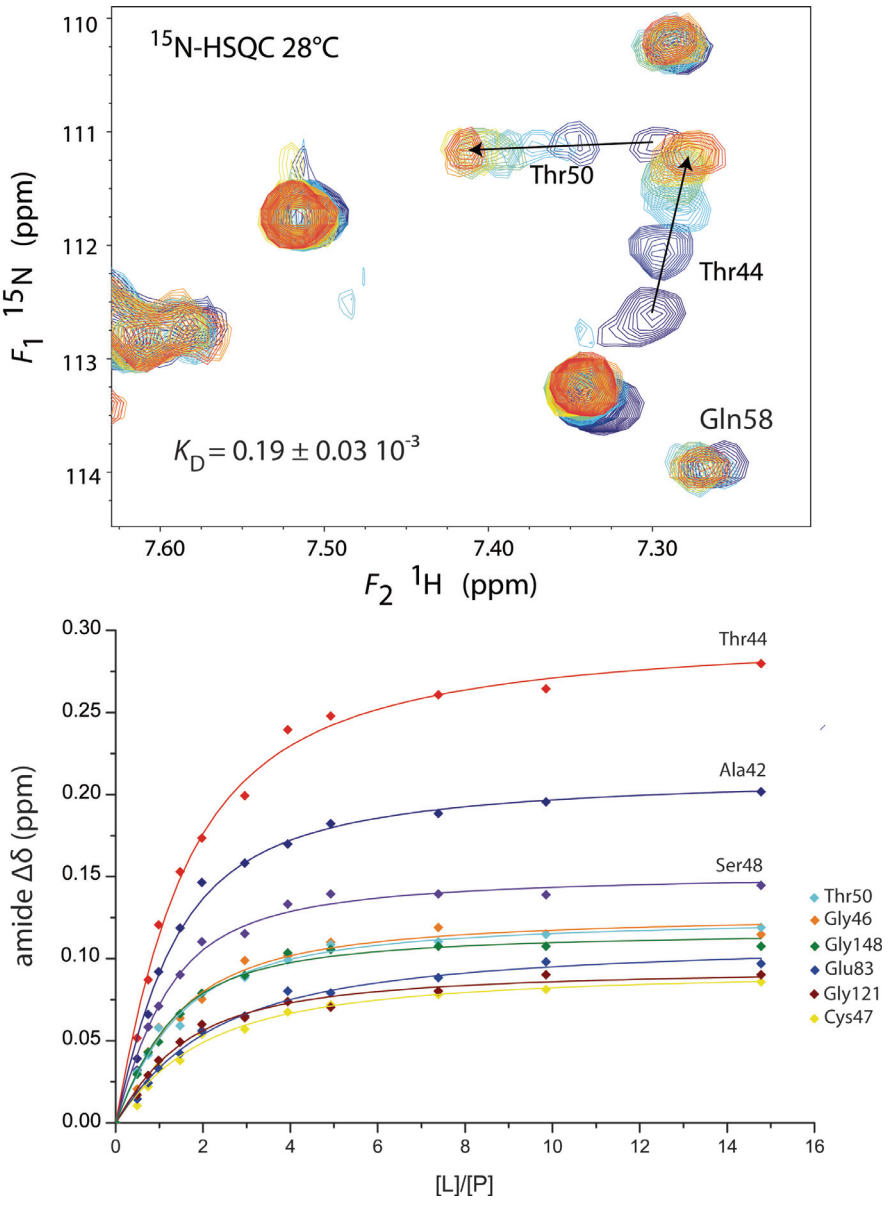

Figure 6 – NMR assay of affinity of 4-*tert*-butylcatechol for reduced hPrx5. The top panel shows superimposed expanded regions of the ^{15}N HSQC experiment, including the Thr50, Thr44, and Gln58 amide signals for protein/ligand ratios ([L]/[P]) ranging from 0 (blue) to 15 (red). The experiments were conducted at a ^{1}H frequency of 600 MHz in PBS (pH 7.4) at 28 °C. The arrows indicate the CSPs induced at equilibrium by ligand binding. The bottom panel is a plot of the combined Δδ amide ^{1}H and ^{15}N CSPs (see Materials and Methods) vs [L]/[P].

4.4.7 Type of inhibition

In identifying how the catechol derivatives could bind and inhibit hPrx5, we examined the inhibition mechanism using steady-state kinetics. As in the IC_{50} assays, hPrx5 activity was monitored using five concentrations of the inhibitors (above and below the IC_{50} value) against a range of H_2O_2 concentrations (0−500 μM).

To understand the inhibition mechanism, changes in the Michaelis−Menten constant (K_M) and maximal velocity constant (V_{max}) were assessed. By plotting the reaction rates against the concentration of H_2O_2 through Michaelis−Menten (rate vs [H_2O_2]) (Figure 8) and Hanes−Woolf ([H_2O_2]/rate vs [H_2O_2]) plots (Figures S16 and S17A−C), we interpreted the K_M and V_{max} trends (Tables S1 and S2). Plotting using both methods yielded similar K_M and V_{max} values. All three catechol derivatives followed identical trends with increasing concen- trations of the inhibitor; the K_M increased while the V_{max} decreased. Therefore, it was determined that the catechol derivatives inhibit hPrx5 in a noncompetitive manner. This inhibition model is represented by an inhibitor binding to the free enzyme and ES (Figure 9). Furthermore, the inhibition constants (K_I and K_I') were determined to provide more details about the subtype of the noncompetitive mechanism. The inhibition mechanisms were analyzed with DynaFit and interpreted under rapid equilibrium-state and steady-state kinetics in the absence of an inhibitor. DynaFit's analysis was validated under both hypotheses. The equilibrium dissociation constant ($K_S = k_{-1}/k_1$) is equivalent to the Michaelis−Menten constant (K_M) under these experimental settings and complied with the relation $k_{cat} \ll k_{-1}$. Thus, the rapid equilibrium hypothesis was used to determine the inhibition mechanism using Dynafit and nonlinear regression methods.[42,43]

For each inhibitor, the reaction rate for each concentration was plotted against the concentration range of H_2O_2 and was fitted to several inhibition mechanism types. All the

catechol derivatives were determined to best fit as the partial mixed noncompetitive inhibition mechanism described in Figure 9. For this model, the catechol derivatives can bind to both the hPrx5 and the ES complex. Comparing the inhibition constants (Table 2), the catechol derivatives preferred to bind and inhibit hPrx5. In addition, hPrx5 activity was not fully impaired by the catechol derivatives binding as H_2O_2 could be reduced to water. Two catalytic turnover rates could be determined from ES (k_{cat} or k_2 in eq 1) or the ternary ESI complex (k_{cat}') as shown in Table 2.

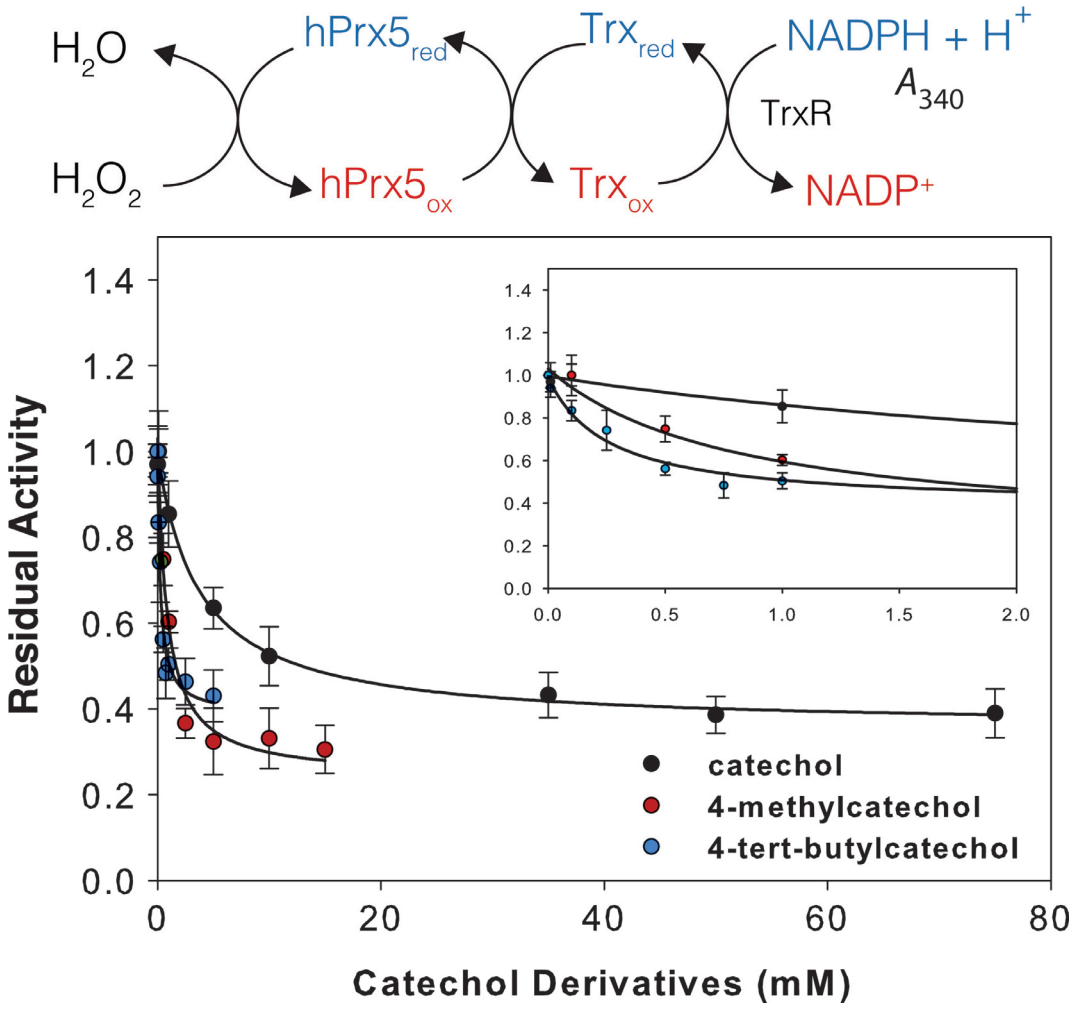

Figure 7- Enzymatic coupling assay used to measure hPrx5 activity and IC_{50}. The top panel shows hPrx5 activity is coupled to NADPH oxidation monitored at 340 nm through thioredoxin (Trx) and thioredoxin reductase (TrxR). The bottom panel is a plot for the concentration-dependent inhibition of hPrx5 by catechol derivatives (Table 2). The reactions were conducted at 23 °C with hPrx5 (0.15 μM) yTrx1 (15 μM), yTrxR1 (2 μM), H_2O_2 (25 μM), and NADPH (200 μM).

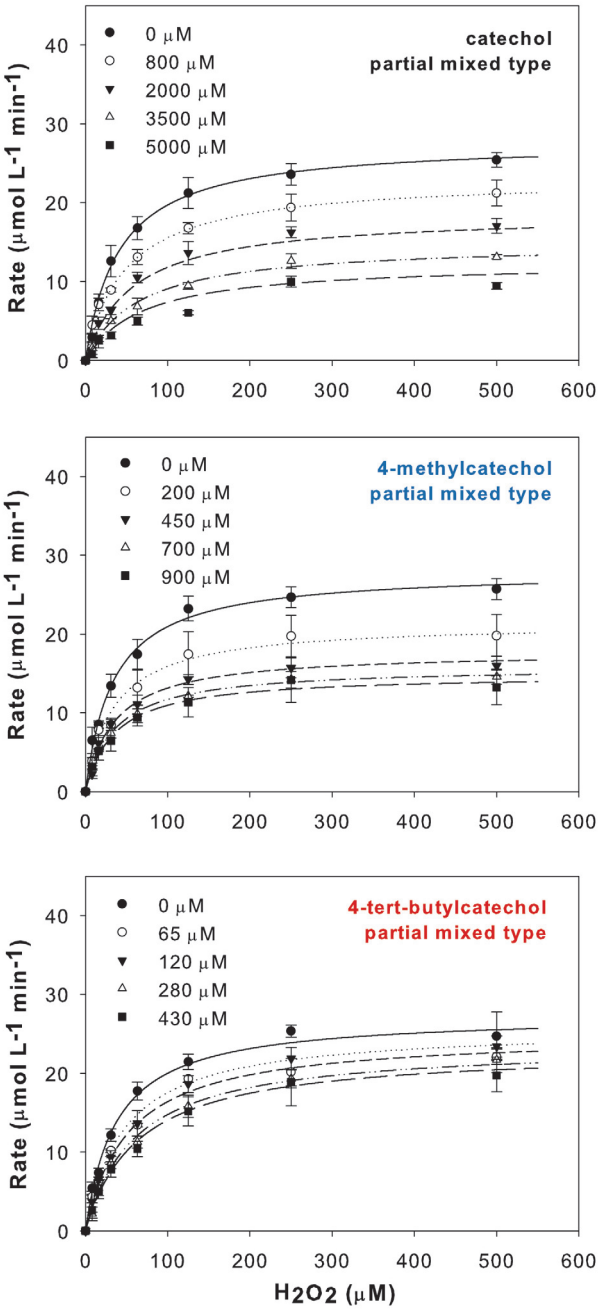

Figure 8 – DynaFit plots for hPrx5 reducing H_2O_2 in the presence of different concentration of catechol (upper), 4-methyl-catechol (middle) and 4-*tert*-butylcatechol (bottom). The initial rates for each inhibitor concentration were plotted vs substrate concentration. The data were fitted using a nonlinear fitting method against several types of inhibition models to determine the best inhibition model using Dynafit. The reactions were conducted at 23 °C with hPrx5 (0.15 μM), Trx (15 μM), TrxR (2 μM), H_2O_2 (0−500 μM), NADPH (200 μM), and the catechol derivatives at various concentrations.

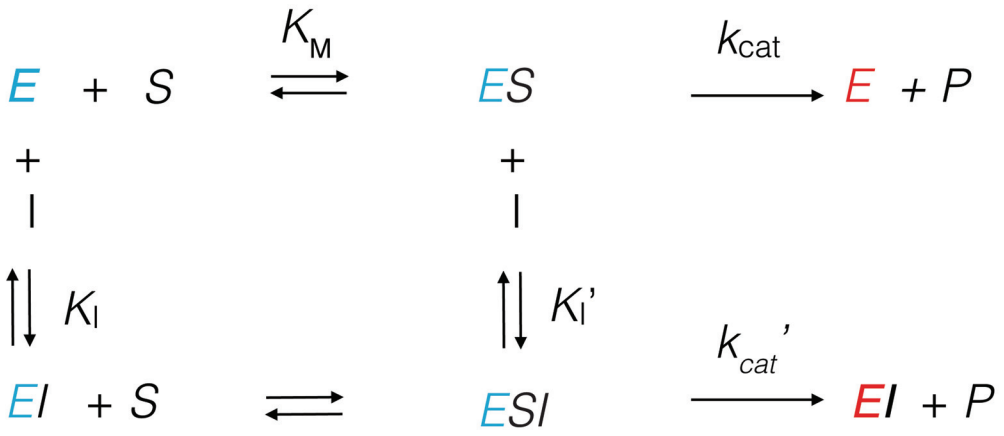

Figure 9 – Partial mixed type noncompetitive inhibition model for the catechol derivatives against hPrx5. When hPrx5 (blue) (E) is inhibited by an inhibitor (I), there are two pathways. The I can bind to either the free enzyme or the Michaelis−Menten complex (ES). Under these conditions, hPrx5 is not fully inhibited and can produce product (P): either by ES or ESI represented by rate constant k_{cat} or k_{cat}', respectively. The oxidized hPrx5 state is colored red (Cys47-SOH or sulfenic acid) and can be regenerated to its reduced state by the thioredoxin system (see Figure 7).

Table 2. Binding affinities of the catechol derivatives and inhibition properties of hPrx5. The mode of inhibition by the catechol derivatives of hPrx5 was identified as being partial mixed type noncompetitive (partial). Kinetic parameters K_M, k_{cat}, and k_{cat}' and inhibition constants K_I and K_I' are averaged over three independent repeats with the error being the standard error. [b]From ref 8. [c]See Discussion.

	catechol	**4-methylcatechol**	**4-*tert* -butylcatechol**
NMR ^{15}N-HSQC			
K_D **(mM)**	4.50 ± 0.60[b]	1.00 ± 0.20[b]	0.19 ± 0.03
IC_{50}			
IC_{50} **(mM)**	3.73 ± 0.85	0.82 ± 0.14	0.25 ± 0.06
DynaFit Model Discrimination			
Best Model Type	Partial	Partial	Partial
K_s **(μM)**	40.7 ± 4.0	33.7 ± 4.6	36.9 ± 4.4
K_I **(mM)**	1.81 ± 0.46	0.33 ± 0.13	0.09 ± 0.04
K_I**' (mM)**	4.04 ± 1.13	0.36 ± 0.12	0.18 ± 0.10
k_{cat} **(s^{-1})**	3.08 ± 0.08	3.11 ± 0.01	3.05 ± 0.10
k_{cat}**' (s^{-1})**	~0 [c]	1.07 ± 0.25	2.35 ± 0.18
k_{cat} **/** K_s **(M^{-1} s^{-1})**	(1.14 ± 0.14) x 10^5	(9.24 ± 1.10) x 10^4	(8.25 ± 0.82) x 10^4

4.5 Discussion

In investing of the binding of the catechol derivatives to hPrx5, FM and solution NMR experiments provided microscopic details to improve our understanding of the interaction conformations. The catechol derivatives were determined to bind and interact with hPrx5. Also, the catechol derivatives were identified as inhibitors impeding hPrx5 catalytic activity. By examining the outcomes of the various techniques used, we found parallels with FM and the inhibitory in vitro assays. Therefore, the possibility of utilizing FM computational modeling to assist in validating ligands as future inhibitors for drug design development is introduced.

4.5.1 Ligand binding affinity correlates to inhibition

From the ^{15}N HSQC NMR titration experiments, 4-tert- butylcatechol was determined to bind hPrx5 with a K_D of 0.19 mM. The NMR titrations identified the residues perturbed within the active site of hPrx5 and near catalytic Cys47.[8,46] 4- tert-Butylcatechol had a binding affinity for hPrx5 significantly greater than those of the other catechol derivatives (see Table 2). Additionally, the catechol derivatives, with a binding affinity for hPrx5, were also determined to inhibit hPrx5 catalytic activity. The IC_{50} assay confirmed 4-tert-butylcatechol to be the most potent inhibitor. These findings were supported by a previous study in which 4-methylcatechol was determined to be more potent than catechol, 4-methylcatechol and catechol inhibiting hPrx5 activity with IC_{50} values of 26 and 105 μM, respectively.[37]

4.5.2 Catechol derivatives inhibition mechanism

The mechanism of inhibition of the catechol derivatives by hPrx5 provided further insight into the binding and inhibition properties. All the catechol derivatives were

determined to inhibit in a partial mixed type noncompetitive model (Figure 9). In examining of the inhibitory constant values, the K_I' was greater than or equal to K_I, indicating the inhibitors prefer to bind the free enzyme rather than the ES complex. From a partial mixed type noncompetitive inhibition model, hPrx5 catalysis activity was also not totally abolished. There are two pathways for converting hydrogen peroxide represented by k_{cat} and k_{cat}'.

In examining of 4-tert-butylcatechol and 4-methylcatechol inhibition properties, their k_{cat}' values are not as reduced in comparison to their k_{cat} values. This suggested that these two inhibitors do not bind to the ES complex very well (Table 2), whereas for catechol, the k_{cat}' value was practically zero. Therefore, this would indicate that the ESI complex is catalytically inactive and the mechanism could be a mixed type noncompetitive mechanism. However, the catechol's inhibition data fit poorly to this precise model (Figure S18). Upon comparison of the inhibitory constants (K_I and K_I'), the turnover rate values (k_{cat} and k_{cat}'), and the Michaelis−Menten constant (K_M), there were discrepancies in the trends found for the other catechol derivatives. As a result, these differences suggested that catechol does not completely fit to the partial mixed type noncompetitive model but is the closest model.

4.5.3 FM simulating hPrx5 *ES* formation

FM simulations provided valuable details about the reversible binding interactions of H_2O_2 prior to its catalytic conversion. Also, the knowledge of the hPrx5 ES complex is important because the catechol derivatives were determined to inhibit in a noncompetitive manner, affecting the free hPrx5 and ES complex. FM as well as NVT MD trajectories identified a very loose ES complex. H_2O_2 appears to be a very small substrate that diffuses very quickly in solution with no particular affinity for hPrx5 during the trajectory. The unrestrained NVT trajectories indicated only short residence times on the order of 10^{-9} s. During the binding periods, hydrogen peroxide made a H-bond with the catalytic thiolate and

formed a weakly stabilized ES complex. When FM simulations are manipulated, it should be noted that FM increases the number of binding events but the protein dynamics remain unchanged. As a result, this reveals the limitation from FM, and there could be some biased effects in estimating the ES $\Delta G_b°$, for instance, if the hPrx5 needs a longer time scale to transit to another conformation to bind H_2O_2 (a different unknown ES complex).

4.5.4 MD with ligands

In the unbiased NVT molecular dynamic studies, interaction of hPrx5 with the ligands revealed the same various binding conformations as in FM. This indicated that the external funnel potential reproduced the most important interactions well within the active site region. Previously, evaluating the interaction of catechol and 4-methylcatechol with hPrx5 showed that the active site and the whole homodimer are subjected to small conformational changes upon ligand binding. In particular, the 4-methylcatechol active site was observed to induced a small shrinkage of the active site to optimize the interaction with the enzyme.[8] However, in this case when 4-tert-butylcatechol bound, it caused the active site to slightly expand instead of retracting. The active site expansion is probably contributed to the 4-tert-butylcatechol being a bulkier ligand and the active site cavity adapting to its size to bind. As also observed in the MD trajectories, the ligands could transit from one bound conformation to another without the need to fully unbind from the active site. These possible transitions are likely related to the fact that the three catechol derivatives still represent low-affinity ligands with K_D values ranging from ~10^{-3} to 10^{-4} M. Overall, MD and FM simulations contributed to a general understanding of how the catechol derivatives interact and bind to hPrx5. These microscopic aspects of protein−ligand interaction could be advantageous for the production of ideal ligands to become inhibitors of enzymes.

4.5.5 Combining FM and enzyme inhibition

Studying the inhibition mechanism against hPrx5, we determined the catechol derivatives inhibited binding to the E and ES complex. FM modeling simulations examined the binding of the catechol derivatives to the E and ES complex. In analyzing the ES complex, we simulated a proposed ES conformation by maintaining hydrogen peroxide bound to hPrx5 through a H- bond to Cys47 thiolate using a distance limiting potential. For each catechol derivative interacting with the mimicked ES complex, there was a drop in the $\Delta G_b°$ values of 1−2 kcal mol^{-1}. Accompanying the changes in the $\Delta G_b°$ were alternative modes of binding of the catechol derivatives to the ES complex. For 4-methylcatechol and 4-tert-butylcatechols (see Figures 4 and 5), there were additional binding modes mainly seen at the periphery of the hPrx5 active site. These additional binding modes could be attributed to the increased residual affinity of 4- methylcatechol and 4-tert-butylcatechol when simulating ES from the extra aliphatic groups present on the catechol backbone. By monitoring the FM simulation, we found 4- methylcatechol and 4-tert-butylcatechol interacted with ES but not specifically with Cys47 forming a H-bond. This would be the origin of the significance of the k_{cat}' values noticed for 4- methylcatechol and 4-tert-butylcatechol for the inhibition mechanism. However, for catechol, these alternative binding modes were less favorable upon interaction with ES. Catechol's reduced affinity for ES could be associated with the simple structural features of catechols and the inability to make interactions stabilized with Leu116, Ile199, and Phe120 mentioned in Figures 4 and 5.

4-*tert*-Butylcatechol improved binding interactions, which can be attributed to its aliphatic group enhancing noncovalent interactions with the hPrx5 free enzyme state. Also, for interactions of 4-tert-butylcatechol with ES, the ligand had alternative binding modes and could complement the retracement in the active site assisting in binding more efficiently. Although these catechol derivatives bound to hPrx5 with a low binding affinity, these microscopic features could be used to improve the design of better ligands to bind to hPrx5.

Overall, FM simulations are sufficiently sensitive to measure binding of a ligand to E and ES to discriminate different binding capabilities.

4.5.6 Concluding remarks

Utilizing NMR techniques, there was early evidence supporting the hypothesis that the catechol derivatives could bind specifically to the active site and do not interact with other catalytic proteins of hPrx5. Accompanied by the NMR results, the FM simulations of the free reduced enzyme and ES complex provided more binding interaction explanations at the microscopic level. Therefore, one could make an inference that FM simulations could be used to predict the inhibition mechanism of a ligand. The estimated $\Delta G_b°$ for both the free enzyme and a simulated ES from FM had common a trend with respect to the inhibition constants (K_I and K_I'). Consequently, one could anticipate the inhibition model as being a noncompetitive mechanism specifically for the catechol derivatives against hPrx5.

Here this study shows how integrating solution NMR and MD simulations can be a valuable tool in understanding the protein−ligand interaction at the microscopic level. Specifically, MD analysis can contribute to the details used for preliminary predictions of potential ligands being inhibitors and the proposal of an inhibition mechanism. This is one example of how MD simulations can be used in drug design to improve drug development. However, additional studies using MD to predict ligands as potential inhibitors will strengthen and improve the value of computational simulations. Overall, MD can contribute to improving drug screening time and costs, benefiting the in vitro investigation level in the pharmaceutical industry.

4.6 References

(1) Henri,V.(1902)Theóriegeńeŕaledel'actiondequelques diastases. C. R. Acad. Sci. Paris 135, 916−919.

(2) Michaelis, L., and Menten, M. L. (1913) Kinetik der Invertinwirkung. Biochem. Zeitung 49, 333−369.

(3) Johnson, K. A., and Goody, R. S. (2011) The Original Michaelis Constant: Translation of the 1913 Michaelis−Menten Paper. Biochemistry 50, 8264−8269.

(4) Segel, I. (1993) Enzymes Kinetics. Behavior Analysis of Rapid Equilibrium and Steady-State Enzymes Systems, Wiley Classics Library Edition, Wiley, New York.

(5) Cornish-Bowden, A. (2015) One hundred years of Michaelis− Menten kinetics. Persp. Sci. 4, 3−9.

(6) Changeux, J. P. (2011) 50th anniversary of the word ″allosteric″. Prot. Sci. 20, 1119−1124.

(7) Harvey, M. J., and De Fabritiis, G. (2012) High-throughput molecular dynamics: the powerful new tool for drug discovery. Drug Discovery Today 17, 1059−1062.

(8) Troussicot, L., Guilliere, F., Limongelli, V., Walker, O., and Lancelin, J. M. (2015) Funnel-metadynamics and solution NMR to estimate protein-ligand affinities. J. Am. Chem. Soc. 137, 1273−1281.

(9) Limongelli, V., Bonomi, M., and Parrinello, M. (2013) Funnel metadynamics as accurate binding free-energy method. Proc. Natl. Acad. Sci. U. S. A. 110, 6358−6363.

(10) Karplus, P. A. (2015) A primer on peroxiredoxin biochemistry. Free Radical Biol. Med. 80, 183−190.

(11) Perkins, A., Nelson, K. J., Parsonage, D., Poole, L. B., and Karplus, P. A. (2015) Peroxiredoxins: guardians against oxidative stress and modulators of peroxide signaling. Trends Biochem. Sci. 40, 435− 445.

(12) Wood, Z. A., Schroder, E., Robin Harris, J., and Poole, L. B. (2003) Structure, mechanism and regulation of peroxiredoxins. Trends Biochem. Sci. 28, 32−40.

(13) Wood, Z. A., Poole, L. B., and Karplus, P. A. (2003) Peroxiredoxin evolution and the regulation of hydrogen peroxide signaling. Science 300, 650−653.

(14) Seo, M. S., Kang, S. W., Kim, K., Baines, I. C., Lee, T. H., and Rhee, S. G. (2000) Identification of a new type of mammalian peroxiredoxin that forms an intramolecular disulfide as a reaction intermediate. J. Biol. Chem. 275, 20346−20354.

(15) Perkins, A., Poole, L. B., and Karplus, P. A. (2014) Tuning of Peroxiredoxin Catalysis for Various Physiological Roles. Biochemistry 53, 7693−7705.

(16) Fujii, J., and Ikeda, Y. (2002) Advances in our understanding of peroxiredoxin, a multifunctional, mammalian redox protein. Redox Rep. 7, 123−130.

(17) Nystrom, T., Yang, J., and Molin, M. (2012) Peroxiredoxins, gerontogenes linking aging to genome instability and cancer. Genes Dev. 26, 2001−2008.

(18) Shichita, T., Hasegawa, E., Kimura, A., Morita, R., Sakaguchi, R., Takada, I., Sekiya, T., Ooboshi, H., Kitazono, T., Yanagawa, T., Ishii, T., Takahashi, H., Mori, S., Nishibori, M., Kuroda, K., Akira, S., Miyake, K., and Yoshimura, A. (2012) Peroxiredoxin family proteins are key initiators of post-ischemic inflammation in the brain. Nat. Med. 18, 911−917.

(19) Haraldsen, J. D., Liu, G., Botting, C. H., Walton, J. G. A., Storm, J., Phalen, T. J., Kwok, L. Y., Soldati-Favre, D., Heintz, N. H., Muller, S., Westwood, N. J., and Ward, G. E. (2009) Identification of conoidin A as a covalent inhibitor of peroxiredoxin II. Org. Biomol. Chem. 7, 3040−3048.

(20) Liu, C. X., Yin, Q. Q., Zhou, H. C., Wu, Y. L., Pu, J. X., Xia, L., Liu, W., Huang, X., Jiang, T., Wu, M. X., He, L. C., Zhao, Y. X., Wang, X. L., Xiao, W. L., Chen, H. Z., Zhao, Q., Zhou, A. W., Wang, L. S., Sun, H. D., and Chen, G. Q. (2012) Adenanthin targets peroxiredoxin I and II to induce differentiation of leukemic cells. Nat. Chem. Biol. 8, 486−493.

(21) Wei, W., Ma, C., Cao, Y., Yang, L., Huang, Z., Qin, D., Chen, Y., Liu, C., Xia, L., and Wang, T. (2016) Identification of H7 as a novel peroxiredoxin I inhibitor to induce differentiation of leukemia cells. Oncotarget 7, 3873−3883.

(22) Zhao, Q., Ding, Y., Deng, Z., Lee, O.-Y., Gao, P., Chen, P., Rose, R. J., Zhao, H., Zhang, Z., Tao, X.-P., Heck, A. J. R., Kao, R., and Yang, D. (2015) Natural products triptolide, celastrol, and withaferin A inhibit the chaperone activity of peroxiredoxin I. Chem. Sci. 6, 4124− 4130.

(23) Parker, A. R., Petluru, P. N., Nienaber, V. L., Badger, J., Leverett, B. D., Jair, K., Sridhar, V., Logan, C., Ayala, P. Y., Kochat, H., and Hausheer, F. H. (2015) Cysteine specific targeting of the functionally distinct peroxiredoxin and glutaredoxin proteins by the investigational disulfide BNP7787. Molecules 20, 4928−4950.

(24) Hall, A., Parsonage, D., Poole, L. B., and Karplus, P. A. (2010) Structural evidence that peroxiredoxin catalytic power is based on transition-state stabilization. J. Mol. Biol. 402, 194−209.

(25) Bernstein, F. C., Koetzle, T. F., Williams, G. J., Meyer, E. F., Jr., Brice, M. D., Rodgers, J. R., Kennard, O., Shimanouchi, T., and Tasumi, M. (1978) The Protein Data Bank: a computer-based archival file for macromolecular structures. Arch. Biochem. Biophys. 185, 584− 591.

(26) Cornell, W. D., Cieplak, P., Bayly, C. I., Gould, I. R., Merz, K. M., Ferguson, D. M., Spellmeyer, D. C., Fox, T., Caldwell, J. W., and Kollman, P. A. (1995) A Second Generation Force Field for the Simulation of Proteins, Nucleic Acids, and Organic Molecules. J. Am. Chem. Soc. 117, 5179−5197.

(27) Hornak, V., Abel, R., Okur, A., Strockbine, B., Roitberg, A., and Simmerling, C. (2006) Comparison of multiple Amber force fields and development of improved protein backbone parameters. Proteins: Struct., Funct., Genet. 65, 712−725.

(28) Lindorff-Larsen, K., Piana, S., Palmo, K., Maragakis, P., Klepeis, J. L., Dror, R. O., and Shaw, D. E. (2010) Improved side-chain torsion

potentials for the Amber ff99SB protein force field. Proteins: Struct., Funct., Genet. 78, 1950−1958.

(29) Jorgensen, W. L., and Madura, J. D. (1983) Quantum and statistical mechanical studies

of liquids. 25. Solvation and con- formation of methanol in water. J. Am. Chem. Soc. 105, 1407−1413.

(30) Wang, J., Wolf, R. M., Caldwell, J. W., Kollman, P. A., and Case, D. A. (2004) Development and testing of a general amber force field. J. Comput. Chem. 25, 1157−1174.

(31) Wang, J., Wang, W., Kollman, P. A., and Case, D. A. (2006) Automatic atom type and bond type perception in molecular mechanical calculations. J. Mol. Graphics Modell. 25, 247−260.

(32) Harvey, M. J., Giupponi, G., and Fabritiis, G. D. (2009) ACEMD: Accelerating Biomolecular Dynamics in the Microsecond Time Scale. J. Chem. Theory Comput. 5, 1632−1639.

(33) Feenstra, K. A., Hess, B., and Berendsen, H. J. C. (1999) Improving efficiency of large time-scale molecular dynamics simulations of hydrogen-rich systems. J. Comput. Chem. 20, 786−798.

(34) Bonomi, M., Branduardi, D., Bussi, G., Camilloni, C., Provasi, D., Raiteri, P., Donadio, D., Marinelli, F., Pietrucci, F., Broglia, R. A., and Parrinello, M. (2009) PLUMED: A portable plugin for free-energy calculations with molecular dynamics. Comput. Phys. Commun. 180, 1961−1972.

(35) Humphrey, W., Dalke, A., and Schulten, K. (1996) VMD: Visual molecular dynamics. J. Mol. Graphics 14, 33−38.

(36) Declercq, J. P., Evrard, C., Clippe, A., Stricht, D. V., Bernard, A., and Knoops, B. (2001) Crystal structure of human peroxiredoxin 5, a novel type of mammalian peroxiredoxin at 1.5 A resolution. J. Mol. Biol. 311, 751−759.

(37) Barelier, S., Linard, D., Pons, J., Clippe, A., Knoops, B., Lancelin, J. M., and Krimm, I. (2010) Discovery of fragment molecules that bind the human peroxiredoxin 5 active site. PLoS One 5, e9744.

(38) Delaglio, F., Grzesiek, S., Vuister, G. W., Zhu, G., Pfeifer, J., and Bax, A. (1995) NMRPipe: a multidimensional spectral processing system based on UNIX pipes. J. Biomol. NMR 6, 277−293.

(39) Johnson, B., and Blevins, R. (1994) NMR View: A computer program for the visualization and analysis of NMR data. J. Biomol. NMR 4, 603−614.

(40) Farmer, B. T., 2nd, Constantine, K. L., Goldfarb, V., Friedrichs, M. S., Wittekind, M., Yanchunas, J., Jr., Robertson, J. G., and Mueller, L. (1996) Localizing the NADP+ binding site on the MurB enzyme by NMR. Nat. Struct. Biol. 3, 995−997.

(41) Kim, I., Lee, K. S., Hwang, J. S., Ahn, M. Y., Li, J., Sohn, H. D., and Jin, B. R. (2005) Molecular cloning and characterization of a peroxiredoxin gene from the mole cricket, Gryllotalpa orientalis. Comp. Biochem. Physiol., Part B: Biochem. Mol. Biol. 140, 579−587.

(42) Kuzmič, P. (2009) DynaFit: A Software Package for Enzymology. In Methods in Enzymology, Chapter 10, pp 247−280, Academic Press, San Diego.

(43) Kuzmic,˘ P. (1996) Program DYNAFIT for the Analysis of Enzyme Kinetic Data: Application to HIV Proteinase. Anal. Biochem. 237, 260−273.

(44) Laio, A., and Gervasio, F. L. (2008) Metadynamics: a method to simulate rare events and reconstruct the free energy in biophysics, chemistry and material science. Rep. Prog. Phys. 71, 126601.

(45) Barducci, A., Bussi, G., and Parrinello, M. (2008) Well- Tempered Metadynamics: A Smoothly Converging and Tunable Free- Energy Method. Phys. Rev. Lett. 100, 020603.

(46) Aguirre, C., ten Brink, T., Guichou, J. F., Cala, O., and Krimm, I. (2014) Comparing binding modes of analogous fragments using NMR in fragment-based drug design: application to PRDX5. PLoS One 9, e102300.

(47) Copeland, R. A. (2005) Evaluation of enzyme inhibitors in drug discovery. A guide for medicinal chemists and pharmacologists. Methods Biochem. Anal. 46, 1−265.

5 Discussion

The purpose of this thesis was to investigate the hypotheses that catechol derivatives (catechol, 4-methylcatechol, and 4-*tert*-butylcatechol) can bind and also inhibit hPrxs peroxidase activity and understand the types of MMOAs. Currently, there are limited drugs available for treatment against post-ischemic inflammation of stroke patients and there is interest to identify new lead inhibitors as possible drugs. The binding interaction and affinities of the catechol derivatives were examined through NMR spectroscopy techniques and computational modeling. Identifying if the catechol derivatives could bind to hPrx1, hPrx2, and hPrx5, the inhibition properties of the catechol derivatives were studied to understand the inhibition MMOA. Knowledge of the catechol derivatives binding and inhibition MMOA to hPrxs can further insight to help in distinguishing key features for improvements in drug design.

5.1 Catechol derivatives bind to hPrxs

5.1.1 Characterizing the binding interactions by NMR spectroscopy

Simple ligand binding to a protein is the basis for identifying inhibitors to be as leads and possibly drugs. To determine if the catechol derivative could bind to hPrx5, hPrx2 and hPrx1, the binding interactions were measured by NMR spectroscopy techniques: ^{15}N-HSQC and STD. All the catechol derivatives were identified to bind to all the hPrxs and 4-*tert*-butylcatechol had the greatest binding affinity in comparing the K_d values. Table 12 is a summary of the catechol derivatives binding affinities to the hPrxs.

^{15}N-HSQC was conducted measuring the interaction of the catechol derivatives to hPrx5 as a high quality ^{1}H-^{15}N 2D spectrum could be obtained for hPrx5. 4-*tert*-butylcatechol was determined to have the greatest binding affinity to hPrx5 amongst catechol and 4-methylcatechol. 4-*tert*-butylcatechol bound to hPrx5 interacting with the amino acids within

the active site (Ala42, Thr44, Gly46, Cys47 (C_p), Ser48, and Thr50) and the loop connected to α-helix surrounding the active site (Leu 116, Ser118, IIe 119, Gly121, Thr147) of hPrx5 were involved in binding (Chow *et al.* 2016). The amino acids of hPrx5 identified in interacting with 4-*tert*-butylcatechol were also similar to past studies determined for hPrx5 binding interaction to catechol and 4-methylcatechol determined by ^{15}N-HSQC [27,32]. Additionally, the binding conformations observed for the catechol derivatives to hPrx5 by ^{15}N-HSQC NMR were also identified in co-crystallized structure obtained for the catechol derivatives bound to hPrx5 too [27].

Evaluating the binding of the catechol derivatives to hPrx1 and hPrx2, STD NMR was used instead of ^{15}N-HSQC since the ^{1}H-^{15}N 2D spectra obtained for hPrx1 and hPrx2 had poor quality presumably only detecting the His-tag. The catechol derivatives protons in contact with hPrxs were delineated through group epitope mapping [54,76]. All the catechol derivatives were found to bind to hPrx1 and hPrx2. The protons within the catechol ring were identified to be more involved in the binding interaction as opposed to the methyl or *tert*-butyl groups. The interaction of the catechol derivative proton's to hPrx1 and hPrx2 was similar to previously STD NMR results examined for the catechol derivatives binding interaction to hPrx5 [27]. Therefore, this suggested the binding interaction might occur in the active site of hPrx1 and hPrx2. Although, further characterizing of hPrx1 and hPrx2 in their dimeric state would be beneficial to carrying out ^{15}N-HQSC to identify the exact amino acids of the hPrxs and location on the proteins that are implicated in the binding. Therefore, computational modeling was used to inquire the possible binding interaction of the catechol derivatives at the active sites specifically for hPrx2.

Table 12: Comparing the K_d and IC_{50} values for the catechol derivatives to the hPrxs.

The K_d values are from the STD NMR spectroscopy (hPrx1 and hPrx2), 2D ^{1}H-^{15}N HSQC NMR spectroscopy (hPrx5) and FM simulations experiments. Also, are the IC_{50} values determined for the 4-*tert*-butylcatechol to the hPrxs. Shown here are hPrx1 **(A)**, hPrx2 **(B)** and hPrx5 **(C)**.

A. hPrx1

	STD or HSQC NMR	FM	Inhibition
	K_d (mM)	K_d (mM)	IC_{50} (mM)
Catechol	95.64 ± 14.57	-	-
4-methylcatechol	26.82 ± 20.34	-	-
4-*tert*-butylcatechol	26.02 ± 7.01	-	0.13 ± 0.04

B. hPrx2

	K_d (mM)	K_d (mM)	IC_{50} (mM)
Catechol	55.54 ± 9.42	14.5 ± 7.2	-
4-methylcatechol	54.12 ± 13.07	84.0 ± 110.0	-
4-*tert*-butylcatechol	5.86 ± 0.98	5.60 ± 1.80	0.19 ± 0.06

C. hPrx5

	K_d (mM)	K_d (mM)	IC_{50} (mM)
Catechol	4.50 ± 0.60 *	6.90 ± 2.10 *	4.04 ± 0.94
4-methylcatechol	1.00 ± 0.20 *	2.40 ± 1.60 *	0.70 ± 0.16
4-*tert*-butylcatechol	0.19 ± 0.03 ♯	0.11 ± 0.09 ♯	0.25 ± 0.07

* Troussicot *et al*. 2015[32]
♯ Chow *et al.* 2016

5.1.2 Characterizing the binding interactions by FM simulations

To understand the binding interactions at the microscopic level computational simulations by funnel-metadynamics (FM) were utilized to provide further details. FM was used as it enhances the binding events at the active sites of hPrxs and following the unbinding and binding events of the catechol derivatives in solution [32,59]. Analyzing the binding interactions of the catechol derivatives to the reduced dimer states of hPrx5 and hPrx2, all the catechol derivatives were determined to bind. hPrx2 was only modeled and not hPrx1 since the structural overlays of the two hPrxs were determined to be similar and also their actives sites highly conserved and homologous [39]. Comparing the K_d values, 4-*tert*-butylcatechol was found to have the greatest binding affinity than catechol and 4-methylcatechol amongst hPrx5 and hPrx2 (see Table 12). Assessing the differences between the hPrxs, 4-*tert*-butylcatechol bound with ~ 50 folds higher binding affinity to hPrx5 than hPrx2.

The improved binding interaction for 4-*tert*-butylcatechol to hPrx5 than hPrx2 could be attributed to several structural differences. As mentioned, hPrx5 is apart of the atypical 2-Cys class that forms intramolecular disulfide bonds between the C_p and C_r during the catalytic reaction. hPrx1-4 are apart of the typical 2-Cys class that form intermolecular disulfide bonds between C_p and C_r. hPrx5 dimer is formed through A-type interface contacts between α-helices (α-3) and hPrx1-4 dimer contact site is between β-sheets (β-7) represented by B-type interface (see Figure 43) [9,39]. Aligning hPrx2 and hPrx5 amino acid sequences, hPrx5 has less amino acids in the overall sequence length than hPrx2, and hPrx5 lacks some β-sheets and α-helices found at the C-terminus. Also, hPrx5 does not have the GGLG and YF motifs seen in hPrx1-4 which, these regions are known to contribute to sensitivity to overoxidation [9]. Within the active site **P**XXX**T**XX**C** motif, there are some variations in the conserved amino acids present between hPrx2 and hPrx5 (see Figure 44). hPrx2 active site motif region has more amino acids involved in the binding interaction with the catechol derivatives than hPrx5 (Pro43, Leu44, Thr47, Phe48 and Cys50). While, hPrx5 has more amino acids involved in the binding interaction in a linker region including Leu116, Ile119 and Phe120 and this region

is absent in hPrx1-4 (see Figure 44– key amino acids in green #180-190 region). Also, hPrx2 has more amino acids from its second monomer involved in the binding contacts in the active site than hPrx5 (amino acids in orange). Therefore, these structural alterations between hPrx5 and hPrx2 maybe a contributing factor influencing the binding interactions of the catechol derivatives in the active site.

5.2 Characterizing recombinant redox proteins

All the recombinant redox proteins required to setup the peroxidase assay were expressed and purified. Upon successfully expressing the proteins, their purity and MW were examined by SDS-PAGE. yTrx1, yTrxR1, hPrx1 and hPrx2 MWs under reducing conditions were confirmed to be their MWs and were compared to past studies reaffirming I obtained our proteins of interest [71,87–91]. Additionally, a protein fingerprint of each recombinant redox protein was acquired by ^{15}N-HSQC NMR spectroscopy. Only yTrx1 acquired a high-quality 2D ^{1}H-^{15}N spectrum, which was comparable to past ^{15}N-HSQC spectrum for yTrx2 confirming its structural properties. Whereas for yTrxR1, hPrx1 and hPrx2, they all had poor quality 2D ^{1}H-^{15}N spectra with sparse peaks observed which, presumably represented the exposed region of the proteins being the His-tag. While, the rest of the protein structure was not observed, as the N-H signals were lost and can be attributed to HMW proteins having fast transverse relaxation rates. Therefore, this suggested the recombinant proteins were HMW oligomers in solution. However, the possibility the recombinant redox proteins were HMW oligomers was not surprising since TrxR and Prxs are known to function as homodimers or oligomers for their redox activity [29,92].

SEC confirmed the recombinant redox proteins were highly ordered oligomers in solution except yTrx1. yTrx1 was determined to be a monomer in solution with an MW ~ 11 kDa which, corroborated to past studies by SEC and also, is representative of its known

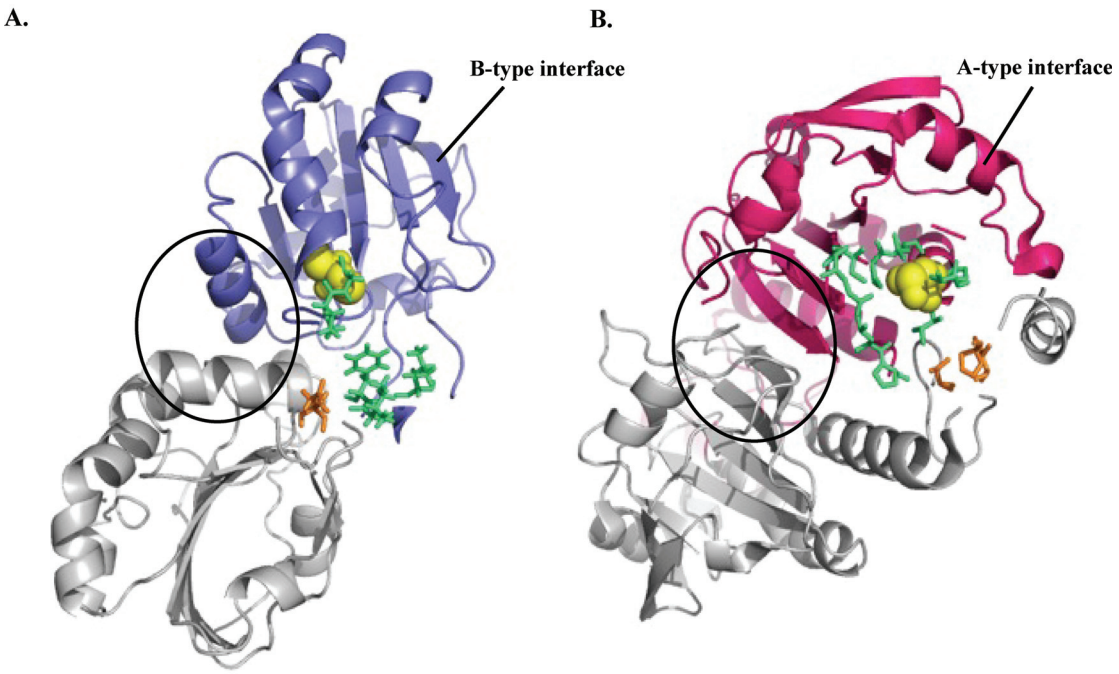

Figure 43: Comparing hPrx5 and hPrx2 structural properties.

Shown here is hPrx5 (A) and hPrx2 (B) highlighting the binding contacts determined in the interaction with 4-*tert*-butylcatechol within the active site by FM simulations. Yellow sphere represent the catalytic cysteine (C_p), the green sticks represent the amino acids in the first monomeric chain involved in binding and the orange sticks represent the amino acids in the second monomeric chain. There are distinctive structural differences between hPrx5 and hPrx2 (colours correspond to amino acid sequence alignment). In the formation hPrx5 forms a dimer with an A-type interface with the α-helices and hPrx2 forms a dimer with B-type interface with β-sheets circled on the proteins. Also, hPrx2 active site was more open and has more amino acids within active site involved in catechol derivative binding compared to hPrx5. hPrx5 active site is more closed and has less amino acids in the active site involved in binding but more so from the surround loop connected to the α-helix.

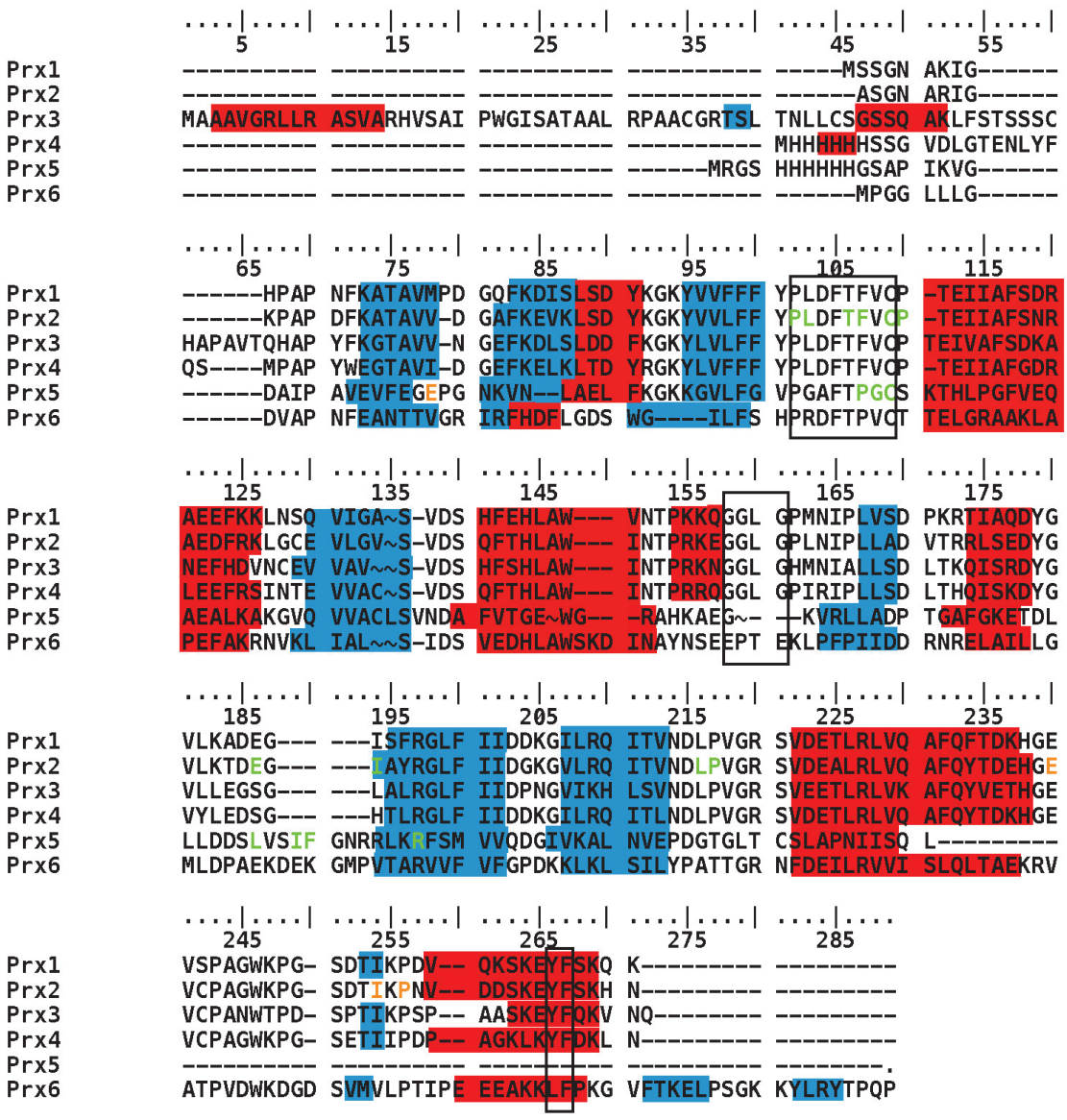

Figure 44: Amino acid sequence alignment for hPrx1-6.

The sequence alignment for all 6 hPrxs isoforms with the proteins secondary structures indicated. α-helices are represented in red and β-sheets are represented in blue. Highlighted with a black box represents the active site motif characterized by PXXXTXXC and also the GGLG and YF motifs representing the regions of hPrxs sensitive to H_2O_2 exposure influencing their redox activity [78]. yTrxR1, hPrx1 and hPrx2 were determined to have MWs to highly ordered oligomers. yTrxR1 apparent MW of ~ 55.6 kDa was a little underestimated since a dimer would represent the MW of 70 kDa. In examining the calibration curve (see and overoxidation. In green are the amino acid contact sites in chain A and in orange are the amino acid contact sites on chain B of the Prx. The amino acid sequence alignment was completed by PRALINE multiple sequence alignment program and edited by BioEdits.

functional redox state [78]. yTrxR1, hPrx1 and hPrx2 were determined to have MWs to highly ordered oligomers. yTrxR1 apparent MW of ~ 55.6 kDa that was a little underestimated since a dimer would represent the MW of 70 kDa. In examining the calibration curve (see Figure 22 from the results section pg 64), the standards proteins were well separated and the plot fit well to the linear regression fit. Therefore, yTrxR1 MW being underestimated was probably attributed to the protein being a homodimer in solution with its diameter similar or slightly larger to the large pores to the stationary phase of the column. This would result in yTrxR1 to partially entered the porous volume of the particles and not be well separated. yTrxR1 would elute sooner than expect and have a smaller retention volume and its MW would be underestimated [93]. yTrxR1 could have been separated on a column with larger pore sizes to accommodate the larger MW. Nevertheless, yTrxR1 was confirmed to be approximately a dimer in solution and these findings were comparable to a past study that determined yTrxR1 to be approximately a MW between 64-80 kDa through sedimentation velocity ultracentrifugation separating 4 mg/ml of yTrxR1 (SEC used ~ 3 mg/ml of yTrxR1) [94]. Overall, yTrxR1 large MW (~56 kDa) reaffirmed the difficulties observed for not achieving a high quality spectrum by ^{15}N-HQSC spectroscopy.

While for hPrx1 and hPrx2 had MWs ~290 and ~ 314 kDa representing highly ordered oligomers under reduced conditions. Even under oxidizing conditions hPrx1 and hPrx2 were oligomers similar to their MW in the reduced state. In separating the proteins by their sizes, hPrx2 separated well with one distinct peak indicating a homogeneous oligomeric state of the protein. In contrast to hPrx1, the protein did separate into one main peak but also had several other small peaks suggesting, the protein could be under oligomeric exchange and its MW could be slightly under or over estimated as the retention volume was take for the main peak to determine the MW (see Figure 23 from the results section pg 65). The MWs for hPrx1 and hPrx2 were not exactly comparable to past results by Lee *et al.* which, determined hPrx1 to have a MW of 340 kDa and hPrx2 a MW of 67 kDa (see Table 2 pg 65) [82].

Differences could have arisen from the calibration curve in how well the standard proteins were separated and the fitted to the curve. Shown in Figure 21 (results section pg 63) is the separation for the HMW standards in which, the column separated the proteins but could have been improved to achieve more distinct individual peaks although a slow flow rate of 0.5ml/min was used but could be due to proteins not well solubilized in the buffer. The variation in the peak separation can be seen in fitting the calibration curve plotting the K_{av} versus MW. Most of the points fit well to a linear regression but a few points. These discrepancies in the curve fitting would influence the exact MW by either over or underestimating ~ 10% error [95]. This is an issue with SEC with the consistency in separating proteins and the lifespan of the columns to have the best accuracy. Lee *et al.* did not disclose their calibration curve to determine how accurate the MW determination was in comparison to what I achieved. Experimental differences by SEC could be due to the elution buffer ionic strength and pH, flow rate, the amount of protein separated and also the proteins did not have His-tag [93]. Since Cao *et al.* recently proved that the presence of a His-tag at the N-terminus of purified bovine Prx3 had an influence on the stability in maintaining the oligomeric state of Prx3 as a dodecamer [93,96]. Therefore, the slightly larger MW determined for hPrx1 and hPrx2 could be due to their His-tag. Also, studies assessing the oligomeric formation state by isothermal titration microcalorimetry (ITC) determined 2-Cys Prxs from plants and human forms had a critical concentration to form oligomers between 1-2 μM [97]. The concentration of hPrx1 and hPrx2 (~ 136 μM) loaded onto the column to be separated could have influenced the oligomeric form too. The oligomeric formation is dependent on several factors such as the pH, temperature, ionic strength, concentration, phosphorylation and redox state [29]. There are a variety of factors affecting the oligomeric formation. Nevertheless, both hPrx1 and hPrx2 were determined to be oligomers in solution and similar to yTrxR1 reaffirmed the challenges in obtaining a 2D ^{1}H-^{15}N spectra. Table 2 (pg 65) is a summary of the results determined for characterizing all the proteins through the various methods.

5.3 Monitoring different hPrxs isoforms peroxidase activity

The focus of this thesis was to setup a peroxidase assay and assess if the catechol derivatives could inhibit hPrxs peroxidase activity. After purifying and characterize the proteins, the ideal experimental conditions to monitor hPrxs activity were determined. All the hPrxs were confirmed to be active in reducing H_2O_2. Comparing the peroxidase activities between the hPrxs, there were differences observed in their reaction rates when testing varying H_2O_2 concentrations. Shown in Figure 27 & Figure 28 (pg 71), hPrx5 was less sensitive to H_2O_2 and required higher concentrations of H_2O_2 (K_m value was ~ 25 μM for hPrx5 compared to hPrx1/2 < 5 μM). In contrast hPrx1 and hPrx2 reached their maximum peroxidase activity with H_2O_2 concentrations ~ 10-15 μM. Examining the catalytic values, hPrx1 and hPrx2 had K_m of < 5 μM and a V_{max} of ~ 1 μmol min^{-1} mg^{-1}, suggested both hPrx1 and hPrx2 have a higher affinity for H_2O_2 than hPrx5 with a K_m of ~ 25-38 μM and a V_{max} of ~ 10-12 μmol min^{-1} mg^{-1} (see Table 3 pg 73). hPrx1 and hPrx2 sensitivity to H_2O_2 and being active at low H_2O_2 concentrations is comparable to a study that examined bovine hPrx3 peroxidase activity and found that maximum activity was achieved at 10 μM or less of H_2O_2 [96]. hPrx1 and hPrx2 are apart of the typical 2-Cys Prx class and have amino acid sequences with homology > 70% [39]. Also, hPrx1 and hPrx2 have the GGLG and YF motifs that are known to be sensitive to H_2O_2 than hPrx5 that lacks these motifs [37]. hPrx1 and hPrx2 having similar sensitivities to H_2O_2 was not surprising. In monitoring hPrx1 and hPrx2 activity reduced H_2O_2 quickly posed some challenges to determine an accurate K_m value for H_2O_2 and also the limitation of the UV-Vis spectrophotometer were reach to measure large enough changes in absorbance to evaluate the initial rate properly (see Figure 27 and Figure 28 from the results section pg 71). As a result, hPrx1 and hPrx2 had K_m values for H_2O_2 < 5 μM and was less than hPrx5. Although, it has been reported to prior experimental conditions monitoring hPrxs activity to have K_m values < 20 μM for hPrx1-3 via coupling assay measuring the oxidation of NADPH and as low as 0.7 μM for hPrx2 via a fluorescent assay [98,99].

In comparing the catalytic turnover (k_{cat}) and efficiencies (k_{cat}/K_m) for the hPrxs, they had similar values in reducing H_2O_2 (see Table 3 pg 73). The k_{cat} represents the maximum rate the hPrxs consumes and reduces H_2O_2 into H_2O. hPrx1 and hPrx2 had k_{cat} values of ~ 2 s^{-1} and hPrx5 had a k_{cat} value of ~ 3 s^{-1}. In addition, the k_{cat}/K_m represents the efficiency for the hPrxs to reduce H_2O_2 and all the hPrxs had a similar affinity for H_2O_2. All the hPrxs catalytic efficiencies were between 10^4-10^5 $M^{-1}s^{-1}$ which was comparable to previous studies observing hPrx efficiencies ranges from ~ 10^5 to 10^8 M^{-1} s^{-1} [9,91,100]. Overall, the hPrx assay was setup well in determining if the catechol derivatives can inhibit their activities.

5.4 Catechol derivatives inhibit specific hPrxs

Identifying all the catechol derivatives have a binding affinity to hPrx1, hPrx2 and hPrx5 their ability to inhibit their peroxidase activity was examined. The IC_{50} assay determined all the catechol derivatives could inhibit hPrx5 and 4-*tert*-butylcatechol was the most potent inhibitor and catechol was the least potent inhibitor (see Table 12). The ranking of the catechol derivatives inhibition potency corroborates to past studies finding 4-methylcatechol was more potent than catechol with IC_{50} values of 26 μM and 105 μM [18].

Additionally, 4-*tert*-butylcatechol was determined to have a greater binding affinity to hPrx1 and hPrx2 out of the catechol derivatives and its inhibitory effects was examined too. 4-*tert*-butylcatechol was also identified to inhibit hPrx1and hPrx2 but with varying degrees of inhibition. 4-*tert*-butylcatechol inhibited hPrx1 with an IC_{50} value of 0.13 mM, and hPrx2 with an IC_{50} value of ~ 0.20 mM. Ranking the IC_{50} values 4-*tert*-butylcatechol would inhibit hPrx1 the best. However, when examining the IC_{50} curve, 4-*tert*-butylcatechol appeared to inhibit hPrx5 better than hPrx1 and hPrx2 comparing the final relative activity maintained (see Figure 42 pg 105). 4-*tert*-butylcatechol inhibited hPrx5 with relative activity at ~ 0.40 (represents ~ 60% is inhibited), in contrast to hPrx1 and hPrx2 with relative activity at ~ 0.80 (represents ~ 20% is inhibited) and ~ 0.65 (represents ~ 35% is inhibited). The difference in

inhibitory effects of 4-*tert*-butylcatechol to the hPrxs could be attributed to the experimental conditions influencing the inhibitory response. The IC_{50} assays were conducted with the concentration of H_2O_2 at 25 μM, corresponding to the K_m value initially determined for hPrx5. Whereas, for hPrx1 and hPrx2 were found to have a lower K_m for H_2O_2 <5 μM. Therefore, potentially hPrx1 and hPrx2 being exposed to higher concentrations of H_2O_2 could have been partially hyperoxidized with the proteins to be less active and as a result 4-*tert*-butylcatechol would not be as potent inhibiting hPrx1 and hPrx2. The possibility of observing to hPrx1 and hPrx2 to be hyperoxidized is not as evident since the experimental conditions are maintained with the concentration of yTrx1 at saturating levels essentially protecting the proteins from the rate-limiting step transitioning from the oxidized to reduced state [99]. However, to ensure 4-*tert*-butylcatechol is an inhibitor at lower levels of H_2O_2, the inhibitory effects of 4-*tert*-butylcatechol against hPrx2 were measured at H_2O_2 concentration at 2.5 μM (instead of 25 μM). 4-*tert*-butylcatechol was found to inhibit hPrx2. The IC_{50} value was slightly improved from the 0.2 mM but the relative inhibitory effect still had a relative activity level at ~ 0.65 suggesting overall 4-*tert*-butylcatechol is not as potent of an inhibitor to hPrx2 compared to hPrx5.

Furthermore, the potency of 4-*tert*-butycatechol could be contributed by the binding affinities measured to the hPrxs. 4-*tert*-butycatechol bound better to hPrx5 with a K_d of ~ 0.19 mM compared to hPrx1 and hPrx2 with a K_d of ~ 26.00 and ~ 5.86 mM (see Table 12). The improved binding affinity of 4-*tert*-butylcatechol could be attributed to binding to the active site of hPrx5 detected through HSQC NMR. In contrast, 4-*tert*-butylcatechol binding affinity to hPrx1 and hPrx2 was detected through STD NMR, only identifying there were binding affinities and not the binding location on the hPrxs. So potentially the higher K_d values identified for hPrx1 and hPrx2 may represent 4-*tert*-butylcatechol binding outside of the active sites or could be effected due to the different structural arrangement of the active site, leading to a reduced binding affinity. Therefore, the reduced binding affinity can be linked to the reduced potency observed for hPrx1 and hPrx2. Future experiments could be

completed to provide more details of the exact binding conformation between 4-*tert*-butylcatechol and hPrx1 and hPrx2 to decipher to the differences observed.

Nevertheless, in determining the catechol derivatives could inhibit hPrx5 the inhibition MMOA was explored. The catechol derivatives were detected to bind and inhibit hPrx5 in a rapid reversible manner, which corresponded the non-covalent bond types determined through FM simulation. However, FM simulations only assessed if the catechol derivative bound in a reversible manner, and not the chemical reaction, therefore this was a coincidence. Also, the catechol derivatives were found to exclusively bind and interact to hPrx5, and not interact to the other coupling reaction reagents, which were confirmed by the ^{1}H and ^{15}N-HQSC NMR experiments. All the catechol derivatives were found to inhibit in a partial mixed type non-competitive conformation MMOA (see Figure 35 pg 87 for the inhibition mechanism scheme). The catechol derivatives did not fully disrupt hPrx5 peroxidase activity and H_2O_2 could still be reduced to H_2O. Also, the catechol derivatives bound and inhibited both free hPrx5 and hPrx5-H_2O_2 complex but preferred to bind to the hPrx5 alone in comparing the inhibitor constant values (K_i'> K_i). In evaluating the catechol derivatives inhibition mechanism, there were discrepancies in deciphering best inhibition model as catechol fit between both partial and/or partial mixed type non-competitive inhibition manners. In comparing the inhibitory constant value trends and model fittings determined by DynaFit to 4-methylcatechol and 4-*tert*-butylcatechol, catechol fit best to the partial mixed type non-competitive inhibition mechanism. The challenges in determining catechol ideal inhibition mechanism against hPrx5 could be associated to hPrx5 conformational modifications in binding event and contacts of the catechol derivatives. It was observed during the MD trajectories that when 4-methylcatechol bound to hPrx5 the active site cavity contracted a bit whereas, for 4-*tert*-butylcatechol bound hPrx5 active site slightly expanded to accommodate the bulkier *tert*-butyl group when examining the FM simulations binding events. For catechol binding to hPrx5, there were no conformational changes observed in the active site as the ligand was smaller in size but also there was a reduced binding affinity [32] (Chow *et al.* 2016).

Consequently, these structural properties of hPrx5 conforming to the catechol derivative structure could have influenced the binding and inhibitory properties.

There have been other studies that have identified inhibitors to have specificity and varying inhibitory potencies as seen with the catechol derivatives to hPrx5. There are interest to find inhibitors to other hPrx1, hPrx2, and hPrx6 identified as other hPrxs isoforms in the post-inflammation cascade after a stroke. Other ligands identified to inhibit various Prxs such as conoidin A, conoidin B, adenanthin, H7 and AMRI-59 [19–21,23–25]. From these inhibitors, adenanthin was determined to be the most potent and specific inhibitor. Adenanthin was found to inhibit hPrx1 and hPrx2 with IC_{50} values of 1.5 μM and 15 μM but not hPrx5. Adenanthin inhibited the hPrxs in two-step inhibition mechanism. First by a slow initial binding phase that was reversible and eventually converted into chemical conversion covalently linking adenanthin to the hPrxs [19]. There is an importance in understanding an inhibitor's MMOA because the overall impact of the inhibitor might not be desired in completely stopping the peroxidase reaction as seen for adenanthin whereas, the catechol derivatives partially impaired the reaction. Although, adenanthin was found to inhibit hPrxs follow up studies identified adenanthin to not explicitly bind and inhibit to hPrx1 and hPrx2 but also could to other redox proteins TrxR, glutathione reductase and glutaredoxin [101]. In determining an inhibitor potent and specific to hPrxs is challenging to accommodate the many factors in drug design. Upon identifying inhibitors potent at the enzymatic level, there is need for development at the cellular and animal model levels.

Distinguishing the catechol derivatives can bind and inhibit hPrx5 at the enzymatic level there have been advancements at the cellular level bringing hope to the potential use of catechol derivatives as possible treatment for brain injuries. Recently, catechol derivatives been identified to bind and inhibit the microglial cells, resident brain cell. Zheng *et al.* determined catechol, 3-methylcatechol, 4-methylcatechol and 4-*tert*-butylcatechol could inhibit BV-2 microglial cells and prevent the production of pro-inflammatory factors nitric oxide (NO), and tumor necrosis factor (TNF-α). As a result, 3-methylcatechol was the most

potent inhibitor (IC_{50} value of 0.61 ± 0.12 μg/ml) followed by catechol, 4-methylcatechol, and lastly the least potent inhibitor 4-tert-butylcatechol (2.08 ± 0.23 μg/ml). Although, more research is required to assess if the catechol derivatives can cross the blood brain barrier (BBB) and lead to the desired effect to in prevent inflammation[26]. Therefore, this study highlighted the prospective that catechol derivatives could be a candidate inhibitor to treat ischemic stroke patients in controlling the inflammation cascade inhibit brains cells along with hPrxs. Future adaptation to the catechol derivative backbone is of course still required to improve binding and inhibition potency.

5.5 Understanding the binding and inhibition interactions of the catechol derivatives to predict the affect on other hPrxs

Identify and understanding how key ligands bind and inhibit proteins is important in lead inhibitors to be developed into drugs for therapeutic treatment. Analyzing the binding interaction of the catechol derivatives to the hPrxs, there were correlations in the binding affinities between NMR and FM simulation experiments. Emphasizing the advantageous tools FM simulations could be utilized to assist in early screening processed to predict lead ligands as potential inhibitors. As the FM simulations were robust enough to in modeling both the *E* and mimicked *ES* complex, in which the binding affinities of the catechol derivatives to hPrx5 and hPrx5-H_2O_2 states had trends correlating to the enzymatic inhibition mechanism analysis.

Investigating the binding properties of the catechol derivatives to hPrx1, hPrx2 and hPrx5 by FM simulations provided insight of key features with the amino acids within and around the active site involved. Therefore, this knowledge could assist in predicting the binding and inhibition properties for the other hPrxs. There is interest to identify drugs to bind and inhibit hPrx1, hPrx2, hPrx5 and hPrx6 causing a response in delaying the effect of post-inflammation cascade after an ischemic stroke.

Analyzing the amino acid sequence alignment, amongst the hPrxs there is ~ 50% conserved residues located within the functional sites of the proteins which include the active

site motif, Arg 123, Trp 84, Ser74, and Glu60 (in reference to hPrx5 sequence) [39]. Identifying the catechol derivatives can bind in the active site of the hPrxs, hPrx2 active site is homologous for hPrx1, hPrx3, and hPrx4 with the same active site motif amino acid sequence (**P**LDF**T**FV**C**) and the other key amino acids found in the C-terminus are the same too (Leu145, Pro146, and Val170, Ile182, Pro184 from the second monomer; in reference to hPrx2 sequence). Due to the homology in these regions, this would suggest the catechol derivatives could bind to hPrx1, hPrx3, and hPrx4 within their active site regions. However, there is some variation in amino acids around the region of Glu121 and Ile123 (in reference to hPrx2). This same region is where hPrx5 has amino acids involved in binding contacts with the catechol derivatives. Therefore, possibly due to lack of homology could contribute to the differences in the degree of binding affinity. Recently, Yang *et al*. determined AMRI-59 could bind and inhibit hPrx1-4 and there was variation in degree of inhibition with hPrx1 inhibited the best with an IC_{50} of 12 μM in contrast to hPrx4 being poorly inhibited with IC_{50} > 100 μM [21].

In predicting if the catechol derivatives could bind to hPrx6 is a little more challenging. hPrx6 is apart of the 1-Cys class and has only one catalytic cysteine involved in the peroxidase activity and is reduced by glutathione than thioredoxin [10]. There is no homology in the active site motif in comparison to the other hPrxs besides maintain the **P**XXX**T**XX**C** composition, and the amino acids differ in the C-terminal region too. However, hPrx6 has the amino acid linker region as seen in hPrx5 but that lacks in hPrx1-4. Also, hPrx6 has additional β-sheets at the C-terminus. Therefore, hPrx6 amino acid sequence has more diversity than the other hPrxs and might bind the catechol derivatives in the active site but it would have to be further explored.

6 Conclusion and future direction

6.1 Conclusion

The long-term goal of this research was to identify potential inhibitors for therapeutic treatment for ischemic strokes. Recently, hPrxs were distinguished as key initiators of the post-inflammation cascade in the brain after a stroke. The first approach was determining if the catechol derivatives (catechol, 4-methylcatechol and 4-*tert*-butylcatechol) could bind to hPrx1, hPrx2 and hPrx5. Previous graduate students have identified catechol, 4-methylcatechol and 4-*tert*-butylcatechol could bind hPrx5. My research focused on further exploring if the catechol derivatives bind to hPrx1 and hPrx2 too.

After examining the binding interactions of the catechol derivatives to hPrx1 and hPrx2, it was determined the catechol derivatives could bind to them too. Additionally, computation modeling was also, able to determine the catechol derivatives could bind to hPrxs. Both approaches of exploring the binding interaction had similarities. Comparing the binding affinities (K_d) values of the catechol derivatives to hPrx1, hPrx2 and hPrx5 there was evident the catechol derivatives had a greater binding affinity to hPrx5. Also, 4-*tert*-butylcatechol had the best binding affinity to all of the hPrxs than 4-methylcatechol and catechol. Therefore, this suggested there could be selectivity in the binding interaction for the catechol derivatives to the hPrxs and this property may influence their inhibition properties.

These hypotheses were further assessed with the second approach in determining if the catechol derivatives could also inhibit the hPrxs in an enzymatic peroxidase activity. All three catechol derivatives were determined to inhibit hPrx5 and 4-*tert*-butylcatechol the most potent inhibitor. Also, 4-*tert*-butylcatechol was discovered to inhibit hPrx1 and hPrx2 too. Comparing the inhibitory effects of 4-*tert*-butylcatechol to the hPrxs, hPrx5 was inhibited the better than hPrx1 and hPrx2. The differences in binding and inhibiting between the catechol derivatives and hPrxs could be attributed to structural differences. Amongst the family of hPrxs, there is homology in the amino acid sequence but there are key amino acids as shown to be involved in the binding interactions contributing to variations between hPrxs. Overall,

this shows developing potential inhibitors against hPrxs requires understanding of the individual hPrxs to achieve the desired inhibition effect.

In assessing these hypotheses, the catechol derivatives have specificity in binding and inhibiting hPrxs. Using various methods such as NMR and FM can be advantageous to assist in the initial screening process. Identifying lead ligands known to have a binding to proteins of interest does not always translate into inhibition effects. There is importance in the *in vitro* and *in vivo* exploration with key ligands of distinguishing the desired affect in causing inhibition.

6.2 Future direction

Future work includes to further understanding the oligomeric formation in hPrx1 and hPrx2. These proteins are posed to be challenging in assessing their structure characteristics under NMR spectroscopy analysis. More knowledge of the elementary states, monomeric or dimeric forms, could be beneficial in designing ligands to be future drugs. FM simulations identified the catechol derivatives could bind to the active site of hPrx1 and hPrx2 but possibly other regions of these proteins could be more ideal to cause inhibition.

Also, further investigating if the catechol derivatives can also bind and inhibit hPrx3, hPrx4 and hPrx6. Computational modeling such as FM could be utilized to assess if they bind in the active site pocket of the proteins and the amino acids involved in the interaction. Also, the inhibitory effect and potentially the MMOA of the catechol derivatives binding to the other hPrxs could be investigated too. Therefore, these studies could assist in identifying specificity characteristics for catechol derivatives involved in binding interaction and be utilized to develop more improved ligands with an increased potency than 4-*tert*-butylcatechol. My lab colleague, Laura Troussicot, is in the process of currently exploring improvements to the catechol backbone skeleton to develop new ligands. Since Aguirre *et al.* investigated the addition of benzene rings from the basic catechol ring backbone and found

these structural modifications did not improve the binding affinities to hPrx5 [27]. Possibly more simple structure additions as seen with the *tert*-butyl group are more ideal to improve the binding affinity to hPrxs.

Presently, all the inhibitors identified to inhibit Prxs have been discovered to bind in the active site disrupting the catalytic activity either locking the protein it its oxidized redox state or inhibiting oligomerization or partially inhibited the peroxidase activity [22,25]. There is interest to identify inhibitors to hPrxs that do bind in areas other than the active site. Shichita *et al.* have found antibodies binding to the surface area of hPrxs such as α-helix 3, β-sheet 4 region as it is highly conserved across Prxs. Antibodies targeting the regions 68-90 on hPrx5 and 66-93 on hPrx6 were identified to bind and inhibit hPrxs phenotype in a mouse model induced with ischemic strokes. As the mice were administered anti-Prx5 and anti-Prx6, and the antibodies were found to suppress the activation of inflammatory cytokines expression infiltrating immune cells (macrophages, T-cells) and reduce the brain tissue damage (infarct volume growth). In which the antibodies were able inhibit and prevent hPrxs relaying neurotoxic danger signals in triggering Toll-Like Receptors (TLRs) 2 and TLR4 leading to the inflammation cascade and causing brain damage (Figure 1 pg 6 post-inflammation cascade). Testing potential inhibitors at the *in vivo* level on mice can provide insight if a desirable response it achieved.

As there has also been testing of other prospective inhibitors H7 against hPrx1 on mice too. H7 was found to reduce in the expression of hPrx1 and induced the differentiation of leukemia cells. It was purposed H7 could be a potential therapeutic agent to treat acute myeloid leukemia (AML)[20]. These studies are examples of the advancements in inhibitor development of hPrxs at the *in vivo* level. There are still many factors to consider such as toxicity of the inhibitors, MMOAs, the time duration the inhibitors work and if treating the brain can these inhibitors cross the blood brain barrier to lead to there anticipated effect.

Studying the binding and inhibitory effects of the catechol derivatives to hPrx1, hPrx2 and hPrx5 revealed how complex at the molecular level is to design lead ligands.

Characterizing the binding, location and key amino acids involved in the binding interaction were distinguished. NMR and FM modeling identified the catechol derivatives can bind to the active site interacting with the catalytic cysteine. In particular, 4-*tert*-butycatechol bound the best amongst the catechol derivatives and this was found for hPrx1, hPrx2 and hPrx5. Also, the catechol derivatives were discovered to inhibit hPrxs too. 4-*tert*-butylcatechol was most potent inhibitor and inhibited the best against hPrx5 than to hPrx1 and hPrx2. To understand the catechol derivatives binding affinities and inhibitory effects, the MMOA was assessed for hPrx5. The catechol derivatives were determined to bind and inhibit more effectively to hPrx5 in contrast to the hPrx5-H_2O_2 complex in a partial mixed non-competitive manner. Overall, a greater understanding of the binding affinities and inhibitory effects of lead ligands is important in the drug development to treat patients with various diseases and disorders such as brain inflammation after a stroke.

Bibliography

1. Perkins, A., Nelson, K. J., Parsonage, D., Poole, L. B. & Karplus, P. A. Peroxiredoxins: guardians against oxidative stress and modulators of peroxide signaling. *Trends Biochem. Sci.* **40,** 435–445 (2015).
2. Karplus, P. A. A primer on peroxiredoxin biochemistry. *Free Radic. Biol. Med.* **80,** 183–90 (2015).
3. Rhee, S. G., Jeong, W., Chang, T.-S. & Woo, H. A. Sulfiredoxin, the cysteine sulfinic acid reductase specific to 2-Cys peroxiredoxin: its discovery, mechanism of action, and biological significance. *Kidney Int. Suppl.* **72,** S3–8 (2007).
4. Mitsumoto, A., Takanezawa, Y., Okawa, K., Iwamatsu, A. & Nakagawa, Y. Variants of peroxiredoxins expression in response to hydroperoxide stress. *Free Radic. Biol. Med.* **30,** 625–35 (2001).
5. Jönsson, T. J., Johnson, L. C. & Lowther, W. T. Structure of the sulphiredoxin-peroxiredoxin complex reveals an essential repair embrace. *Nature* **451,** 98–101 (2008).
6. Perkins, A., Poole, L. B. & Karplus, P. A. Tuning of Peroxiredoxin Catalysis for Various Physiological Roles. *Biochemistry* **53,** 7693–7705 (2014).
7. Knoops, B., Argyropoulou, V., Becker, S., Ferté, L. & Kuznetsova, O. Multiple Roles of Peroxiredoxins in Inflammation. *Mol. Cells* **39,** 60–64 (2016).
8. Rhee, S. G., Kang, S. W., Chang, T.-S. S., Jeong, W. & Kim, K. Peroxiredoxin, a novel family of peroxidases. *IUBMB Life* **52,** 35–41 (2001).
9. Wood, Z. A., Schröder, E., Robin Harris, J. & Poole, L. B. Structure, mechanism and regulation of peroxiredoxins. *Trends Biochem. Sci.* **28,** 32–40 (2003).
10. Fujii, J. & Ikeda, Y. Advances in our understanding of peroxiredoxin, a multifunctional, mammalian redox protein. *Redox Rep.* **7,** 123–130 (2002).
11. Shichita, T. *et al.* Peroxiredoxin family proteins are key initiators of post-ischemic inflammation in the brain. *Nat. Med.* **18,** 911–7 (2012).
12. Shichita, T., Sakaguchi, R. & Ito, M. Mini Review Peroxiredoxin triggers cerebral post-ischemic inflammation. **33,** 150–155 (2013).
13. Garcia-Bonilla, L. & Iadecola, C. Peroxiredoxin sets the brain on fire after stroke. *Nat. Med.* **18,** 858–9 (2012).
14. Moskowitz, M. A., Lo, E. H. & Iadecola, C. The science of stroke: Mechanisms in search of treatments. *Neuron* **67,** 181–198 (2010).
15. Lakhan, S. E., Kirchgessner, A. & Hofer, M. Inflammatory mechanisms in ischemic stroke: therapeutic approaches. *J. Transl. Med.* **7,** 97 (2009).
16. del Zoppo, G. J. Plasminogen activators in ischemic stroke: introduction. *Stroke.* **41,** (2010).
17. Mehta, R. & Shapiro, A. D. Plasminogen activator inhibitor type 1 deficiency. *Haemophilia* **14,** 1255–1260 (2008).
18. Barelier, S. *et al.* Discovery of fragment molecules that bind the human peroxiredoxin 5 active site. *PLoS One* **5,** e9744 (2010).
19. Liu, C.-X. *et al.* Adenanthin targets peroxiredoxin I and II to induce differentiation of leukemic cells. SUPPLEMENT DATA. *Nat. Chem. Biol.* **8,** 486–93 (2012).
20. Wei, W. *et al.* Identification of H7 as a novel peroxiredoxin I inhibitor to induce differentiation of leukemia cells. *Oncotarget* **7,** (2016).
21. Yang, Y. J. *et al.* Effective Killing of Cancer Cells Through ROS-Mediated Mechanisms by AMRI-59 Targeting Peroxiredoxin I. *Antioxid. Redox Signal.* **00,** 1–17 (2015).
22. Zhao, Q. *et al.* Natural products triptolide, celastrol, and withaferin A inhibit the chaperone activity of peroxiredoxin I. *Chem. Sci.* **6,** 4124–4130 (2015).
23. Liu, G. *et al.* Optimisation of conoidin A, a peroxiredoxin inhibitor. *ChemMedChem* **5,**

41–5 (2010).
24. Haraldsen, J. D. *et al.* Identification of conoidin A as a covalent inhibitor of peroxiredoxin II. *Org. Biomol. Chem.* **7,** 3040–3048 (2009).
25. Nguyen, J. B. *et al.* Peroxiredoxin-1 from the human hookworm ancylostoma ceylanicum forms a stable oxidized decamer and is covalently inhibited by conoidin a. *Chem. Biol.* **20,** 991–1001 (2013).
26. Zheng, L. T., Ryu, G.-M., Kwon, B.-M., Lee, W.-H. & Suk, K. Anti-inflammatory effects of catechols in lipopolysaccharide-stimulated microglia cells: inhibition of microglial neurotoxicity. *Eur. J. Pharmacol.* **588,** 106–13 (2008).
27. Aguirre, C., Brink, T. Ten, Guichou, J. F., Cala, O. & Krimm, I. Comparing binding modes of analogous fragments using NMR in fragment-based drug design: Application to PRDX5. *PLoS One* **9,** 1–11 (2014).
28. Matés, J. M., Pérez-Gómez, C. & Núñez de Castro, I. Antioxidant enzymes and human diseases. *Clin. Biochem.* **32,** 595–603 (1999).
29. Barranco-Medina, S., Lázaro, J.-J. & Dietz, K.-J. The oligomeric conformation of peroxiredoxins links redox state to function. *FEBS Lett.* **583,** 1809–16 (2009).
30. Rhee, S. G., Woo, H. A., Kil, I. S. & Bae, S. H. Peroxiredoxin functions as a peroxidase and a regulator and sensor of local peroxides. *J. Biol. Chem.* **287,** 4403–10 (2012).
31. C., I. & J., A. The immunology of stroke: from mechanism to translation. *Nat. Med.* **17,** 796–808 (2012).
32. Troussicot, L., Guillière, F., Limongelli, V., Walker, O. & Lancelin, J.-M. Funnel-Metadynamics and Solution NMR to Estimate Protein–Ligand Affinities. *J. Am. Chem. Soc.* **137,** 1273–1281 (2015).
33. Macrez, R. *et al.* Stroke and the immune system: from pathophysiology to new therapeutic strategies. *Lancet. Neurol.* **10,** 471–80 (2011).
34. Kumar, S., Selim, M. H. & Caplan, L. R. Medical complications after stroke. *Lancet Neurol.* **9,** 105–118 (2010).
35. Balami, J. S., Chen, R. L., Grunwald, I. Q. & Buchan, A. M. Neurological complications of acute ischaemic stroke. *Lancet Neurol.* **10,** 357–371 (2011).
36. Flohe, L. & Robin Harris, J. *Peroxiredoxin Systems*. *Subcell. Biochem.* **44,** (Springer Netherlands, 2007).
37. Knoops, B., Goemaere, J., Van der Eecken, V. & Declercq, J.-P. Peroxiredoxin 5: structure, mechanism, and function of the mammalian atypical 2-Cys peroxiredoxin. *Antioxid. Redox Signal.* **15,** 817–29 (2011).
38. Wood, Z. A., Poole, L. B., Hantgan, R. R. & Karplus, P. A. Dimers to doughnuts: Redox-sensitive oligomerization of 2-cysteine peroxiredoxins. *Biochemistry* **41,** 5493–5504 (2002).
39. Nelson, K. J. *et al.* Analysis of the peroxiredoxin family: Using active-site structure and sequence information for global classification and residue analysis. *Proteins Struct. Funct. Bioinforma.* **79,** 947–964 (2011).
40. Lian, F. M. *et al.* Structural snapshots of yeast alkyl hydroperoxide reductase Ahp1 peroxiredoxin reveal a novel two-cysteine mechanism of electron transfer to eliminate reactive oxygen species. *J. Biol. Chem.* **287,** 17077–17087 (2012).
41. Jönsson, T. J. & Lowther, W. T. The peroxiredoxin repair proteins. *Subcell. Biochem.* **44,** 115–41 (2007).
42. Woo, H. A. *et al.* Inactivation of Peroxiredoxin I by Phosphorylation Allows Localized H2O2 Accumulation for Cell Signaling. *Cell* **140,** 517–528 (2010).
43. Wood, Z. A., Poole, L. B. & Karplus, P. A. Peroxiredoxin evolution and the regulation of hydrogen peroxide signaling. *Science* **300,** 650–3 (2003).
44. Jang, H. H. *et al.* Two enzymes in one; two yeast peroxiredoxins display oxidative stress-dependent switching from a peroxidase to a molecular chaperone function. *Cell* **117,** 625–35 (2004).

45. Copeland, R. A. *Evaluation of enzyme inhibitors in drug discovery. A guide for medicinal chemists and pharmacologists.* (John Wiley & Sons, Inc., 2005). doi:10.1002/9781118540398
46. Swinney, D. C. & Anthony, J. How were new medicines discovered? *Nat. Rev. Drug Discov.* **10,** 507–19 (2011).
47. Macalino, S. J. Y., Gosu, V., Hong, S. & Choi, S. Role of computer-aided drug design in modern drug discovery. *Arch. Pharm. Res.* **38,** 1686–1701 (2015).
48. Lee, J. & Bogyo, M. Target deconvolution techniques in modern phenotypic profiling. *Curr. Opin. Chem. Biol.* **17,** 118–126 (2013).
49. Pellecchia, M. *et al.* Perspectives on NMR in drug discovery: a technique comes of age. *Nat. Rev. Drug Discov.* **7,** 738–745 (2008).
50. Carr, R. A. E., Congreve, M., Murray, C. W. & Rees, D. C. Fragment-based lead discovery: Leads by design. *Drug Discov. Today* **10,** 987–992 (2005).
51. Williams, M. A. *Protein-Ligand Interactions*. **1008,** (Humana Press, 2013).
52. Pellecchia, M., Sem, D. S. & Wüthrich, K. NMR in drug discovery. *Nat. Rev. Drug Discov.* **1,** 211–9 (2002).
53. Dias, D. M. & Ciulli, A. NMR approaches in structure-based lead discovery: Recent developments and new frontiers for targeting multi-protein complexes. *Prog. Biophys. Mol. Biol.* **116,** 101–112 (2014).
54. Angulo, J. & Nieto, P. M. STD-NMR: Application to transient interactions between biomolecules-a quantitative approach. *Eur. Biophys. J.* **40,** 1357–1369 (2011).
55. Mayer, M. & Meyer, B. Group epitope mapping by saturation transfer difference NMR to identify segments of a ligand in direct contact with a protein receptor. *J. Am. Chem. Soc.* **123,** 6108–17 (2001).
56. Borhani, D. W. & Shaw, D. E. The future of molecular dynamics simulations in drug discovery. *J. Comput. Aided. Mol. Des.* **26,** 15–26 (2012).
57. Stanley, N. & De Fabritiis, G. High throughput molecular dynamics for drug discovery. *Silico Pharmacol.* **3,** 3–6 (2015).
58. Durrant, J. D. & McCammon, J. A. Molecular dynamics simulations and drug discovery. *BMC Biol.* **9,** 71 (2011).
59. Limongelli, V., Bonomi, M. & Parrinello, M. Funnel metadynamics as accurate binding free-energy method. *Proc Natl Acad Sci U S A* **110,** 6358–6363 (2013).
60. Strelow, J. *et al. Mechanism of Action Assays for Enzymes*. *Assay Guid. Man.* (2004). at <http://www.ncbi.nlm.nih.gov/pubmed/22553872>
61. Goddard, J. P. & Reymond, J. L. Recent advances in enzyme assays. *Trends Biotechnol.* **22,** 363–370 (2004).
62. Copeland, R. A. *Enzymes: a practical introduction to structure, mechanism, and data analysis*. (John Wiley & Sons, 2000). at <http://eu.wiley.com/WileyCDA/WileyTitle/productCd-0471359297.html>
63. Segel, I. H. *Enzyme kinetics behavior and analysis of rapid equilibrium and steady state enzyme systems*. (A Wiley-Interescience Publication, 1993).
64. Swinney, D. C. Biochemical mechanisms of drug action: what does it take for success? *Nat. Rev. Drug Discov.* **3,** 801–8 (2004).
65. Schweigert, N., Zehnder, A. J. B. & Eggen, R. I. L. Chemical properties of catechols and their molecular modes of toxic action in cells, from microorganisms to mammals. *Environ. Microbiol.* **3,** 81–91 (2001).
66. Baron, R., Zayats, M. & Willner, I. Dopamine-, L-DOPA-, adrenaline-, and noradrenaline-induced growth of Au nanoparticles: Assays for the detection of neurotransmitters and of tyrosinase activity. *Anal. Chem.* **77,** 1566–1571 (2005).
67. Huang, W., Zhang, H., Liu, W. & Li, C. Survey of antioxidant capacity and phenolic composition of blueberry, blackberry, and strawberry in Nanjing. *J. Zhejiang Univ. Sci. B* **13,** 94–102 (2012).
68. Parmigiani, R. B. *et al.* HDAC6 is a specific deacetylase of peroxiredoxins and is

involved in redox regulation. *Proc. Natl. Acad. Sci.* **105,** 9633–9638 (2008).
69. Declercq, J. P. *et al.* Crystal structure of human peroxiredoxin 5, a novel type of mammalian peroxiredoxin at 1.5 A resolution. *J. Mol. Biol.* **311,** 751–9 (2001).
70. Mendham, J., Denney, R. C., D, B. J. & K, T. M. J. *Vogel's Textbook of Quantitative Chemical Analysis*. *New York* **6th,** (Pearson Education Limited, 2000).
71. Kim, J.-A., Park, S., Kim, K., Rhee, S. G. & Kang, S. W. Activity assay of mammalian 2-cys peroxiredoxins using yeast thioredoxin reductase system. *Anal. Biochem.* **338,** 216–23 (2005).
72. Kuzmič, P. Program DYNAFIT for the Analysis of Enzyme Kinetic Data: Application to HIV Proteinase. *Anal. Biochem.* **237,** 260–273 (1996).
73. Marquardt, D. W. An Algorithm for Least-Squares Estimation of Nonlinear Parameters. *J. Soc. Ind. Appl. Math.* **11,** 431–441 (1963).
74. Savitzky, A. & Golay, M. J. E. Smoothing and Differentiation of Data by Simplified Least Squares Procedures. *Anal. Chem.* **36,** 1627–1639 (1964).
75. Kay, L. E., Keifer, P. & Saarinen, T. Pure Absorption Gradient Enhanced Heteronuclear Single Quantum Correlation Spectroscopy with Improved Sensitivity. *J. Am. Chem. Soc.* 10663–10665 (1992). doi:10.1021/ja00052a088
76. Mayer, M. & Meyer, B. Characterization of ligand binding by saturation transfer difference NMR spectroscopy. *Angew. Chemie - Int. Ed.* **38,** 1784–1788 (1999).
77. Hall, T. A. BioEdit: a user-friendly biological sequence alignment editor and analysis program for Windows 95/98/NT. *Nucleic Acids Symp. Ser.* **41,** 95–98 (1999).
78. Weichsel, a, Gasdaska, J. R., Powis, G. & Montfort, W. R. Crystal structures of reduced, oxidized, and mutated human thioredoxins: evidence for a regulatory homodimer. *Structure* **4,** 735–751 (1996).
79. Arnér, E. E. S. & Holmgren, A. Physiological functions of thioredoxin and thioredoxin reductase. *Eur. J. Biochem.* **267,** 6102–9 (2000).
80. Pinheiro, A. S., Amorim, G. C., Netto, L. E. S., Almeida, F. C. L. & Valente, A. P. NMR solution structure of the reduced form of thioredoxin 1 from Sacharomyces cerevisiae. *Proteins Struct. Funct. Bioinforma.* **70,** 584–587 (2007).
81. Doucleff, M., Hatcher-Skeers, M. & Crane, N. J. *Pocket Guide to Biomolecular NMR*. (Springer Berlin Heidelberg, 2011). doi:10.1007/978-3-642-16251-0
82. Lee, W. *et al.* Human peroxiredoxin 1 and 2 are not duplicate proteins: the unique presence of CYS83 in Prx1 underscores the structural and functional differences between Prx1 and Prx2. *J. Biol. Chem.* **282,** 22011–22 (2007).
83. Nelson, K. J. & Parsonage, D. Measurement of peroxiredoxin activity. *Curr. Protoc. Toxicol.* **Chapter 7,** Unit7.10 (2011).
84. Lu, J. & Holmgren, A. The thioredoxin antioxidant system. *Free Radic. Biol. Med.* **66,** 75–87 (2014).
85. Bhunia, A., Bhattacharjya, S. & Chatterjee, S. Applications of saturation transfer difference NMR in biological systems. *Drug Discov. Today* **17,** 505–513 (2012).
86. Kuriyan, J., Konforti, B. & Wemmer, D. in *Mol. Life* 1–58 (Garland Science, 2013).
87. Kwon, S. J., Park, J. W., Choi, W. K., Kim, I. H. & Kim, K. W. Inhibition of Metal-Catalyzed Oxidation Systems by a Yeast Protector Protein in the Presence of Thioredoxin. *Biochem. Biophys. Res. Commun.* **201,** 8–15 (1994).
88. Zhang, Y., Bao, R., Zhou, C.-Z. & Chen, Y. Expression, purification, crystallization and preliminary X-ray diffraction analysis of thioredoxin Trx1 from Saccharomyces cerevisiae. *Acta Crystallogr. Sect. F. Struct. Biol. Cryst. Commun.* **64,** 323–5 (2008).
89. Horecká, T., Perecko, D., Kutejová, E., Muchová, K. & Kollárová, M. Purification and partial characterization of two thioredoxins from Streptomyces aureofaciens. *Biochem. Mol. Biol. Int.* **40,** 497–505 (1996).
90. Zhang, Z. *et al.* Crystal structure of Saccharomyces cerevisiae cytoplasmic thioredoxin reductase Trr1 reveals the structural basis for species-specific recognition of thioredoxin. *Biochim. Biophys. Acta* **1794,** 124–8 (2009).

91. Peskin, A. V. *et al.* The high reactivity of peroxiredoxin 2 with H2O2 is not reflected in its reaction with other oxidants and thiol reagents. *J. Biol. Chem.* **282,** 11885–11892 (2007).
92. Oliveira, M. A. *et al.* Insights into the specificity of thioredoxin reductase-thioredoxin interactions. A structural and functional investigation of the yeast thioredoxin system. *Biochemistry* **49,** 3317–26 (2010).
93. Fekete, S., Beck, A., Veuthey, J.-L. & Guillarme, D. Theory and practice of size exclusion chromatography for the analysis of protein aggregates. *J. Pharm. Biomed. Anal.* **101,** 161–73 (2014).
94. Gonzalez Porqué, P., Baldesten, A. & Reichard, P. Purification of a thioredoxin system from yeast. *J. Biol. Chem.* **245,** 2363–70 (1970).
95. Trathnigg, B. Size-Exclusion Chromatography of Polymers. *Encycl. Anal. Chem.* 8034–8088 (2000). doi:10.1002/9780470027318.a2032
96. Cao, Z., Bhella, D. & Lindsay, J. G. Reconstitution of the Mitochondrial PrxIII Antioxidant Defence Pathway: General Properties and Factors Affecting PrxIII Activity and Oligomeric State. *J. Mol. Biol.* **372,** 1022–1033 (2007).
97. Barranco-Medina, S., Kakorin, S., Lázaro, J. J. & Dietz, K. J. Thermodynamics of the dimer-decamer transition of reduced human and plant 2-cys peroxiredoxin. *Biochemistry* **47,** 7196–7204 (2008).
98. Chae, H. Z., Kim, H. J., Kang, S. W. & Rhee, S. G. Characterization of three isoforms of mammalian peroxiredoxin that reduce peroxides in the presence of thioredoxin. *Diabetes Res. Clin. Pract.* **45,** 101–12 (1999).
99. Yang, K.-S. K.-S. *et al.* Inactivation of human peroxiredoxin I during catalysis as the result of the oxidation of the catalytic site cysteine to cysteine-sulfinic acid. *J. Biol. Chem.* **277,** 38029–36 (2002).
100. Manta, B. *et al.* The peroxidase and peroxynitrite reductase activity of human erythrocyte peroxiredoxin 2. *Arch. Biochem. Biophys.* **484,** 146–154 (2009).
101. Soethoudt, M. *et al.* Interaction of adenanthin with glutathione and thiol enzymes: Selectivity for thioredoxin reductase and inhibition of peroxiredoxin recycling. *Free Radic. Biol. Med.* **77C,** 331–339 (2014).

Appendix

An example script used to discriminate the various conformation inhibition mechanisms by DynaFit. Note: the rate values units are in μmol min^{-1} L^{-1}.

```
Model discrimination analysis - mechanisms of enzyme inhibition

Enzyme: Peroxiredoxin5

Substrate: H2O2

Inhibitor: TBCat

No set Ks or kcat

;------------------------------------------------------------

[task]

   task   = fit

   data   = rates

   approx = rapid-equilibrium

   model  = Competitive ?

[mechanism]

   E + S <===> ES    :  Ks    dissoc

   ES ---> E + P     :  kcat

   E + I <===> EI    :  Ki    dissoc

[constants]

   Ks = 25 ?, kcat = 1000 ?

   Ki = 20 ?

[responses]

   P = 1

[concentrations]

   E = 0.15

[data]


   variable      S

   set gti0 | concentration I = 0

   set gti65 | concentration I = 65
```

```
   set gti120 | concentration I = 120
   set gti280 | concentration I = 280
   set gti430 | concentration I = 430

[output]
   directory ./
;_____________________________________________________________
[task]
   task   = fit
   data   = rates
   approx = rapid-equilibrium
   model  = Uncompetitive ?
[mechanism]
   E + S <===> ES       :  Ks     dissoc
   ES ---> E + P        :  kcat
   ES + I <===> ESI     :  Kis    dissoc
[constants]
   Ks = 25 ?, kcat = 1000 ?
   Kis = 20 ?
[responses]
   P = 1
[concentrations]
   E = 0.15
[data]
  variable      S
   set gti0 | concentration I = 0
   set gti65 | concentration I = 65
   set gti120 | concentration I = 120
```

```
   set gti280 | concentration I = 280
   set gti430 | concentration I = 430

[output]

   directory ./
;_____________________________________________________________
[task]
   task   = fit
   data   = rates
   approx = rapid-equilibrium
   model  = Mixed-type noncompetitive ?

[mechanism]
   E + S <===> ES      :  Ks    dissoc
   ES ---> E + P       :  kcat
   E + I <===> EI      :  Ki    dissoc
   ES + I <===> ESI    :  Kis   dissoc

[constants]
   Ks = 100 ?, kcat = 4000 ?
   Ki = 30 ?,  Kis = 1000 ?
[responses]
   P = 1
[concentrations]
   E = 0.15
[data]
   variable      S
   set gti0 | concentration I = 0
```

```
   set gti65 | concentration I = 65
   set gti120 | concentration I = 120
   set gti280 | concentration I = 280
   set gti430 | concentration I = 430
[output]
  directory ./
;_____________________________________________________________

[task]
   task   = fit
   data   = rates
   approx = rapid-equilibrium
   model  = Partial mixed-type ?

[mechanism]
   E + S <===> ES    :  Ks    dissoc
   ES ---> E + P     :  kcat
   E + I <===> EI    :  Ki    dissoc
   ES + I <===> ESI  :  Kis   dissoc
   ESI ---> EI + P   :  kcat'
 [constants]
   Ks = 25 ?, kcat = 2000 ?
   Ki = 10 ?, Kis = 10 ? , kcat' = 500 ?
[responses]
   P = 1
[concentrations]
   E = 0.15
[data]
```

```
   variable      S
   set gti0 | concentration I = 0
   set gti65 | concentration I = 65
   set gti120 | concentration I = 120
   set gti280 | concentration I = 280
   set gti430 | concentration I = 430
[output]

  directory ./
;_____________________________________________________________
[task]
   task   = fit
   data   = rates
   approx = rapid-equilibrium
   model  = Dual site partial mixed-type ?
[mechanism]
   E + S <===> ES      :  Ks    dissoc
   ES ---> E + P       :  kcat
   E + I <===> EI      :  Ki    dissoc
   ES + I <===> ESI    :  Kis   dissoc
   ESI ---> EI + P     :  kcat'
   EI + I <===> EII    :  Ki2   dissoc
[constants]
   Ks = 25 ?, kcat = 2000 ?
   Ki = 10 ?, Kis = 10 ?, kcat' = 500 ?, Ki2 = 100 ?

[responses]
```

```
   P = 1
[concentrations]
   E = 0.15
[data]
   variable      S
   set gti0 | concentration I = 0
   set gti65 | concentration I = 65
   set gti120 | concentration I = 120
   set gti280 | concentration I = 280
   set gti430 | concentration I = 430

[output]

   directory ./
;_____________________________________________________________
[task]
   task   = fit
   data   = rates
   approx = rapid-equilibrium
   model  = Partial mixed-type, optimized E ?
[mechanism]
   E + S <===> ES      :  Ks    dissoc
   ES ---> E + P       :  kcat
   E + I <===> EI      :  Ki    dissoc
   ES + I <===> ESI    :  Kis   dissoc
   ESI ---> EI + P     :  kcat'
[constants]
   Ks = 25.3?, kcat = 2000 ?
   Ki = 10 ?, Kis = 10 ?, kcat' = 500 ?
```

```
[responses]
   P = 1
[concentrations]
   E = 0.15
[data]
   variable      S

   set gti0 | concentration I = 0
   set gti65 | concentration I = 65
   set gti120 | concentration I = 120
   set gti280 | concentration I = 280
   set gti430 | concentration I = 430

[output]
   directory ./
;_____________________________________________________________
[task]
   task   = fit
   data   = rates
   approx = rapid-equilibrium
   model  = Dual site partial mixed-type, optimized E ?

[mechanism]
   E + S <===> ES      :   Ks    dissoc
   ES ---> E + P       :   kcat
   E + I <===> EI      :   Ki    dissoc
   ES + I <===> ESI    :   Kis   dissoc
   ESI ---> EI + P     :   kcat'
```

```
   EI + I <===> EII    :   Ki2   dissoc

[constants]

   Ks = 25.3?

   kcat = 2000 ?, kcat' = 500 ?

   Ki = 10 ?, Kis = 10 ?, Ki2 = 100 ?

[responses]

   P = 1

[concentrations]

   E = 0.15

[data]

   variable      S

   set gti0 | concentration I = 0

   set gti65 | concentration I = 65

   set gti120 | concentration I = 120

   set gti280 | concentration I = 280

   set gti430 | concentration I = 430


[output]

   directory ./

;_____________________________________________________________

[set:gti0]

S .uM    rate (I=0)

0        0
8        6.5019295501
16       7.1519880367
31       11.0531073472
63       18.2052874816
125      19.5055965525
250      24.0569664474
500      26.0075261026
```

```
;_____________________________________________________________

[set:gti65]

S .uM    rate (I=65)


0        0
8        4.5513698948
16       6.5019295501
31       9.7527982763
63       13.6539175868
125      20.1558471368
250      16.904786313
500      20.1558471368

;_____________________________________________________________

[set:gti120]

S .uM    rate (I=120)


0        0
8        5.8516789658
16       5.8516789658
31       8.4524892053
63       12.3536085158
125      17.5550368973
250      20.8059056235
500      21.4561562078

;_____________________________________________________________

[set:gti280]

S .uM    rate (I=280)


0        0
8        1.3003090709
16       5.2014283815
31       9.102547692
63       12.3536085158
125      17.5550368973
250      21.4561562078
500      20.8059056235

;_____________________________________________________________

[set:gti430]

S .uM    rate (I=430)


0        0
8        3.2508687262
16       5.8516789658
31       7.1519880367
63       11.0531073472
125      13.6539175868
250      18.8553459682
500      22.1064067921


[end]
```

The software, DynaFit, used the following parameters to fit the inhibition mechanism. Specifically, the Levenberg-Marquardt algorithm[73] and the Savitzky-Golay algorithm[74] was used to fit and smooth the data.

```
{DynaFit}
   RandomizationSeed                = 4357 ; | 0 for system time

{ODESolver}
   Iterations                       = 1000
   AbsoluteError                    = 1.e-14
   RelativeError                    = 1.e-8

{Marquardt}
   IterationsPerParameter           = 100
   RestartPerturbation              = 0.1
   Restarts                         = 2
   RestartsConfidence               = 1
   RobustFit                        = n
   EqualizeDatasets                 = n
   FixRedundantParameters           = y

{ConfidenceIntervals}
   LevelPercent                     = 95
   OnlyConstants                    = n
   InferenceBand                    = confidence ; | prediction
   JointProbability                 = n
   MaxSteps                         = 30
   SquaresIncreasePercent           = 0 ; | 10 for continuous assays

{DifferentialEvolution}
   PopulationSizeFixed              = 0
   PopulationSizeMinimal            = 1000
   PopulationSizePerParameter       = 5
   PopulationSizePerOrderOfMag      = 3
   MinimumGenerationsPerParameter   = 5
   MaximumGenerationsPerParameter   = 100
   MaximumEvolutions                = 6
   MinimumEvolutions                = 6
   RandomSeed                       = 1234

{Constraints}
   Constants                        = 1000000
   Responses                        = 1000000
   Concentrations                   = 1000
   AllParametersConstrained         = y
   AllParametersRelativeBound       = 1000000

{Filter}
   PointsPerDataset                 = 0
   ExponentialSpacing               = n
   ReadEveryNthPoint                = 0
   SkipFirstNPoints                 = 0
   TimeMin                          = 0
   TimeMax                          = 0
   TimeShift                        = 0
   TimeFirstMesh                    = 0
   TimeInitialRate                  = 1
   PrintInitialRate                 = y
```

```
   SmoothData                     = n
   SmoothingMethod                = savitzky-golay ; | average
   SavitzkyGolayWindow            = 10
   SavitzkyGolayDegree            = 4
   ExtrapolationMethod            = quadratic ; | linear
   SmoothingPasses                = 4
   AverageReplicates              = n
   ZeroBaselineSignal             = n

{PieceWiseLinearFit}
   Points                         = 0
   Segments                       = 4
   Time                           = 0
   Overlap                        = n

{Output}
   UseDefaultDirectory            = y
   Autocorrelations               = n
   InferenceBands                 = n
   WriteTXT                       = n
   WriteEPS                       = n
   ColorEPS                       = y
   ResidualsEPS                   = y
   WriteTeX                       = n
   XAxisLabel                     =
   YAxisLabel                     =
   BlackBackground                = y
   IncludeYZero                   = n
   InitialRateDigits              = 4
   StartDefaultBrowser            = n
   PlotRatesLogarithmic           = n
   PlotStateLogarithmic           = n

{MonteCarlo}
   PerformInitialFit              = y
   Runs                           = 1000
   RandomizationMethod            = simulate  ;  | shuffle | shift
   Distribution                   = normal    ;  | cauchy |
logistic | uniform
   StandardDeviationSource        = fit       ;  | data | explicit
   StandardDeviation              = 1.2
   SignificantDigits              = 4
   HistogramBuckets               = 20
   TruncateMeanPercent            = 5
   ColorOutput                    = y
   RandomizationSeed              = 1267
   ConcentrationErrorPercent      = 0
   OriginalEstimates              = n
   ConfidenceLevel                = 100

{EstimateScan}
   ReportSizeMax                  = 1000
   RefineMarquardt                = 10
```

```
{ExponentialFit}
   Degree                        = 4
   Automatic                     = y
   AllowOscillations             = n
   TinyAmplitudes                = 0 ; or 0.000001
   RefineMarquardt               = n

{OptimalDesign}
   Algorithm                     = AS ; | DE | BFGS
   Function                      = D  ; | T  | E  | V  ; see
manual
```

RÉSUMÉ

COMPRÉHENSION DES EFFETS DE L'INHIBITION DES PROTÉINES PEROXYRÉDOXINES HUMAINES POUR LE TRAITEMENT POTENTIEL DE L'INFLAMMATION POST-ISCHÉMIQUE CÉRÉBRALE

Les accidents vasculaires cérébraux (AVC) sont la seconde cause d'invalidité à long terme et du mortalité dans le monde entier qui résulte d'une interuption de flux sanguin cérébral. Il y a actuellement peu de médicaments pour traiter les accidents vasculaires cérébraux. Pourtant, il y a un intérêt pour trouver un traitement, ciblant spécifiquement la cascade post-inflammatoire. Il y a une attention particulière pour inhiber les protéines peroxyrédoxines humaines (hPrx) qui sont des initiateurs clés de l'inflammation. Les protéines hPrx sont des enzymes qui dégradent les peroxydes et aussi protègent les cellules du stress oxydatif. Cette thèse est centrée sur l'étude de ligands potentiels des hPrx, dérivés du catéchol, susceptibles de devenir des agents thérapeutiques potentiels pour traiter les AVC. Basées sur différents ligands potentiels criblés par RMN et modélisation moléculaire, nos études ont révélé que ces dérivés du catéchol pouvaient se lier à plusieurs hPrx. Deuxièmement, la capacité des dérivés du catéchol à inhiber l'activité des hPrx a été examinée au travers de tests enzymatiques *in vitro*. Il a été montré que tous les dérivés du catéchol étudiés étaient capables de les inhiber. En utilisant des simulations de dynamique moléculaire, nous avons pu expliquer le mécanisme d'action moléculaire d'inhibition. D'un point de vue général, cette recherche fournit un aperçu des ligands qui pourrait être développés pour devenir un médicament pour aider dans le processus de rétablissement de patients atteints d'attaque cérébrale.

Mots clés: peroxyrédoxines humaines, dérivés de catéchol, cinétique enzymatique, RMN

UNDERSTANDING THE EFFECTS OF INHIBITING HUMAN PEROXIREDOXIN PROTEINS FOR POTENTIAL TREATMENT AGAINST POST-ISCHEMIC BRAIN INFLAMMATION

Strokes are the second leading cause of long-term disability and death worldwide that result from a sudden loss of blood supply to the brain. Currently, there are limited drugs to treat patients when having a stroke. However, there is now interest focused on treatment after a stroke, specifically the post-inflammation cascade. In particular, there is attention to inhibit human peroxiredoxin proteins, which are key initiators of inflammation. Human peroxiredoxins are enzymes that degrade peroxides and also, protect the cells against oxidative stress. This thesis focuses on studying ligands, catechol derivatives, to bind and inhibit human peroxiredoxin proteins to become potential therapeutic agents for strokes. First, the ligands were screened to identify if they could bind to various human peroxiredoxin isoforms with NMR and computational modeling techniques. This study revealed the catechol derivatives could indeed bind to several human peroxiredoxins. Second, the ability for the catechol derivatives to inhibit human peroxiredoxin peroxidase activity was examined through an *in vitro* enzymatic assay. All the catechol derivatives were determined to inhibit several human peroxiredoxins. In utilizing molecular dynamic simulations, it assisted in explaining the *in vitro* inhibition molecular mechanism of action. Overall, this research provides insight of molecules that could be further developed to become possibly a drug to aid in stroke patients recovery process.

Key words: human peroxiredoxins, catechol derivatives, enzymatic kinetics, inhibition mechanism, NMR.